Folic acid derivatives for PET imaging and therapy addressing folate receptor positive tumors

Dissertation

zur Erlangung des Grades eines

“Doktor rerum naturalium (Dr. rer. nat.)”

im Promotionsfach Chemie

am Fachbereich Chemie, Pharmazie und Geowissenschaften

der Johannes Gutenberg-Universität Mainz

Hanno Schieferstein

geb. in Bad Schwalbach

Mainz 2013

Die vorliegende Arbeit wurde unter der Betreuung von ..... in der Zeit von 2010 bis 2013 am Institut für Kernchemie der Johannes Gutenberg-Universität Mainz angefertigt.

„I hereby declare that I wrote the dissertation submitted without any unauthorized external assistance and used only sources acknowledged in the work. All textual passages which are appropriated verbatim or paraphrased from published and unpublished texts as well as information obtained from oral sources are duly indicated and listed in accordance with bibliographical rules. In carrying out this research, I complied with the rules of standard scientific practice as formulated in the statutes of Johannes Gutenberg-University Mainz to insure standard scientific practice."

_____

Dekan:

1. Berichterstatter:

2. Berichterstatter:

Tag der mündlichen Prüfung:

Table of Contents

II

List of Abbreviations

AIBN	azobisisobutyronitrile	Da	dalton
approx.	approximately	L	liter
Bq	bequerel	LG	leaving group
CAT	chloramine-T	i.v.	intravenous
$CDCl_3$	deuterated chloroform	L-Dopa	L–3,4-dihydroxyphenylalanine
CMC	critical micelle concentration	LMA	lauryl methacrylate
CPM	count per minute	m	multiplett (NMR)
CT	computed tomography	M	molar
CTA	chain transfer agent	MeCN	acetonitrile
CuAAC	copper(I)-catalyzed azide-alkyne cycloaddition	MeOH	methanol
d	day	min	minute
d	dublett (NMR)	M_n	number average molecular weight
Da	dalton	max.	maximum
DMF	dimethylformamide	MIP	maximum intensity projection
DMSO	dimethyl sulfoxide	MR	magnetic resonance
DNA	deoxyribonucleic acid	MRI	magnetic resonance imaging
DOTA	1,4,7,10-tetraazacyclododecanetetraacetic acid	MRS	magnetic resonance spectroscopy
Dox	doxorubicin	M_w	weight average molecular weight
e^+	positron	n	neutron
e.g.	for example (*exempli gratia*)	NaCl	sodium chloride
EDG	electron donating group	n.d.	not determined
EPR	enhanced permeability and retention	NMR	Nuclear Magnetic Resonance
EWG	electron withdrawing group	OG	Oregon Green Cadaverine 488
FCS	Fluorescence correlation spectroscopy	o-/*p*-Ps	*ortho*-/*para*-positronium
[^{18}F]FETos	2-[^{18}F]fluorethyl tosylate	OSEM	Ordered Subset Expectation Maximization
[^{18}F]SFB	N-succicimidyl 4-[^{18}F]fluorobenzoate	p	proton
g	gram	PBS	phosphate buffered saline
GPC	gel permeation chromatography	PDI	polydispersity index
h	hour	PDLLA	poly-DL-lactide
HPLC	high pressure liquid chromatography	PEG	polyethylene glycole
HPMA	N-(2-hydroxypropyl)methacrylamide	PET	positron emission tomography
Hz	Hertz	PFPMA	pentafluorphenyl methacrylate
ID	injected dose	p.i.	post injection

ppm	parts per million (NMR)
prop	propargyl
q	quartett (NMR)
RAFT	Reversible Addition Fragmentation Chain Transfer
RCY	radiochemical yield
R_h	hydrodynamic radius
ROI	region of interest
s	singulett (NMR)
sec	second
SEC	size exclusion chromatograpy
SEM	standard error of the mean
SEM	scanning electron microscopy
SD	Sprague Dawley
SEPCT	single photon emission computed tomography
SER	serine
SUV	standardized uptake value
THF	tetrahydrofuran
TLC	thin layer chromatography
VEGF	vascular endothelial growth factor
VOI	volume of interest
W 256	Walker 256 mammary carcinoma of the rat
µPET	small animal PET

Abstract:

Folic acid, also known as vitamin B_9, is the oxidized form of 5,6,7,8-tetrahydrofolate, which serves as methyl- or methylene donor (C1-building blocks) during DNA synthesis. Under physiological conditions the required amount of 5,6,7,8-tetrahydrofolate for survival of the cell is accomplished through the reduced folate carrier (RFC). In contrast, the supply of 5,6,7,8-tetrahydrofolate is insufficient under pathophysiological conditions of tumors due to an increased proliferation rate. Consequently, many tumor cells exhibit an (over)expression of the folate receptor. This phenomenon has been applied to diagnostics (PET, SPECT, MR) to image FR-positive tumors and on the other hand to treat malignancies related to a FR (over)expression. Based on this concept, a new ^{18}F-labeled folate for PET imaging has been developed and was evaluated *in vivo* using tumor-bearing mice. The incorporation of oligoethylene spacers into the molecular structure led to a significant enhancement of the pharmacokinetics in comparison to previously developed ^{18}F-folates. The liver uptake could be reduced by one sixth by remaining a tumor uptake of 3%ID/g leading to better contrast ratios. Encouraged by these results, a *clickable* ^{18}F-labeled serine-based prosthetic group has been synthesized, again with the idea to improve the metabolic and pharmacokinetic profile of hydrophilic radiotracers. Therefore, an alkyne-carrying azido-functionalized serine derivative for coupling to biomolecules was synthesized and a chlorine leaving group for ^{18}F-labeling, which could be accomplished using a microwave-assisted synthesis, a $[K\subset2.2.2]^+$/carbonate system in DMSO. Radiochemical yields of 77±6% could be achieved.

The promising results obtained from the FR-targeting concept in the diagnostic field have been transferred to the boron neutron capture therapy. Therefore, a folate derivative was coupled to different boron clusters and cell uptake studies were conducted. The synthesis of the folate-boron clusters was straightforward. At first, a linker molecule based on maleic acid was synthesized, which was coupled to the boron cluster via Michael Addition of a thiol and alkene and subsequently coupled to the targeting moiety using CuAAC. The new conjugates of folate and boron clusters led to a significant increase of boron concentration in the cell of about 5-times compared to currently used and approved boron pharmaceuticals.

Moreover, azido-folate derivatives were coupled to macromolecular carrier systems (pHPMA), which showed an enhanced and specific accumulation at target sites (up to 2.5-

times) during *in vivo* experiments. A specific blockade could be observed up to 30% indicating an efficient targeting effect. A new kind of nanoparticles consisting of a PDLLA core and p((HPMA)-*b*-LMA)) as surfactants were developed and successfully radiolabeled via ^{18}F-click chemistry in good RCYs of 8±3%

The nanoparticles were obtained via the miniemulsion technique in combination with solvent evaporation. The ^{18}F-labeled nanoparticles were applied to *in vivo* testing using a mouse model. PET imaging showed a "*mixed*" biodistribution of low molecular weight as well as high molecular weight systems, indicating a partial loss of the ^{18}F-labeled surfactant.

In conclusion, the presented work successfully utilized the FR-targeting concept in both, the diagnostic field (PET imaging) and for therapeutic approaches (BNCT, drug delivery systems). As a result, the high potential of FR-targeting in oncological applications has been shown and was confirmed by small animal PET imaging.

Zusammenfassung:

Folsäure, Vitamin B_9, ist die oxidierte Form der 5,6,7,8-Tetrahydrofolsäure, welche in der DNS Biosynthese als Lieferant u.a. von Methyl- und Methylenbausteinen (C1-Bausteine) fungiert. Unter physiologischen Bedingungen ist die Aufnahme der notwendigen Menge an 5,6,7,8-Tetrahydrofolat in die Zelle über den Reduced Folate Carrier (RFC) gewährleistet, wohingegen unter pathophysiologischen Bedingungen der erhöhte Bedarf an DNS Bausteinen aufgrund der gesteigerten Proliferationsrate, durch eine (Über)Expression des Folatrezeptors (FR) kompensiert wird. Diese (Über)Expression wird zum einen für die Diagnostik (PET, SPECT, MR) von FR-positiven Tumoren und zum anderen zur gezielten Therapie von malignen Tumoren eingesetzt. Auf dieser Grundlage wurde ein neues ^{18}F-markiertes Radiofolate für die PET entwickelt und evaluiert. Der Einbau von Oligoethylenspacern bewirkte eine deutlich verbesserte Pharmakokinetik. Dies spiegelt sich durch eine um ein sechstel erniedrigte Anreicherung des Tracers in der Leber wieder, wobei die Tumoranreicherung bei einem ähnlichen Wert von 3%ID/g blieb im Vergleich zu ähnlichen Tracern. Dies führte zu einer deutlichen Verbesserung des Kontrasts. Auf diesen Erkenntnissen wurde eine serinbasierte prosthetische Gruppe entwickelt, die sich nahe am endogenen Serin orientiert und somit zu einer nochmaligen Verbesserung der Pharmakokinetik von Biomolekülen führen sollte. Dazu wurde ein Serinderivat dargestellt, welches eine Alkinfunktion für die Biomolekülanbindung und Chlor als Abgangsgruppe trug. Die Radiomarkierung konnte mittels einer mikrowellengestützten Synthese und eines Karbonat/Kryptofix Systems in DMSO durchgeführt werden.

Die erfolgreiche Anwendung von Folatstrukturen in der Diagnostik konnte auch auf Therapieansätze übertragen werden. Hierbei wurden Folatborclusterderivate dargestellt, welche in der Bor Neuronen Einfangtherapie Anwendung finden. Dabei wurde zuerst das Borcluser über eine Michael Additionsreaktion eines Thiols mit einem Alken an das Linkermolekül angebunden. In einer zweiten CuAAC wurde nun das Folat gekoppelt. Darüber hinaus wurden die dargestellten Folsäurederivate an makromolekulare Trägersysteme (pHPMA) übertragen. Erste Zellaufnahmestudien zeigten eine deutliche Verbesserung der Anreicherung (Faktor 5) von Bor in den Zellen im Vergleich zu bisher verwendeten zugelassenen Borpharmazeutika. Die verwendeten Borcluster wurden über

ein Linkermolekül mit der Folatstruktur gekoppelt. Durch die Verwendung des aktiven FR-targeting Konzepts konnte eine erhöhte Anreicherung (bis zu 2.5-fach) im Tumor während *in vivo* Experimenten gezeigt werden. Darüber hinaus konnte eine spezifische Blockade von 30% beobachtet werden, was nochmals die Effizienz des aktiven Targetings zeigte. Eine nochmalige Verbesserung der *in vivo* Eigenschaften wurde sich durch die Verwendung von nanopartikulären Systeme (PDLLA-Kern und p((HPMA)-*b*-(LMA)) Tenside), die mit Folsäure konjugiert sind, versprochen. Die über die Miniemulsion in Kombination mit der Solvent Evaporation Technik synthetisierten Systeme, noch ohne Folsäureanbindung, wurden hierbei erstmals mit Fluor-18 mit RCA von 8±3% markiert und im Mausmodell evaluiert. Die Systeme zeigten interessanterweise das Verhalten von sowohl niedermolekularen als auch hochmolekularen Systemen. Zusammenfassend konnte die erfolgreiche Anwendung des FR-targeting Konzepts in Diagnostik (PET)- und Therapieansätzen (BNCT, Drug Delivery) demonstriert werden.

1. Introduction

The human body consists of trillions cells, which are diploid and eukaryotic.[1] One cell has twenty-three sets of chromosomes, whereas twenty-two sets are autosomal and the twenty-third pair is the sex determining one. Those sets of chromosomes undergo proliferation in distinct intervals, meaning a cell duplicate is produced. This requires that all parts of the cell have to be doubled, avoiding mutations during the replication of deoxyribonucleic acid (DNA). The DNA itself is a twisted double-stranded helix, whereby a stand consists of a phosphate-backbone, attached sugars (deoxyribose) and nucleobases (guanine, adenine, thymine, and cytosine).[2] There are four types of nucleobases which are complementary to each other, meaning that only guanine and cytosine or adenine and thymine are able to form stable hydrogen bridge bonds.[2] Adenine and guanine are purines; in contrast thymidine and cytosine are pyrimidines. The biosynthesis of these nucleobases requires a number of enzymes and building blocks, whereas 5-methyl-5,6,7,8-tetrahydrofolate (5-methyl-THF), a folic acid derivative, represents one important one-carbon donor for the build-up synthesis of purines.[3] Since folic acid or folates cannot be synthesized by the human body due to the lack of two key enzymes for an endogenous biosynthesis, they have to be admitted through the diet. Therefore, the human body has mechanisms to ensure folate supply using several kinds of receptors and carriers.[4] Furthermore, these mechanisms can be relevant to health science, in oncology, where these receptors have been found to be suitable as targeting structures for diagnostics and therapy.

Most malignancies are dependent on an enhanced supply of nutrients, since they have a fast proliferation rate.[5] This characteristic of malignant cells has been recognized as unique feature in the field of molecular imaging, where various receptor ligands have been modified and introduced to e.g. magnetic resonance imaging, near-infrared optical imaging, single-photon emission computed tomography or positron emission tomography. These ligands can target recognition structures on the cell surface (VEGF[6],

FR[7], antigens[8]), structures in the cytosol (signaling pathways)[9], or structures in the cell nucleus (nuclear receptors)[10]. However, there is still a lack of selective, effective and readily accessible compounds to target the folate receptor, in particular, for diagnostic and therapeutic purposes, facilitating a personalized, quality of life improving therapy/cure.

1.1 Molecular Imaging

The term "molecular imaging" has been used over decades, but never a proper definition has been made, which changed in 2007, when a task force of fourteen members developed standard definitions for all types of communications, advocacy, and educational activities. These definitions describe molecular imaging as followed:

"*Molecular imaging is the visualization, characterization, and measurement of biological processes at the molecular and cellular levels in humans and other living systems. To elaborate; Molecular imaging typically includes 2- or 3-dimensional imaging as well as quantification over time. The techniques used include radiotracer imaging/nuclear medicine, MR [magnet resonance] imaging, MR spectroscopy, optical imaging, ultra-sound, and others.*"[11]

The principle behind these techniques, especially the radiotracer imaging/nuclear medicine techniques is the "tracer principle", which was first described by Georg de Hevesy in 1913 using lead-212 as a radiotracer. Since lead is known to be toxic in larger amounts, the idea in using lead-212 was to apply smallest amounts to avoid a pharmacological effect.

Single photon emission computed tomography (SPECT) is one of the before mentioned 3-dimensional imaging techniques belonging to the area of radiotracer imaging/nuclear medicine, which is non-invasive, kinetic and repetitive for imaging biochemical processes. Briefly, this technique is based on the detection of photons from a γ-emission as a result of the decay of a radionuclide or isomeric transition. These photons can be detected using a gamma-camera, which consists of a collimator, a scintillator, fiber optics, a

photomultiplier and an analyzer. To generate a 3-dimensional imaging, the gamma-camera rotates around the subjects. Typical radionuclides used for SPECT are shown in Table 1.

Table 1. Radionuclides relevant for medical purposes in SPECT.

Nuclide	Half-life	γ-Energy	γ-Emission yield
Iodine-123	13.2 h	159 keV	83.3%
Iodine-131	8.04 d	364.5 keV	81.2%
Technecium-99m	6.01 h	140.5 keV	87.2%
Thallium-201	3.05 d	68.9 keV	26.9%
		70.82 keV	46%
		140.5 keV	16.1%
Gallium-67	3.26 d	184.6 keV	20.4%
Indium-111	2.82 d	171.3 keV	90.24%
		245.4 keV	94%

Many routinely used radiotracers have been developed for SPEC imaging, including various folate-based tracers.[12] In contrast, radiotracers for the folate receptor system and the use in positron emission tomography (PET) are still lacking, which is the major base and rationale for this work. PET is another 3-dimensional imaging technique for imaging biochemical processes, but differs from the SPECT in this way, that it is based on the process of positron emission (β^+-decay). Two major advantages of PET are a very high spatial resolution and the ability of a precise quantification of the radiotracer concentration *in vivo*. Indeed the measured species during PET studies are two photons, deriving from the annihilation of an electron and the positron as product of a β^+-decay. Radionuclides available for PET imaging, either cyclotron-produced or generator-based are listed in Table 2.

Table 2. PET nuclides with their characteristics.

Nuclide	Half-life	β^+-Branching	β^+-Energy (max)	Range (H_2O)
Carbon-11	20.3 min	99.8%	0.96 MeV	4.1 mm
Nitrogen-13	9.96 min	100%	1.19 MeV	5.4 mm
Oxygen-15	2.03 min	99.9%	1.70 MeV	8.2 mm
Fluorine-18	109.7 min	96.9%	0.63 MeV	2.4 mm
Gallium-68	67.71 min	89.1%	1.90 MeV	13.6 mm
Yttrium-86	15.7 d	31.4%	1.18 MeV	5.3 mm
Scandium-44	3.93 h	88%	1.48 MeV	
Arsenium-72	25.9 h	88%	3.34 MeV	
Copper-64	12.7 h	17.6%	0.65 MeV	
Niobium-90	14.6 h	53%	1.50 MeV	

The property that all PET nuclides have in common is an excess of protons in their nucleus. During the β^+-decay, a proton is converted into a neutron, whereas a positron (β^+-particle) and an electron neutrino are emitted. The emitted positron is able to move a certain distance (proportional to its energy), before it reaches its resting energy. From that point, it pairs with an electron from the environment, forms an intermediate positronium and annihilates. However, the positronium has two appearances, an *ortho*- and *para*-positronium (*o*-/*p*-Ps). The *o*-Ps annihilates with a higher probability (75%, triplet state) under a continuous γ-spectrum, which makes a coincident detection impossible. On the other hand, the *o*-Ps can transform into a *p*-Ps due to interaction with the environment. In contrast to the *o*-Ps, the *p*-Ps (25% probability, singlet state) possesses distinct angles after annihilation enabling the detection of two photons with an angle of nearly 180° and an energy of 511 keV each, which reflects the resting energy of the positron or electron, respectively. By using a tomograph equipped with a ring of scintillation crystals, fiber optics, a photomultiplier and an analyzer, it is possible to detect the photons in the 180° angle, coincidently, and re-constructing the origin of this event (*line of response*, LOR) (Figure 1). As already mentioned, the travelled distance of the e^+, which correlates with the resolution, is mainly dependent on the β^+-energy of the

particle, featuring resolutions from 5 to 3 mm for human PET cameras and 2.0 to 0.7 mm for small animal PET cameras. After subtraction of dead-time, scattered photons, detector sensitivity and attenuation, an image can be reconstructed in 2D or 3D via rendering the regions or volumes of interest. This whole processing leads to different intensities in different areas of interest, representing the amount of radiotracer in distinct e.g. tissues or organs, which can be assigned to biological process rates, if measured dynamically over time.[13]

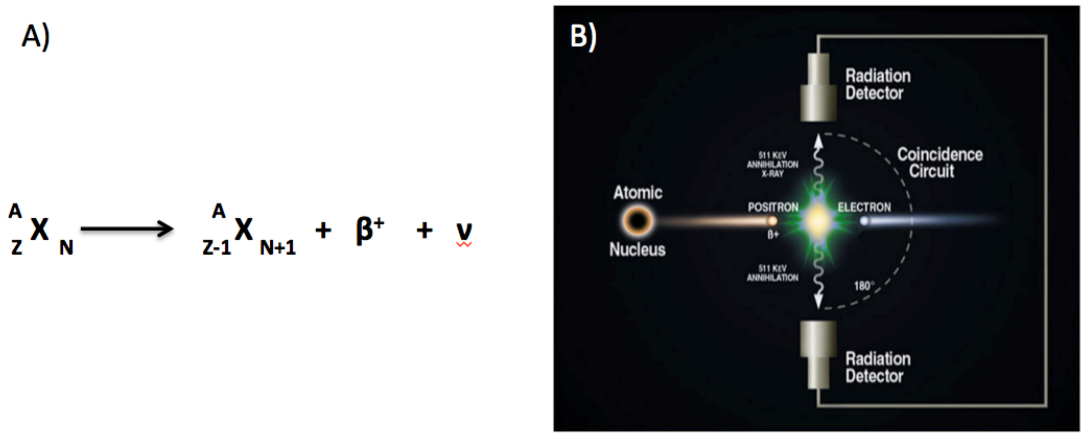

Figure 1. **A**) β^+-decay on nuclear level; **B**) Schematic setup for PET imaging principle.[14]

1.2 Folic Acid

(2*S*)-2-[(4-{[(2-amino-4-hydroxypteridin-6-yl)methyl]amino}phenyl)formamido]pentane-dioic acid or folic acid (Scheme 1) is an essential nutrient belonging to the vitamins. Folic acid itself is also known as vitamin B_9 and was discovered in 1941 by Esmond Snell, who simmered and filtered four tons of spinach to get enough amount of a compound, which he later named after the latin word for leaf, *folium*.[15] This was the birth of folic acid in nutrition science, particularly when a folate deficiency during pregnancy was related to neural tube defects, like *spina bifida*.[16]

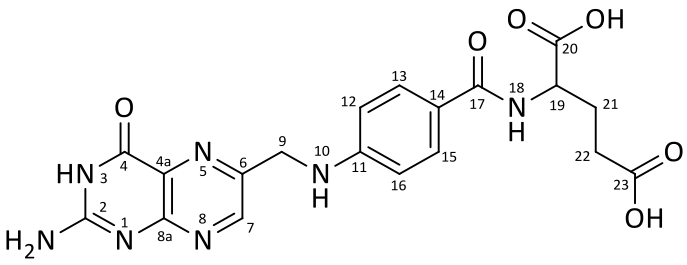

Scheme 1. Chemical structure and IUPAC carbon nomenclature of folic acid.

Under physiological conditions folic acid plays a crucial role in the early stage of deoxyribonucleic acid (DNA) synthesis, more precisely in the one-carbon metabolism of nucleotide synthesis.[17] During DNA synthesis, it is not folic acid itself, which is metabolized, but there are several reduced forms of folic acid, which are the responsible bioactive compounds in the synthesis of nucleotides. The most relevant reduced forms are listed in Table 3.

Table 3. Roles of different folates in metabolism.[4]

Position	Substituent	Derivative	Metabolic step
5,6,7,8	-H	5,6,7,8-Tetrahydrofolate	Generation of formate
N^5	$-CH_3$	5-Methyl-5,6,7,8-tetrahydrofolate	Homocysteine to methionine
N^5	$-CNH_2$	Formiminotetrahydrofolate	Histidine metabolism
N^5	-CHO	Folinic acid	Synthesis of purines
N^{10}	-CHO	10-Formyltetrahydrofolate	Synthesis of purines
N^{5-10}	-CH-	5,10-Methenyltetrahydrofolate	Synthesis of purines
N^{5-10}	$-CH_2-$	5,10-Methylenetetrahydrofolate	Synthesis of thymidylate

As already mentioned, folic acid cannot be synthesized by the human body, meaning that folates are essential nutrients obtained through the diet (Figure 2).

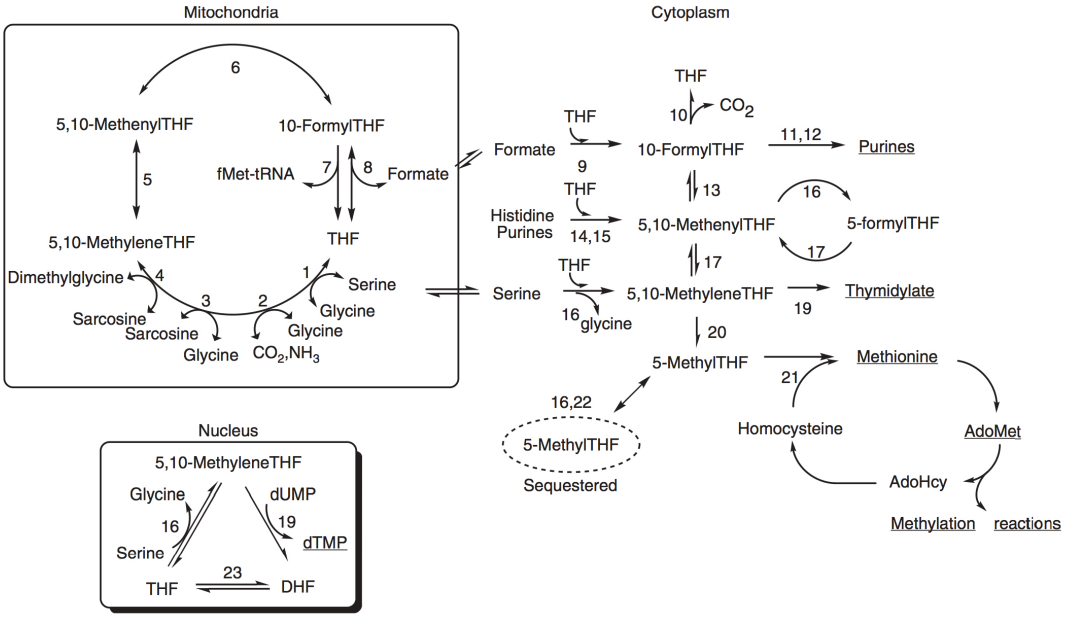

Figure 2. Folate-mediated one-carbon circle. **1**, mitochondrial serine hydroxymethyltransferase; **2**, aminomethyltransferase; **3**, sarcosine dehydrogenase; **4**, dimethylglycine dehydrogense; **5**, 5,10-methylenetetrahydrofolate dehydrogenase (NAD-dependent); **6**, 5,10-methenyltetrahydrofolate cyclohydrolase; **7**, methionyl-tRNA formyltransferase; **8**, 10-formyltetrahydrofolate synthetase; **9**, 10-formyltetrahydrofolate synthetase; **10**, 10-formyltetrahydofolate dehydrogenase; **11** and **12**, phosphoribosylglycinamide formyltransferase and phosphoribosylaminoimidazolecarboxamide formyltransferase; **13**, 5,10-methenyltetrahydrofolate cyclohydrolase; **14** and **15**, glycine formiminotransferase/formimidoyltetrahydrofolate cyclodeaminase and glutamate formiminotransferase/formimidoyltetrahydrofolate cyclo- deaminase; **16**, cytoplasmic serine hydroxymethyltransferase; **17**, methenyltetrahydrofo- late synthetase; **18**, 5,10-methylenetetrahydrofolate dehydrogenase (NADP-dependent); **19**, thymidylate synthase; **20**, methylenetetrahydrofolate reductase; **21**, methionine synthase; **22**, glycine N-methyltransferase; **23**, dihydrofolate reductase.[17]

The most common form of folic acid in the plasma is 5-methyl-5,6,7,8-tetrahydrofolate (5-methyl-THF) with plasma levels from 5-30 nM. Generally, serum folates exist in the monoglutamate form, which enables them to be transported through the cell membranes by various transporters, but mainly the reduced folate carriers (RFCs). Once a folate entered a cell it can be converted to a polyglutamte, which is the trapped form in the cell. Since folate is essential for various metabolic steps, it is subjected to strict recycling machinery in the kidneys of various folate transport proteins, like α-folate receptors (α-FRs), reduced folate carriers (RFCs), proton-coupled folate transporters (PCFTs), organic anion transporters (OATs), and multidrug resistance proteins (MRPs).

Due to the more and more focus drawn on folic acid or folates, epidemiological studies showed that an imbalance in folic acid metabolism compromised vitality and is involved in pathologies and developmental abnormalities like neural tube defects (NTD)[16], cardiovascular disease[18,19], and cancer[20–24]. This reflects the importance of folic acid derivatives for cell viability and life in general leading to an increased interest of researchers to investigate the fade of folic acid derivatives *in vivo*. In 1961, *John et al.* injected [^{3}H]folic acid and native folic acid at different concentrations into men and measured the activity in the urine over 2 h and found out that renal reabsorption could be saturated by co-injection of native folic acid.[25] This was the first report about exploring the *in vivo* behavior for diagnostic purposes of folic acid using a radiolabeled tag.

1.3 Folic Acid and Folates in Therapy and Diagnostics

Based on the essential roles of folates in multiple biochemical processes, like synthesis of DNA and RNA, gene regulation, and amino acid metabolism, folate derivatives became a promising candidate for diagnostic and therapeutic questions.[26] Additionally, the chemical properties of folates, which are described as hydrophilic and anionic, demand effective and specific transport over cell membranes, which is facilitated through a variety of transport proteins, like the reduced folate carrier (RFC)[27,28] and the proton coupled folate-transporter (PCFT)[29,30]. The RFC is located on almost all physiological working cells to supply 5-methyl-THF, the form that circulates in the blood stream. Recently, the PCFT was discovered and assigned to folate transportation under acidic conditions, which can be found in the intestines. In contrast, to these carriers systems, there is also a receptor family summarized under the name folate binding protein (FBP), with high affinity (~1 nM) to the oxidized form of folate and only 5-methyl-THF of the reduced forms.[31,32] This family can be divided into three receptor subtypes, the α-folate receptor (α-FR), the β-folate receptor (β-FR) and the γ-folate receptor (γ-FR), whereas the α-FR and FR-β are *N*-glycolsylated and clinched to the cell surface. But the occurrence of the α-FR and β-FR is limited to distinct tissues and organs, like the lung (α-FR), the choroid plexus (α-FR), the

placenta (α-FR/β-FR), and kidneys (α-FR), where it is expressed on the apical side of the epithelial cells, consequently not directly reachable through the blood stream by circulating (radio)folates.[33–35] In contrast, it has been shown that the β-FR is often (over)expressed on activated macrophages in synovial fluid from inflamed joints of rheumatoid arthritis in humans and rat models.[36–39]

The importance of folates during, especially DNA synthesis, explains the fact, that the α-FR is overexpressed in many common types of cancer, like ovarian, cervix and endometrium. The biological properties of folates, meaning the rapid uptake in cells or tissues with FR-expression and the fast clearance in healthy tissues, makes them attractive for tumor targeting in molecular imaging and therapeutic approaches, e.g. the first imaging approach of metastatic cancer in mice was done in 2003, when *Kennedy et al.* used a fluorescein-folate conjugate.[40] Since the potential of folate has been esteemed, the development of various folate-based imaging agents for magnetic resonance (MR) imaging[41], near-infrared (NR) optical imaging[42,43] as well as molecular imaging probes using radioactivity, e.g. ^{125}I-labeled pteroylglutamic acid[44], were promoted.

1.4 SPECT-Folates

There are several radiofolates for single-photon emission computed tomography (SPECT), whereas the most used radionuclides are ^{67}Ga-, ^{99m}Tc- and ^{111}In.[7] A prominent radiofolate using deferoxamine (DFO) as chelate was published by *Wang et al*. [45] In this case a deferoxamine mesylate was coupled to the activated ester form of folic acid. The resulting regioisomeric mixture was separated by anion-exchange chromato-graphy to obtain the γ-derivatized folate carrying the DFO as chelate, showing a tumor uptake of 5.2±1.5%ID/g 4 h post injection (p.i.).[46] Beside the folates attached to an open-chain chelate, like DFO, there have also been folates synthesized carrying cyclic chelates, like 1,4,7,10-tetraazacyclododecane-1,4,7,10-tetraacetic acid (DOTA). The attachment to the chelate can vary, meaning the folate part was clicked to the chelate via copper(I)-catalyzed cycloaddition (CuAAC)[47] or just coupled using amide-bonding[48,49], achieving around 6%ID/g tumoruptake for all variants after 4 h. Another radionuclide widely used in

SPECT is indium-111. One, often as “gold standard” termed, radiofolate is the ^{111}-In-diethylenetriaminepentaacetic acid (DTPA) folate. In a first step, the activated *N*-hydroxysuccinimide (NHS) ester of folic acid is generated with *N,N'*-dicyclohexyl-carbodiimide (DCC) as coupling agent and reacted directly with ethylenediamin (EDA). The resulting mixture of regioisomers was separated via high-performance liquid chromatography (HPLC), whereas the γ-folate was reacted with DTPA dianhydride in a second step under basic conditions. After radiolabeling with [^{111}In]$InCl_3$ the tracer showed a rapid blood clearance and a low accumulation of the activity in the intestines by maintaining the high tumor affinity *in vivo*. This led to the ^{111}In-DTPA folate in clinical trials (Phase I & II) for human ovarian cancer and also the development of a kit formulation for routine use.[50,51] Another approach was again to vary the coupling strategy between folate and chelate by using the CuACC to simplify radiosynthesis.[47] The ^{111}In-labeled “click” folate showed results close to the original ^{111}In-DTPA folate.

Due to the relatively long half-life of the ^{111}In-folates Ilgan *et al.* published a new radiofolate labeled with technicium-99m. The best scanning point for optimal contrast was reached after 1 h, but this folate consisting of folic acid, ethylenediamine spacer and ethylenedicystein showed low tumor uptake values less than 0.1%ID/g 4 h p.i.[52] The only reason that could be imagined was the use of an unsuitable tumor model. Further research led to the development of ^{99m}Tc-hydrazinonicotinic acid (HYNIC) folates. A ^{99m}Tc-HYNIC-pteroyllysine conjugate, which showed an efficient labeling, was synthesized by reacting hydrazine with the NHS-ester of folic acid. After isolation of the γ-derivate using anion-exchange chromatography the derivate was reacted with chloronicotinic acid yielding the final precursor for ^{99m}Tc-labeling. The tracer showed specific and good uptake, and moreover, the undesired specific kidney uptake could be reduced by co-administration of native folic acid.[53] The widely used folate Etarfolatide® (formerly ^{99m}Tc-EC20), which has already entered phase III in clinical trials coordinates technecium-99m by complexation using a peptide structure, which has been synthesized on a Wang resin.[54] The results, like uptake and background levels, were comparable to the ^{111}In-DTPA folate, since all experiments were carried out in the same cell lines. These

promising results led to intensive investigations to use Etarfolatide® for patient selection, who were particularly promising for a folate-based therapy.[55] The ultimate approach using Etarfolatide® for patient selection and therapy monitoring, in combination with the vincaalkaloid desacetylvinblastine hydrazide folatconjugate EC145 *Vintafolide*® (Endocyte/Merck/MSD, USA) for therapy depict the high potential of the combined diagnostic/therapy approach for a personalized treatment plan. The application of this combinational therapy is frequently used to tread women with a cis-platinum resistant ovarian carcinoma.[56]

The tricarbonyl-complexes are one more method to form stable complexes with technecium-99m. Therefore, $^{99m}Tc(CO)_3$ folates have been developed using, e.g. three carbonyls and a histidine tag for comlexation.[57,58] This folate showed good labeling results and seemed to be a good candidate for further evaluation, however, these tracers suffered from the increased lipophilicity of the tricarbonyl-structure.

But as already mentioned to use molecular imaging techniques like SPECT or PET for selection and staging of patients, there is a need for real quantification of activity, which can be contrived with SPECT during small animal imaging, but when it comes to human use it is too imprecise, and therefore inferior to PET.

1.5 PET-Folates

The great potential of molecular imaging techniques, especially PET has already been described. But there is still a lack of PET-folates suitable for routine application to warranty personalized patient care for best therapeutic results. The most widespread PET-folates are labeled with gallium-68, copper-64 and fluorine-18. The metal-based PET-folates are similar to the SPECT-folates due to their *in vivo* behavior, only differing in the radionuclide, which emits positrons.

A major focus of this work should be set on ^{18}F-labeled folates, whereas two main strategies were prosecuted, the direct ^{18}F-fluorination and the ^{18}F-labeling via prosthetic group (Table 4). The direct ^{18}F-fluorination approach is often very challenging, in respect

to precursor synthesis or radiolabeling. During the precursor synthesis on the one hand a complex protecting group chemistry is needed to circumvent problems during ^{18}F-labeling and on the other hand the introduction of leaving groups suitable for nucleophilic aromatic substitutions has to be accomplished. The labeling reaction itself leads mostly to low radiochemical yields and secondly, the essential protecting groups for ^{18}F-labeleing bear always risks during deprotection, leading to either decomposition (acidic or basic conditions; high temperatures), or do not react at all. In contrast, the labeling via an ^{18}F-labeled prosthetic group can be favorable, because often no protection groups are required and the labeling occurs under mild conditions. There are three different types for prosthetic group labeling used in combination with folates, yielding three different kinds of bonding (Scheme 2).

A) amide formation

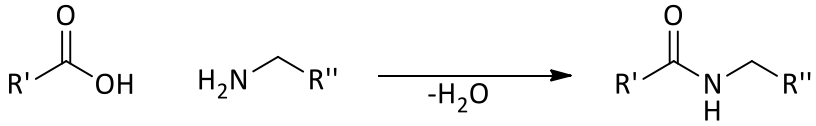

B) copper-catalyzed cycloadditons

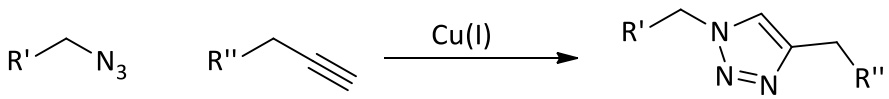

C) oxime-formation

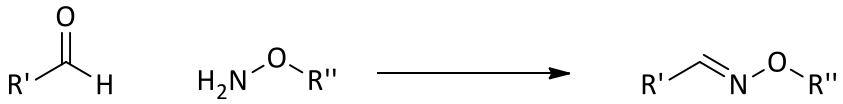

Scheme 2. Common used coupling strategies for the synthesis of radiofolates via prosthetic group labeling.

The last coupling between the folate part and the prosthetic group via oxime-formation seems to be very questionable, because the *in vivo* data show an uptake in the kidneys of 1.49%ID/g only, which was blocked with 50%, indicating that the tracer might degrade *in vivo*.[59]

The formation of amide bonds has been used routinely to protect tracers from degradation. The first ^{18}F-labeled folate of Bettio *et al.* used amide coupling of 4-[^{18}F]fluorobenzylamine ([^{18}F]FBA) and the NHS-activated ester of (native) folic acid for synthesis.[60] The resulting regioisomeric mixture (5% RCY) was not separated though, but the ^{18}F-folate(s) showed good *in vivo* characteristics with a specific tumor uptake of 6%ID/g in tumor bearing mice (human KB-tumors) and was, moreover, the first ^{18}F-folate applied to preclinical PET imaging studies. Further ^{18}F-folates were synthesized in 2006, but evaluated only in 2011 by Al-Jammaz *et al*., who also used the amide bond formation for coupling folic acid to the prosthetic group, showing uptake values of 6%ID/g.[61,62] Therefore, *N*-succinimidyl-4-[^{18}F]fluorobenzoate or 4-[^{18}F]fluorobenzenecarbohydrazide were used as prosthetic groups. One drawback of these ^{18}F-folates was the undefined regiospecificity after labeling and purification, which led to the development of ^{18}F-folates, synthesized via copper(I)-catalyzed cycloaddition (CuAAC) as coupling reaction. This type of reaction seemed to be very promising, since the prosthetic group labeling gave high RCYs as well as the coupling reaction to the folic acid part. Additionally, the CuAAC is likely very fast, robust, high yielding and regiospecific, and therefore particularly suitable for radioactive labeling reactions.

The first ^{18}F-folate synthesized through CuAAC by Ross *et al.* showed the desired features during radiosynthesis, but had some undesired *in vivo* properties. Indeed the tracer showed a highly specific uptake in the FR-rich tissues like KB-tumors (3%ID/g) and kidney (17%ID/g), but also a strong hepatobiliary excretion, impairing the background signal in the abdominal area of the body.[63] The strong hepatobiliary excretion of this ^{18}F-folate was referred to the relatively high lipophilicity of the prosthetic group. Therefore, the *k'*-value (HPLC) was introduced to allow comparison between different radiofolates. The *k'*-value or the capacity factor is determined through the following equation:

$$k' = (t_{retention} - t_{solvent})/t_{solvent} \quad (1)$$

However, the *k'*-value is restricted to the use of the same HPLC column as well as the same solvent system, to get revealing values, whereas the HPLC system used is arbitrary, enabling the prediction of the *in vivo* behavior of novel ^{18}F-folates due to their hepatobiliary excretion rate. To overcome the predominant hepatobiliary excretion due to a high lipophilicity Fischer *et al.* combined the highly efficient ^{18}F-CuAAC for radiosynthesis and the very polar properties of 2-[^{18}F]fluoro-2-deoxy-glucose ([^{18}F]FDG) *in vivo*. Therefore, a 2-[^{18}F]fluoro-2-deoxy-glucopyranosyl azide was ^{18}F-labeled and reacted with the corresponding alkynyl-folate (25% RCY), showing a high specific uptake in tumor bearing mice (human KB-tumors) avoiding hepatobiliary excretion and providing a clear tumor visualization.[64]

Table 4. Overview ^{18}F-labeled folates used for PET

Folate	Labeling chemistry (leaving group)	RCY	Time (EOB)	Tumor uptake	Bile to tumor ratio[a]
[^{18}F]fluorobenzenecarboxyhydrazide folate	amide formation	35%	85 min	~ 6%ID/g	n.d.
[^{18}F]fluorobenzenecarboxy-hydrazide folate	amide formation	~80%	45 min	~ 6%ID/g	n.d.
α/γ-[^{18}F]FBA-folates	amide formation	~5%	135 min	~ 6%ID/g	40.5
^{18}F-click folate	CuAAC	35%	90 min	~ 3%ID/g	213.3
[^{18}F]FDG-click folate	CuAAc	25%	180 min	~ 10%ID/g	1
[^{18}F]FDG folate	oxime formation	80%	(20 min)	~ 3%ID/g	n.d.
[^{18}F]fluoro-PEG folate	amide formation	~30%	(73 min)	-	n.d.
2'-[^{18}F]fluorofolic acid	Sn_{Ar} (-NO_2)	4%	80 min	~ 10%ID/g	1.8
γ-[^{18}F]fluorofolic acid	Sn_2 (-OMs)	~5%	120min	~ 8%ID/g	24
3'-aza-2'-[^{18}F]fluorofolic acid	Sn_{Ar} (-Cl)	~9%	110 min	~ 12%ID/g	0.7

[a] sacrifice time points differ, in respect to the optimal scanning time point.

In contrast to the prosthetic group labeling approach, some efforts have been made to synthesize a direct labeling precursors. By taking a closer look at the structure of folic acid there are two parts qualified for direct ^{18}F-labeling, which is derivatization of the glutamate residue (^{18}F-fluorination at the alkyl-chain)[65] or nucleophilic aromatic

substitution (S_NAr) at the aminobenzoylic part of the pteroic acid. The first reported direct ^{18}F-fluorination at the aminobenzoylic part of the pteroic acid was described by Ross *et al.* using the N^2-(*N,N*-dimethylamino-methylene)-2'-nitrofolic acid di-*tert*-butylester.[66] ^{18}F-Fluorination could be accomplished under harsh labeling conditions, followed by a deprotection step in 4M hydrochloric acid solution. Unfortunately, partial degradation of precursor and product was mainly observed. Therefore, the conditions have been studied and optimized to minimize the degradation and increasing RCY, ending up with an overall RCY of 4%. This derivative showed an excellent *in vivo* behavior and a tumor uptake of 10%ID/g, since it is very similar to native folic acid. To optimize the RCY during the S_NAr with ^{18}F-fluoride, there was a need to activate the aromatic ring for nucleophilic attacks. Therefore, Betzel and coworkers substituted the original aminobenzoylic part with an aminopyridinoylic ring resulting in 9% RCY, almost 12%ID/g in the tumor and additionally low background signals (Figure 3).[67]

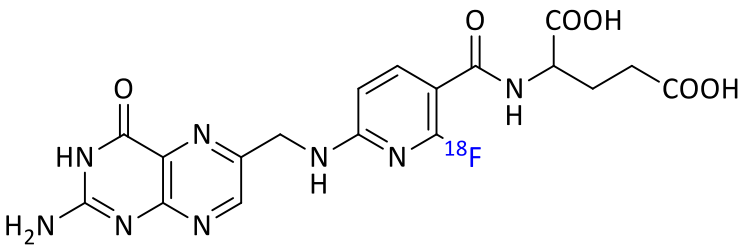

Figure 3. Molecular structure of 3'-Aza-2'-[^{18}F]fluorofolic acid.[67]

This whole group of ^{18}F-labeled folates shows the continuous improvement of both, ^{18}F-labeling strategies and *in vivo* behavior on the road to develop a clinically applicable ^{18}F-labeled folate.

1.6 Endoradiotherapy using Folates

The use of radiofolates for diagnostic purposes is just an expedient, meaning that not only the localization of tumors is the main goal; rather it is to support therapeutic approaches for personalized therapies. One successful folate-based approach is the

theranostic pair Etarfolatide and EC145, where a molecular imaging (SPECT) component is used as screening tool for patient identification and monitoring towards a folate-based chemotherapy. As already described, there are quite a number of radiofolates (e.g. SPECT, PET) for imaging FR-positive tumors, although a radiofolate for PET is not yet available for humans. As located a FR-positive tumor, therapeutic strategies can be planned using either folate-based chemotherapeutics, like EC145 (vincaalcaloide-folate), or therapeutic radioisotopes, like lutetium-177, yttrium-90 as β^--emitters or bismuth-213 and actinium-225 as α-emitting isotopes attached to FR-targeting structures. This approach has already been investigated preclinically using ^{177}Lu-labeled DOTA-folate conjugate for treatment of small tumors and metastases.[47,68] The initial animal studies showed promising results and uptake values of 7.5%ID/g 4 h p.i. The ^{177}Lu-DOTA folate showed also a favorable biodistribution since it was rapidly cleared from the blood stream and had very low unspecific binding in non-targeted tissues. However, an expected kidney uptake (57.22%ID/g) was observed, leading to serious kidney damage and aggravating the evaluation process. Generally, the use of particle emitting isotopes seemed to be very potent and promising, but the high accumulation of the tracer in the kidneys hinders the application in further trials.

Boron neutron capture therapy (BNCT)

Boron neutron capture therapy is a non-invasive method for treatment of melanoma[69], head-neck cancer[70] and adenocarcinoma[71]. The treatment is based on the nuclear reaction of boron-10 with thermal neutrons and first used at the Brookhaven National Laboratory (BNL) in the early 1950s to treat glioblastoma multi-form.[72] Boron-10 has a high cross-section for thermal neutrons (3838 barns)[73] making the neutron capture very effective, forming an instable compound nucleus, which decays with 96% under emission of an α-particle (1.47 MeV), a lithium-7-nucleus (0.84 MeV) and one prompt γ-ray (0.48 MeV) and can be seen in Figure 4. In 4%, no γ-ray is emitted. Due to the short range of these high-energy particles, they possess a very high linear energy transfer (LET), meaning that most of the energy is stored in the volume around the original ^{10}B-atom and

frequently, does not exceed one cell diameter when applied *in vivo*. This very high-energy deposit of the resulting particles has a high radiobiological effect (RBE), e.g. irreversible damage of the cell, triggering cell-death.[74] However, one drawback of this therapeutic approach is a high concentration of a ^{10}B is needed in tumor cells and in a high contrast to normal cells. Consequently, a concentration of around 20 µg/g weight or ~10^9 atoms/cell is a commonly accepted rule of thumb, although these values only derive from one small animal study.[75] A variety of boron-10 containing pharmaceuticals has been synthesized, but only two entered clinical trials and were successfully approved by several authorities (FDA, EMA (formerly EMEA), CFDA, MAH etc.) for the use in BNCT, namely boron phenylalanine (BPA)[76] and sodium mercaptoundecahydrododecaborate (BSH)[77,78]. Additionally, a ^{18}F-labeled BPA was synthesized allowing visualization and treatment by the use of one and the same pharmaceutical facilitated via spiking of BPA with ^{18}F-BPA.[74]

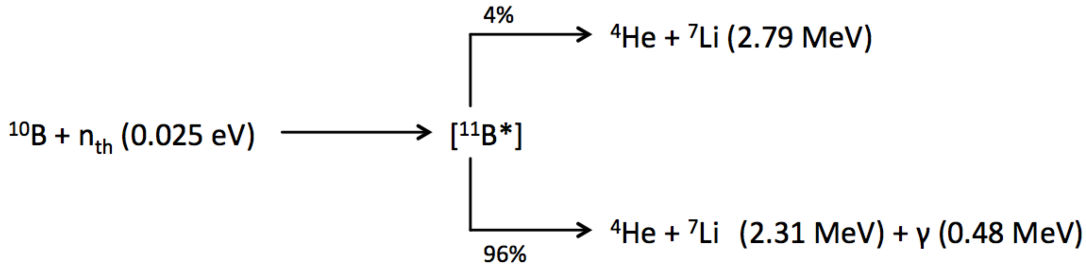

Figure 4. Nuclear reaction during BNCT. ^{10}B reacts with a thermal neutron and decays to highly charged and energetic particles.

Over the past decade, there was effort put in the development of new low- and high-molecular weight boron delivery compounds to increase the ^{10}B-concentration in tumor tissues and enhance tumor-to-healthy tissue contrast (Table 5).

Table 5. Low- and high-molecular weight boron delivery compounds under evaluation.[79]

Boronated unnatural amino acids[77–79]	Carboranyl nucleosides[80,81]
Dodecaborate cluster lipids and cholesterol derivatives[85]	Boronated porphyrins[86–88]
Boron containing immunoliposomes and liposomes[89–91]	Boronated EGF and anti-EGFR and VEGFR MoAbs[92–97]
Boronated DNA intercaltors[98]	Boron-containing nanoparticles[99,100]
Transferrin-polyethylene glycol (TF-PEG) liposomes[101,102]	Carboranyl porphyrazines[103]
Dodecahydro-closo-dodecaborate clusters[85]	Boronated cyclic peptides[104]
	Boron nitride nanotubes[105]

The aim of these new boron-delivery agents is to accumulate in the tumor tissues without a washout, which BPA shows to a certain extend. In contrast, a fast blood clearance is favored and ideally an accumulation in only the tumor tissue to reduce the damage to healthy tissues. This is the main drawback of BPA and BSH that they are not metabolically trapped in the cell and additionally, none shows an effective active targeting. BPA is transported mainly via the LAT-1 (*large neutral amino acid transporter system*), which is bidirectional and thus, BPA also shows a quite rapid efflux. On the other hand, BSH has no active targeting and accumulates via the enhanced permeability and retention (EPR) effect (for details about EPR effect please see next section) intercellular in tumor tissue. One advantage of BSH is the high ^{10}B-loading (B_{12}).

Similarly, some above listed ^{10}B-delivery systems are macromolecular, which is from peculiar charm, that one macromolecular system can transport large amounts of boron-10 to achieve the ^{10}B-concentrations necessary for successful treatments. Many efforts were put in the development of liposomal carrier systems with a high capacity for boron-10 loading, since the most used carboranyl compounds are very lipophilic.[106,107] Accumulation of these macromolecular ^{10}B-delivery systems is again based on the EPR effect, which is defined and explained in the next section, and depicts a passive targeting effect. To enhance tumor accumulation, there was another approach to attach folic acid as targeting vector, showing that it was possible to deliver up to 1584 μg boron-10 per

10^9 cells *in vitro*, whereas only 20 μg/gram tumor or per 10^9 cells is required to maintain the lethal effect of BNCT.[108]

1.7 Macromolecular Carriers

The therapeutic index of (chemo)therapeutic drugs is often narrow and is defined as the ratio between the toxic dose and the therapeutic dose of a drug. Thus high concentrations of the drug have to be administered to reach the steady state that the drug evolves the full effect. There is a demand for novel and innovative drug delivery systems addressing treatment of various diseases, especially cancer. The field of nanomedicine accomplishes many requirements for a successful delivery of various cargos to target sites for treatment of pathophysiological disease.[109] The term nanomedicine envelopes among others liposomes, nanoparticles, polymer therapeutics and block copolymer micelles, which are relevant in clinics (Figure 5).[109]

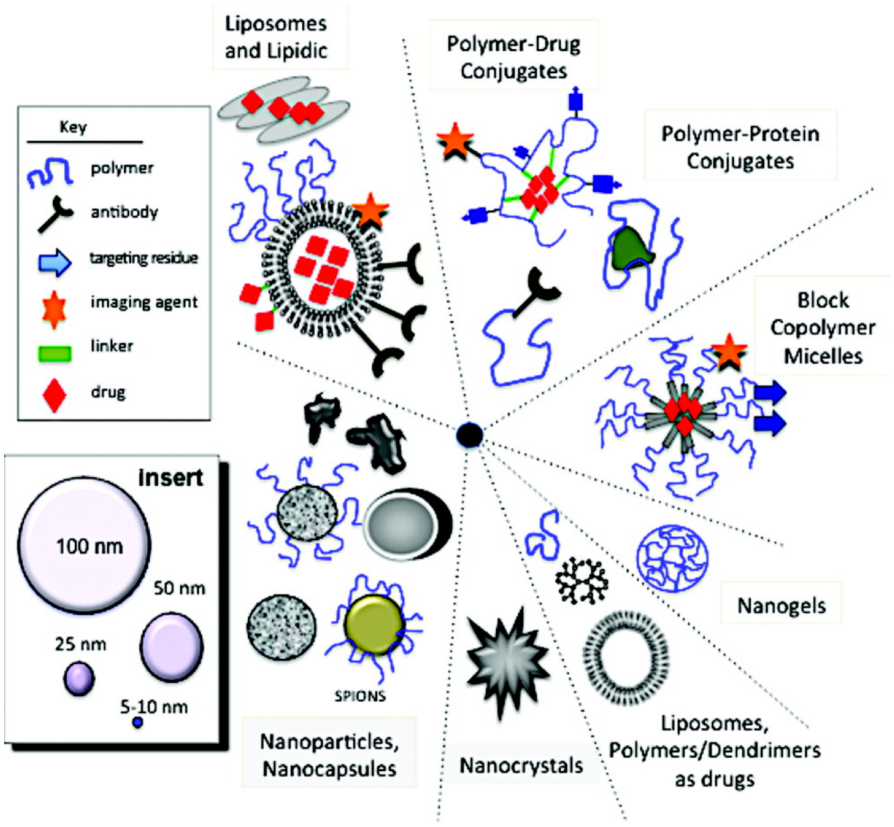

Figure 5. Schematic overview over the main classes of nanomedicines in clinical trial and routine clinical use.[109]

The aim of nanomedicines to deliver (chemo)therapeutics selectively to target sites has been shown several times for various carrier systems.[109,110] Since poly-*N*-(2-hydroxypropyl)methacryamide (pHPMA) is water-soluble, non-toxic and non-immunogenic, it seems to be a promising candidate for drug-delivery *in vivo*, depicting the carrier systems of choice in this work. The use of those systems has been proposed the first time by Ringsdorf *et al.* in the 1970s.[111] The idea was to use a polymeric backbone with a solubilizer, a cleavable drug and a targeting moiety attached to the side-chains. pHPMA was initially used in the 1970s as potential plasma expander for human use.[112] Therefore, the *in vivo* behavior was studied carefully leading to the first synthetic polymer-based drug conjugate PK1 through coupling doxorubicin to pHPMA.[113] The conjugate showed the desired reduced toxicity compared to the free drug and was the dawn of HPMA conjugates used in cancer therapy.[114]

To introduce polymeric systems to health science it is crucial to use polymeric structures as well defined as possible. To obtain these polymeric systems with a defined size and narrow size distribution, living radical polymerization techniques are the methods of choice. Reversible Addition Fragmentation Chain Transfer (RAFT)[115,116] polymerization in combination with a reactive ester approach[117,118] accomplishes many of the above-mentioned established criteria. An expression for determination of the molecular weight distribution is the polydispersity index (PDI), which is determined as followed:

$$PDI = \frac{M_w}{M_n} \quad , \qquad (2)$$

where M_w is the weight average molecular weight and M_n is the number average molecular weight. [119]

The here used pHPMA is based on the RAFT technique in combination with the reactive ester approach, meaning that a precursor polymer is synthesized consisting of reactive ester monomers. This precursor polymer can be reacted with primary amines to form multifunctional pHPMA polymers.[120] While using 2-hydroxypropyl amine it is possible to synthesized pHPMA in a subsequent polymeranalogous reaction or in order to

incorporate targeting vectors, drugs or/and labeling probes it is possible to add these compounds if they are carrying a primary amine. [121–123]

Those modifications at the polymer backbone can lead to amphiphilic polymers, when two different compounds are introduced during the polymeranalogous reaction. If so, they can be characterized by their composition of hydrophilic and hydrophobic segments and their tendency for spontaneous self-assembly in aqueous solution, leading to aggregate formation. The assembly takes place in order to reduce the hydrodynamic radii (R_h), because of the congregation of hydrophobic segments in the copolymer, whereas it does not matter if copolymers, with a distinct separation of hydrophobic/hydrophilic segments, or statistical copolymers with random areas of hydrophobic groups, are used (Figure 6).

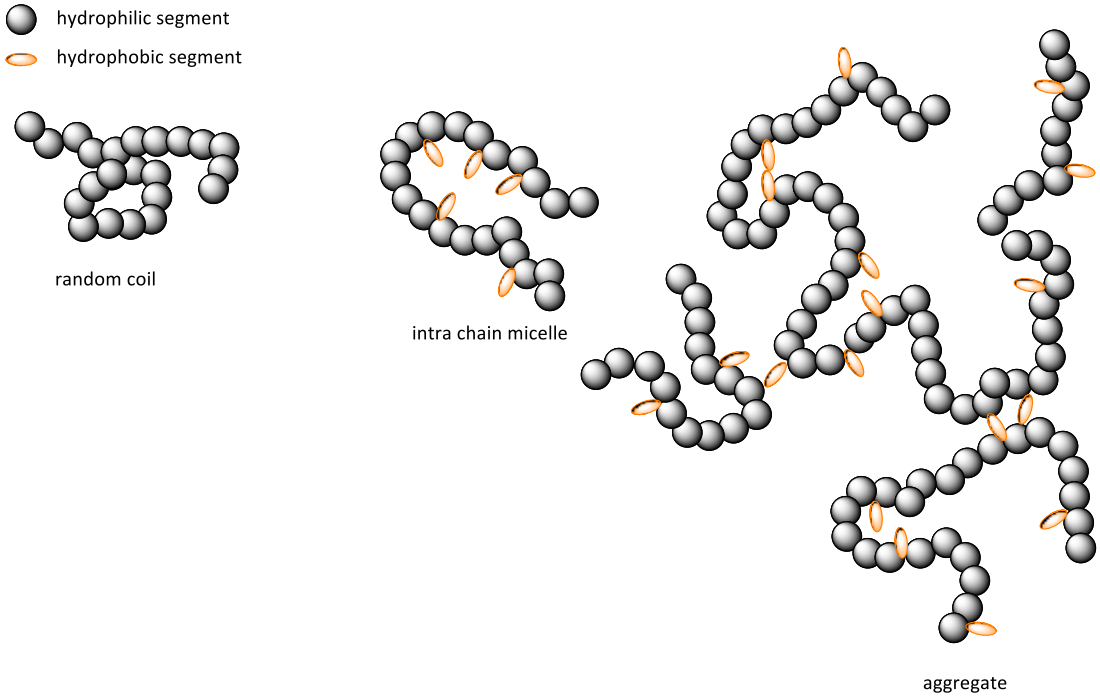

Figure 6. Overview of different polymer assemblies in aqueous solution.

The approach to synthesize pHPMA via RAFT in combination with the reactive ester approach was used to obtain narrow distributed pHPMA polymers having about 3% tyramine incorportated, enabling the radiolabeling with 2-[^{18}F]fluoroethyl tosylated as

prosthetic group to investigate the biodistribution of these poylmers *in vivo* (rat model).[124] In addition, the biodistribution of different size and architectures have been evaluated, like random and block copolymers consisting of laurylmethacrylamide (LMA) and HPMA, as well as their behavior in different tumor models.[125]

The above mentioned drug delivery systems carrying no targeting moieties use the enhanced permeability and retention (EPR) effect alone for accumulation at target sites, which proceeds on the assumption that during tumor growth the lymphatic drainage is flawed and the blood vessels are leaky (fenestration) due to the fast angiogenesis (Figure 7). This reflects the concept of passive targeting, and is mostly used by liposomal, polymeric and micellar systems.[126,127]

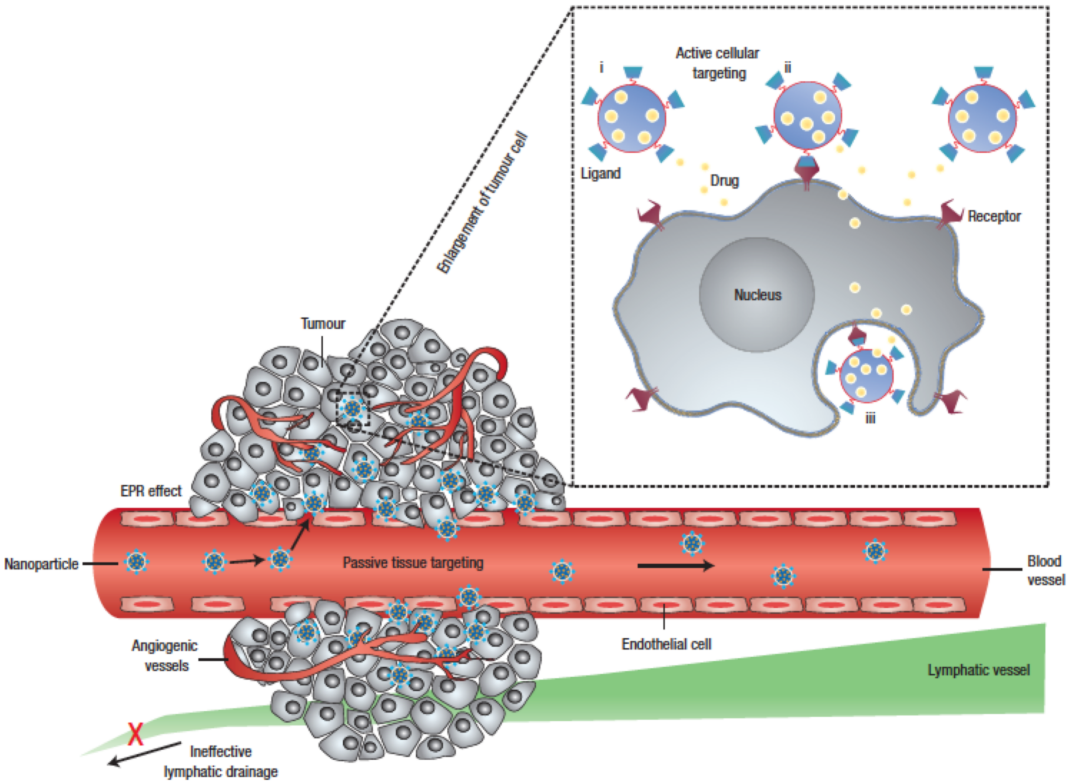

Figure 7. Vascularization of normal and tumor tissue. Tumor tissue shows hyperpermeable vascularization (fenestration) allowing extravasation and accumulation of macromolecules. Active targeting utilizes surface receptors to increase cellular uptake of carrier systems.[128]

Active targeting, on the other hand, utilizes targeting structures like, receptor ligands, antibodies or peptides, which bind to recognition sites on/in target tissue and enhance tumor uptake, the retention time or can provide cell internalization.[129,130] Besides the relatively high-molecular weight targeting vectors, it has been shown that folic acid (FA) bound to pHPMA increases uptake of the FA-pHPMA conjugates into tumor cells *in vitro*.[131] The conjugation of FA to other macromolecular carrier systems, like liposomes, has already been demonstrated, and showing promising results, but also the significance of a selection procedure of patients to guarantee best response rates during treatment has to be considered.[110]

The above-mentioned efforts and insights illustrate how the combination of different techniques and basic approaches bear an opportunity to improve patient care and ideally patient cure. The aim of this present work is to continue and improve the encouraging results for the treatment of malignant disease.

1.8 References

(1) Plattner, H.; Hentschel, J. *Zellbiologie*; 2nd Ed.; Thieme, 1977.

(2) Koolman, J.; Röhm, K.-H. *Taschenatlas der Biochemie*; 3rd Ed.; Thieme, 1994.

(3) Schirch, V.; Strong, W. B. *Arch. Biochem. Biophys.* **1989**, *269*, 371–380.

(4) Damaraju, V. L.; Cass, C. E.; Sawyer, M. B. In *Folic Acid and Folates*; Litwack, G., Ed.; Academic Press, 2008; Vol. 79, pp. 185–202.

(5) Rodríguez-Enríquez, S.; Moreno-Sánchez, R. *Arch. Med. Res.* **1998**, *29*, 1–12.

(6) Stollman, T. H.; Ruers, T. J. M.; Oyen, W. J. G.; Boerman, O. C. *Methods* **2009**, *48*, 188–92.

(7) Müller, C. *Curr. Pharm. Des.* **2012**, *18*, 1058–1083.

(8) Reddy, S.; Robinson, M. K. *Semin. Nucl. Med.* **2010**, *40*, 182–9.

(9) Vogel, R. O.; Janssen, R. J. R. J.; Brand, M. A. M. Van Den; Dieteren, C. E. J.; Verkaart, S.; Koopman, W. J. H.; Willems, P. H. G. M.; Pluk, W.; Heuvel, L. P. W. J. Van Den; Smeitink, J. A. M.; Nijtmans, L. G. J. *Genes Dev.* **2007**, *21*, 615–624.

(10) Feige, J. N.; Gelman, L.; Tudor, C.; Engelborghs, Y.; Wahli, W.; Desvergne, B. *J. Biol. Chem.* **2005**, *280*, 17880–90.

(11) Mankoff, D. A. *J. Nucl. Med.* **2007**, *48*, 18N, 21N.

(12) Müller, C.; Schibli, R. *J. Nucl. Med.* **2011**, *52*, 1–4.

(13) Phelps, M. E. *PET: Molecular Imaging and its Biological Applications*; Springer, 2004.

(14) Herth, M. M. Synthese und 18F-Markierung von Altanserin und MDL 100907-Derivaten für den 5-HT2A-Rezeptor im serotonergen System, 2006, p. 4.

(15) Green, T. Folic acid one of several discoveries that made Esmond Snell world-renowned http://www.utexas.edu/opa/blogs/research/2013/01/17/folic-acid-one-of-several-discoveries-that-made-esmond-snell-world-renowned.

(16) Locksmith, G. J.; Duff, P. *Obstet. Gynecol.* **1998**, *91*, 1027–1034.

(17) Fox, J. T.; Stover, P. J. In *Folic Acid and Folates*; Litwack, G., Ed.; Academic Press, 2008; Vol. 79, pp. 1–44.

(18) Gerhardt, G. T.; Barton, P. *Curr. Opin. Lipidol.* **1999**, *10*, 417–428.

(19) Ueland, P. M.; Refsum, H.; Beresford, S. A.; Vollset, S. E. *Am. J. Clin. Nutr.* **2000**, *72*, 324–332.

(20) Ames, B. N. *J. Nucleic Acids* **2010**, *2010*.

(21) Ames, B. N. *Proc. Natl. Acad. Sci. U. S. A.* **2006**, *103*, 17589–17594.

(22) Choi, S. W.; Mason, J. B. *J. Nutr.* **2000**, *130*, 129–132.

(23) Kim, Y. I.; Pogribny, I. P.; Basnakian, A. G.; Miller, J. W.; Selhub, J.; James, S. J.; Mason, J. B. *Am. J. Clin. Nutr.* **1997**, *65*, 46–52.

(24) Kim, Y. I. *Nutr. Rev.* **1999**, *57*, 314–321.

(25) Johns, D. G.; Sperti, S.; Burgen, A. S. V. *Le J. L'Association Med. Can.* **1961**, *84*, 77–79.

(26) Leamon, C. P.; Low, P. S. *Drug Discovery Today* **2001**, *6*, 44–51.

(27) Sirotnak, F. M.; Tolner, B.; Whetstine, J. R.; Gifford, A. J.; Witt, T.; Liu, X. Y.; Flatley, R. M.; Norris, M.; Haber, M.; Taub, J. W.; Ravindranath, Y.; Matherly, L. H. *Clin. Cancer Res.* **1999**, *7*, 3416–22.

(28) Whetstine, J. R.; Flatley, R. M.; Matherly, L. H. *Biochem J.* **2002**, *640*, 629–640.

(29) Linkers, P. E. G.; Wang, L.; Shi, J.; Kim, Y.; Zhai, S.; Jia, B.; Zhao, H.; Liu, Z.; Wang, F.; Chen, X.; Liu, S. *Mol. Pharmaceutics* **2009**, *6*, 231–245.

(30) Zhao, R.; Goldman, I. D. *Cancer Metastasis Rev.* **2007**, *26*, 129–139.

(31) Antony, A. C. *Annu. Rev. Nutr.* **1996**, *16*, 501–521.

(32) Antony, A. C. *Blood* **1992**, *79*, 2807–2820.

(33) Parker, N.; Turk, M. J.; Westrick, E.; Lewis, J. D.; Low, P. S.; Leamon, C. P. *Anal. Biochem.* **2005**, *338*, 284–93.

(34) Weitman, S. D.; Lark, R. H.; Coney, L. R.; Fort, D. W.; Frasca, V.; Zurawski, V. R.; Kamen, B. A. *Cancer Res.* **1992**, *52*, 3396–3401.

(35) Weitman, S. D.; Weinberg, A. G.; Coney, L. R.; Zurawski, V. R.; Jennings, D. S.; Kamen, B. A. *Cancer Res.* **1992**, *52*, 6708–6711.

(36) Gent, Y. Y.; Weijers, K.; Molthoff, C. F.; Windhorst, A. D.; Huisman, M. C.; Smith, D. E.; Kularatne, S. a; Jansen, G.; Low, P. S.; Lammertsma, A. a; van der Laken, C. J. *Arthritis Res. Ther.* **2013**, *15*, R37.

(37) Nakashima-Matsushita, N.; Homma, T.; Yu, S.; Matsuda, T.; Sunahara, N.; Nakamura, T.; Tsukano, M.; Ratnam, M.; Matsuyama, T. *Arthritis Rheum.* **1999**, *42*, 1609–16.

(38) Van der Heijden, J. W.; Oerlemans, R.; Dijkmans, B. a C.; Qi, H.; van der Laken, C. J.; Lems, W. F.; Jackman, A. L.; Kraan, M. C.; Tak, P. P.; Ratnam, M.; Jansen, G. *Arthritis Rheum.* **2009**, *60*, 12–21.

(39) Paulos, C. M.; Turk, M. J.; Breur, G. J.; Low, P. S. *Adv. Drug Deliv. Rev.* **2004**, *56*, 1205–17.

(40) Kennedy, M. D.; Jallad, K. N.; Thomson, D. H.; Ben-Amotz, D.; Low, P. S. *J. Biomed. Opt.* **2003**, *8*, 636–641.

(41) Konda, S. D.; Aref, M.; Wang, S.; Brechbiel, M.; Wiener, E. C. *MAGMA (N. Y.)* **2001**, *12*, 104–113.

(42) Moon, W. K.; Lin, Y.; O'Loughlin, T.; Tang, Y.; Kim, D.-E.; Weissleder, R.; Tung, C.-H. *Bioconjugate Chem.* **2003**, *14*, 539–545.

(43) Tung, C.-H.; Gerszten, R. E.; Jaffer, F. A.; Weissleder, R. *Chembiochem* **2002**, *3*, 207–211.

(44) Walton, L. *Med Lab Sci* **1981**, *38*, 187–95.

(45) Wang, S.; Lee, R. J.; Mathias, C. J.; Green, M. a; Low, P. S. *Bioconjugate Chem.* **1996**, *7*, 56–62.

(46) Mathias, C. J.; Wang, S.; Lee, R. J.; Waters, D. J.; Low, P. S.; Green, M. A. *J. Nucl. Med.* **1996**, *37*, 1003–1008.

(47) Mindt, T. L.; Müller, C.; Stuker, F.; Salazar, J.-F.; Hohn, A.; Mueggler, T.; Rudin, M.; Schibli, R. *Bioconjugate Chem.* **2009**, *20*, 1940–9.

(48) Fani, M.; Wang, X.; Nicolas, G.; Medina, C.; Raynal, I.; Port, M.; Maecke, H. R. *Eur. J. Nucl. Med. Mol. Imaging* **2011**, *38*, 108–19.

(49) Müller, C.; Vlahov, I. R.; Santhapuram, H. K. R.; Leamon, C. P.; Schibli, R. *Nucl. Med. Biol.* **2011**, *38*, 715–23.

(50) Mathias, C. J.; Wang, S.; Waters, D. J.; Turek, J. J.; Low, P. S.; Green, M. A. *J. Nucl. Med.* **1998**, *39*, 1579–1585.

(51) Siegel, B. A.; Dehdashti, F.; Mutch, D. G.; Podoloff, D. A.; Wendt, R.; Sutton, G. P.; Burt, R. W.; Ellis, P. R.; Mathias, C. J.; Green, M. A.; Gershenson, D. M. *J. Nucl. Med.* **2003**, *44*, 700–707.

(52) Ilgan, S.; Yang, D. J.; Higuchi, T.; Zareneyrizi, F.; Bayhan, H.; Yu, D.; Kim, E. E.; Podoloff, D. A. *Cancer Biother. Radiopharm.* **1998**, *13*, 427–435.

(53) Guo, W.; Hinkle, G. H.; Lee, R. J. *J. Nucl. Med.* **1999**, *40*, 1563–1569.

(54) Leamon, C. P.; Parker, M. A.; Vlahov, I. R.; Xu, L.-C.; Reddy, J. A.; Vetzel, M.; Douglas, N. *Bioconjugate Chem.* **2002**, *13*, 1200–1210.

(55) Fisher, R. E.; Siegel, B. A.; Edell, S. L.; Oyesiku, N. M.; Morgenstern, D. E.; Messmann, R. a; Amato, R. J. *J. Nucl. Med.* **2008**, *49*, 899–906.

(56) Low, P. S.; Kularatne, S. A. *Curr. Opin. Chem. Biol.* **2009**, *13*, 256–62.

(57) Schibli, R.; La Bella, R.; Alberto, R.; Garcia-Garayoa, E.; Ortner, K.; Abram, U.; Schubiger, P. a *Bioconjugate Chem.* **2000**, *11*, 345–51.

(58) Sparr, C.; Michel, U.; Marti R. E. *Synthesis* **2009**, 787–792.

(59) Al Jammaz, I.; Al-Otaibi, B.; Amer, S.; Al-Hokbany, N.; Okarvi, S. *Nucl. Med. Biol.* **2012**.

(60) Bettio, A.; Honer, M.; Müller, C.; Brühlmeier, M.; Müller, U.; Schibli, R.; Groehn, V.; Schubiger, A. P.; Ametamey, S. M. *J. Nucl. Med.* **2006**, *47*, 1153–60.

(61) Al Jammaz, I.; Al-Otaibi, B.; Okarvi, S.; Amartey, J. *J. Labelled Compd. Radiopharm.* **2006**, *49*, 125–137.

(62) Al Jammaz, I.; Al-Otaibi, B.; Amer, S.; Okarvi, S. M. *Nucl. Med. Biol.* **2011**, *38*, 1019–28.

(63) Ross, T. L.; Honer, M.; Lam, P. Y. H.; Mindt, T. L.; Groehn, V.; Schibli, R.; Schubiger, P. A.; Ametamey, S. M. *Bioconjugate Chem.* **2008**, *19*, 2462–70.

(64) Fischer, C. R.; Müller, C.; Reber, J.; Müller, A.; Krämer, S. D.; Ametamey, S. M.; Schibli, R. *Bioconjugate Chem.* **2012**, *23*, 805–13.

(65) Schibli, R.; Moser, R.; Müller, C. M.; Ametamey, S. M.; Ross, T. L.; Groehn, V. WO2010040854 A1, 2010.

(66) Ross, T. L.; Honer, M.; Müller, C.; Groehn, V.; Schibli, R.; Ametamey, S. M. *J. Nucl. Med.* **2010**, *51*, 1756–62.

(67) Betzel, T.; Mu, C.; Groehn, V.; Mu, A.; Fischer, C. R.; Krämer S. D.; Schibli, R.; Ametamey, S. M. *Bioconjugate Chem.* **2013**, *24*, 205–214.

(68) Müller, C.; Mindt, T. L.; de Jong, M.; Schibli, R. *Eur. J. Nucl. Med. Mol. Imaging* **2009**, *36*, 938–46.

(69) Mishima, Y.; Ichihashi, M.; Hatta, S.; Honda, C.; Yamamura, K.; Nakagawa, T. *Pigment Cell Res. Spons. by Eur. Soc. Pigment Cell Res. Int. Pigment Cell Soc.* **1989**, *2*, 226–234.

(70) Kato, I.; Ono, K.; Sakurai, Y.; Ohmae, M. *Appl. Rad. Isotop.* **2004**, *61*, 1069–1073.

(71) Nano, R.; Barni, S.; Chiari, P.; Pinelli, T.; Fossati, F.; Altieri, S.; Zonta, C.; Prati, U.; Roveda, L.; Zonta, A. *Oncol. Rep.* **2004**, *11*, 149–153.

(72) Farr, L. E.; Sweet, W. H.; Robertson, J. S.; Foster, C. G.; Locksley, H. B.; Sutherland, D. L.; Mendelsohn, M. L.; Stickley, E. E. *Am. J. Roentgenol., Radium Ther. Nucl. Med.* **1954**, *71*, 279–293.

(73) Beddoe, A. H. *Br. J. Radiol.* **1997**, *70*, 665–7.

(74) Barth, R. F.; Coderre, J. a; Vicente, M. G. H.; Blue, T. E. *Clin. Cancer Res.* **2005**, *11*, 3987–4002.

(75) Barth, R. F.; Soloway, A. H.; Fairchild, R. G.; Brugger, R. M. *Cancer* **1992**, *70*, 2995–3007.

(76) Aihara, T.; Hiratsuka, J.; Morita, N.; Uno, M.; Sakurai, Y.; Maruhashi, A.; Ono, K.; Harada, T. *Head & Neck* **2006**, *28*, 850–855.

(77) Yokoyama, K.; Miyatake, S.-I.; Kajimoto, Y.; Kawabata, S.; Doi, A.; Yoshida, T.; Asano, T.; Kirihata, M.; Ono, K.; Kuroiwa, T. *J. Neuro-Oncol.* **2006**, *78*, 227–232.

(78) Takagaki, M.; Oda, Y.; Miyatake, S.; Kikuchi, H.; Kobayashi, T.; Sakurai, Y.; Osawa, M.; Mori, K.; Ono, K. *Boron neutron capture therapy: preliminary study of BNCT with sodium borocaptate ($Na_2B_{12}H_{11}SH$) on glioblastoma.*; 1997; Vol. 35, pp. 177–185.

(79) Barth, R.; H Vicente, M. G.; Harling, O.; Kiger, W. S.; Riley, K.; Binns, P.; Wagner, F.; Suzuki, M.; Aihara, T.; Kato, I.; Kawabata, S. *Radiat. Oncol.* **2012**, *7*, 146.

(80) Semioshkin, A.; Nizhnik, E.; Godovikov, I. V. *J. Organomet. Chem.* **2007**, *692*, 4020–4028.

(81) Kabalka, G. W.; Wu, Z.; Yao, M.-L. *Appl. Organomet. Chem.* **2008**, *22*, 516–522.

(82) Kabalka, G. W.; Yao, M. L.; Marepally, S. R.; Chandra, S. *Appl. Radiat. Isot.* **2009**, *67*, S374–S379.

(83) Al-Madhoun, A. S.; Johnsamuel, J.; Barth, R. F.; Tjarks, W.; Eriksson, S. *Cancer Res.* **2004**, *64*, 6280–6286.

(84) Barth, R. F.; Yang, W.; Wu, G.; Swindall, M.; Byun, Y.; Narayanasamy, S.; Tjarks, W.; Tordoff, K.; Moeschberger, M. L.; Eriksson, S. *Proc. Natl. Acad. Sci. U. S. A.* **2008**, *105*, 17493–17497.

(85) Bregadze, V. I.; Sivaev, I. B.; Lobanova, I. A.; Titeev, R. A.; Brittal, D. I.; Grin, M. A.; Mironov, A. F. *Appl. Radiat. Isot.* **2009**, *67*, S101–S104.

(86) Renner, M. W.; Miura, M.; Easson, M. W.; Vicente, M. G. *Anticancer Agents Med. Chem.* **2006**, *6*, 145–157.

(87) Ol'shevskaya, V.; Zaytsev, A.; Savchenko, A. *Bull. Korean Chem. Soc.* **2007**, *28*, 1910–1916.

(88) Kahl, S.; Koo, M. *Prog. Neutron Capture Ther.* **1992**, 223–226.

(89) Nakamura, H. *Boron Sci. New Technol. Appl.* **2012**, 165–179.

(90) Altieri, S.; Balzi, M.; Bortolussi, S.; Bruschi, P.; Ciani, L.; Clerici, A. M.; Faraoni, P.; Ferrari, C.; Gadan, M. A.; Panza, L. *J. Med. Chem.* **2009**, *52*, 7829–7835.

(91) Feakes, D. A. *Boron Sci. New Technol. Appl. Vol. 12* **2011**, 277–292.

(92) Capala, J.; Barth, R. F.; Bendayan, M.; Lauzon, M.; Adams, D. M.; Soloway, A. H.; Fenstermaker, R. A.; Carlsson, J. *Bioconjugate Chem.* **1996**, *7*, 7–15.

(93) Wu, G.; Yang, W.; Barth, R. F.; Kawabata, S.; Swindall, M.; Bandyopadhyaya, A. K.; Tjarks, W.; Khorsandi, B.; Blue, T. E.; Ferketich, A. K. *Clin. Cancer Res.* **2007**, *13*, 1260–1268.

(94) Yang, W.; Wu, G.; Barth, R. F.; Swindall, M. R.; Bandyopadhyaya, A. K.; Tjarks, W.; Tordoff, K.; Moeschberger, M.; Sferra, T. J.; Binns, P. J. *Clin. Cancer Res.* **2008**, *14*, 883–891.

(95) Backer, M. V; Gaynutdinov, T. I.; Patel, V.; Bandyopadhyaya, A. K.; Thirumamagal, B. T.; Tjarks, W.; Barth, R. F.; Claffey, K.; Backer, J. M. *Mol. Cancer Ther.* **2005**, *4*, 1423–1429.

(96) Yang, W.; Barth, R. F.; Wu, G.; Kawabata, S.; Sferra, T. J.; Bandyopadhyaya, A. K.; Tjarks, W.; Ferketich, A. K.; Moeschberger, M. L.; Binns, P. J. *Clin. Cancer Res.* **2006**, *12*, 3792–3802.

(97) Yang, W.; Barth, R. F.; Wu, G.; Huo, T.; Tjarks, W.; Ciesielski, M.; Fenstermaker, R. A.; Ross, B. D.; Wikstrand, C. J.; Riley, K. J.; Binns, P. J. *J. Neuro-Oncol.* **2009**, *95*, 355–365.

(98) Crossley, E. L.; Ziolkowski, E. J.; Coderre, J. A.; Rendina, L. M. *Mini-Rev. Med. Chem.* **2007**, *7*, 303–313.

(99) Zhu, Y.; Yan, K.; Maguire, J. *Curr. Chem. Biol.* **2007**, *1*, 141–149.

(100) Yinghuai, Z.; Cheng Yan, K.; Maguire, J. A. *Boron Sci. New Technol. Appl. Vol. 1* **2007**, 147–163.

(101) Doi, A.; Kawabata, S.; Iida, K.; Yokoyama, K.; Kajimoto, Y.; Kuroiwa, T.; Shirakawa, T.; Kirihata, M.; Kasaoka, S.; Maruyama, K. *J. Neuro-Oncol.* **2008**, *87*, 287–294.

(102) Ito, Y.; Kimura, Y.; Shimahara, T.; Ariyoshi, Y.; Shimahara, M.; Miyatake, S.; Kawabata, S.; Kasaoka, S.; Ono, K. *Appl. Radiat. Isot.* **2009**, *67*, S109–S110.

(103) Pietrangeli, D.; Ricciardi, G. *Appl. Radiat. Isot.* **2009**, *67*, S97–S100.

(104) Mier, W.; Gabel, D.; Haberkorn, U. *Z. Anorg. Allg. Chem.* **2004**, *630*, 1258–1262.

(105) Menichetti, L.; De Marchi, D.; Calucci, L.; Ciofani, G.; Menciassi, A.; Forte, C. *Appl. Radiat. Isot.* **2011**, *69*, 1725–1727.

(106) Hawthorne, M. F.; Shelly, K. *Joural of Neuro-Oncol.* **1997**, *33*, 53–58.

(107) Li, T.; Hamdi, J.; Hawthorne, M. F. *Bioconjugate Chem* **2006**, *17*, 15–20.

(108) Pan, X. Q.; Wang, H.; Shukla, S.; Sekido, M.; Adams, D. M.; Tjarks, W.; Barth, R. F.; Lee, R. J. *Bioconjugate Chem.* **2002**, *13*, 435–442.

(109) Duncan, R.; Gaspar, R. *Mol. Pharm.* **2011**, *8*, 2101–41.

(110) Lammers, T.; Kiessling, F.; Hennink, W. E.; Storm, G. *J. Controlled Release* **2012**, *161*, 175–87.

(111) Ringsdorf, H. *J. Polym. Sci. Poym. Symp* **1975**, *51*, 135–153.

(112) Sprincl, L.; Exner, J.; Kopecek, J. *J. Biomed. Mater. Res.* **1976**, *10*, 953–963.

(113) Vasey, P. A.; Kaye, S. B.; Morrison, R.; Conjugates, A. D.; Twelves, C.; Wilson, P.; Duncan, R.; Thomson, A. H.; Murray, L. S.; Hilditch, T. E.; Murray, T.; Burtles, S.; Fraier, D.; Frigerio, E. *Clin. Cancer Res.* **1999,** *5*, 83–94.

(114) Duncan, R.; Vicent, M. J. *Adv. Drug Deliv. Rev.* **2010**, *62*, 272–82.

(115) Scales, C. W.; Vasilieva, Y. A.; Convertine, A. J.; Lowe, A. B.; McCormick, C. L. *Biomacromolecules* **2005**, *6*, 1846–1850.

(116) Chytil, P.; Etrych, T.; Kříž, J.; Subr, V.; Ulbrich, K. *Eur. J. Pharm. Sci.* **2010**, *41*, 473–482.

(117) Barz, M.; Luxenhofer, R.; Zentel, R.; Kabanov, A. V *Biomaterials* **2009**, *30*, 5682–90.

(118) Barz, M.; Tarantola, M.; Fischer, K.; Schmidt, M.; Luxenhofer, R.; Janshoff, a; Theato, P.; Zentel, R. *Biomacromolecules* **2008**, *9*, 3114–8.

(119) Stepto, R. F. T. *Pure Appl. Chem.* **2009**, *81*, 351–353.

(120) Eberhardt, M.; Mruk, R.; Zentel, R.; Theato, P. *Eur. Polym. J.* **2005**, *41*, 1569–1575.

(121) Barz, M.; Luxenhofer, R.; Zentel, R.; Kabanov, A. V *Biomaterials* **2009**, *30*, 5682–90.

(122) Barz, M.; Tarantola, M.; Fischer, K.; Schmidt, M.; Luxenhofer, R.; Janshoff, a; Theato, P.; Zentel, R. *Biomacromolecules* **2008**, *9*, 3114–8.

(123) Hemmelmann, M.; Knoth, C.; Schmitt, U.; Allmeroth, M.; Moderegger, D.; Barz, M.; Koynov, K.; Hiemke, C.; Rösch, F.; Zentel, R. *Macromol. Rapid Commun.* **2011**, *32*, 712–7.

(124) Herth, M. M.; Barz, M.; Moderegger, D.; Allmeroth, M.; Jahn, M.; Thews, O.; Zentel, R.; Rösch, F. *Biomacromolecules* **2009**, *10*, 1697–703.

(125) Allmeroth, M.; Moderegger, D.; Biesalski, B.; Koynov, K.; Rösch, F.; Thews, O.; Zentel, R. *Biomacromolecules* **2011**, *12*, 2841–9.

(126) Seymour, L. W. *Crit. Rev. Ther. Drug Carrier Syst.* **1992**, *9*, 135–187.

(127) Moghimi, S. M.; Hunter, A. C.; Murray, J. C. *Pharmacol. Rev.* **2001**, *53*, 283–318.

(128) Peer, D.; Karp, J. M.; Hong, S.; Farokhzad, O. C.; Margalit, R.; Langer, R. *Nat. Nanotechnol.* **2007**, *2*, 751–60.

(129) Allen, T. M. *Nature* **2002**, *2*.

(130) Lammers, T.; Hennink, W. E.; Storm, G. *Br. J. Cancer* **2008**, *99*, 392–7.

(131) Barz, M.; Canal, F.; Koynov, K.; Zentel, R.; Vicent, M. J. *Biomacromolecules* **2010**, *11*, 2274–2282.

2 Aims and Objectives

The positron emission tomography represents a powerful non-invasive tool for imaging of *in vivo* processes, especially tumor imaging. Thus, it can support the translation of novel molecular imaging probes from the bench to human to improve diagnostics and therapy, meaning to set up a personalized treatment plan for best response rates.

A prominent diagnostic target is the FR, which is (over)expressed on numerous tumor types. Various ^{18}F-labeled folates for PET imaging have been developed, but some are suffering from a challenging radiosynthesis, others from an unfavorable *in vivo* behavior. By going one step further, folate receptors can be used as targets for therapeutic approaches by direct linkage of either a therapeutic agent, radionuclide or a macromolecular carrier system loaded with therapeutic agents. In the second case, the *in vivo* behavior of those folate-targeted macromolecular carrier systems have to be adjusted and optimized in preclinical studies to guarantee the best-personalized therapy. This displays the huge potential of combining the positron emission tomography with therapeutic approaches, which address the FR.

The scope of this work was to develop an ^{18}F-labeled folate, with a facile radiosynthesis and improved *in vivo* properties, available for imaging FR-positive tumors via PET. Therefore, we investigated the conjugation approach using ^{18}F-click chemistry, which has already proven its outstanding role in ^{18}F-labeling due to high radiochemical yields under mild conditions and a defined regioselectivity. Besides, the *in vivo* behavior should be modulated towards a reduced abdominal background signal by increasing the polarity of the radiofolate. As a result, an amino acid-based ^{18}F-labeled prosthetic group should be synthesized. This prosthetic group was thought to have two main features. First it should resemble an endogenous amino acid, and second it should have the ability to participate in copper(I)-catalyzed azide-alkyne cycloadditions.

Moreover, the FR-targeting concept should be introduced to therapy concepts. The first concept focuses on FR-targeting in combination with the already existing macromolecular carrier systems, consisting of pHPMA, to increase the tumor accumulation of these systems. Whereas the second concept deals with the introduction of the FR-targeting into the boron neutron capture therapy using different boron clusters to enhance the accumulation of the boron pharmaceutics by active targeting (trapping effect).

Since it has been shown that FR-targeting led to an increased accumulation of macromolecular carrier systems at target sites, we applied this concept to pHPMA-systems and planned to track the systems *in vivo* by conjugation of a ^{18}F-label. For that reason, this folate-pHPMA conjugates have to be physicochemically characterized and the conjugation parameters optimized, before preclinical studies can be conducted. The *in vivo* experiments can provide information about how the folate-pHPMA systems have to be enhanced for *in vivo* application. By reconsidering the properties to be accomplished for enhancement of these systems, the use of nanoparticles in respect to drug delivery systems should be investigated. Thus, these nanoparticular systems should primarily be ^{18}F-labeled and the biodistribution explored. These colloids consist of PDLLA as core material and p((HPMA)-*b*-(LMA)) as surfactant, representing a fully biocompatible and partial biodegradable systems, with the ability of multifunctional modifications.

In the second part of the treatment section, boron clusters should be conjugated to a folate derivative via copper(I)-catalyzed cycloadditions. Thus, a new synthetic concept has to be evaluated to make these compounds available. Furthermore, these systems should be tested *in vitro* for comparison with already approved boron-containing pharmaceutics, like BPA or BSH.

This work should make a modest contribution and constitute how the FR-targeting approach can be used in combination to benefit human treatments of malignancies and improving their life quality through a personalized therapy approach.

3 Results and Discussion

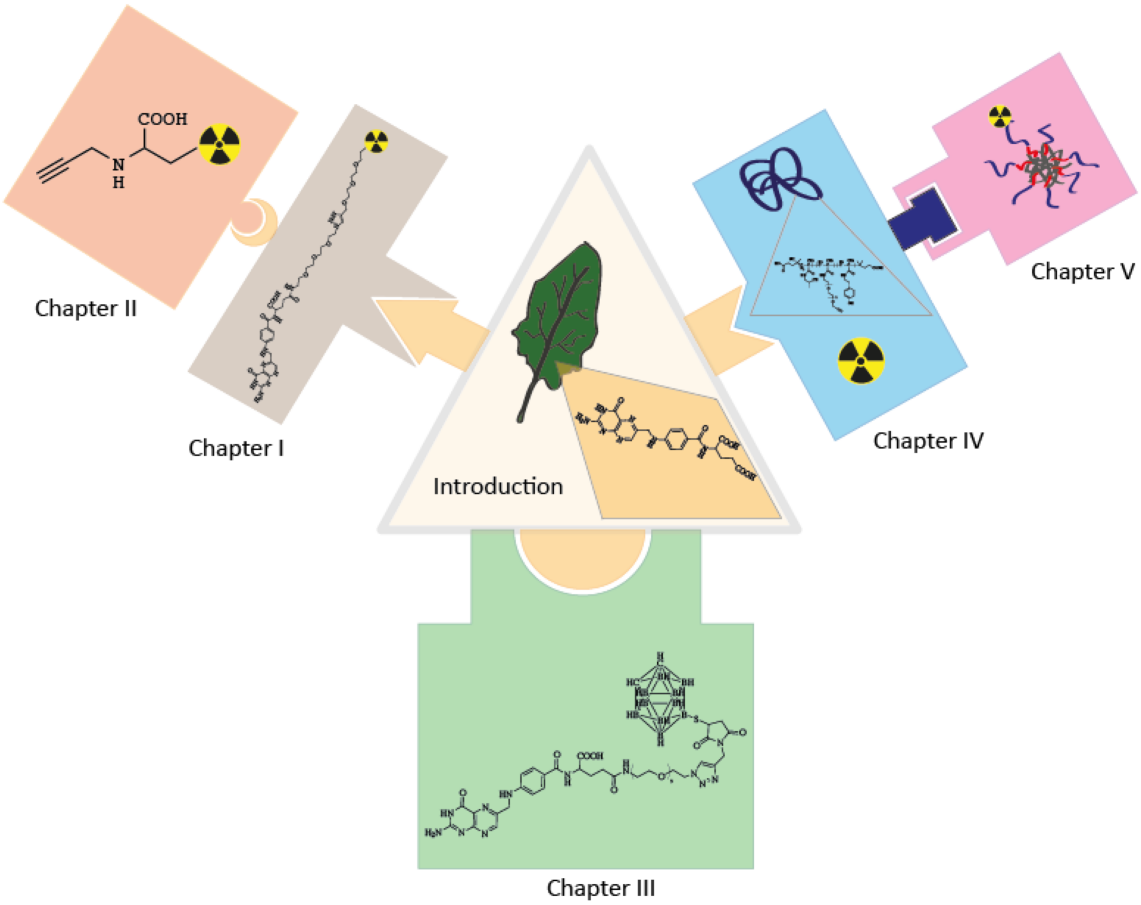

Figure 1. Schematic illustration of the cumulated work.

The following figure depicts the three different approaches for applying the lead structure folic acid to molecular imaging and therapy. Thereby, *Chapter I* contains the synthesis, ^{18}F-click labeling and evaluation of an oligoethylene-based radiofolate (^{18}F-OEG-folate) for PET imaging. *Chapter II* is the sequel of the results obtained in *Chapter I* to improve the *in vivo* behavior of the ^{18}F-OEG-folate or biomolecules in general by using a novel amino acid-based prosthetic group.

The transition to therapy approaches of FR-positive tumors can be found in *Chapter III*, which deals with the coupling of new folate derivatives carrying boron clusters to be able to perform boron neutron capture therapy.

Chapters IV and *V* comprise with ^{18}F-labled folate-pHPMA conjugates to investigate their *in vivo* behavior as potential drug carrier systems, whereas *Chapter V* is based on *Chapter IV* to improve the feasibility of those systems (colloids) for drug delivery and targeting

As outlined in **Aims & Objectives** the goal of this work was to utilize folate derivatives for PET imaging and therapeutic approaches by targeting the FR. The results clearly display that FR-targeting is very suitable for imaging of FR-positive tumors and secondly significantly enhance accumulation at target sites of folate-based structures, including small molecules and folate-pHPMA conjugates. In the following chapter major results and conclusions are portrayed, which are based of the findings in the Chapter **Publications & Ongoing studies**. *Chapters II* and *V* are approaches directly derived from the results of the previous *Chapters I* and *IV*.

The matter of fact, that the FR is a valuable target for tumor imaging and therapy, is known over decades. It is also fact, that the FR is (over)expressed in a very large number of human malignancies. Therefore, quite a number of agents for imaging FR-positive tumors have been developed, especially for SPECT imaging. Up to now, agents for PET imaging are lacking on two different aspects, depending on the labeling strategy pursued (conjugation or integrated approach). Both approaches have drawbacks, meaning the integrated approach is always correlated with a challenging precursor synthesis as well as radiosynthesis. The latter often leads to low RCYs, but the directly ^{18}F-labeled folates provide the best *in vivo* data, so far. In contrast, the conjugation approaches suffer from inferior *in vivo* properties, but being aware of the mostly high RCYs during multi-step radiosyntheses. Especially the here used ^{18}F-click reaction has already proven its outstanding role due to high RCYs under mild conditions, no need of protection groups and a distinct regioselectivity. Three folates based on the ^{18}F-click reaction have yet been published, whereas a clear trend can be observed with respect to *in vivo* characteristics and hydrophilicity of the radiotracer (Figure 2).

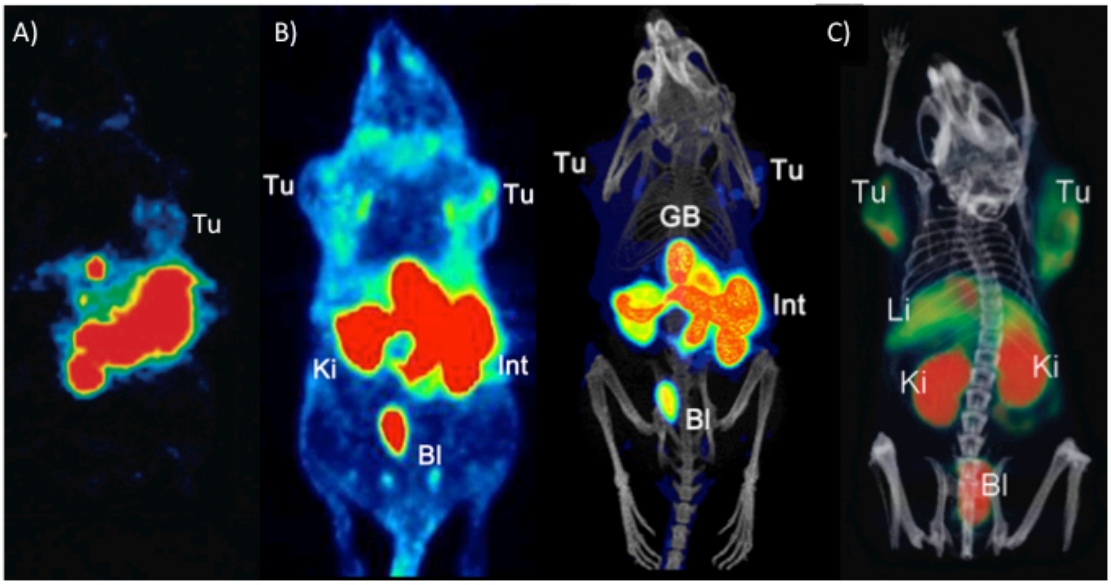

Figure 2. **A**) Horizontal whole body image of ^{18}F-click folate (**1**)[1]; **B**) Maximum intensity projection of ^{18}F-OEG-folate (left) and 3D PET/CT image of ^{18}F-OEG-folate (right); **C**) 3D PET/CT image of [^{18}F]fluoro-deoxy-glucose folate[2].

The first ^{18}F-click folate by Ross and coworkers displays a pronounced hepatobiliary excretion pathway, generally taken by more or less (lipophilic) compounds.[1] This ^{18}F-labeled folate served as lead compound in this work. To increase the polarity of the lead compound, an oligoethylene spacer was incorporated at the γ-position of the glutamate moiety (Scheme 1).

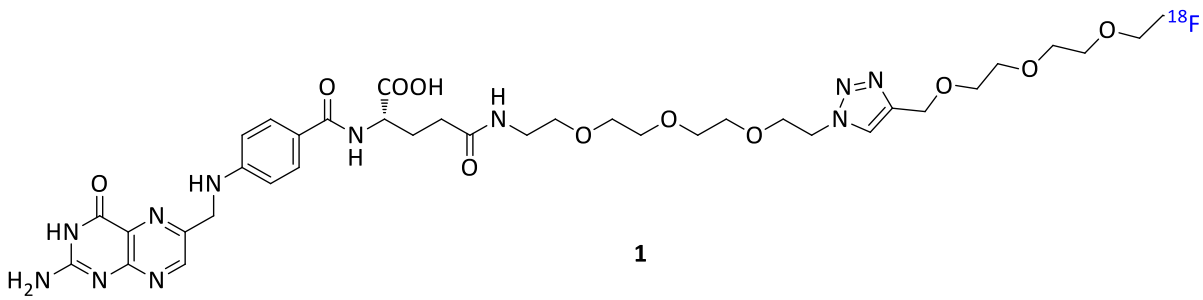

1

Scheme 1. Chemical structure of the new ^{18}F-OEG folate. (**1**)

Additionally, an oligoethylene-based ^{18}F-labeled prosthetic group was used to maintain the oligoethylene character of the molecule. Figure 1 clearly displays the reduction of abdominal background signal leading to the visualization of the tumors in the front forelimbs. The third ^{18}F-click folate represents the tracer with the highest polarity, which could be obtained by conjugation of the folate scaffold to ^{18}F-labeled glucose.[2] This led to an enhanced tumor uptake on the one hand as well as to a significantly reduced background signal in the abdomen. However, an unexpected and distinct liver uptake was observed. The synthesis of the azido-functionalized OEG-folate was straightforward starting from 4-((*tert*-butoxycarbonyl)amino)-5-methoxy-5-oxopentanoic acid (BOC-Glu-OMe). First, a 11-azido-3,6,9-trioxaundecan-1-amine spacer was coupled to the carboxylic acid at the γ-position of the glutamate residue using COMU to activate the carboxylic function for a nucleophilic attack of the primary amine of the spacer, and additionally, to retain the formed water.[3] After acidic cleavage of the BOC-group the glutamate derivative was coupled to 4-(*N*-((2-(((dimethylamino)methylene)amino)-4-oxo-3,4-dihydropteridin-6-yl)methyl)formamido)-benzoic acid using also COMU for activating the carboxylic function. The resulting protected azido-functionalized OEG-folate was deprotected and coupled to the $^{18/19}$F-labeled prosthetic group.

Based on these findings, a novel prosthetic group should be synthesized with the following characteristics: First, the prosthetic group should be as hydrophilic (polar) as possible, second, the prosthetic group should be able to participate in CuAAC, and third, the prosthetic group should be based on and structurally close to an endogenous biomolecule, which limited the scope to an amino acid-based prosthetic group. Serine seemed to be a good choice, because the hydroxyl function can be seen as isoelectronic towards attached fluorine after derivatization, although several functionalities are assembled over a small space (Scheme 2).

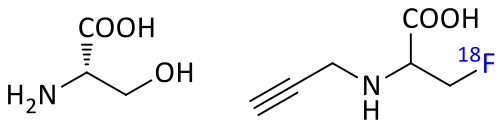

2 **[^{18}F]21**

Scheme 2. Chemical structures of *L*-serine (**2**) and the ultimate clickable ^{18}F-labeled prosthetic group (**[^{18}F]21**).

The idea was to couple methyl 2-(((benzyloxy)carbonyl)amino)-3-(tosyloxy)propanoate (**3**) with propiolic acid, after cleavage of the carboxybenzyl protecting group (Scheme 3).

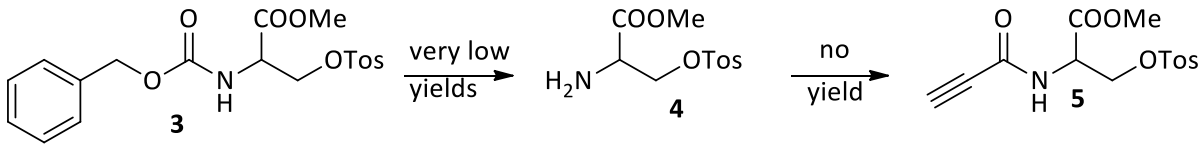

3 **4** **5**

Scheme 3. Original synthetic strategy to the ^{18}F-labeled prosthetic group precursor.

The deprotection of **3** turned out to be very sensitive to hydrogenation no matter which catalyst or conditions were used leading to serine, since the formed C-H bond is stronger than the C-O bond of the oxygen, which is also activated through the sulfonic ester.[4] Consequently, a different approach was needed, which was the use of iodotrimethylsilane for deprotection. In this case, the trimethylsilyl coordinates with the carboxyl function of the Cbz group and activates the methylene group of Cbz group for a nucleophilic attack of the iodide, yielding benzyl iodide, whereas the subsequent addition of methanol leads to the formation of the unprotected primary amine.[5] This procedure finally led to the desired product **4** in very low yields of < 1%, which was intended for coupling to propiolic acid. Unfortunately, this synthetic step was the end of the road, since no amide coupling strategy (DCC/HOBt; HATU, HBTU; COMU; oxalyl chloride; ethyl chloroformate) succeeded – due to the reactivity of the alkyne functionality of the propargylic acid, which can form vinyl acetylenes (exclusion of water) or symmetrical ethers (small amounts of water present).[6]

Thus, an alternative synthetic strategy was evaluated starting with the methyl ester of serine **6** (Scheme 4). After BOC protection, the hydroxyl function of **7** was tosylated under mild conditions using the pyridine/*p*-toluenesulfonyl chloride system in dichloromethane. The subsequent cleavage of the BOC group (quantitative) made the free amino function available for amide coupling of the trimethylsilyl-protected propiolic acid. The coupling could be accomplished by using the DCC/HOBt system in dimethylformamide. Deprotection of the silyl-protected alkyne function was performed in methanol and potassium carbonate at room temperature. The pitfall of this strategy revealed during the ^{18}F-labeling reaction, showing that the ^{18}F-labeling acidified the methylene protons next to the fluorine inducing a ring closure and ending up with an oxazoline derivative (compound **10)**.[7]

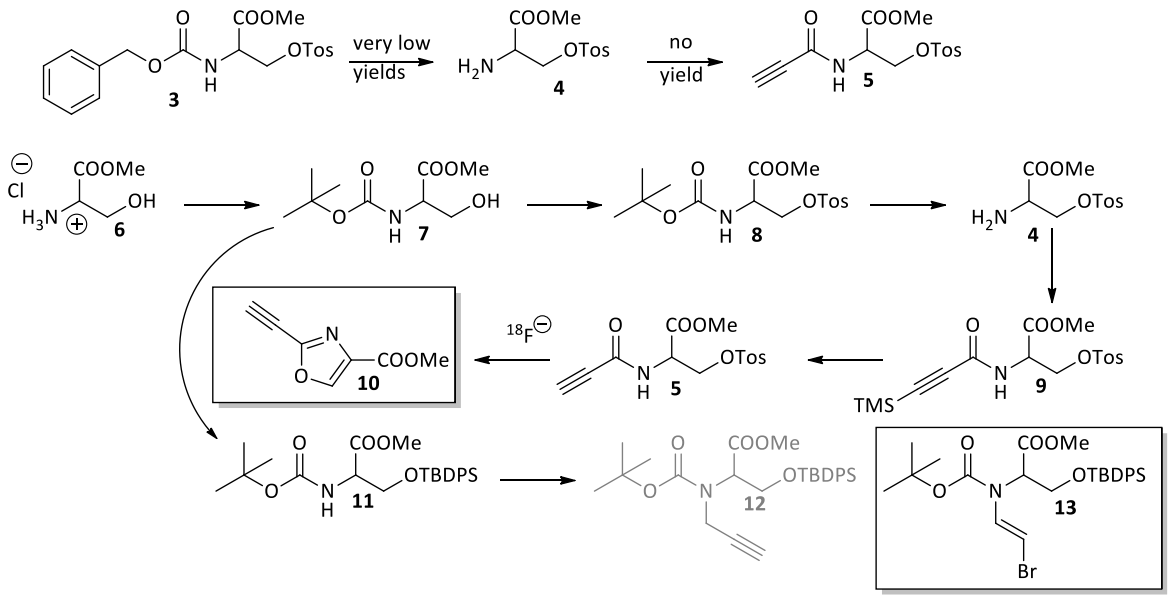

Scheme 4. Preliminary synthetic strategies and dead ends (compound **10** and **13**) to the final prosthetic group.

As a result, a reconsideration of the molecular structure of the prosthetic group was induced and led to the decision that a secondary amine instead of amide bond between serine and alkyne function would be more suitable, because the primary amine is easily derivatized and the resulting secondary amine is protonated under physiological conditions for enhanced polarity. The new synthetic route started with the BOC-protected serine **7**, which was *O*-protected in the next step using *tert*-butyl(chloro)-

diphenylsilane. The resulting fully protected serine derivative **11** was reacted with propargyl bromide, whereas different strong bases (NaH, LDA, phosphazenes) were used, yielding to no product **12**. Rather the terminal proton of propargyl bromide was cleaved, enabling the lone pair to attack the amide bond giving **13** as main product.

Based on these findings, another new synthetic concept was elaborated, which can be seen in Scheme 5.

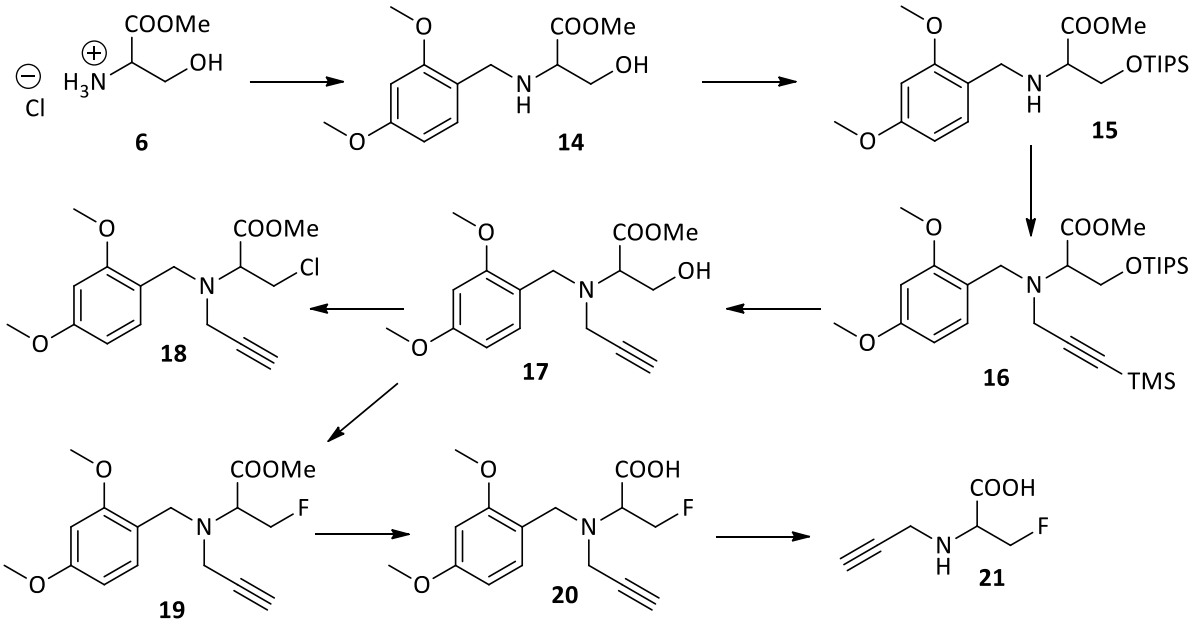

Scheme 5. Synthetic pathway to the labeling precursor and the reference compound of a serine-based prosthetic group.

The synthesis started with the methyl ester of serine (**6**), which was reductively *N*-protected using 2,4-dimethoxybenzaldehyde. Subsequently, the hydroxyl function was protected using triisopropylsilyl chloride, to avoid *O*-alkylation in the following step. The alkyne function was introduced using trimethylsilyl-protected propargyl bromide and reacted with the secondary amine of **15**. The resulting fully protected compound **16** was treated with tetrabutylammonium fluoride to cleave both silyl-based protecting groups yielding **17**, the starting material for either the precursor or reference compound synthesis. This strategy appeared to be very neat, since the high bond energy of the Si-F-bond (D = 565 kJ/mol)[8] leads to an exclusive cleavage of the silyl groups under mild conditions. The final step towards the labeling precursor was faciliated using

toluenesulfonyl chloride and triethylamine in acetonitrile. Typically, a tosylation of the hydroxyl function would be expected, but only chlorination has been observed. The reason for this pattern is due to the relatively high reactivity of tosyl leaving group in the given molecular construct. Therefore, the less reactive mesyl and nosyl leaving groups were tested as well, unfortunately, always resulting in the chlorinated compound **18**. But, considering the assembly of functionalities within the small space, the methylene position next to the leaving group is very activated for any kind of nucleophilic attack. Thereby, the methyl ester and the tosyl group, which are more likely electron withdrawing groups (EWG) and the tertiary amine, which is on the one hand electron withdrawing (χ = 3.0), but possesses also a lone pair to stabilize mesomeric structures (supports elimination), are in direct neighborhood. This illustrates the reaction potential of the small molecule. However, the formed hydrogen chloride itself represents a nucleophile, which replaces the before attached tosylate. Therefore, the use of tosyl and mesyl anhydride, to avoid chloride ions in the reaction mixture, led to the desired products, but still a high reactivity caused decomposition (frequently: hydrolysis) during the purification (column chromatography) of the reaction mixture. In this case, the above-mentioned electronic effect exerts, but the lack of chloride ions led to the formation of the desired products. However, the exposure of the sulfonic esters to humidity led to rapid degradation. This can be on the one hand substitution of the LG with hydroxyl or on the other hand elimination of the acidic proton of serine (α-proton). Thus, methyl 3-chloro-2-((2,4-dimethoxybenzyl)(prop-2-yn-1-yl)amino)propanoate (**18**) became the precursor of choice and was used for the ^{18}F-labeling reactions, because the chlorinated precursor was stable under storage conditions (argon atmosphere, 0 °C). Further LGs, which would be suitable, but a little bit more reactive than the chloride are other halides, like bromide or iodide. It would also be possible to achieve radiolabeling via a ^{19}F/^{18}F isotopic exchange.[9] The major drawback is the relative low specific activities of the obtained labeled compounds, which limits the use of these tracers. However, for the application as prosthetic groups no major influence on the *in vivo* profile of the biomolecule can be expected-due to the low specific activities. An additional opportunity offers the use of silver triflate, which generates one

of the most reactive LGs for nucleophilic substitutions *in situ*. Thus, the chloride LG of **17** is substituted by triflate, while silver chloride is formed.[10]

The synthesis of the reference compound **21** was carried out by starting from **17.** (Diethylamino)sulfur trifluoride was used to fluorinate the hydroxyl function directly to provide the protected reference **19**. Subsequently, a stepwise deprotection was performed. At first, the methyl ester of **19** was cleaved applying an aqueous solution of lithium hydroxide at room temperature. This mild deprotection step gave high yields and additionally prevented from undesired dehydration products during the reaction.[11] Final deprotection was accomplished using a trifluoroacetic acid and dichloromethane mixture for cleaving the 2,4-dimethoxybenzyl group, yielding the reference compound **21**.

The radiosynthesis of the prosthetic group was optimized regarding labeling conditions as well as deprotection conditions (Scheme 6).

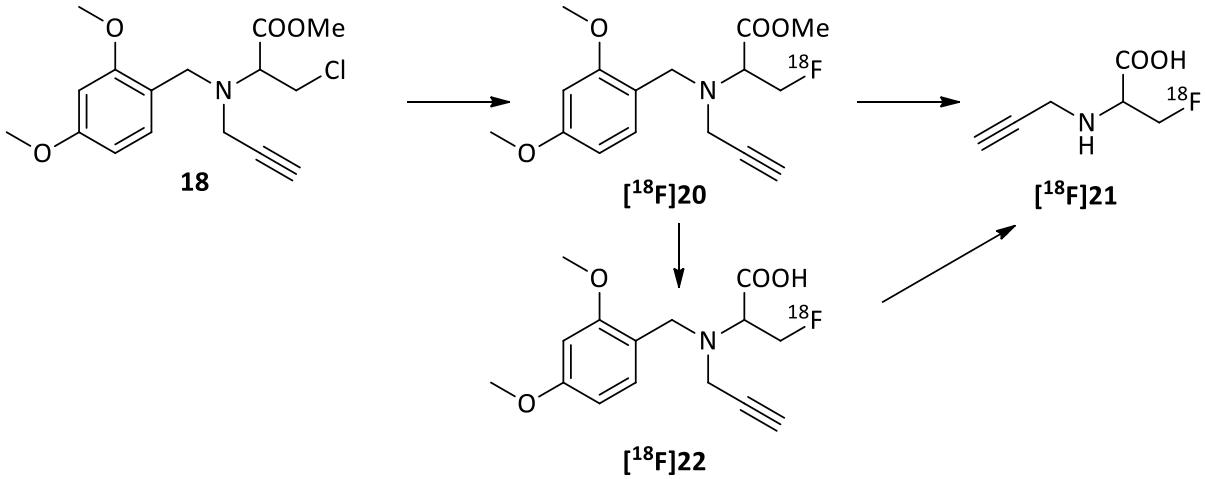

Scheme 6. ^{18}F-labeling of **18** and subsequent deprotection towards the new clickable serine-based ^{18}F-labeled prosthetic group **21**.

Hence, parameters like precursor concentration, base concentration, base system, solvent system, temperature and the mode of energy support (oil-bath; microwave) were screened and optimized. High overall radiochemical yields of 28±5% were obtained using a microwave-supported radiosynthesis and the K222 / potassium carbonate system in dimethyl sulfoxide. Furthermore, it could be shown that the protecting groups of **[^{18}F]20**

could be removed selectively (Figure 3). Finally, the isolated **[^{18}F]21** was successfully coupled to an azido-functionalized cRGD as proof of principle.

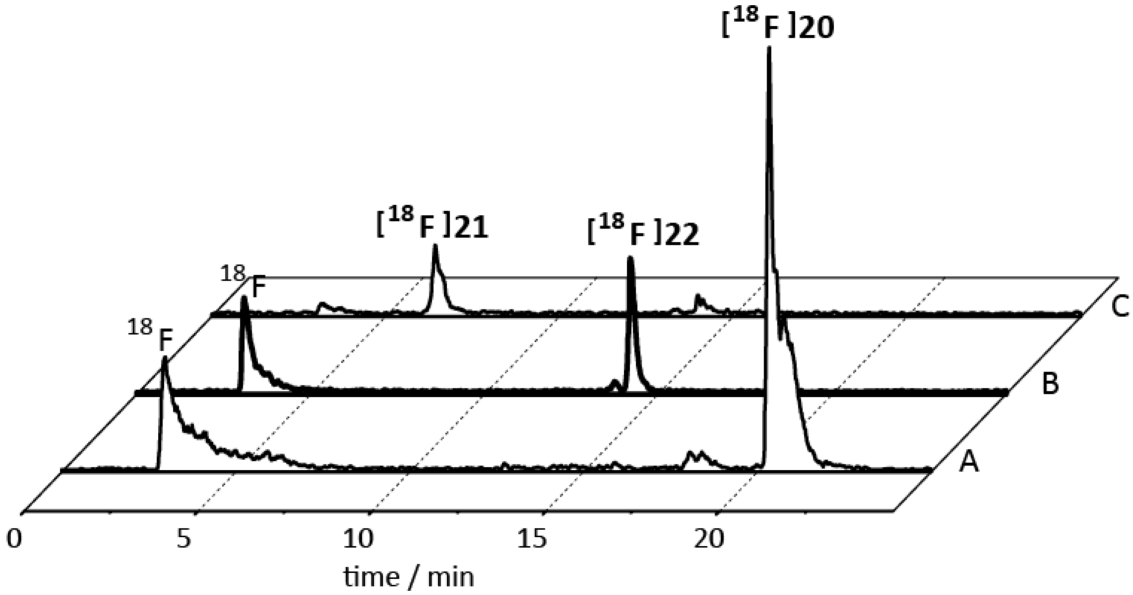

Figure 3. Step-wise deprotection of ^{18}F-labeled protected prosthetic group. **A**) Full protected ^{18}F-labeled prosthetic group. **B**) Partly protected ^{18}F-labeled prosthetic group after methyl ester cleavage. **C**) Fully deprotected ^{18}F-labeled prosthetic group. Relative peak intensities are not normalized for **A**, **B** and **C**.

The following paragraph, *Chapter III*, deals with the development of folate-based constructs for radiation therapy and is considered to bridge the two main areas of this work, radiofolates for diagnostics and folate-functionalized macromolecular carriers for therapy.

The here reported boron containing folate conjugates demonstrate the approach to introduce the FR-targeting concept into BNCT. Currently, BPA and BSH are the predominantly used and only clinically approved (second generation) boron pharmaceuticals in BNCT. In the case of BPA, an inefficient active targeting of the overexpressed *L*-amino acid transporter (LAT1) is utilized, where BPA has no metabolic trapping in tumor cells resulting in a fast efflux of BPA by the bidirectional LAT1. In contrast, BSH uses only passive targeting into the intercellular spacer of tumor tissue via the EPR effect.[5] The aim of a third generation of boron pharmaceuticals is to conjugate boron delivery agents to targeting structures, like proteins, antibodies or liposomes, to overcome the lack of selectivity and poor pharmacokinetics of currently used pharmaceuticals.[6,7,8] Therefore, small molecules consisting of the folate scaffold and a boron cluster have been synthesized in a regioselective multi-step synthesis (Scheme 7).

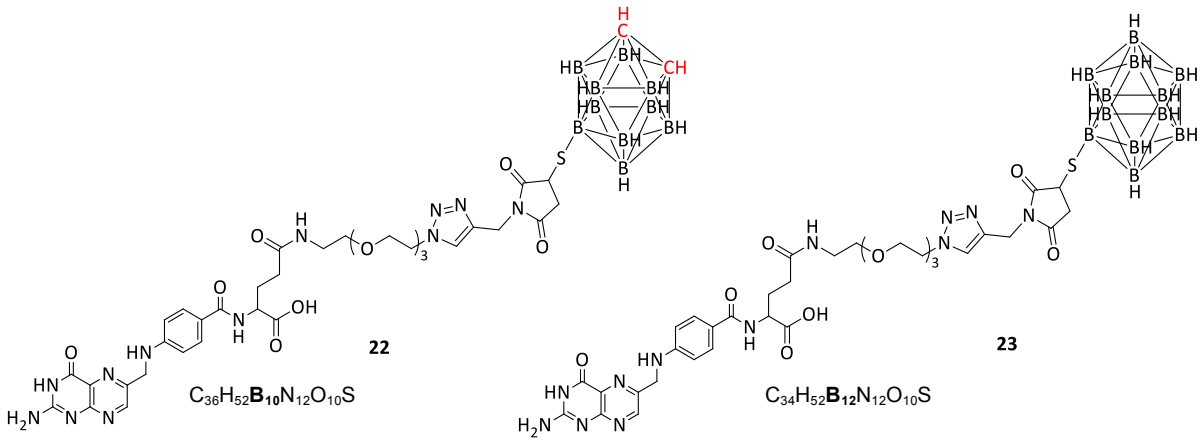

Scheme 7. Chemical structure of the new folate-boron-clusters **22** and **23**.

The targeting structure has been synthesized regioselectively according to our established protocol developed in first part of the presented work[16], yielding the protected γ-azido folate, which was further coupled to a linker-boron cluster system via CuAAC. For the synthesis of the linker-boron cluster system, one challenge was to find a linker, which allowed orthogonal couplings of the boron cluster and the targeting vector (folate). Thus, an alkynylmaleimide structure was selected. This structure was synthesized through a ring opening reaction of maleic anhydride using propargyl amine, followed by a ring re-closure reaction using zinc chloride and hexamethyldisilazane. Earlier approaches using maleimde and propargyl alcohol under Mitsunobu conditions failed. The alkynylmaleimide (highly electron deficient system) was first coupled to the boron cluster via *Thiol-Michael Addition* in good yields. The convenience of this reaction is, again, the mild conditions needed for conversion. In this case, the base-catalyzed mechanism can be applied, since reaction of the thiol group was initiated through addition of a basic sodium acetate buffer solution.[17] Another hind for this reaction pathway is the need of energy during the reaction, which in our case was accomplished through elevated temperatures.[17] Surprisingly, no or only traces of side products could be observed due to the additional introduced alkyne functionality. This also indicates the possibility to use electron deficient "-*ynes*" for Thiol-Michael Additions, which can react twice with a thiol functionality.[18] After the synthesis of the linker-boron cluster, it was then reacted with the protected γ-azido folate in a CuAAC. Subsequent deprotection led to the novel carboran- and BSH-folate conjugates, which were available for *in vitro* testing in cell assays.

To evaluate the *in vitro* behavior of the novel carboran and BSH-folate (**22** and **23**), preliminary cell uptake studies using KB-tumor cells derived from human cervical carcinoma were used. The initial experiments were performed using the carboran-folate **22** for getting a surface impression. The KB cells were seeded in petri dishes and the incubation times as well as different boron folate concentrations (1 ppm/6 ppm) were tested in comparison to BPA, which also uses an active targeting concept via LAT1. The studies clearly displayed an up to 7-times higher cell uptake of the carboran-folate after

1.5 h and 2.5 h at incubation concentrations of 1 ppm. This effect slightly attenuated if incubation concentrations were raised to 6 ppm. Rather at this concentrations the BPA uptake increased and reached values close to the carboran-folate (Figure 4), which can be related to a saturation effect of the FRs by incubating at 6 ppm. Nevertheless, it has to be considered that the uptake of the boron-folate conjugates is not retrogressive, meaning that no efflux of boron-folate conjugates is expected. Further investigations should proof the trapping effect. However, it has to be considered that the uptake of one carboran-folate leads to ten boron atoms in the cell, whereas BPA only carries one boron atom. Therefore, the amount of administered pharmaceutical can be reduced due to the enhanced pharmacokinetics, which would lead to an increased tumor to non-target tissue ratio of the boron-pharmaceutical. Moreover, studies of the supernatants showed that ~10% of the carboran-folate was receptor bound. Under treatment conditions this fraction would also be able to develop a lethal effect on tumor cells (Figure 4). Considering the advantages of the FR-targeting in BNCT, time management between application of born-pharmaceutical and radiation could be optimized.

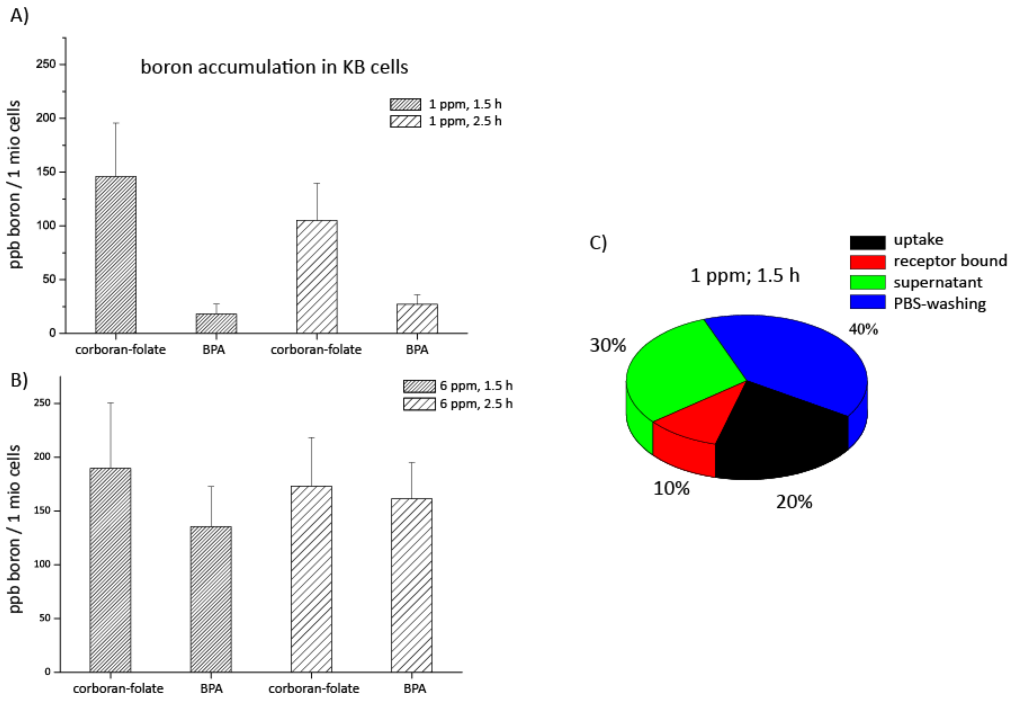

Figure 4. **A**) Boron accumulation in KB cells after incubation with carboran-folate in comparison to BPA uptake at 1 ppm; **B**) Boron accumulation in KB cells after incubation with carboran-folate in comparison to

BPA uptake at 1 ppm **C**) Boron distribution pattern (within one probe) after incubation with carboran-folate **22**.

These results show once again that FR-targeting cannot only be used for diagnostic purposes, rather this concept can be transferred to numerous approaches whether for radiation therapy (*Chapter III*) or therapy using macromolecular carrier systems, which is described in *Chapters IV* and *V*.

Chapter IV involves the research about ^{18}F-labeled folate-pHPMA conjugates for targeting FR-positive tumors. As already mentioned in the Introduction, macromolecular carrier systems have been developed for improving the therapeutic effect of (chemo)therapeutics. These systems can accumulate at target sites due to the EPR effect. Former studies already showed that it was possible to change the biodistribution of pHPMA-based systems by varying the architecture.[19] Additionally, labeling strategies of macromolecular systems have been generally extended. The here reported pHPMA using folate-targeting has already shown its potential in preliminary *in vitro* experiments.[20] However, these results have never been proven in *in vivo* experiments, which would provide significant information about the suitability of these conjugates as potential and effective carrier systems. For the here conducted experiments, a low and a high molecular weight precursor polymer were synthesized (**P1-R** and **P2-R**) to investigate the conjugates' behavior. One (**P1**) exhibiting a size under and the other (**P2**) over the renal threshold. These precursor polymers were reacted, yielding finally four different folate-HPMA conjugates (Table 1). The final conjugation of the γ-azido-folate was facilitated via CuAAC, obtaining folate incorporations of about 8%, which has already been proven to provide highest uptake levels *in vitro*. The γ-azido-folate was synthesized according to our before mentioned protocol.[16]

Table 1. Characterization of pHPMA and folate-pHPMA conjugates

Polymer	M_n [g/mol]	M_w [g/mol]	*Đ*	Tyramine content[2]	Alkyne content[2]	Folic acid content[2]
P1-R	12,800[1]	16,000[1]	1.2[1]	-	-	-
P2-R	64,000[1]	91,500[1]	1.4[1]	-	-	-
P1	8,000[3]	10,000[3]	1.2[3]	3%	10%	-
P2	40,000[3]	57,000[3]	1.4[3]	3%	10%	-
FA-P1	10,500[3]	13,000[3]	1.2[3]	3%	10%	8%
FA-P2	52,500[3]	75,000[3]	1.4[3]	3%	10%	8%
P1-OG[4]	8,000[3]	10.000[3]	1.2[3]	-	10%	-
P2-OG[4]	40,500[3]	58,000[3]	1.4[3]	-	10%	-
FA-P1-OG[4]	10,800[3]	13.000[3]	1.2[3]	-	10%	8%
FA-P2-OG[4]	53,500[3]	76,500[3]	1.4[3]	-	10%	8%

[1] = Determination by GPC in THF as solvent; [2] = Tyramine-, alkyne spacer- and folic acid incorporation ratio determined by ^{1}H-NMR spectroscopy after polymeranalogous reaction; [3] = Calculated from the molecular weight of the reactive ester polymer P-R determined by GPC in THF as solvent; [4] = Oregon Green Cadaverine was incorporated during polymeranalogous reaction (1 mol%).

Furthermore, two of the synthesized conjugates were labeled with *Oregon Green Cadaverine* for fluorescent correlation spectroscopy (FCS) measurements, indicating that the high mw conjugates do form aggregates, whereas the low mw conjugates do not. However, this circumstance was expected for the here-investigated systems since it has been shown that aggregation of such systems occurs in the presence of around 10% of a hydrophobic moiety.[21] After determination of the physicochemical properties of the conjugates **FA-P1** and **FA-P2**, these were ^{18}F-labeled using 2-[^{18}F]FETos. The ^{18}F-labeled conjugates were employed for biodistribution and micro PET studies using Walker mammary carcinoma bearing rats. Figures 5A+B display the whole body images of **[^{18}F]FE-FA-P1** (Figure 5A) and **[^{18}F]FE-FA-P2** (Figure 5B), showing the expected biodistribution pattern for a low and high molecular weight pHPMA polymer, meaning that low mw polymers undergo renal excretion, whereas high mw polymers accumulate in the liver and lungs. Moreover, the tumors in both hind legs of the rat are visible. Henceforth, all values of both, biodistribution and micro PET studies, have been referenced to the testis, representing an area of unspecific accumulation. Now, taking a closer look at the tumor

accumulation of **[^{18}F]FE-FA-P1** and **[^{18}F]FE-FA-P2** it can be seen, that the low mw polymer accumulated in the tumor tissue and the accumulation stayed constant over the whole 240 min (Figure 5C). It was further possible to significantly block the retention of the low mw polymer by administering excess of native folic acid. Additionally, the blocking effect of the FRs in the tumor did not persist over the 240 min indicated by an increase of activity of the low mw polymer over time. Furthermore the high mw polymer showed a similar accumulation profile over the first 120 min by reaching the same accumulation levels as the low mw polymer. However, the activity levels of the high mw polymer increased significantly of about one third towards the low mw polymer. Surprisingly, blocking of the high mw polymer was not significant within the first 120 min, whereas a specific blockade of 30% was possible after 240 min. These results were consistent with the findings obtained in the micro PET studies (Figure 5D). First of all a significant increase of tumor accumulation towards the non-targeted pHPMA could be observed (2.5-fold low mw polymer; 1.5-fold high mw polymer), demonstrating the enhancement of tumor uptake due to folate conjugation and the combination of EPR and active FR-targeting.

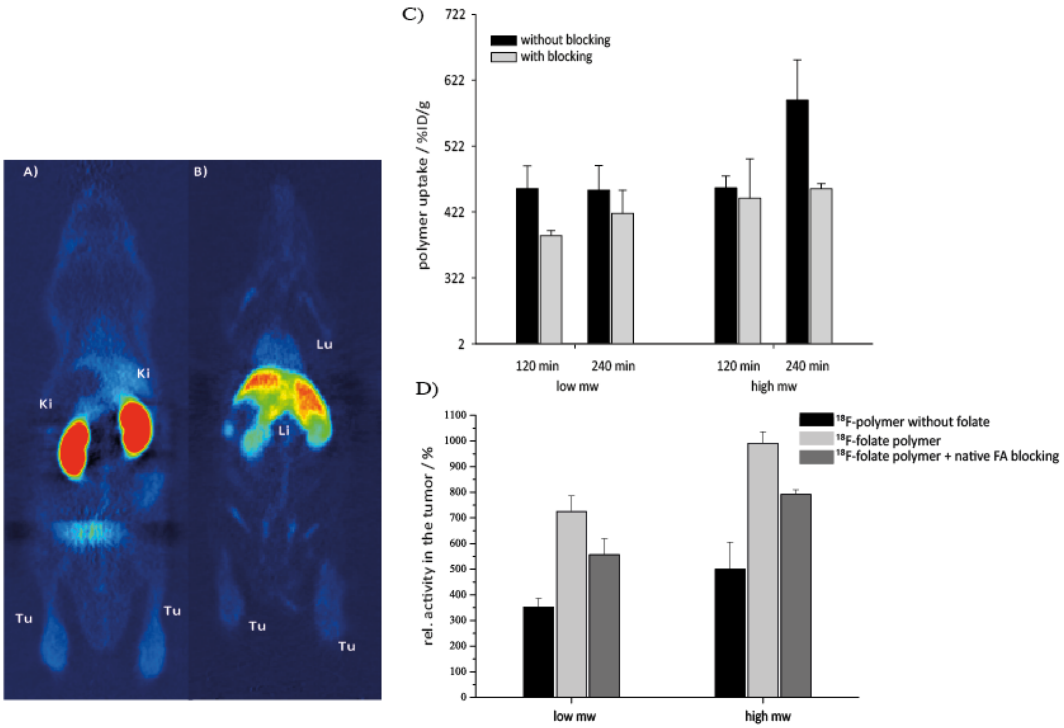

Figure 5. µPET imaging of ^{18}F-labeled folate-pHPMA conjugates. Representative coronar µPET summed images in different depths 120-135 min after i.v. injection. Both tracers show slight accumulation in the tumors (Tu). **A**) Mw = 10.5 kDa homopolymer (**[^{18}F]FE-FA-P1**) showing renal excretion (Ki). **B**) M = 52.5 kDa homopolymer (**[^{18}F]FE-FA-P2**) has a different bodydistribution pattern where the most activity can be found in the liver (Li) and a reduced kidney (Ki) accumulation. **C**) Biodistribution studies of the low mw polymer (left) and high mw polymer (right) under normal and blockade conditions in the tumor and referenced to the testis. **D**) Micro PET studies (2h) of the low and high mw polymers having no-targeting moiety, FA as targeting vector and blockade conditions.

As already seen during biodistribution experiments, the folate accumulation of **[^{18}F]FE-FA-P1** and **[^{18}F]FE-FA-P2** could be blocked through administration of native folic acid confirming the high specificity of the active FR-targeting. The high mw polymer showed the highest uptake/binding enhancement, although physicochemical *in vitro* studies showed aggregation of the polymers due to the folate conjugation. An explanation could be the relative number of folate segments in a polymer chain. For the low mw polymer only seven folates are available for binding to the FR, therefore, no aggregation was observed during FCS measurements. In contrast, the high mw polymer is carrying 7-times more folates per polymer chain, resulting in aggregation. But, if there are only a couple of folates responsible for aggregation there are still a bigger number of folates available for FR-binding. Moreover, the hydrodynamic radii of the high mw polymer aggregates could

indeed lead to a slower immigration of the polymers into tissues, but certainly to a diminished efflux from the tumor tissue, which could also result in the increased contrast levels during the *in vivo* studies. Considering the demands towards macromolecular drug delivery systems, the low mw polymer is clearly superior compared to the high mw polymer.[22] The presence of defined structures of polymers for biological applications is impassable and represents the foundation of this research field; to that effect the aggregation of the high mw polymer leads to undefined structures and an unpredictable *in vivo* behavior.

By considering the results obtained from *Chapter IV* that aggregate formation was observed resulting in a lowered amount of folates available for binding to the FR, the question arose how to force the FA pointing to the outside and secondly, how to increase the number of folates available for binding. A neat opportunity is the use of nanoparticles obtained by the miniemulsion process in combination with solvent evaporation yielding nanoparticles consisting of a PDLA core and a p((HPMA-*b*-(LMA)) copolymer as surfactants on the shell. By incorporating folic acid into the hydrophilic block an orientation of the FA towards the aqueous medium would be achieved. Moreover, solely the size of these nanoparticles allows conjugation of a large number of targeting vectors. Thus, *Chapter V* deals with the evaluation of those non-targeted systems as drug carrier systems starting with the synthesis and characterization of the nanoparticles. Furthermore, preliminary *in vivo* experiments using ^{18}F-labeled nanoparticles were conducted to investigate the biodistribution and pharmacokinetics of these new nanoparticles (Figure 6).

For the synthesis of these nanoparticles via miniemulsion process in combination with solvent evaporation, low molecular weight block copolymers consisting of HPMA and 10% LMA were synthesized. The block copolymers, which in the end act as surfactants, in turn were synthesized via RAFT polymerization in combination with a reactive ester approach. The copolymers were additionally modified with an oligoethylene-based azido spacer, which served as azido constituent during ^{18}F-labeling via CuAAC. Subsequently, these copolymers were introduced into the miniemulsion process in combination with the

solvent evaporation process. The unique feature of using this combined process, is the ability to use numerous pre-fabricated polymers as core material, which cannot be obtained via the miniemulsion polymerization.[23] The core of the used nanoparticles consisted of PDLLA, which represents a fully biocompatible and biodegradable material and is very suitable to embed drugs of various kinds and characteristics.

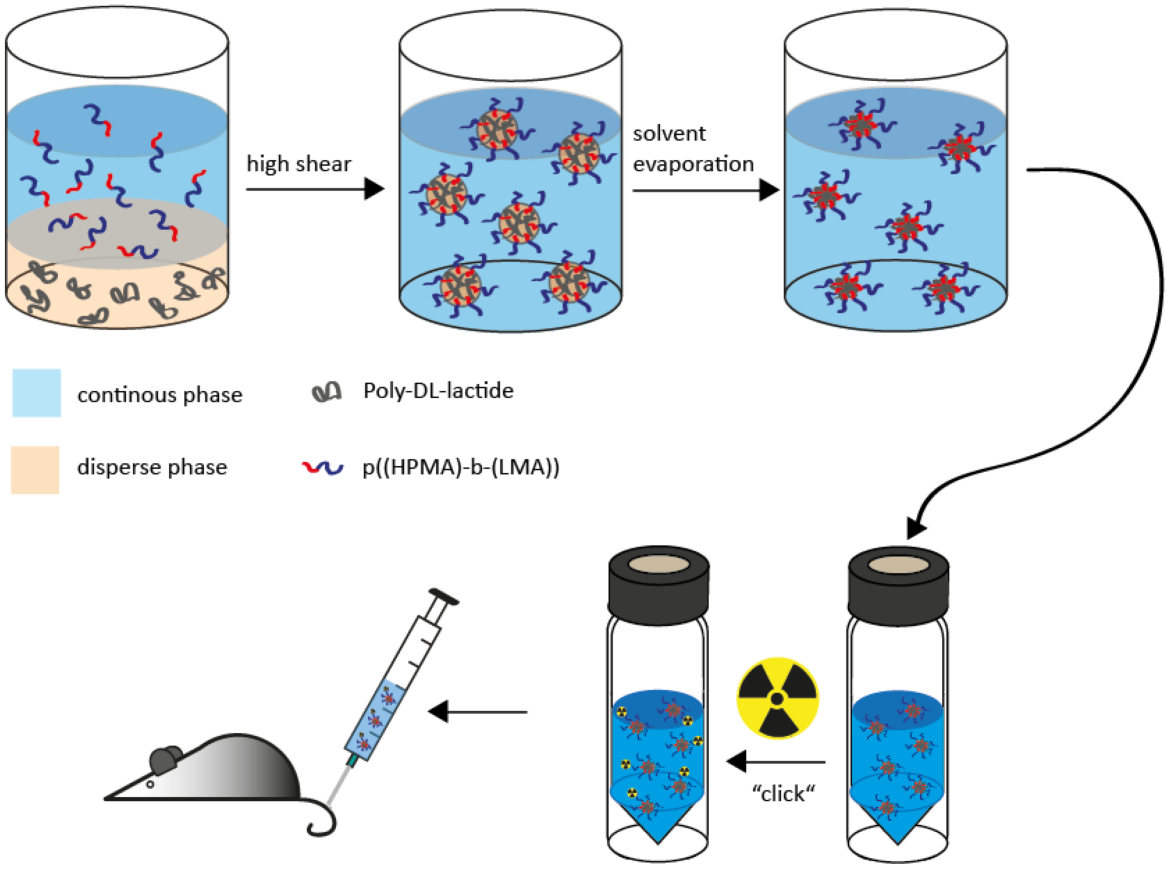

Figure 6. From Schlenk flasks over screw led glasses to *in vivo* micro PET experiments. Synthesis of new nanoparticles via miniemulsion process in combination with solvent evaporation.

The obtained azido-functionalized nanoparticles were ^{18}F-labeled via CuAAC. Therefore, a ^{18}F-labeled alkyne-functionalized prosthetic group was synthesized and subsequently "*clicked*" to the nanoparticle. Two major challenges during radiosynthesis were on the one hand, the restricted usage of aqueous solvent systems and on the other hand, the sensitivity towards heat - due to the PDLLA core. Ultimately, a PBS-buffered system at

40 °C and a reaction time of 20 min was superior leading to an overall RCY of 8±3% including purification via size exclusion chromatography.

Finally, the ^{18}F-labeled nanoparticles were evaluated in C57BL/6 mice. Therefore, micro PET measurements and *ex vivo* biodistribution studies were performed. The mirco PET scan (MIP) showed that high radioactivity levels have been excreted through renal filtration, although the sizes of the nanoparticles were around 200 nm in diameter and far above the renal threshold of about 5-8 nm (Figure 7A).

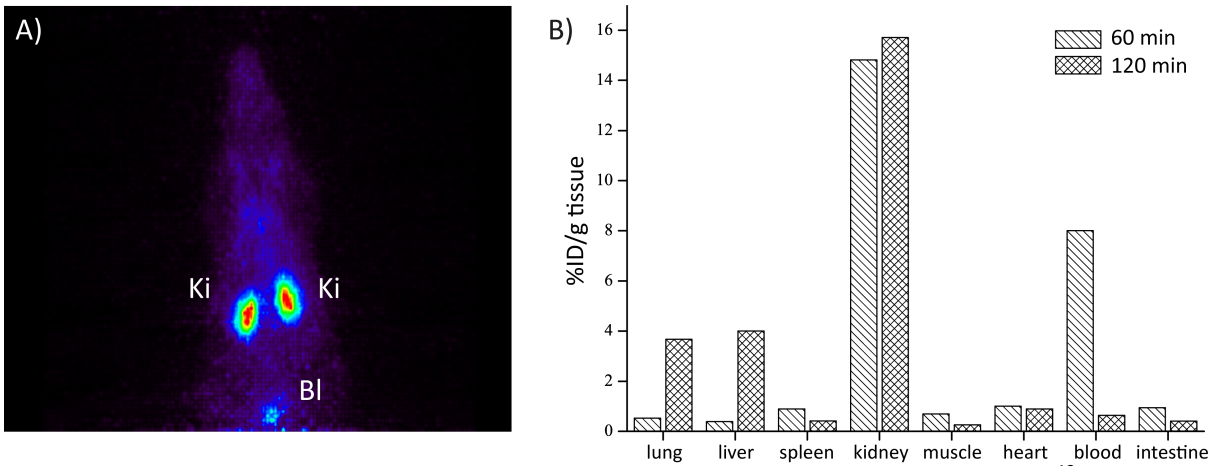

Figure 7. **A**) MIP of a 30 min micro PET scan of a C57BL/6 mouse injected with 2 MBq of the ^{18}F-labeled nanoparticles; Ki: kidney, Bl: bladder. **B**) Biodistribution of the ^{18}F-labeled nanoparticles after 60 min and 120 min after i.v. injection.

The predominantly excretion of radioactivity over the kidneys could be confirmed by *ex vivo* biodistribution studies at 60 min and 120 min p.i. (Figure 7B). Furthermore, a high blood accumulation (8%ID/g) could be observed, whereas in the liver and lungs only tracer activities below 1%ID/g were measured. However, this pattern changed after 120 min, when the tracer was cleared from the blood and the radioactivity levels in the liver and lungs increased to ~4%ID/g. The *in vivo* behavior of the new ^{18}F-labeled nanoparticles displays the distribution pattern of low and high mw macromolecules.[19] It is assumed either there is an dynamic equilibrium of the p((HPMA)-*b*-(LMA)) copolymers on the surface of the nanoparticles, or the copolymers simply dissociate from the surface area. The high blood levels of labeled nanoparticles is clearly assigned to the unimpaired

nanoparticle, whereas the high activity in the kidney can be referred to a dissociated fraction of the ^{18}F-labeled p((HPMA)-*b*-(LMA)) copolymer.

To conclude, this work itself describes the possibility to perform a personalized diagnostic and therapy of FR-positive tumors by using the ^{18}F-labeled OEG-folate for patient selection and localization of the malignancies. If the tumor to background levels are too low, a ^{18}F-labeled serine-folate conjugate could be used to further improve the pharmacokinetics. After visualization of the tumors, FR-targeted BNCT and/or the macromolecular drug delivery systems can be used for an effective treatment by preventing healthy tissues from damage.

3.1 References

(1) Ross, T. L.; Honer, M.; Lam, P. Y. H.; Mindt, T. L.; Groehn, V.; Schibli, R.; Schubiger, P. A.; Ametamey, S. M. *Bioconjugate Chem.* **2008**, *19*, 2462–70.

(2) Fischer, C. R.; Müller, C.; Reber, J.; Müller, A.; Krämer, S. D.; Ametamey, S. M.; Schibli, R. *Bioconjugate Chem.* **2012**, *23*, 805–13.

(3) Junkers, M. *Aldrich Chem Files* **2010**, *10*, 2–5.

(4) Krishnamurthy, S.; Brown, H. C. *J. Org. Chem.* **1976**, *41*, 3064–3066.

(5) Brenner, E.; Baldwin, M.; Tamagnan, G. *Tetrahedron Lett.* **2004**, *45*, 3607–3610.

(6) McCulloch, A. W.; McInnes, A. G. *Can. J. Chem.* **1974**, *52*, 3569–3576.

(7) Wipf, P.; Graham, T. H. *Org. Biomol. Chem.* **2005**, *3*, 31–5.

(8) Cottrell, T. L. *The Strengths of Chemical Bonds*; 1958.

(9) Liu, S.; Lin, T.-P.; Li, D.; Leamer, L.; Shan, H.; Li, Z.; Gabbaï, F. P.; Conti, P. S. *Theranostics* **2013**, *3*, 181–9.

(10) Iwata, R.; Pascali, C.; Bogni, A.; Furumoto, S.; Terasaki, K.; Yanai, K. *Appl. Radiat. Isot.* **2002**, *57*, 347–52.

(11) Dayal, B.; Salen, G.; Toome, B.; Tint, G. S.; Shefer, S.; Padia, J. *Steroids* **1990**, *55*, 233–7.

(12) Sibrian-Vazquez, M.; Vicente, M. G. H. *Boron Sci.: New Technol. Appl.* **2011**, 203–232.

(13) Nakamura, H. *Boron Sci.: New Technologies and Applications*; Hosmane, N., Ed.; CRC Press, 2011; pp. 203–232.

(14) Mier, W.; Gabel, D.; Haberkorn, U. *Z. Anorg. Allg. Chem.* **2004**, *630*, 1258–1262.

(15) Zhu, Y.; Yan, K.; Maguire, J. *Curr. Chem. Biol.* **2007**, *1*, 141–149.

(16) Schieferstein, H.; Betzel, T.; Fischer, C. R.; Ross, T. L. *EJIMMI Res.* **2013**, *3*, 68.

(17) Wang, C.; Qi, C. *Tetrahedron* **2013**, *69*, 5348–5354.

(18) Kuroda, H. *Polymer* **1997**, *38*, 6049–6054.

(19) Allmeroth, M.; Moderegger, D.; Biesalski, B.; Koynov, K.; Rösch, F.; Thews, O.; Zentel, R. *Biomacromolecules* **2011**, *12*, 2841–9.

(20) Barz, M.; Canal, F.; Koynov, K.; Zentel, R.; Vicent, M. J. *Biomacromolecules* **2010**, *11*, 2274–2282.

(21) Hemmelmann, M.; Kurzbach, D.; Koynov, K.; Hinderberger, D.; Zentel, R. *Biomacromolecules* **2012**, *13*, 4065–74.

(22) Duncan, R.; Vicent, M. J. *Adv. Drug Deliv. Rev.* **2010**, *62*, 272–82.

(23) Landfester, K. *Angew. Chem. Int. Ed. Engl.* **2009**, *48*, 4488–507.

4 Summary

The high potential to target the FR has already proven its outstanding role in the diagnostic field as well as in numerous therapeutic approaches. Especially, in the field of ^{18}F-labeled folates for PET imaging a facile and robust synthesis route to an ^{18}F-labeled folate for routine application is still lacking. However, many approaches have been made to overcome this gap. Additionally, the FR-targeting concept has also been used in many therapeutic approaches as targeting vector for radiotherapy ligands or macromolecular carrier systems.

This dissertation deals on the one hand with the evaluation of a novel ^{18}F-labeled folate and the advancement of the used prosthetic group labeling by developing an amino acid-based (serine) prosthetic group and on the other hand with the *in vivo* evaluation of folate-pHPMA conjugates as potential drug delivery systems. Furthermore, the synthesis of ^{18}F-labeled nanoparticles obtained via the miniemulsion process in combination with solvent evaporation has been shown.

The ^{18}F-labeled folate displayed the highly efficient and robust ^{18}F-click labeling in combination with an oligoethylene-based spacer approach to introduce polarity into the molecule. *Ex vivo* biodistribution and *in vivo* micro PET studies showed an enhancement of the *in vivo* behavior with a strongly reduced background signal compared to the original ^{18}F-click folate, which is alkyl spacer-based. Based on these promising results, a serine derivative as new *clickable* ^{18}F-labeling prosthetic group was developed and tested in first ^{18}F-labeling studies of a RDG-peptide. The amino acid approach enables on the one hand the introduction of a very hydrophilic prosthetic group and on the other hand a very biocompatible compound since serine is an endogenous amino acid.

For the first time, the FR-targeting concept could be transferred to the BNCT for enhancing tumor uptake and contrast of ^{10}B-pharmaceuticals. Up to date most clinically approved ^{10}B-phramaceuticals use only inefficient or passive targeting to accumulate at tumor sites. For this reason, the folate scaffold has been conjugated to two different

boron clusters (carboran and BSH), which were evaluated *in vitro* showing that FR-targeting resulted in a significant increase of the boron concentration in tumor cells.

The FR-targeting concept, however, is not restricted to the conjugation of small molecules. It could also been demonstrated that FA was successfully coupled to pHPMA polymers (low and high mw polymers), which were evaluated in *in vivo* micro PET studies and biodistribution experiments after ^{18}F-labeling. The physicochemical properties were investigated showing aggregation *in vitro* of the high mw polymers after conjugation to FA. *In vivo* experiments indicated that the low mw polymer accomplishes more criteria for the application in health science as drug delivery systems. Furthermore, PDLLA-based colloids could be ^{18}F-labeled for the first time using the highly efficient and mild CuAAC reaction and the biodistribution was investigated using dissection and micro PET imaging.

To summarize this broad positioned work, we could successfully demonstrate that the FR-targeting concept can be applied in multifarious applications from improved diagnostics to effective therapeutics to make a small contribution to patient identification and staging for individualized and personalized cancer treatment based on FR-targeting.

5 Publications and Ongoing Studies

"^{18}F-click labeling and preclinical evaluation of a new ^{18}F-folate for PET imaging"

Hanno Schieferstein, Thomas Betzel, Cindy R. Fischer, Tobias L. Ross

EJNMMI Res. 2013, *3*:68

"Highly Polar ^{18}F-Labeled Serines for Convenient Amino Acid-based Click-Labeling of Biomolecules"

Hanno Schieferstein, Tobias L. Ross

Angew. Chem., Int. Ed., *submitted*

"Synthesis and Evaluation of Boron Folates for Boron-Neutron-Capture-Therapy (BNCT)"

Kathrin Kettenbach, **Hanno Schieferstein**, Catrin Grunewald, Dorothée Iffland, Christian Schütz, Gabriele Hampel, Nicolas Bings, Tobias L. Ross

Mol. Cancer Ther., *in preparation for submission*

"^{18}F-Radiolabeling and Evaluation of Folate-pHPMA Conjugates via PET"

Hanno Schieferstein, Annette Kelsch, Achim Reibel, Kaloian Koynov, Matthias Barz[2], Hans-Georg Buchholz, Nicole Bausbacher, Oliver Thews, Rudolf Zentel, Tobias L. Ross

Biomacromolecules., *in preparation for submission*

"Bodydistribution of ^{18}F-labeled Nanoparticles stabilized by HPMA-based Block Copolymers"

Annette Kelsch*, **Hanno Schieferstein***, Nicole Bausbacher, Tobias L. Ross, Katharina Landfester, Rudolf Zentel

* both authors have contributed equally

in preparation for submission

^{18}F-click labeling and preclinical evaluation of a new ^{18}F-folate for PET imaging

Hanno Schieferstein, Thomas Betzel, Cindy R Fischer, Tobias L Ross

Institute of Nuclear Chemistry, Johannes Gutenberg University Mainz, Mainz 55128, Germany

Center for Radiopharmaceutical Sciences of ETH, PSI and USZ, Institute of Pharmaceutical Sciences, ETH Zürich, Zurich 8093, Switzerland

Radiochemistry/Radiopharmacy, Department of Nuclear Medicine, Hannover Medical School, Hannover 30623, Germany

Background

Since the folate receptor (FR) is a well-established target in tumor imaging and tumor therapy, many radiofolates and chemotherapeutics based on the natural ligand folic acid have been developed and investigated.[1] Folic acid is a vitamin essential for *de novo* DNA synthesis in eukaryotic cells where it is converted into the co-enzyme 5,6,7,8-tetrahydrofolate and acts as a carrier of C1 building blocks.[2] The FR is a glycosyl phosphatidylinositol-anchored protein which has a high affinity for folic acid (K_d ~ 1 nM) and is (over)expressed in many types of human tumors, e.g., ovarian cancer or endometrial cancer.[3-5] The expression of the FR in healthy tissues, directly accessible from the bloodstream, is limited to the proximal tubules of the kidneys, where it is involved in the recycling of folic acid from renal excretion.[6,7] Hence, specific accumulation of an intravenously administered radiofolate is mostly associated with a pathophysiological cause. Therefore, many folate conjugates, featuring different radionuclides for various applications, have been developed and evaluated in the past two decades.[8] The introduction of FR targeting to tumor diagnostics in the field of nuclear imaging goes back to 1981 using ^{125}I-labeled *pteroylglutamic acid* (equals folic acid)[9], which was not particularly promising. In spite of that, a number of radiofolates have been reported, many of which feature radionuclides useful in single photon emission computed tomography. Examples are ^{111}In-diethylenetriamine pentaacetic acid-folates, ^{99m}Tc-folates, and ^{67}Ga-folates, which showed promising results in preclinical *in vivo* tumor targeting.[10-13] In 2006, Bettio and co-workers synthesized a ^{18}F-labeled folate for application in positron emission tomography (PET), formed by amide coupling of the prosthetic group 4-[^{18}F]fluorobenzylamine and native folic acid. The coupling afforded a mixture of α- and γ-regioisomers, which was not separated before *in vivo* animal PET studies.[14] Good visualization of FR-positive tumors was achieved; however, one major drawback was the time-consuming multistep radiosynthesis, the regioisomeric mixture, and low radiochemical yields. To overcome the complicated radiosynthesis and provide a regioselective product, another radiofolate was developed using the copper-catalyzed azide-alkyne cycloaddition (CuAAC, click reaction). The structural isomerism was

circumvented by a regioselective derivatization at the carboxylic acid in the γ-position of the folate precursor.[15] The radio-CuAAC clearly simplified the radiosynthesis and gave the first ^{18}F-click-labeled folate in high radiochemical yields within ≤90 min. However, *in vivo* animal PET imaging revealed an unfavorable biological distribution profile with a poor signal-to-noise ratio and a very high abdominal background, which were assumed to be related to the loss of hydrophilicity of the tracer. To retain the polarity of the radiofolate, which is obviously necessary for favorable *in vivo* characteristics, a radiofolate was developed by coupling a folate carbohydrazide with 2-[^{18}F]fluoro-2-deoxy-d-glucose ([^{18}F]FDG) via oxime formation with the open-chain form of glucose.[16] Another approach of Fischer and co-workers also used the efficiency of CuAAC for ^{18}F-radiolabeling in combination with the inevitable polarity of [^{18}F]FDG to enhance pharmacodynamics.[17] In this case, a ^{18}F-labeled azido-FDG derivative was used as a prosthetic group and coupled via CuAAC to an alkyne-carrying γ-folate. This derivative gave promising results, with significantly enhanced tumor-to-background ratios due to a high tumor uptake and reduced background. An alternative to folate radioconjugates is the derivatives synthesized by direct ^{18}F-fluorination approaches, which led to the development of 2′-[^{18}F]fluorofolic acid, synthesized via a nucleophilic aromatic ^{18}F-flourination at the 2′-position of folic acid.[18] Preclinical evaluation showed excellent *in vivo* behavior with a clear-cut visualization of FR-positive KB tumors and healthy tissues (kidneys). However, the direct ^{18}F-fluorination of folic acid requires protecting group chemistry with cleavage under harsh conditions, resulting in degradation and poor radiochemical yields. Very recently, an optimized version of 2′-[^{18}F]fluorofolic acid was reported.[19] The intended aromatic ring was exchanged by a pyridine to further reduce the electron density in the 2′-position for the nucleophilic ^{18}F-fluorination. As a result, the radiochemical yield was significantly improved and, besides an increased liver uptake, the pharmacokinetic characteristics were excellent for *in vivo* PET imaging. In respect to the ^{18}F-folates via prosthetic group conjugates, a new ^{18}F-polyethylene glycol (PEG)-folate was developed very recently and published while this manuscript was in preparation. The new ^{18}F-PEG-folate was not primarily intended for tumor imaging, but for targeting the FR-β on

activated macrophages in a rat model of arthritis.[20] The major objective was to reduce background signal in the periarticular tissue by following a similar strategy as for the here presented work to improve pharmacokinetics by introducing oligoethylene glycol spacers.[21]

The aim of this study was to investigate the influence of oligoethylene glycol spacers on the polarity of a conjugated ^{18}F-labeled radiofolate, when introduced at the γ-position of the glutamate residue, since many drugs showed improved pharmacokinetics due to PEGylation.[21] In this paper, the synthesis, radiolabeling, and preclinical evaluation of a new ^{18}F-labeled γ-radiofolate are reported. The radiofolate features oligoethylene glycol spacers for enhanced polarity and is radiolabeled via the highly efficient radio-CuAAC reaction.

Methods

General

Reagents and solvents were purchased from Sigma-Aldrich Co. (St. Luois, MO, USA), Acros (Geel, Belgium), or Merck AG (Darmstadt, Germany) and used without further purification, unless otherwise stated. The building block N^2-*N*,*N*-dimethylaminomethylene-10-formylpteoric acid was generously provided by Merck & Cie AG (Schaffhausen, Switzerland). ^{3}H-folic acid was purchased from Moravek Biochemicals Inc. (Brea, CA, USA). Reactions were monitored by thin layer chromatography (performed on Merck silica gel 60 F254, not modified, pre-coated silica gel on aluminum-supported plates) or high-performance liquid chromatography (HPLC).

Radiosyntheses were performed either in a manipulator-equipped hot cell by conventional heating (starting activities >5 GBq [^{18}F]fluoride) or manually in a lead-shielded fume hood (starting activities ≤5 GBq [^{18}F]fluoride) using a focused laboratory microwave (CEM Discover, Matthews, NC, USA) in the following mode: 1-min pre-run, 10-min reaction time, and a maximum power of 300 W.

Information about compound characterizations and analytical or preparative HPLC as well as radio-HPLC conditions can be found in Additional file 1.

Small animal PET imaging was performed on a *GE eXplore Vista PET/CT* scanner (GE Healthcare, Little Chalfont, UK).

*Synthesis of the 2-(2-(2-(prop-2-yn-1-yloxy)ethoxy)ethoxy)ethyl 4-methylbenzenesulfonate (**10**)*

The 2-(2-(2-(prop-2-yn-1-yloxy)ethoxy)ethoxy)ethyl 4-methylbenzenesulfonate was prepared using a modified method of that described by Li and co-workers.[22] Briefly, 2-[2-(2-hydroxyethoxy)ethoxy]ethanol (**7**) (5 g, 33 mmol) was added to a suspension of sodium hydride (1.3 g, 33 mmol) in dimethylformamide (15 mL) cooled to 0°C, and propargyl bromide (3.5 mL, 33 mmol) was added. The reaction mixture was then allowed to warm to room temperature and stirred. After 24 h, the solvent was removed and the crude reaction mixture purified by silica gel column chromatography (ethyl acetate/*n*-hexane, 1:2) to give **8** as a pale yellow oil in 42% yield (2,6 g, 14 mmol).

Compound **8** (1 g, 5 mmol) and *p*-toluenesulfonyl chloride (1.9 g, 10 mmol) were dissolved in anhydrous dichloromethane (10 mL) and cooled to 0°C. 1,4-Diazabicyclo[2.2.2]octene (560 mg, 5 mmol), dissolved in 5 mL dichloromethane, was added dropwise to the solution. The reaction mixture was stirred for 2 h at room temperature and gave, after purification by column chromatography, **10** as a colorless oil (54%, 940 mg, 2.7 mmol).

*Synthesis of 3-(2-(2-(2-fluoroethoxy)ethoxy)ethoxy)prop-1-yne (**9**)*

Compound **8** (200 mg, 1 mmol) was dissolved in anhydrous dichloromethane (5 mL) and cooled to 0°C. To this solution, *N*,*N*-diaminosulfur trifluoride (132 µL, 1 mmol) was added, and the reaction mixture maintained at 0°C for 1 h, before allowing it to warm to room temperature and stirring for additional 5 h. After removal of the solvent *in vacuo*, the

crude reaction mixture was purified via column chromatography to give **9** as a pale yellow oil (40%, 80 mg, 0.4 mmol).

*Synthesis of γ-(11-azido-3,6,9-trioxaundecanyl)folic acid amide (**5**)*

N-(*tert*-butoxycarbonyl)glutamic acid α-methyl ester (**1**) (200 mg, 0.7 mmol) was reacted with 11-azido-3,6,9-trioxaundecan-1-amine (152 mg, 0.7 mmol) using 298 mg (0.7 mmol) 1-cyano-2-ethoxy-2-oxoethylidenaminooxy)dimethylamino-morpholino-carbenium hexafluorophosphate (COMU) as coupling agent and 2 eq. of 2,2,6,6-tetramethylpiperidine (TMP) as base. The reaction was performed in acetonitrile and stirred at room temperature for 16 h. The crude residue was re-dissolved in dichloromethane (20 mL) and washed successively with aqueous hydrochloric acid (0.1M, 2 × 10 mL) and aqueous sodium hydrogen carbonate (0.1M, 3 × 10 mL), dried over sodium sulfate, and filtered, and the solvent was removed under reduced pressure. Purification by silica gel column chromatography (ethyl acetate/hexane, 10:1) afforded a colorless oil (86%, 274 mg, 0.6 mmol). Compound **2** was deprotected using dichloromethane/trifluoroacetic acid (1:1, 10 mL) at room temperature for 12 h. The mixture was co-evaporated with toluene (3 × 5 mL) and used in the next step without further purification. After deprotection, **3** was coupled to the activated ester of protected pteroic acid (230 mg, 0.6 mmol) prepared by adding COMU (256 mg, 0.6 mmol) and TMP (2 eq.) in anhydrous dimethylformamide (5 mL) to give the activated ester complex. The deprotected **3** was added dropwise to the solution, and the mixture was stirred at 40°C for 12 h, after which the solvent was removed *in vacuo*. The crude reaction mixture was re-dissolved in dichloromethane and extracted analogously to the coupling reaction of **1** and 11-azido-3,6,9-trioxaundecan-1-amine. The mixture was purified first by aluminum oxide column chromatography (dichloromethane/methanol, 15:1) followed by a second *flash* chromatography on silica gel (ethyl acetate/methanol, 5:1), giving 103 mg (0.14 mmol) of **4** as a yellow powder.

For deprotection of **4**, 30 mg (0.04 mmol) was dissolved in a 1M sodium hydroxide solution (1 mL) and stirred at room temperature for 16 h. After 16 h, the pH was adjusted

to 2 using a 2M hydrochloric acid solution resulting in the precipitation of the product. After centrifugation, the supernatant was removed and the product was washed twice with water, leading to 19 mg (0.03 mmol) of the final azido-folate **5** (Scheme 1).

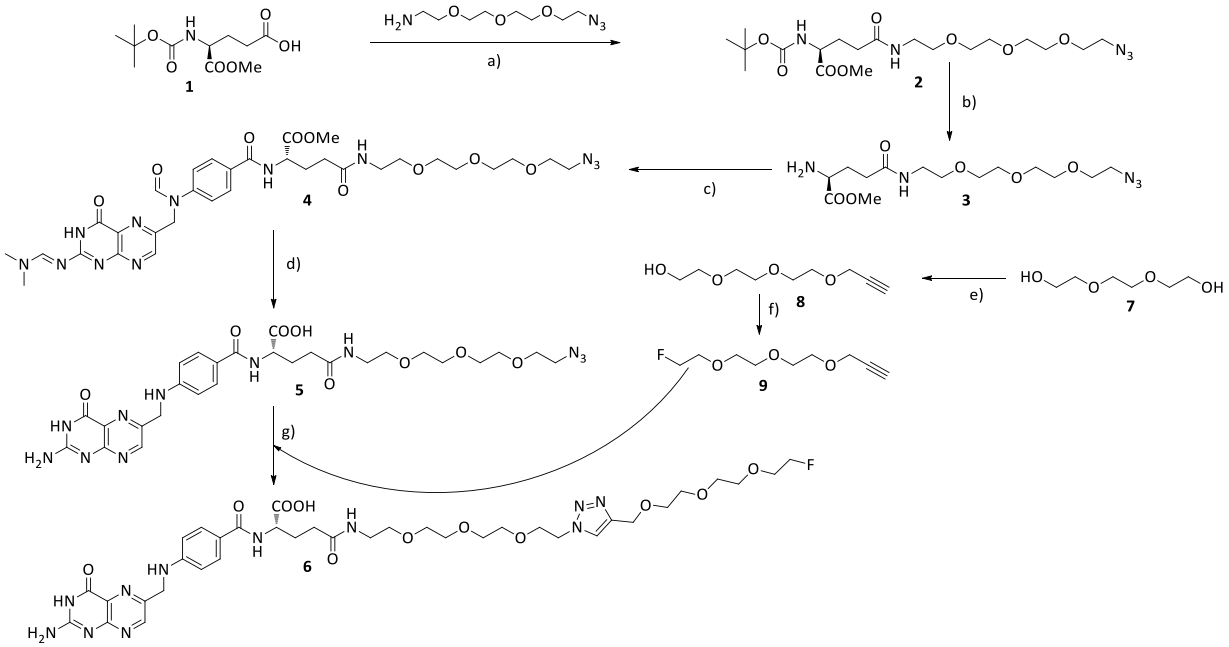

Scheme 1. Synthesis of the azido-folate (5) and the reference compound (6). (a) COMU, TMP, MeCN, rt. (b) DCM/TFA (1:1), rt. (c) COMU, TMP, DMF, rt. (d) 1M NaOH (aq.), rt. (e) NaH, DMF, 0°C to rt. (f) DCM, DAST, 0°C to rt. (g) Cu(I)I, sodium ascorbate, MeCN, 0.05M phosphate buffer, DIPEA/2,6-lutidine (1:1), microwave.

*Synthesis of the 16-(4-(((2-amino-4-oxo-3,4-dihydropteridin-6-yl)methyl)amino)benz-amido)-1-(4-(2-(2-(2-fluoroethoxy)ethoxy)ethoxy)-1H-1,2,3-triazol-1-yl)-13-oxo-3,6,9-trioxa-12-azaheptadecan-17-oic acid (**6**)*

Compound **5** (5 mg, 0.02 mmol), copper(I) iodide (0.5 eq.), and a mixture of diisopropylethyl amine (DIPEA)/2,6-lutidine (1 eq.) were dissolved in 2 mL acetonitrile. The reaction was allowed to react for 15 min before 15 mg (0.02 mmol) of **9**, dissolved in 2 mL of 0.05 M phosphate buffer, was added in one portion to the reaction mixture. The mixture was reacted at 130°C for 9 min in a sealed vessel using a laboratory microwave at 55 W and purified by semi-preparative HPLC. The combined fractions were lyophilized and re-dissolved in water (1 mL) and the pH was adjusted to 2, leading to the precipitation of the product, which was separated by centrifugation (10,000 rpm, 8 min).

The supernatant was removed and the precipitate was lyophilized, yielding 9 mg (0.01 mmol) of **6** as a yellow solid.

*Synthesis of 16-(4-(((2-amino-4-oxo-3,4-dihydropteridin-6-yl)methyl)amino)benzamido)-1-(4-(2-(2-(2-[^{18}F]fluoroethoxy)ethoxy)ethoxy)-1H-1,2,3-triazol-1-yl)-13-oxo-3,6,9-trioxa-12-azaheptadecan-17-oic acid (**[^{18}F]12**)*

No-carrier-added (n.c.a.) [^{18}F]fluoride was produced via the ^{18}O(p,n)^{18}F nuclear reaction. Isotopically enriched [^{18}O]water (97% enrichment) was irradiated by an 18-MeV proton beam and trapped on an anion exchange resin (Sep-Pak Light Waters Accell Plus QMA Cartridge, Waters Corporation, Milford, MA, USA), which was pre-conditioned with a 1M potassium carbonate solution (10 mL) and rinsed with pure water (20 mL). The n.c.a. [^{18}F]fluoride was eluted with 1 mL of a methanolic tetrabutylammonium hydroxide solution (95.7 mg tetrabutylammonium hydroxide (TBA-OH) × 30 H_2O in 2 mL methanol) into a 5-mL sealed reaction vial. After azeotropic drying using three portions of acetonitrile, 800 µL of acetonitrile was added to the dry [^{18}F]fluoride-base mixture. The 2-(2-(2-(prop-2-yn-1-yloxy)ethoxy)ethoxy)ethyl 4-methylbenzenesulfonate **10** (6 mg, 17 µmol) was dissolved in 200 µL acetonitrile and subsequently added to the [^{18}F]fluoride solution. The reaction time was 12 min at 110°C, followed by quenching with 5 mL of 50 mM phosphate buffer. After HPLC purification (t_R([^{18}F]**11**), 15 min) the fraction of the ^{18}F-labeled prosthetic group was diluted by addition of 25 mL of water and trapped on a Phenomenex Strata X-C18 cartridge (Torrance, CA, USA). After washing with 5 mL of water, the final prosthetic group **11** was eluted into a 5-mL reaction vial with 800 µL acetonitrile, which was equipped with copper(II) acetate (1.5 mg in 500 µL), sodium ascorbate (9 mg in 500 µL of 0.05M phosphate buffer), and **5** (2 mg in 500 µL of 0.05 M phosphate buffer). The click reaction was performed at 110°C. After 13 min, the reaction was quenched with 0.05M phosphate buffer and filled to a final volume of 5 mL. Purification was performed using the semi-preparative radio-HPLC system described before. The product fraction was acidified by addition of 500 µL of a 1-M hydrochloric acid solution and passed through a Phenomenex Strata X-C cartridge. After washing with

5 mL of water, the final radiotracer was eluted with 2.5 mL phosphate-buffered saline containing 10% ethanol.

Relative lipophilicity (*k'* value)

The relative lipophilicity of **6** was determined as capacity factor *k*' (*k*' = ($t_{retention} - t_{solvent}$) / $t_{solvent}$) by reversed-phase HPLC using a methanol-phosphoric acid buffer eluent system at pH 2. Under these conditions, the retention time (t_R) was 4.49 min, which equals a *k*' value of 1.12. This method has already been described elsewhere.[18]

In vitro binding affinity assays

Displacement studies using [^{3}H]folic acid and the non-radioactive reference compound **6** were carried out according to the previously described procedure[18]

In vitro metabolite studies in fetal calf serum

A solution of [^{18}F]**12** (50 µL, approximately 5 MBq) was incubated with 500 µL of fetal calf serum (FCS) at 37°C and the mixture shaken at 900 rpm. The time points were set between 0 and 90 min using 500 µL of FCS and 50 µL of the radiotracer for each time point. Plasma proteins were precipitated by addition of cold acetonitrile (300 µL), followed by centrifugation (10,000 rpm, 10 min). An aliquot of each time point (15, 30, 60, and 90 min, 100 µL) was injected into the analytical radio-HPLC system for analytics.

In vivo studies

All animal experiments were approved by the local veterinary department and complied with Swiss and local laws on animal protection. Female CD-1 nude mice (Charles River, Sulzfeld, Germany) were fed with a folate-deficient rodent diet (Harlan Laboratories, Indianapolis, IN, USA). After an acclimatization period of 5 to 7 days, human KB tumor cells (5 × 10^6 cells in 0.1 mL sterile phosphate-buffered saline (PBS)) were inoculated subcutaneously on both shoulders of each mouse. Twelve days later, the animals were

intravenously injected with [^{18}F]**12** (approximately 5 MBq, 100 µL). Blocking studies were performed with excess folic acid dissolved in PBS (100 µg in 100 µL) injected 5 min prior to [^{18}F]**12**. Animals were euthanized at the indicated time points, and selected organs and tissues were collected, weighed, and measured in a γ-counter. The incorporated radioactivity was expressed as percentage injected dose per gram (%ID/g) of tissue. PET/computed tomography (CT) experiments were performed with a dedicated small-animal PET/CT scanner (eXplore Vista PET/CT, Sedecal, Algete, Spain/GE Healthcare). Animals were intravenously injected with [^{18}F]**12** (approximately 13 MBq, 100 µL). For scanning, mice were anesthetized with isoflurane in an air/oxygen mixture. The PET scans were acquired from 60 to 90 min post-injection (p.i.) followed by a CT. After acquisition, PET data were reconstructed in user-defined time frames, and the fused datasets of PET and CT were analyzed with PMOD software (version 3.4).

Results and discussion

Organic chemistry

The regioselective buildup synthesis of the γ-azido-folate **5** was straightforward. Starting with the selectively protected glutamic acid **1**, which had its γ-position free for derivatization, it gave the desired glutamic acid derivative **2** after coupling of 11-azido-3,6,9-trioxaundecan-1-amine in good yields of 86% (Scheme 1). The incorporation of the oligoethylene glycol spacer carrying a terminal azido moiety enabled conjugation via the CuAAC reaction, which had previously been applied as an efficient and high-yielding radiolabeling protocol [15]. After Boc removal at the glutamate **2**, it was coupled to protected pteroic acid. As reported by Subiros-Funosas and co-workers[23], a side reaction occurs using COMU as coupling agent. The protected azido-folate **4** was purified in two steps: first by aluminum oxide column chromatography, followed by a second column based on silica gel. As a consequence of two purification steps in particular, the pure product was obtained only in moderate to low yields of 20%. Deprotection of azido-folate (prot.) **4** by addition of a 1M sodium hydroxide solution, followed by precipitation at pH 2

and washing with pure water, afforded the final azido-folate **5** in 50% yield. The azido-folate **5** was employed as a precursor for the synthesis of the reference compound and the radiotracer. In this respect, the counterpart of the CuAAC reaction, 3-(2-(2-(2-fluoroethoxy)ethoxy)ethoxy)prop-1-yne **9**, was synthesized according to the literature.[22] Triethylene glycol was reacted with propargyl bromide to introduce the alkyne functionality into the prosthetic group for the CuAAC. The free hydroxyl group was either fluorinated via diethylaminosulfur trifluoride (DAST) for the reference

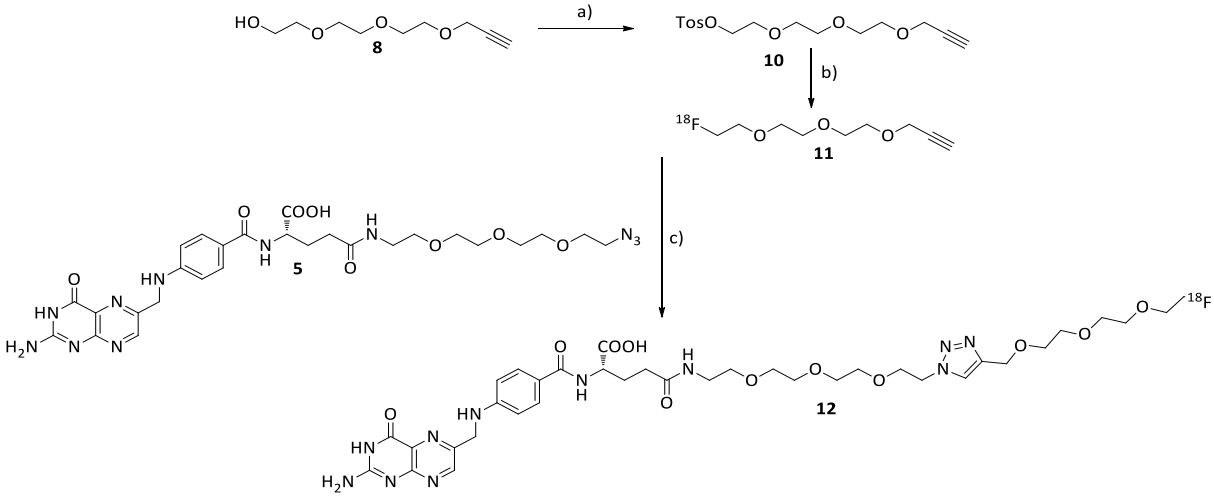

Scheme 2. Synthesis of the prosthetic group precursor (10), followed by radiosynthesis of the ^{18}F-labeled prosthetic group **[^{18}F]11** and ^{18}F-labeled radiofolate **[^{18}F]12**. (a) DCM, TEA, Tos-Cl, rt. (b) TBA-OH, acetonitrile, 110°C. (c) Cu(II)acetate, sodium ascorbate, 110°C, acetonitrile/water/0.05M phosphate buffer.

compound or tosylated to act as a radiolabeling precursor for the nucleophilic aliphatic ^{18}F-fluorination (Scheme 2). The synthesis of the reference compound was screened in terms of the catalyzing copper species, base, solvent system, and type of heating (Table 1). Optimized conditions comprised Cu(I)I; DIPEA/2,6-lutidine; a mixture of water, buffer, and acetonitrile; and microwave-supported heating. This combination clearly reduced unfavorable side reactions and product degradation during reference compound synthesis.

Table 1. Results of the CuAAC reaction for different catalysts and heating conditions

	Cu(I)I (%)	Cu(I)I + sodium ascorbate (%)	Cu(II)acetate + sodium ascorbate (%)	Cu(II)sulfate + sodium ascorbate (%)
Microwave[a]	60 ± 3	22	45	n.d.
Oil bath[b]	20	n.d.	30	15

For all reactions, the used copper concentration was kept constant, whereby that for reactions using copper(II) ascorbate was used in tenfold excess. Yields were determined by HPLC, and for the superior conditions, $n = 3$. [a]Performed at 110°C for 10 min and a mode with 1-min pre-run and a maximum power of 300 W; [b]performed at 65°C. n.d., no data.

Relative lipophilicity (k' value)

The capacity factor k' ($k' = (t_{retention} - t_{solvent}) / t_{solvent}$) was determined using reversed-phase HPLC and enables different (radio)folates to be compared based on their polarity. The values determined can be used to give hint to the *in vivo* behavior in terms of the degree of hepatobiliary excretion by comparison with literature examples. The ^{18}F-click folate[15] and the 2'-[^{18}F]fluorofolic acid[18] have k' values of 2.28 and 0.53, respectively, of which the latter shows an excellent *in vivo* profile while the former is unfavorable in terms of its abdominal background. The determined k' value of 1.12 for compound **12** was between these two values of the previously synthesized radiofolates, suggesting that it might be a promising candidate for *in vivo* imaging applications.

Radiochemistry

The established radio-CuAAC approach was used for labeling as it has been proven to produce high radiochemical yields and obviates the need for protecting groups. The prosthetic group [^{18}F]**11** was synthesized by following a modified protocol of Li et al.[22] using tetrabutylammonium hydroxide as base during ^{18}F-fluorination instead of the Kryptofix 2.2.2/potassium carbonate system. In agreement with the findings of Li et al.[22], the radiofluorination showed a strong temperature dependency with a conversion of greater than 75% achieved with conventional heating at 110°C. The crude reaction mixture was purified by semi-preparative HPLC that resulted in 58% radiochemical yield (RCY). After dilution, the prosthetic group [^{18}F]**11** was trapped on a Phenomenex Strata X-

C18 cartridge and eluted directly into a vial containing the azido-folate **5**, the copper catalyst, and sodium ascorbate. This final setup was a result of an extensive optimization process, as the conditions used during the non-radioactive reference synthesis could not be successfully translated into radiolabeling. The use of Cu(I)I and a mixture of DIPEA/2,6-lutidine led to significant degradation of the precursor **5** and thus resulted in poor RCYs of 5% to 10%. Therefore, the system described above with no additional base was found optimal. A much higher RCY (≥90%) was achieved through microwave-supported radio-CuAAC; however, such a protocol was not applicable in the manipulator-equipped hot cell used for productions of [^{18}F]**12** for animal studies. For the radiolabeling of the prosthetic group by conventional heating, higher amounts of radioactivity (40 to 100 GBq) were used to compensate for reduced RCY (58%) and prolonged reaction times. Final purification of the radiofolate was achieved using a semi-preparative HPLC system, followed by acidification (pH 1) and subsequent fixation on a Phenomenex Strata X-C cartridge. The loaded cartridge was flushed with water and the product [^{18}F]**12** eluted with PBS buffer containing 10% of ethanol. Sterile filtration of the eluate gave the final product [^{18}F]**12** in a very high radiochemical purity of ≥97% and good overall RCY of 8.7% within a total radiosynthesis time of approximately 2.5 h (end of bombardment (EOB)) for the hot cell-based synthesis. The overall radiosynthesis time could be reduced to approximately 90 min (EOB) using microwave-supported hands-on synthesis in a lead-shielded hood.

In vitro metabolite studies in fetal calf serum

The stability of the new radiotracer, [^{18}F]**12**, was evaluated in the presence of FCS. For this purpose, [^{18}F]**12** was added to FCS and incubated at 37°C. At certain time points (15, 30, 60, and 90 min), aliquots were extracted and proteins removed by precipitation. The integrity of the radiotracer was determined by analytical radio-HPLC. No degradation or defluorination of the radiotracer [^{18}F]**12** was observed over 90 min, and therefore, [^{18}F]**12** can be considered stable for the general duration of a microPET (µPET) scan.

In vitro binding affinity assays

FR-positive human KB cells were kept under folate-deficient conditions to adjust the folate concentration levels to that of the human serum.[24] The half maximal inhibitory concentration (IC_{50}) values of native folic acid and the reference compound **6** were determined by displacement studies using [^{3}H]folic acid. The displacement curves indicated a slightly higher IC_{50} value for **6** of 3.1 nM (n = 3) compared to that of native folic acid (0.9 nM (n = 3)) (Figure 1). Using the Cheng-Prusoff equation[25], a K_i value of 1.6 nM was calculated, assuming a K_d value for [^{3}H]folic acid of 1 nM [4,5,26]. This value is in the very low nanomolar range and close to the K_d value of native folic acid (approximately 1 nM), indicating a very high affinity of **6** to the folate receptor.

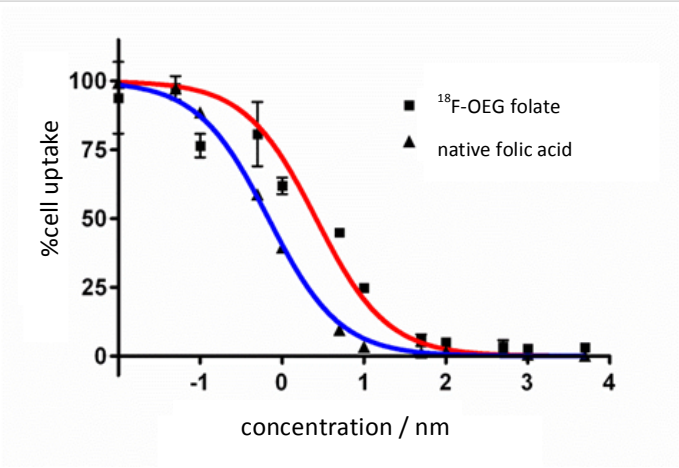

Figure 1. Displacement assay. Displacement assay of native folic acid and ^{18}F-OEG-folate **6** using [^{3}H]folic acid and human KB cells in cell suspension. Experiments were conducted in triplicate (n = 3).

Ex vivo biodistribution studies

Biodistribution studies of the new ^{18}F-folate [^{18}F]**12** were performed using human KB tumor-bearing nude mice, determined at 30, 60, and 90 min post-injection. Additionally, a blocking experiment after 60 min using native folic acid was done, whereby 100 µg of native folic acid in PBS buffer (100 µL) was injected 2 min before radiotracer administration. At 30 min post-injection, it was found that the tracer [^{18}F]**12** accumulated in the tumor (3.4%ID/g) and in the kidneys (42%ID/g), remaining constant over 90 min

(Table 2). Selective blocking of the folate receptors led to a decrease in specific radiotracer accumulation of 94% in KB tumors and 99% in kidneys (Figure 2). The strong blocking effect reflected the high specificity of the tracer to the FR *in vivo*. Unspecific liver uptake decreased from 5.2%ID/g to 2.1%ID/g over 90 min similar to the background radioactivity in the feces and gall bladder (Table 2), which is believed to be a beneficial effect of the increased polarity of this novel radiofolate. Compared to the biodistribution profile at 45 min post-injection of the former ^{18}F-click folate by Ross and co-workers, the specific uptake of the original ^{18}F-click folate in KB tumors was retained, whereas the specific kidney uptake more than doubled. This indicated a stronger tendency to renal excretion, more likely a result of the increased polarity of the new ^{18}F-folate [^{18}F]**12**. Additionally, the highest unspecific background accumulation in the gall bladder was reduced by half. This background reduction correlated with the more renal excretion and the two times lower *k*' value as an indicator of lipophilicity of the here presented radiofolate.[15] Similarly, the unspecific accumulation in the liver, feces, and empty intestine was noticeably reduced compared to that of the ^{18}F-click folate. On the other hand, the still increased uptake levels in the gall bladder and feces were evidence of a prominent hepatobiliary elimination pathway of [^{18}F]**12**. However, distinct changes in the molecular structure of the folate-based radioconjugate [^{18}F]**12** induced a higher polarity into the lead molecule ^{18}F-click folate and a significant reduction of the *in vivo* background. The new ^{18}F-folate still showed abdominal background levels, which might impede *in vivo* PET imaging in this region. However, as our results and very recent results of the new and similar ^{18}F-PEG-folate demonstrated[20], such radiofolates have high potential for *in vivo* PET imaging of FR-positive tissues.

Table 2. *Ex vivo* biodistribution studies of ^{18}F-OEG-folate 12 in mice at various time points and ^{18}F-click folate

	30 min p.i. (*n* = 3)	**60 min p.i. (*n* = 3)**	**90 min p.i. (*n* = 3)**	**60 min p.i. blockade[a] (*n* = 3)**	***^{18}F-click folate* 45 min p.i.[b] (*n* = 4)**
%ID/g					
Blood	0.20 ± 0.02	0.18 ± 0.01	0.16 ± 0.02	0.04 ± 0.01	0.13 ± 0.01
Heart	1.81 ± 0.61	1.09 ± 0.07	0.79 ± 0.16	0.02 ± 0.01	0.90 ± 0.22
Lung	1.21 ± 0.15	1.02 ± 0.7	0.86 ± 0.17	0.04 ± 0.03	0.85 ± 0.04
Spleen	0.53 ± 0.14	0.49 ± 0.04	0.43 ± 0.08	0.06 ± 0.03	0.33 ± 0.12
Kidneys	*41.80 ± 2.58*	*40.77 ± 4.34*	*41.04 ± 7.04*	*0.26 ± 0.08*	*16.53 ± 2.22*
Stomach (empty)	2.18 ± 0.76	1.39 ± 0.13	0.96 ± 0.37	0.12 ± 0.11	2.50 ± 0.6
Intestines (empty)	23.52 ± 7.37	4.56 ± 2.31	1.92 ± 0.52	14.72 ± 19.32	19.59 ± 5.26
Feces	164.2 ± 72.5	29.48 ± 19.04	11.36 ± 4.29	105.5 ± 128.7	56.00 ± 27.64
Liver	5.24 ± 1.57	4.05 ± 0.67	2.30 ± 0.54	0.21 ± 0.09	1.71 ± 0.14
Gall bladder	309.3 ± 187.6	133.2 ± 67.38	55.13 ± n.d.	775.5 ± 206.5	667.4 ± 530.1
Muscle	1.91 ± 0.25	1.64 ± 0.46	1.17 ± 0.03	0.08 ± 0.09	n.d.
Bone	1.47 ± 0.05	1.13 ± 0.21	0.84 ± 0.16	0.06 ± 0.06	0.13 ± 0.01
Salivary glands	8.01 ± 1.16	9.28 ± 1.68	7.03 ± 1.98	0.20 ± 0.18	n.d.
Tumor	*3.39 ± 0.54*	*3.39 ± 0.44*	*3.54 ± 0.68*	*0.19 ± 0.07*	*3.13 ± 0.83*
Ratio of tumor to organ or tissue					
Blood	16.81 ± 3.13	18.95 ± 2.68	22.72 ± 6.73		24,08 ± 0.82
Liver	0.69 ± 0.22	0.86 ± 0.19	1.55 ± 0.15		1.18 ± 0.69
Kidney	*0.08 ± 0.02*	*0.08 ± 0.01*	*0.09 ± 0.01*		*0.19 ± 1.38*

[a]In the blockade group, each animal received 100 µg/100 µL of folic acid in PBS 5 min before radiotracer injection; [b]biodistribution data of the ^{18}F-click folate were taken from.[15] n.d., no data.

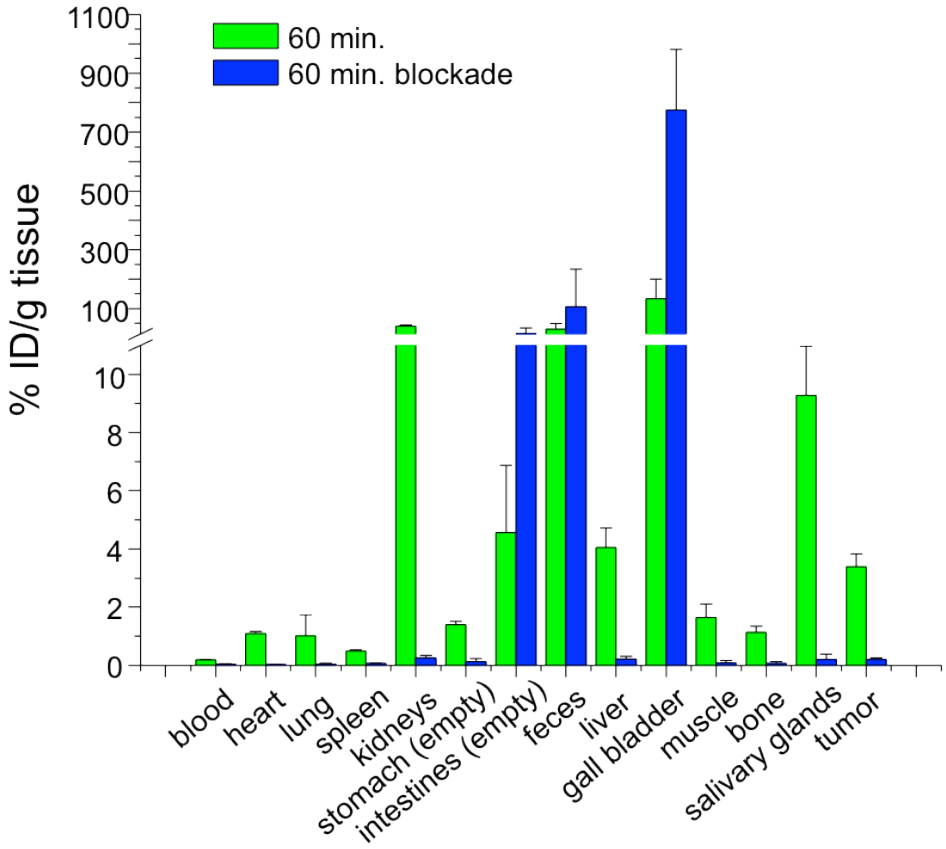

Figure 2. Results of *ex vivo* biodistribution studies under control and blockade conditions using [^{18}F]12 in mice. The human KB tumor-bearing nude mice were euthanized 60 min post-injection. Data are expressed as percentage injected dose per gram tissue (%ID/g). In the blockade group (*n = 3*), 100 µg of native folic acid was injected into each animal 5 min prior to the radiotracer administration, whereas the control group (*n* = 3) received a corresponding volume of PBS.

In vivo µPET studies

µPET studies were performed using KB tumor-bearing mice, in which tumors were located in the area above the left and right shoulders. The animals were scanned 60 to 90 min after radiotracer injection to fade out noise signals from perfusion and renal excretion in order to get a higher tumor-to-background contrast. As expected from *ex vivo* biodistribution studies, the kidneys and abdomen (gall bladder, intestines, liver) showed the highest tracer uptake. This caused a poor tumor-to-background contrast in the maximum intensity projection (Figure 3). Tumors are clearly visible in selected coronal

slices of µPET scans. In agreement with findings of earlier investigations[14,15], the tracer accumulation was observed only in the outer rim of tumors, indicating that the tumor perfusion is very heterogeneous and the blood supply into the tumor center is believed to be hindered or even blocked. These results are assumed to be due to a high internal tumoral pressure or even a necrotic tumor center of such fast growing xenograft models as already demonstrated in previous studies.[27-29] Increased radioactivity accumulation was observed in the abdominal area, which led to an elevated background. This unspecific accumulation is mainly due to the pronounced hepatobiliary excretion. Despite this prominent background, [^{18}F]**12** showed a significantly reduced hepatobiliary excretion compared to the previously synthesized ^{18}F-click folate and most importantly facilitated visualization of FR-positive tumors on the maximum intensity projection. The elevated abdominal background points to a lipophilicity of [^{18}F]**12** not yet being optimal, although the HPLC capacity factor (*k*' value) of the non-radioactive reference compound **6** indicated that. The uptake in the gall bladder, liver, feces, and intestine could strongly be reduced compared to the original ^{18}F-click folate.[15]

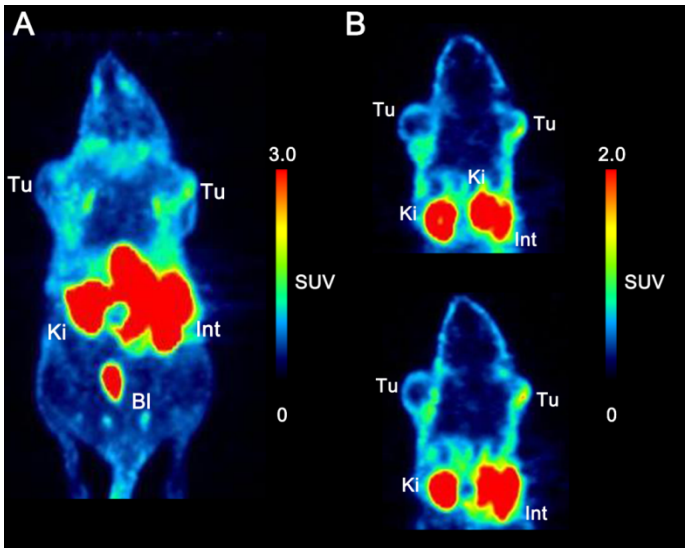

Figure 3. PET images of a KB tumor-bearing mouse. Scanned 60 to 90 min after injection of [^{18}F]-OEG-folate **12** (approximately 13 MBq). **(A)** Maximal intensity projection. **(B)** Two representative coronal slices. Tu, tumor; Ki, kidneys; Bl, urinary bladder; Int, intestines/feces; SUV, *standardized uptake value.*

Conclusions

There is a demand for ^{18}F-labeled radiofolates with superior *in vivo* behavior, which can be produced using a facile and robust radiosynthesis transferrable into routine productions for clinical applications. To this end, a novel ^{18}F-radio folate, with high affinity to the folate receptor and increased polarity compared to the original lead compound (^{18}F-click folate), was developed. ^{18}F-labeling of the prosthetic group and the radio-CuAAC reaction were optimized to give excellent RCYs and purities within short reaction times. ^{18}F-click chemistry, by providing a facile and robust labeling procedure, again confirmed its outstanding potential and its particular suitability for ^{18}F-labeling of folate derivatives. *Ex vivo* biodistribution experiments showed a highly specific uptake in FR-positive human KB tumors and kidneys. Compared to the previously developed ^{18}F-click folate, the new radiofolate [^{18}F]**12** showed significantly reduced hepatobiliary excretion while maintaining the tumor uptake. In *in vivo* µPET studies, human KB tumor xenografts were visualized, while a moderate tumor-to-background contrast was found for [^{18}F]**12**. Coronal slices of the PET imaging clearly showed a heterogeneous uptake of [^{18}F]**12** in the outer rim of KB xenografts. In comparison to the previously developed [^{18}F]fluoro-deoxy-glucose folate, the new ^{18}F-OEG-folate showed similar background levels. On the other hand, the threefold higher tumor uptake of the [^{18}F]fluoro-deoxy-glucose folate with significantly increased contrast values led to a much better tumor visualization. However, the very recently reported ^{18}F-PEG-folate with structural similarities to the new ^{18}F-OEG-folate gave promising results in imaging FR-expressing activated macrophages in inflammatory diseases. This study confirms the suitability of such PEGylated ^{18}F-folates for *in vivo* PET imaging of FR-positive tissue and their broad potential. In summary, the newly developed ^{18}F-labeled radiofolate has excellent radiochemical availability and exhibits a high and specific affinity to the folate receptor.

Acknowledgements

The authors thank Dr. Cristina Müller and Stephanie Haller for performing biological *in vitro* assays and *ex vivo* biodistribution studies. We also thank Merck & Cie AG (Switzerland) for kindly providing the protected pteroic acid. This work has further been supported by the research cluster SAMT of the Johannes Gutenberg University Mainz.

References

(1) Xia, W.; Low, P. S. *J. Med. Chem.* **2010**, *53*, 6811–24.

(2) Leamon, C. P.; Low, P. S. *Drug Discov. Today* **2001**, *6*, 44–51.

(3) Parker, N.; Turk, M. J.; Westrick, E.; Lewis, J. D.; Low, P. S.; Leamon, C. P. *Anal. Biochem.* **2005**, *338*, 284–93.

(4) McHugh, M. *J. Biol Chem.* **1979**, *254*, 11312–11318.

(5) Antony, A. C. *Annu. Rev. Nutr.* **1996**, *16*, 501–521.

(6) Weitman, S. D.; Weinberg, A. G.; Coney, L. R.; Zurawski, V. R.; Jennings, D. S.; Kamen, B. A. **1992**, 6708–6711.

(7) Low, P. S.; Henne, W. A.; Doorneweerd, D. D. *Acc. Chem. Res.* **2008**, *41*, 120–9.

(8) Müller, C. *Curr. Pharm. Des.* **2012**, *18*, 1058–1083.

(9) Walton, L. *Med. Lab. Sci.* **1981**, *38*, 187–95.

(10) Wang, S.; Lee, R. J.; Mathias, C. J.; Green, M. a; Low, P. S. *Bioconjugate Chem.* **1996**, *7*, 56–62.

(11) Mindt, T. L.; Müller, C.; Melis, M.; de Jong, M.; Schibli, R. *Bioconjugate Chem.* **2008**, *19*, 1689–95.

(12) Müller, C.; Vlahov, I. R.; Santhapuram, H. K. R.; Leamon, C. P.; Schibli, R. *Nucl. Med. Biol.* **2011**, *38*, 715–23.

(13) Mathias, C. J.; Wang, S.; Waters, D. J.; Turek, J. J.; Low, P. S.; Green, M. A. *J. Nucl. Med.* **1998**, *39*, 1579–1585.

(14) Bettio, A.; Honer, M.; Müller, C.; Brühlmeier, M.; Müller, U.; Schibli, R.; Groehn, V.; Schubiger, A. P.; Ametamey, S. M. *J. Nucl. Med.* **2006**, *47*, 1153–60.

(15) Ross, T. L.; Honer, M.; Lam, P. Y. H.; Mindt, T. L.; Groehn, V.; Schibli, R.; Schubiger, P. A.; Ametamey, S. M. *Bioconjugate Chem.* **2008**, *19*, 2462–70.

(16) Al Jammaz, I.; Al-Otaibi, B.; Amer, S.; Al-Hokbany, N.; Okarvi, S. *Nucl. Med. Biol.* **2012**, *39***,** 864–870.

(17) Fischer, C. R.; Müller, C.; Reber, J.; Müller, A.; Krämer, S. D.; Ametamey, S. M.; Schibli, R. *Bioconjugate Chem.* **2012**, *23*, 805–13.

(18) Ross, T. L.; Honer, M.; Müller, C.; Groehn, V.; Schibli, R.; Ametamey, S. M. *J. Nucl. Med.* **2010**, *51*, 1756–62.

(19) Betzel, T.; Mu, C.; Groehn, V.; Mu, A.; Reber, J.; Fischer, C. R.; Kra, S. D.; Schibli, R.; Ametamey, S. M. **2013**, *24*, 205 – 214.

(20) Gent, Y. Y.; Weijers, K.; Molthoff, C. F.; Windhorst, A. D.; Huisman, M. C.; Smith, D. E.; Kularatne, S. a; Jansen, G.; Low, P. S.; Lammertsma, A. a; van der Laken, C. J. *Arthritis Res. Ther.* **2013**, *15*, R37.

(21) Harris, J. M.; Martin, N. E.; Modi, M. *Clin. Pharmacokinet.* **2001**, *40*, 539–551.

(22) Li, Z.-B.; Wu, Z.; Chen, K.; Chin, F. T.; Chen, X. *Bioconjugate Chem.* **2007**, *18*, 1987–94.

(23) Subiros-Funosas, R.; Acosta, G. A.; El-Faham, A.; Albericio, F. *Tetrahedron Lett.* **2009**, *50*, 6200–6202.

(24) Antony, A. C.; Kane, M. A.; Portillo, R. M.; Elwood, P. C.; Kolhouse, J. F. *J. Biol. Chem.* **1985**, *260*, 14911.

(25) Cheng, Y.; Prusoff, W. H. *Biochem. Pharmacol.* **1973**, *22*, 3099–3108.

(26) Kamen, B. A.; Capdevila, a *Proc. Natl. Acad. Sci. U. S. A.* **1986**, *83*, 5983–7.

(27) Zanzonico, P.; O'Donoghue, J.; Chapman, J. D.; Schneider, R.; Cai, S.; Larson, S.; Wen, B.; Chen, Y.; Finn, R.; Ruan, S.; Gerweck, L.; Humm, J.; Ling, C. *Eur. J. Nucl. Med. Mol. Imaging* **2004**, *31*, 117–28.

(28) Müller, C.; Schibli, R.; Forrer, F.; Krenning, E. P.; de Jong, M. *Nucl. Med. Biol.* **2007**, *34*, 603–8.

(29) Mathias, C. J.; Lewis, M. R.; Reichert, D. E.; Laforest, R.; Sharp, T. L.; Lewis, J. S.; Yang, Z.-F.; Waters, D. J.; Snyder, P. W.; Low, P. S.; Welch, M. J.; Green, M. a. *Nucl. Med. Biol.* **2003**, *30*, 725–731.

Supplementary Data

^{18}F-click labeling and preclinical evaluation of a new ^{18}F-folate for PET imaging

Hanno Schieferstein*, Thomas Betzel, Cindy R Fischer, Tobias L Ross*

Institute of Nuclear Chemistry, Johannes Gutenberg University Mainz, Mainz 55128, Germany

Center for Radiopharmaceutical Sciences of ETH, PSI and USZ, Institute of Pharmaceutical Sciences, ETH Zürich, Zurich 8093, Switzerland

Radiochemistry/Radiopharmacy, Department of Nuclear Medicine, Hannover Medical School, Hannover 30623, Germany

Organic Chemistry

^{1}H and ^{13}C nuclear magnetic resonance experiments

^{1}H and ^{13}C nuclear magnetic resonance spectra were recorded on either a Bruker 300 MHz or 400 MHz spectrometer. Chemical shifts (δ) to solvent are reported in parts per million (ppm) relative to tetramethylsilane and referenced; the following abbreviations are used in the experimental section for the description of ^{1}H-NMR spectra: singlet (s), doublet (d), triplet (t), multiplet (m), broad singlet (br). The chemical shifts of complex multiplets are given as the range of their occurrence.

Low-resolution mass spectra (LR-MS) and high-resolution mass spectra (HR-MS)

Low-resolution mass spectra (LR-MS) and high-resolution mass spectra (HR-MS) were recorded on either a Micromass Quattro micro API LC-ESI or a Finnigan MAT90-Spectrometer.

High-Pressure Liquid Chromatography

For analysis and purification via radio-HPLC, a 50 mM phosphate buffer at pH 7.4 was used (11.29 mmol/L $NaH_2PO_4 \times H_2O$ and 38.71 mmol/L $Na_2HPO_4 \times 2H_2O$). Analytical radio-HPLC was performed on an Agilent 1100 series HPLC system, equipped with a 100 µL loop and a GabiStar radiodetector (Raytest). A reversed-phase column (Gemini C18, 5 µm, 4.6 × 250 mm, Phenomenex®) was used at a flow rate of 1 mL/min with a method as follows: 0-5 min 15% **B** (isocratic), 5-50 min 15-50% **B** (gradient) with **A**=50 mM phosphate buffer and **B**=methanol).

For semipreparative purification, a semi-preparative radio-HPLC was used, equipped with a Smartline Pump 1000, Smartline Manager 5000, Smartline UV-detector 2500 (Knauer), GabiStar radiodetector (Raytest) and a 5 mL loop. A reversed-phase column (Gemini C18, 5 µm, 10 × 250 mm, Phenomenex®) was used. The labeled synthon, [^{18}F]fluoroethoxy)ethoxy)ethoxy)-1H-1,2,3-triazol-1-yl)-13-oxo-3,6,9-trioxa-12-

azaheptadecan-17-oic acid ([^{18}F]**11**) was purified, using a flow rate of 3.6 mL/min under isocratic conditions (30% **B**).

For the purification of the radiotracer ^{18}F-OEG folate the following method was used at a flow of 5 mL/min: 0-5 min 100% **A** (isocratic), 5-25 min 0-55% **B** (gradient), 25-35 min 55% **B** (isocratic).

Determination of relative lipophilicity was performed on Dionex ICS-5000 system equipped with a photo diode detector (PDA) using a reversed-phase (Gemini 5μ C18 250 × 4.6 mm, Phenomenex®) column and an isocratic solvent system as follows: 80% aqueous solution (pH 2 with *ortho*phosphoric acid) and 20% acetonitrile.

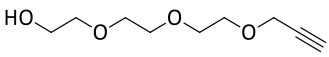

^{1}H NMR (300 MHz, $CDCl_3$) δ 4.16 (d, 2H), 3,71-3.62 (m, 10H), 3.57 (m, 2H), 2.60 (br, 1H), 2.41 (t, 1H) ppm.

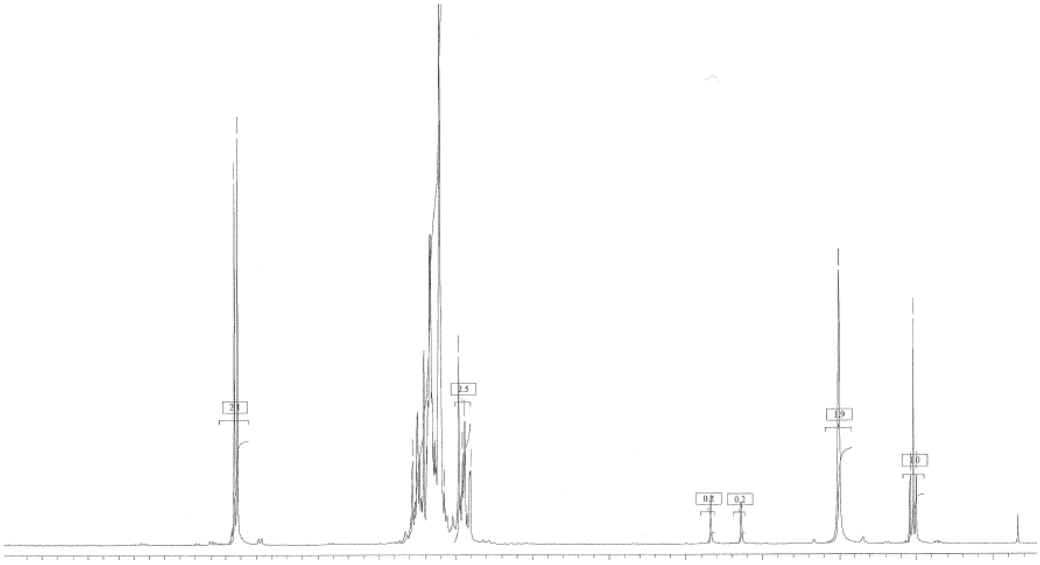

Figure 1. ^{1}H NMR; 300MHz, $CDCl_3$

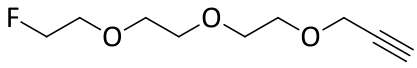

^{1}H NMR (300 MHz, $CDCl_3$) δ 4.61 (t, 1H), 4.44 (t, 1H), 4.17 (d, 2H), 3.67-3.65 (m, 10H), 2.40 (t, 1H) ppm. LR-MS: $[M+H]^+$ = 191.5 (calc. for $C_9H_{15}FO_3$: 191.1).

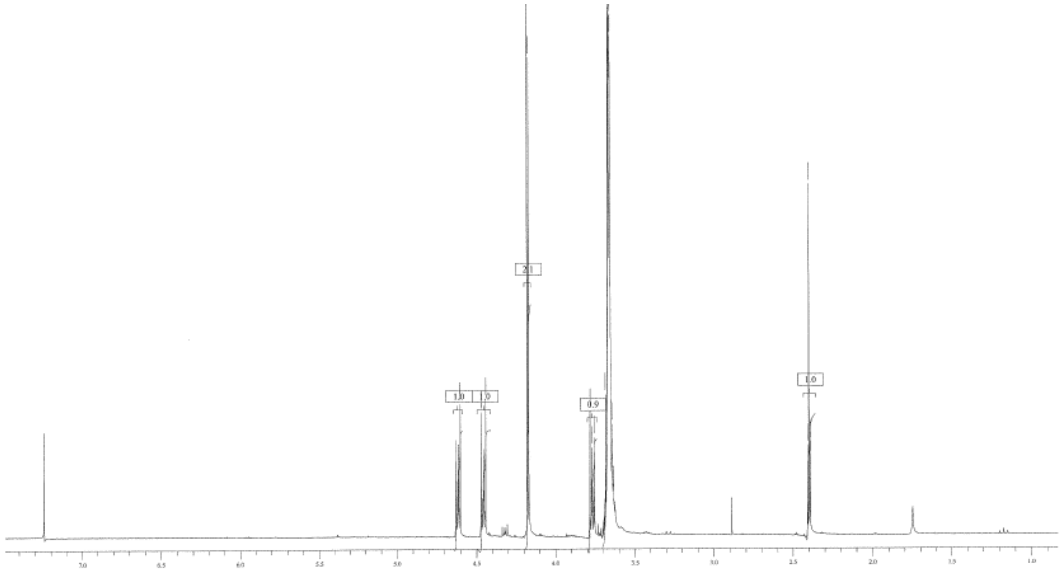

Figure 2. ^{1}H NMR; 300MHz, $CDCl_3$

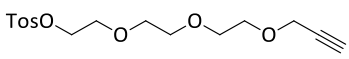

^{1}H NMR (300 MHz, $CDCl_3$) δ 7.75 (d, 2H), 7.30 (d, 2H), 4.15-4.11 (m, 4H), 3.67-3.59 (m, 6H), 2.41 (s, 3H), 2.40 (t, 1H) ppm. ^{13}C NMR (75 MHz, $CDCl_3$) δ 132.96, 129.79, 127.96, 79.59, 74.54, 70.70, 70.53, 70.41, 69.21, 69.04, 68.65, 58.36, 21.61 ppm. LR-MS: $[M+H]^+$ = 343.5 (calc. for $C_{16}H_{22}O_6S$: 343.1).

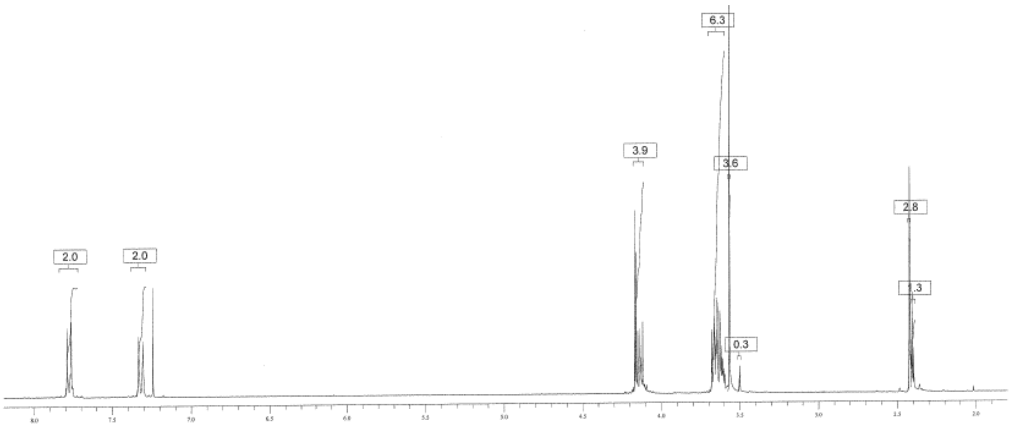

Figure 3. ^{1}H NMR; 300MHz, $CDCl_3$

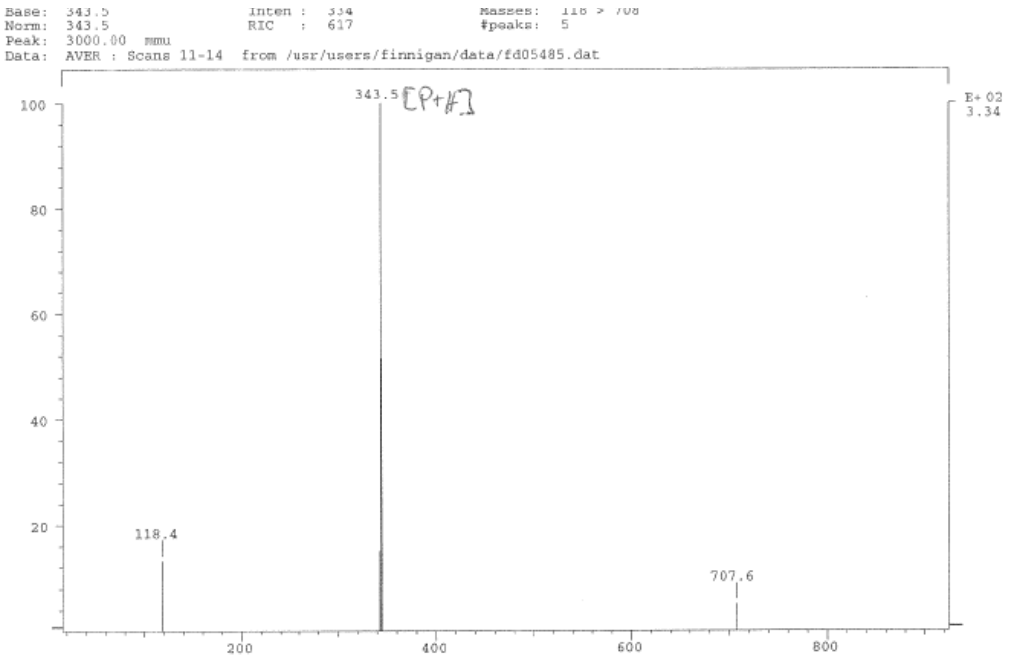

Figure 4. FD-MS; CH_2Cl_2

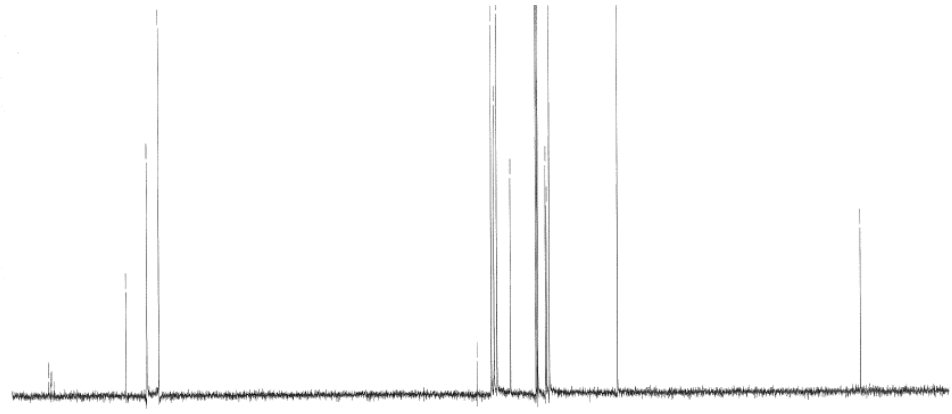

Figure 5. ^{13}C NMR; 300MHz, $CDCl_3$

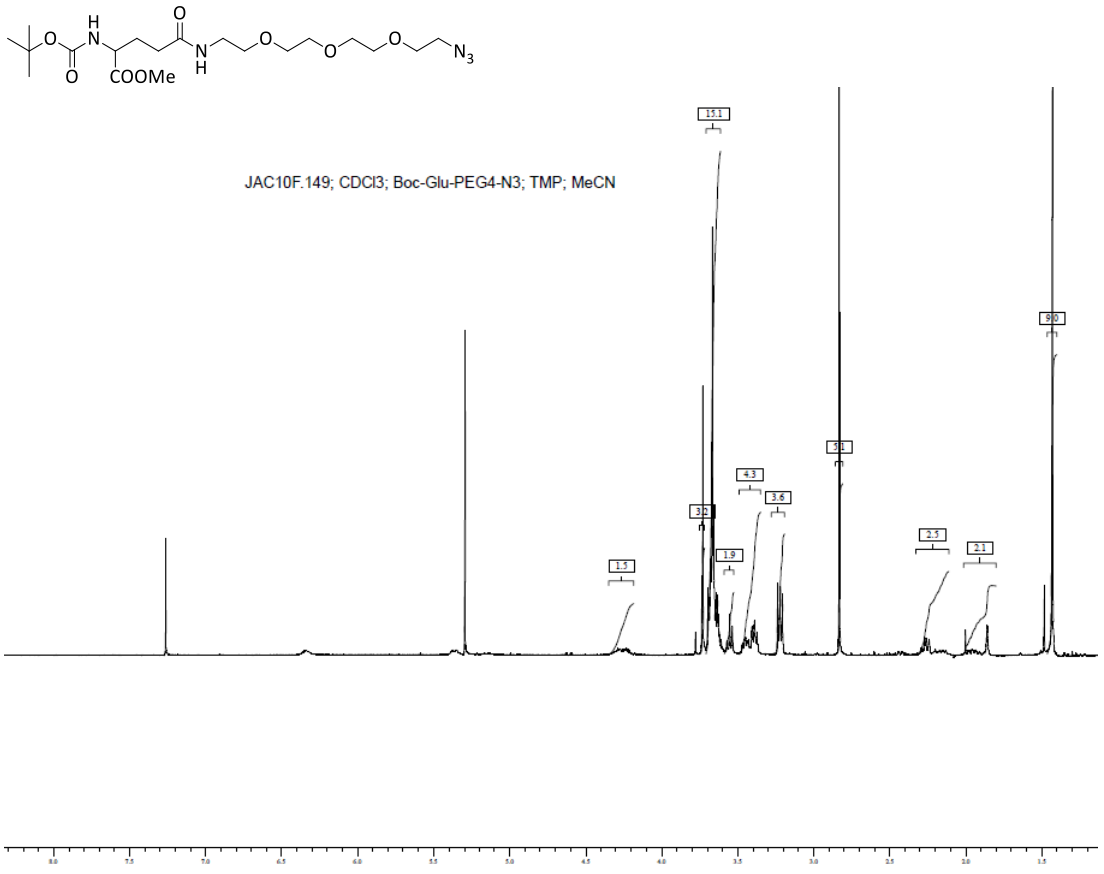

Figure 6. ^{1}H NMR; 300MHz, $CDCl_3$

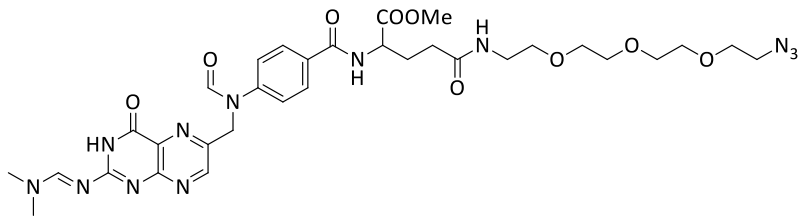

^{1}H NMR (400 MHz, $CDCl_3$) δ 8.91 (s, 1H), 8.70 (d, 2H), 7.87 (d, 2H), 7.30 (d, 2H), 5.29 (s, 2H), 4.61-4.56 (m, 1H), 3.70 (s, 3H), 3.60-3.40 (m, 12H), 3.36 (m, 2H), 3.34 (t, 2H), 3.19 (s, 3H), 3.12 (s, 3H), 2.45-2.32 (m, 2H), 2.20-2.13 (m, 2H) ppm. LR-MS: $[M+H]^+$ = 739.36, $[M+Na]^+$ = 761.33 (calc. for $C_{32}H_{42}N_{12}NaO_9$: 761.31).

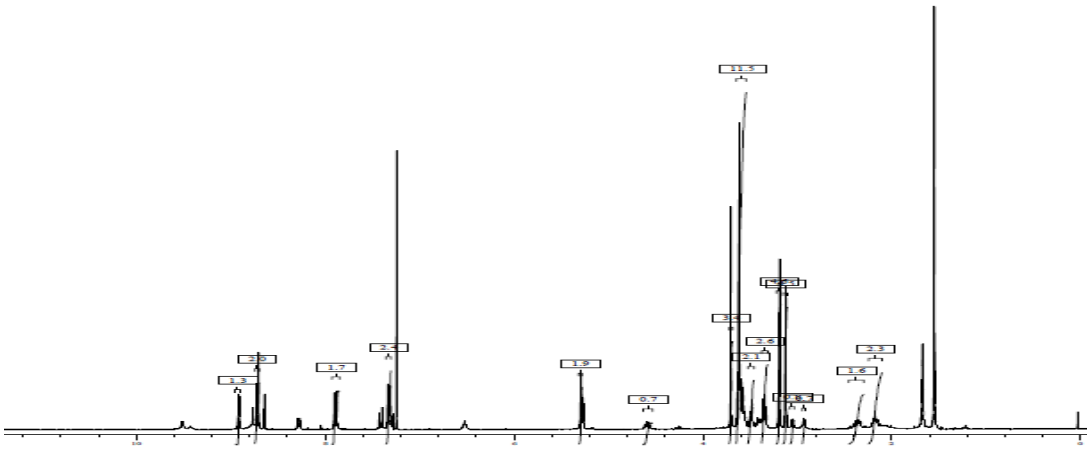

Figure 7. ^{1}H NMR; 400MHz, $CDCl_3$

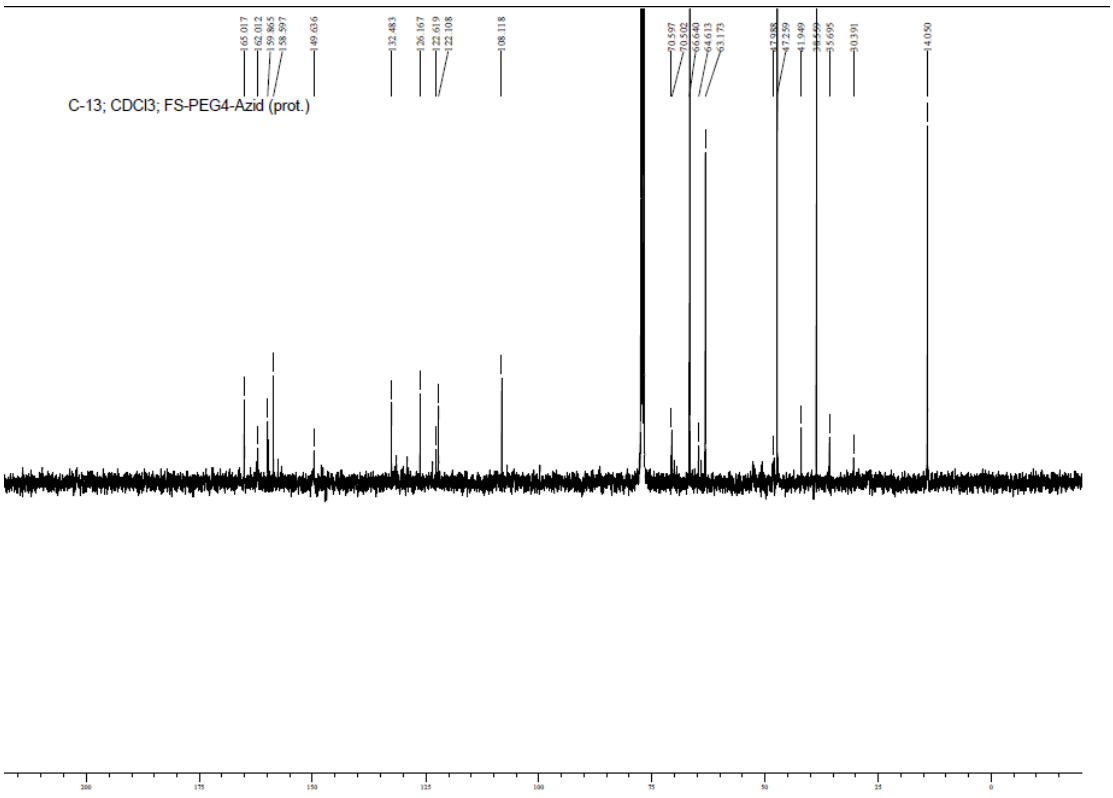

Figure 8. ^{13}C NMR; 300MHz, $CDCl_3$

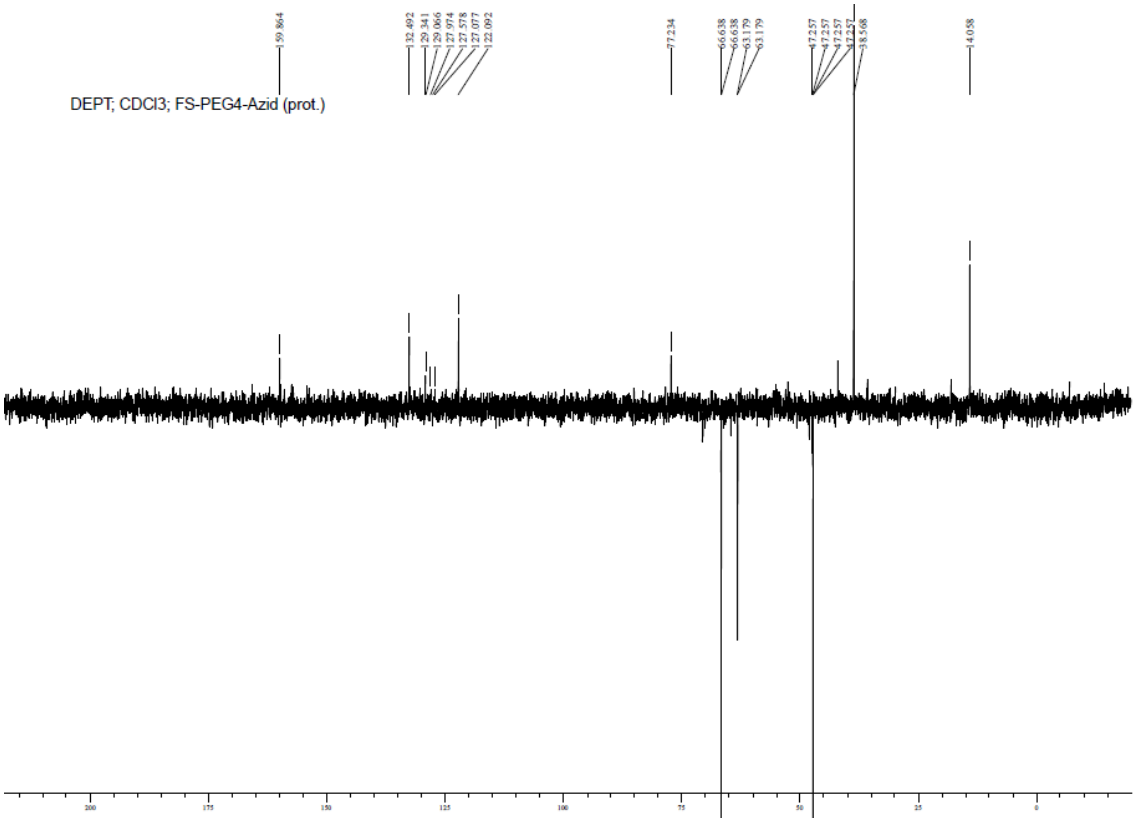

Figure 9. DEPT-135 NMR; 400MHz, $CDCl_3$

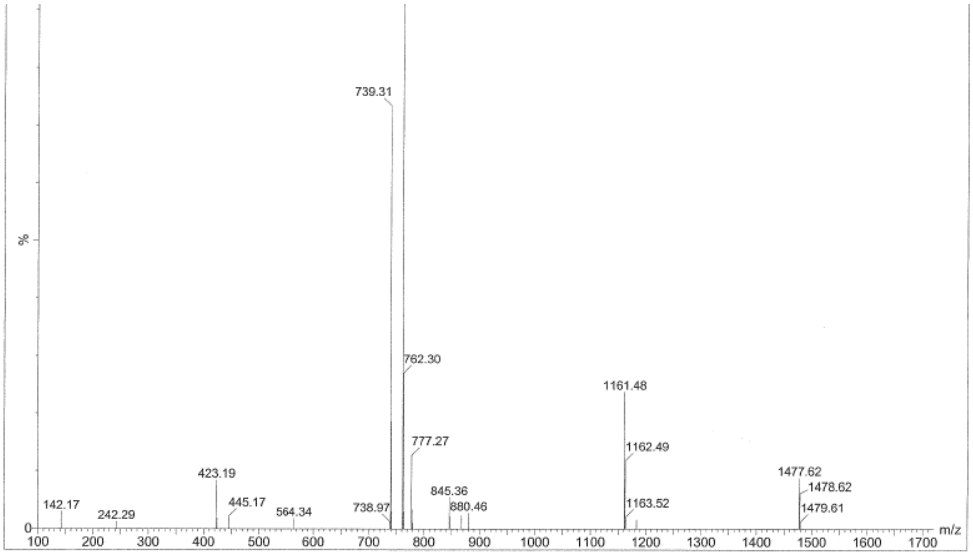

Figure 10. ESI-MS^{+}; MeCN

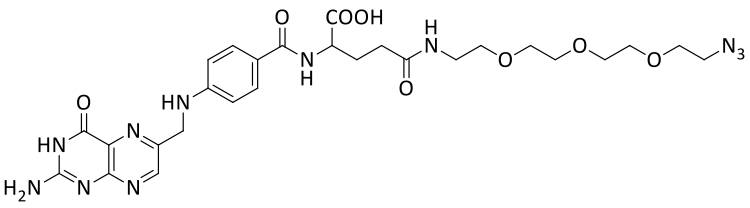

^{1}H NMR (400 MHz, DMSO-d_6) δ 11.52 (br, 1H), 8.63 (s, 1H), 7.62 (d, 2H), 6.61 (d, 2H), 4.46 (s, 2H), 4.26-4.24 (m, 1H), 3.57 (t, 2H), 3.52-3.35 (m, 10H), 3.17 (m, 2H), 2.18 (m, 2H), 2.06-1,99 (m, 1H), 1.93-1.83 (m, 1H) ppm. ^{13}C NMR (100 MHz, DMSO-d_6) δ 174.32, 172.14, 166.70, 154.26, 151.21, 149.13, 129.59, 129.41, 128.41, 121.80, 111.61, 72.79, 70.22, 70.17, 70.12, 70.0, 69.69, 60.65, 52.70, 50.42, 46.36, 32.40, 27.04 ppm. $[M+Na]^+$ = 664.28 (calc. for $C_{27}H_{35}N_{11}NaO_8$: 664.26) HR-MS: $[M+H]^+$ = 642.2746 (calc. for $C_{27}H_{35}N_{11}O_8$: 642.2748).

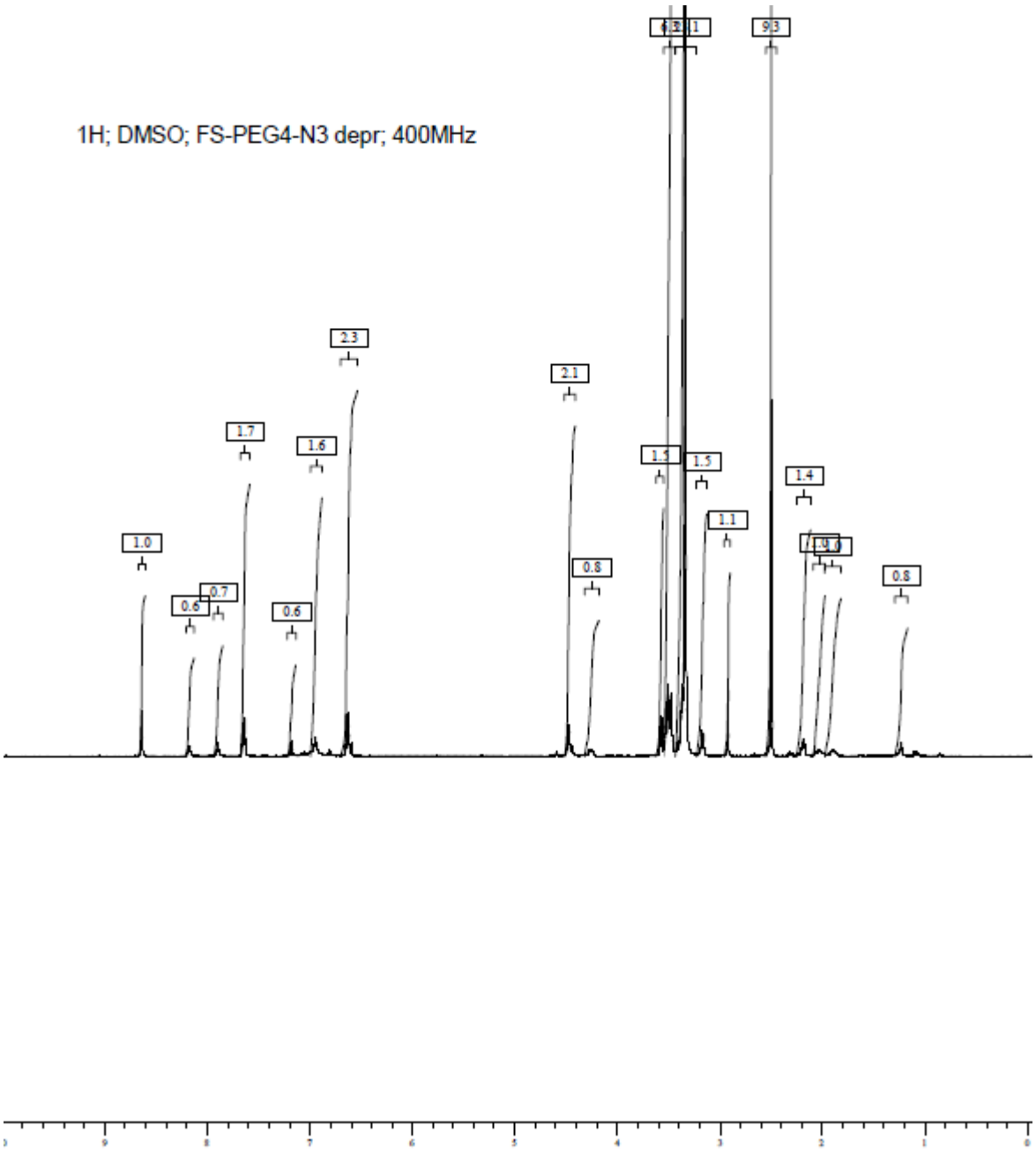

Figure 11. ^{1}H NMR; 400MHz, $CDCl_3$

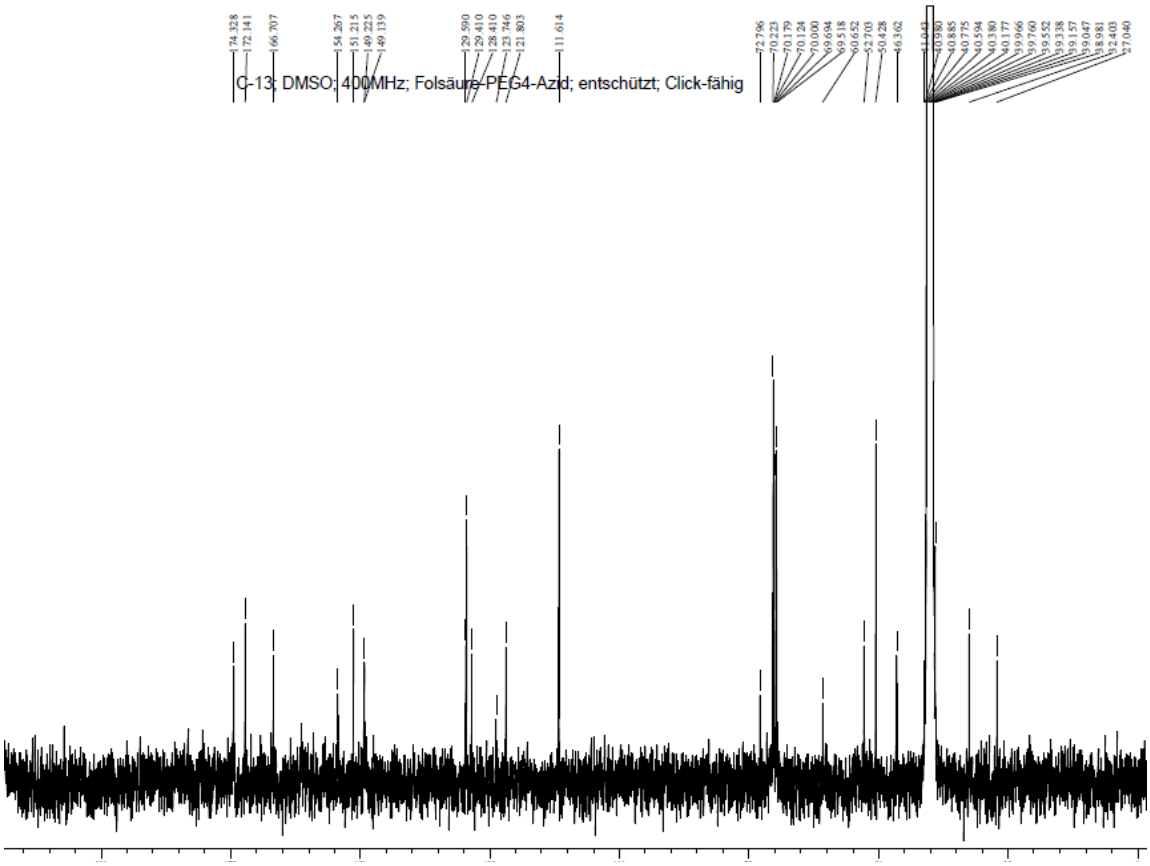

Figure 12. ^{13}C NMR; 400MHz, $CDCl_3$

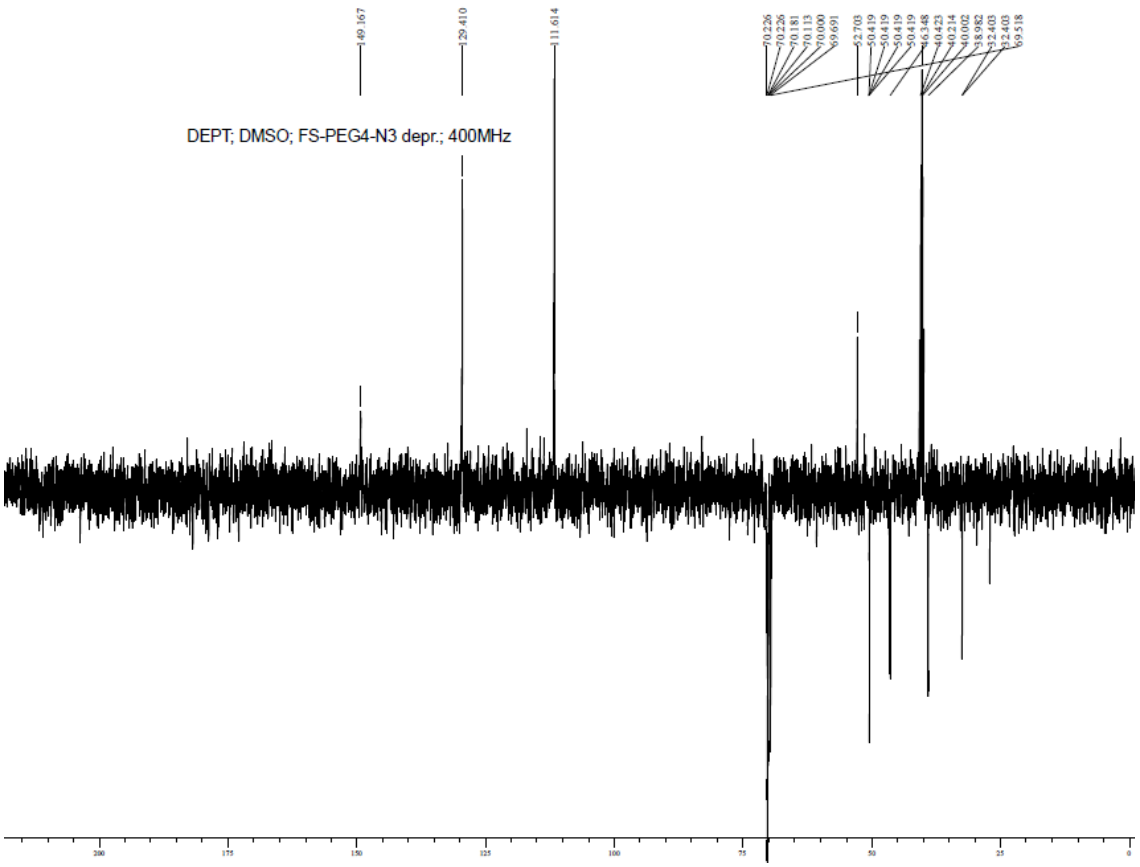

Figure 13. DEPT-135 NMR; 400MHz, $CDCl_3$

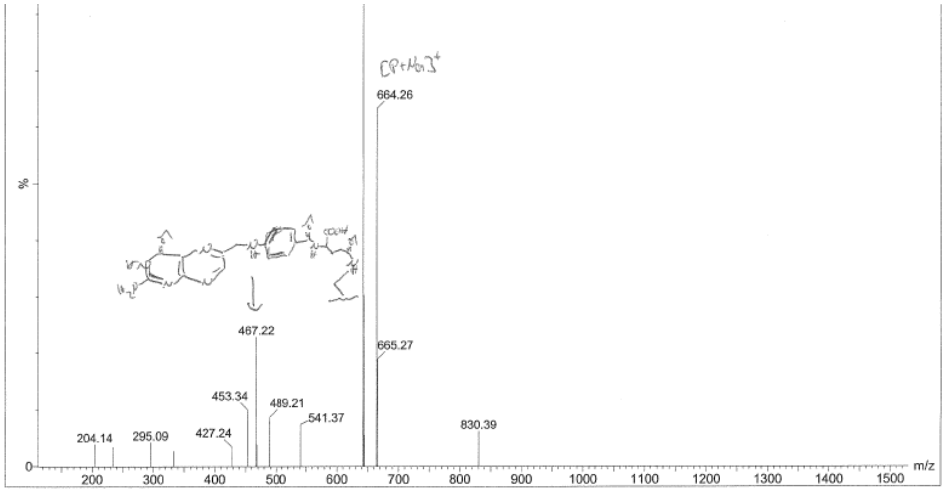

Figure 14. ESI-MS^+; NH_4HCO_3-Buffer (0.05 M)

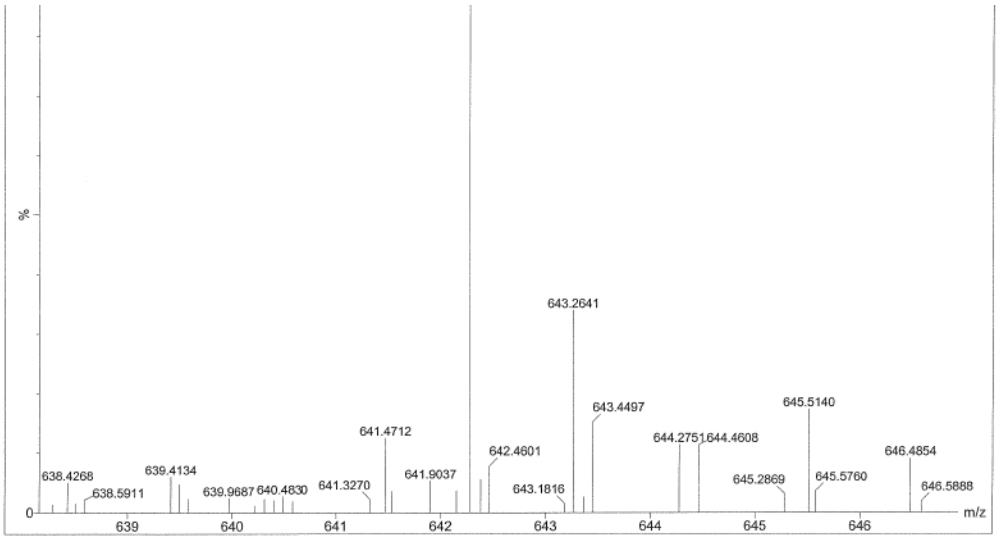

Figure 15. ESI-MS^+ (high resolution); NH_4HCO_3-buffer (0.05 M)

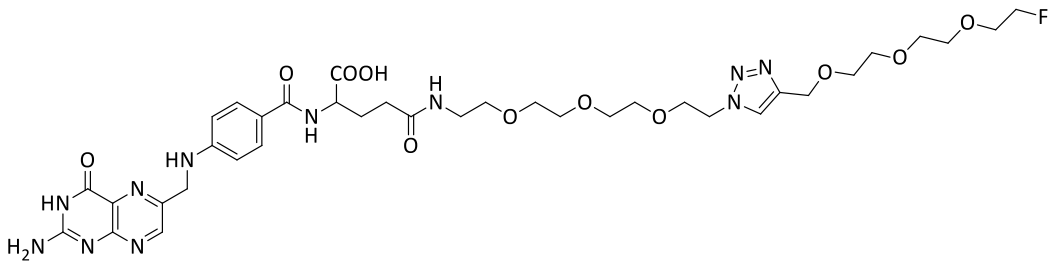

^{1}H NMR (400 MHz, DMSO-d_6) δ 11.58 (br, 1H), 8.63 (s, 1H), 8.18 (d, 1H), 7.93-7.88 (d, 2H), 7.63 (d, 2H), 6.98-6.94 (m, 2H), 6.62 (d, 2H), 4.55 (t, 1H), 4.50 (s, 2H), 4.43 (t, 1H), 4.28-4.22 (m, 1H), 3.87 (t, 2H), 3.65 (t, 2H), 3.58 (t, 2H), 3.55-3.41 (m, 22 H), 3.35 (t, 2H), 3.18-3.12 (m, 2H), 2.20-2.16 (m, 2H), 2.07-1.98 (m, 1H), 1.93-1.84 (m, 1H) ppm. ^{13}C NMR (100 MHz, DMSO-d_6) δ 174.44, 172.13, 166.69, 161.26, 151.22, 149.17, 148.89, 144.88, 129.42, 124.56 121.69, 111.53, 84.42, 82.56, 70.25, 70.21, 70.13, 70.1, 70.03, 69.50, 69.40, 69.14, 64.05, 52.67, 49.74, 46.35, 32.47, 26.73 ppm. LR-MS: $[M+K]^+$ = 870.36 (calc. for $C_{36}H_{50}FKN_{11}O_{11}$: 870.33), $[M+2K]^+$ = 908.32 (calc. for $C_{36}H_{49}FK_2N_{11}O_{11}$: 908.29), $[M+2K]^{2+}$ = 454.65 (calc. for $C_{36}H_{49}FK_2N_{11}O_{11}$: 454.15).

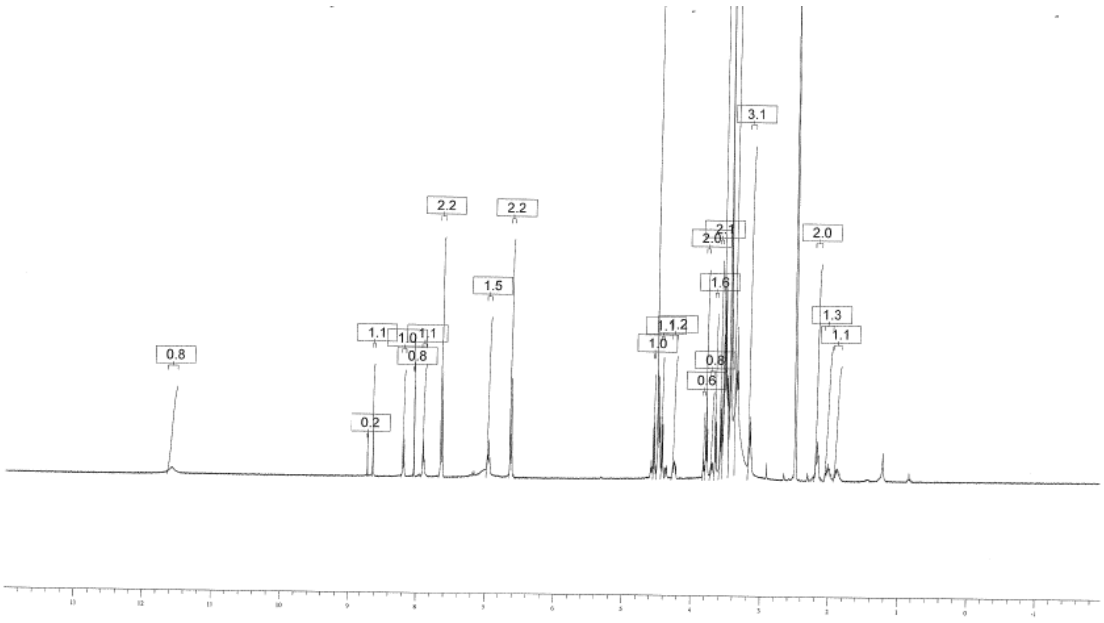

Figure 16. ^{1}H NMR; 400MHz, DMSO-d_6

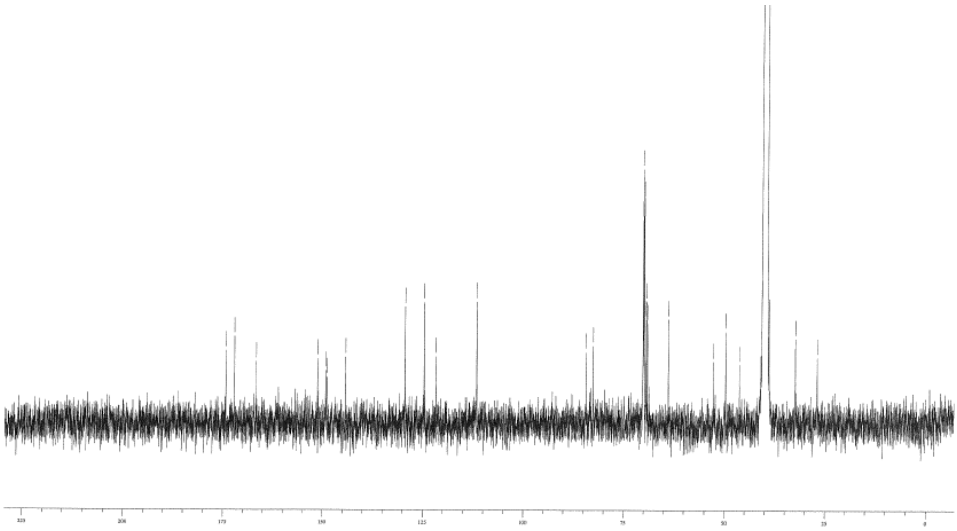

Figure 17 ^{13}C NMR; 400MHz, DMSO-d_6

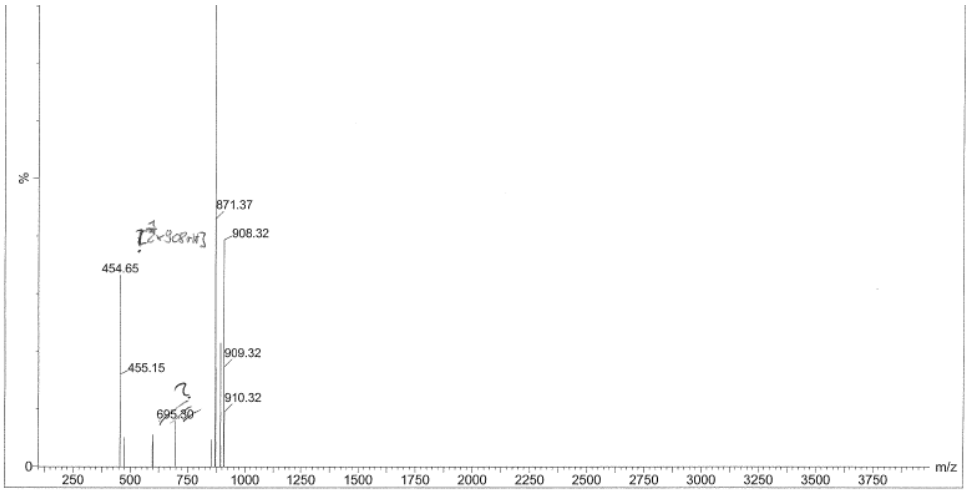

Figure 18. ESI-MS^+; Na/K-phosphate-buffer (0.05 M)

Radiochemistry

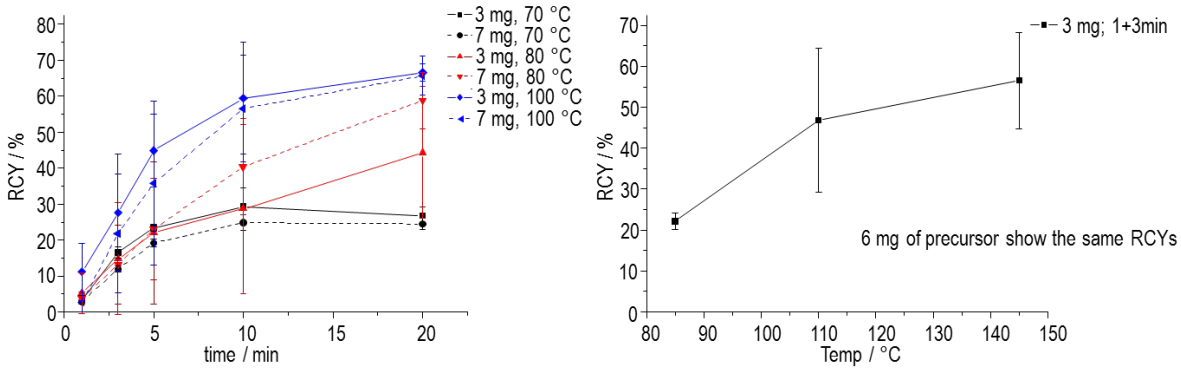

Figure 19. Optimization of the radiolabeling of the prosthetic group. Reaction was performed using acetonitrile and TBA-OH as bas. Conventional heating on the left side and the µwave supported synthesis on the right side.

Prosthetic group synthesis

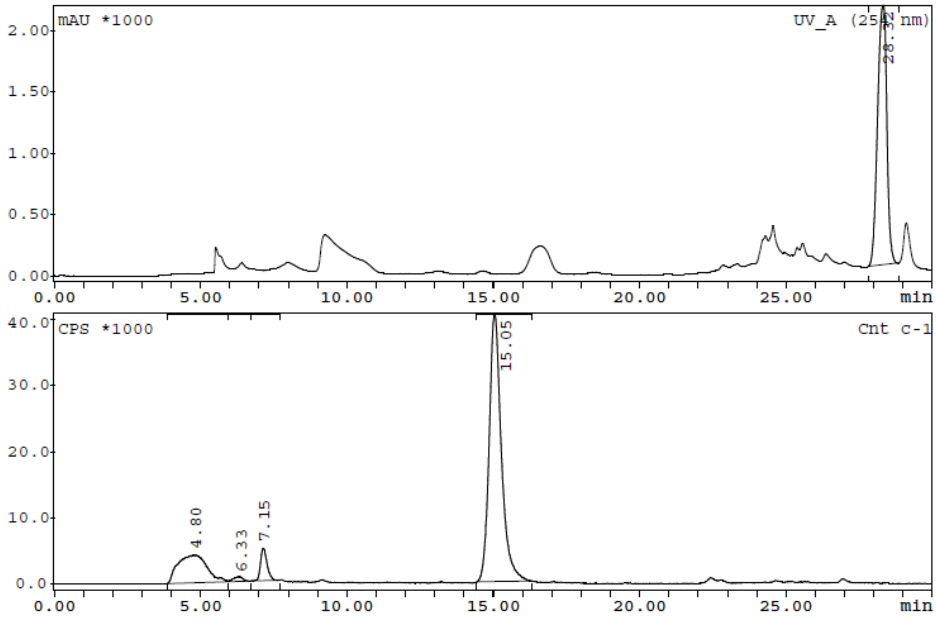

Integration Cnt c-1

Substance	R/T min	Type	Area Counts	%Area %
Reg #1	4.80	BD	287528	18.61
Reg #2	6.33	DD	15000	0.97
Reg #3	7.15	DB	74406	4.82
Reg #4	15.05	BB	1167944	75.60
Sum in ROI			1544877	
Area			1931345	
Ext. BKG			0.00 CPS	

Integration UV_A (254 nm)

Substance	R/T min	Type	Area mAU*min	%Area %
Reg #1	28.32	BB	46365.18	100.00
Sum in ROI			46365.18	

[^{18}F]OEG-folate synthesis

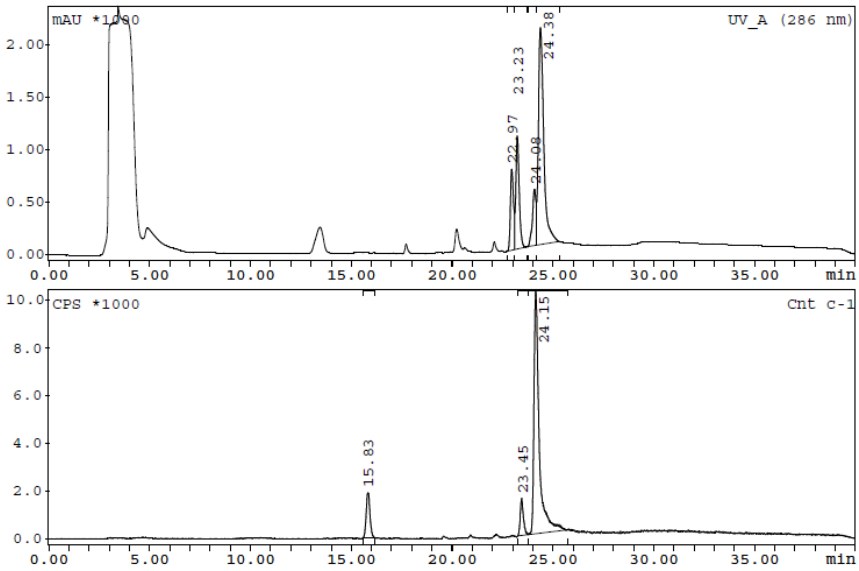

Integration Cnt c-1

Substance	R/T min	Type	Area Counts	%Area %
Reg #1	15.83	BB	24249.9	10.82
Reg #2	23.45	BD	16478.8	7.35
Reg #3	24.15	DB	183438.2	81.83
Sum in ROI			224166.9	
Area			530601.0	
Ext. BKG			0.00 CPS	

Integration UV_A (286 nm)

Substance	R/T min	Type	Area mAU*min	%Area %
Reg #1	22.97	BD	8101.82	12.30
Reg #2	23.23	DB	12854.45	19.51
Reg #3	24.08	BD	6307.47	9.57

Quality Control

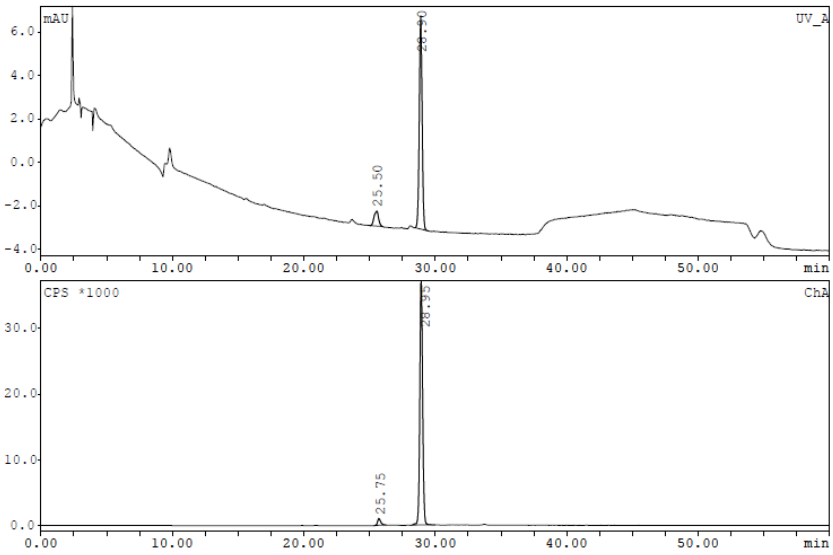

Integration ChA

Substance	R/T min	Type	Area Counts	%Area %
Reg #1	25.75	BB(	16888.9	2.95
Reg #2	28.95	BB(	555790.3	97.05
Sum in ROI			572679.1	
Area			692413.2	
Ext. BKG			0.00 CPS	

Integration UV_A

Substance	R/T min	Type	Area mAU*min	%Area %
Reg #1	25.50	BB(	16.4580	9.97
Reg #2	28.90	BB(	148.5847	90.03
Sum in ROI			165.0427	

Coinjection

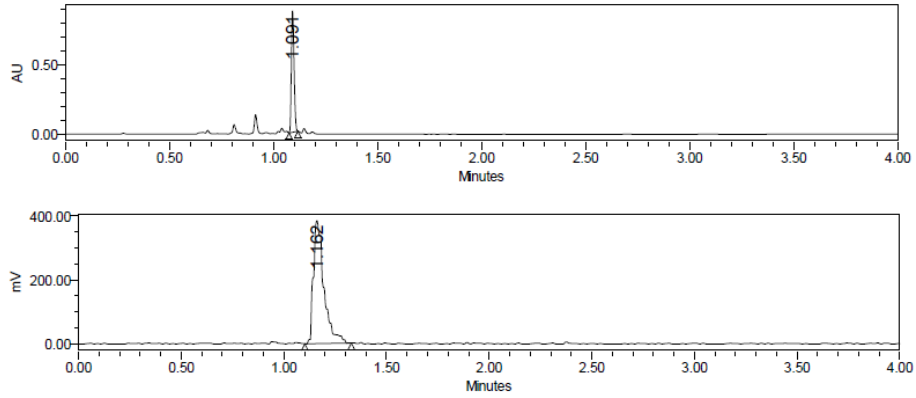

Channel Description: Channel 1, PDA Ch1 254nm@1.2nm

	RT	Area	% Area	Height
1	1.091	784850	100.00	874810

Channel Description: Channel 1

	RT	Area	% Area	Height
1	1.162	1376165	100.00	384444

Biology

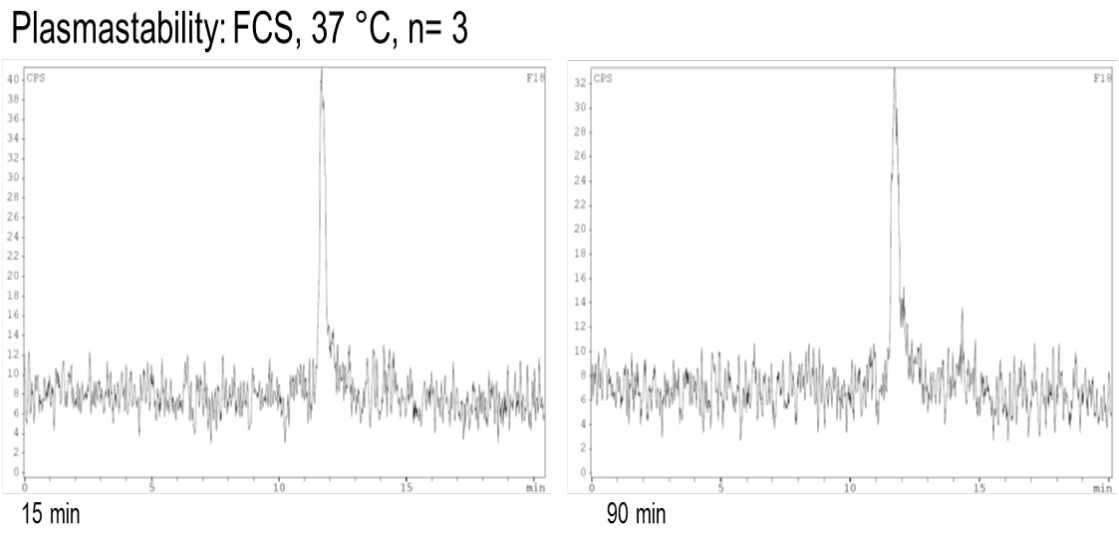

Figure 20. Plasmastability tests using fetal calve serum. Tracer was incubated over 90 min at 37 °C. Aliquots were taken after various time points and injected into an analytical HPLC-system after plasmaproteins have been precipitated.

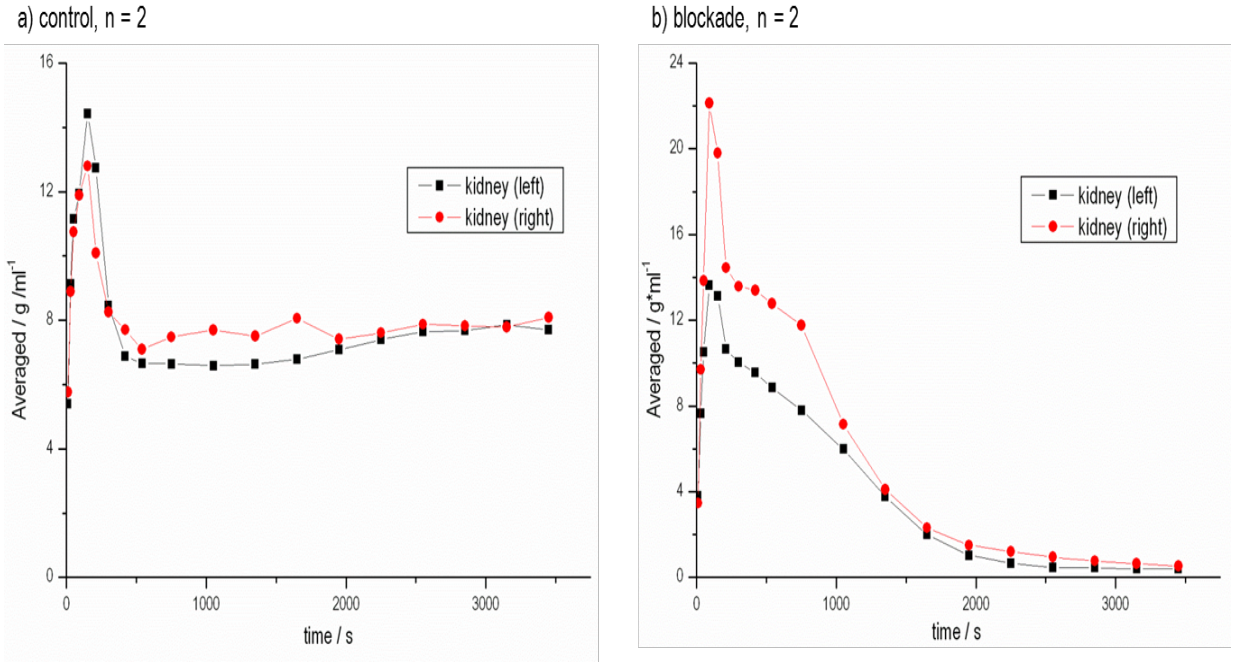

Figure 21. Preliminary µPET studies. left) male healthy CD rats (230 – 310 g), ID 20 – 30 MBq, scanning 60 min dynamic; right) blockade 4 mg/kg 10 min before tracer administration.

Highly Polar ^{18}F-Labeled Serine for Convenient Amino Acid-based Click-Labeling of Biomolecules

Hanno Schieferstein and Tobias L. Ross*

Institute of Nuclear Chemistry, Johannes Gutenberg-University Mainz, Mainz 55128, Germany

Radiopharmaceutical Chemistry, Department of Nuclear Medicine, Hannover Medical School, Hannover 30623, Germany

Abstract:

Click it like serine: The endogenous amino acid serine was derivatized to be able to participate in copper(I)-catalyzed cycloadditions and to carry a ^{18}F-label. The organic synthesis and the ^{18}F-labeling were screened and optimized. Finally, the ^{18}F-labeled prosthetic group was "*clicked*" to an azido-functionalized cRGD as proof of principle.

The positron emission tomography (PET) is one of the most powerful non-invasive methods for molecular imaging. This enables the visualization of *in vivo* processes and pharmacokinetics of radiolabeled molecules.[1] Fluorine-18, as the most widely used PET-nuclide, with a half-life of 110 min, has one major advantage – the possibility to do multi-step radiosyntheses.[2–4] The incorporation of fluorine-18 into biomolecules has emerged a field in radiochemistry, dedicated to the development of labeling strategies other than direct ^{18}F-fluorination or labeling with [^{18}F]fluoroaliphatic derivatives such as 2-[^{18}F]fluoroethyl tosylate.[5–7] Over the past couple of years, many encouraging methods have been developed dealing with ^{18}F-prosthetic group labeling, showing that radiolabeling is no longer limited to small molecules.[8,9] Rather small molecules were used to indirectly radiolabel complex structures, which ask for mild reaction/labeling conditions since they are sensitive to the commonly used harsh conditions for direct ^{18}F-labeling.[10–12] A prominent example is the copper(I)-catalyzed cycloaddition (CuAAC), which enables regioselective and efficient ^{18}F-labeling under mild conditions.[13–15] However, some approaches already demonstrated, how the *in vivo* behavior of compounds is affected due to conjugation of a structural differing prosthetic group. Further investigations showed that the metabolic profile of a peptide strongly altered by the usage of different prosthetic groups.[16–18] More recently it has been shown, that switching from an alkyl-based ^{18}F-prosthetic group to an oligoethylene-based ^{18}F-prosthetic group can enhance the pharmacokinetic profile of ^{18}F-labeled folates.[19] In similar approaches, a glucose-based prosthetic group was introduced as a biologically relevant molecule into the ^{18}F-click labeling concept. As a result, the high potential of the

combination of ^{18}F-click labeling and a very hydrophilic and biologically cognate prosthetic group could be impressively demonstrated by efficient ^{18}F-labeling and drastically improved pharmacokinetics of the radiolabeled biomolecule *in vivo*.[2,20] Numerous radiolabeled amino acids have been used for diagnostic purposes and have shown great potential and clinical usefulness as radiotracers.[21–24] However, to our best knowledge, an endogenous amino acid-based clickable ^{18}F-prosthetic group has not been reported, yet, although many relevant biomolecules are based on amino acids.

This encouraged us to develop a prosthetic group for ^{18}F-labeling of biomolecules, which is based on an amino acid, *L*-serine. *L*-serine seemed very suitable since the hydroxyl functionality and fluorine can be seen as a chemical corresponding (isoelectronic) pair, having no influence on the chemical *in vivo* properties and be as hydrophilic as native amino acids under physiological conditions to reduce unspecific binding and unfavorable pharmacokinetics. In addition, this amino acid derivative should be able to participate in CuAACs and was functionalized with an alkyne moiety. Consequently, a labeling precursor and a non-radioactive reference compound were synthesized. The ^{18}F-labeling reaction was optimized to establish a high yielding and robust radiosynthesis. Finally, the ^{18}F-labeled prosthetic group was reacted with an azido-functionalized cRGD-peptide as a model system and an important vector for angiogenesis targeting.[14,25,26]

The synthesis of the alkyne-functionalized reference compound (**9**) as well as the ^{18}F-labeling of the corresponding precursor (**6**) is depicted in Scheme 1, starting from commercially available *L*-serine methyl ester (**1**). In a first step the amino functionality of **1** was protected by 2,4-dimethoxybenzyl via reductive amination using sodium cyanoborohydride. To ensure regioselectivity, the first synthetic route encompassed the selective silyl-protection of the hydroxyl function of **2**. For this purpose the triisopropylsilyl protecting group was employed, which can be cleaved conveniently and under mild conditions with tetrabutylammonium fluoride. Since the hydroxyl group was protected, only the secondary amine was able to perform alkylation reactions. Therefore, compound **3** was *N*-alkylated using 3-bromo-1-(trimethylsilyl)-1-propyne, enabling the participation in CuAACs through the alkyne function. Subsequently, the fully protected

intermediate **4** was deprotected using a 1M tetrabutylammonium fluoride solution in tetrahydrofuran at room temperature, yielding **5**, which is used as starting material for both, the labeling precursor **6** and the reference compound **9**. Additionally, an alternative route from **2** to **5** without the selective protection of the hydroxyl function of *L*-serine was tested, leading to methyl 2-((2,4-dimethoxybenzyl)(3-(trimethylsilyl)prop-2-yn-1-yl)amino)-3-hydroxypropanoate where only traces of *N*-alkylation could be observed. The following deprotection of the methyl 2-((2,4-dimethoxybenzyl)(3-(trimethylsilyl)prop-2-yn-1-yl)amino)-3-hydroxypropanoate with tetrabutyammonium fluoride in tetrahydrofuran at room temperature led quantitatively to the starting material **5**. For the synthesis of the labeling precursor, compound **5** was reacted with *p*-toluolsulfonyl chloride using triethylamine as base.[27] But only chlorination was observed during the tosylation reaction. Even the addition on trimethylamine hydrochloride in catalytic amounts was not successful to avoid or reduce the chlorination reaction, indicating that the tosyl leaving group-carrying compound has an elevated reactivity.[27,28] To avoid the chlorination, toluolsulfonyl anhydride was used, leading to the desired product, but only detectable in mass-spectroscopy. Purification and isolation of the product was not successful in our hands, due to a rapid degradation (hydrolysis) of the tosylated product during column chromatography. Alternatively, the mesylate precursor was synthesized to introduce a less reactive leaving group, but it turned out that degradation during the purification process took place as well. In the end, the chlorinated compound **6** became our precursor of choice for ^{18}F-labeling (Scheme 1), although sulfonic acid-based leaving groups are preferable. The reference compound of the alkyne-functionalized prosthetic group was synthesized through ^{19}F-fluorination of **5** using DAST ((diethylamino)sulfur trifluoride) at low temperatures of 0 °C. Deprotection of **7** was accomplished in two steps. At first, the methyl ester was cleaved under basic conditions using 1M lithium hydroxide solution, obtaining **8** in 60% yield. Subsequently, compound **8** was deprotected using trifluoroacetic acid in dichloromethane, whereas completion was indicated by a color change of the reaction mixture into deep purple, giving the final racemic reference compound **9**.[30]

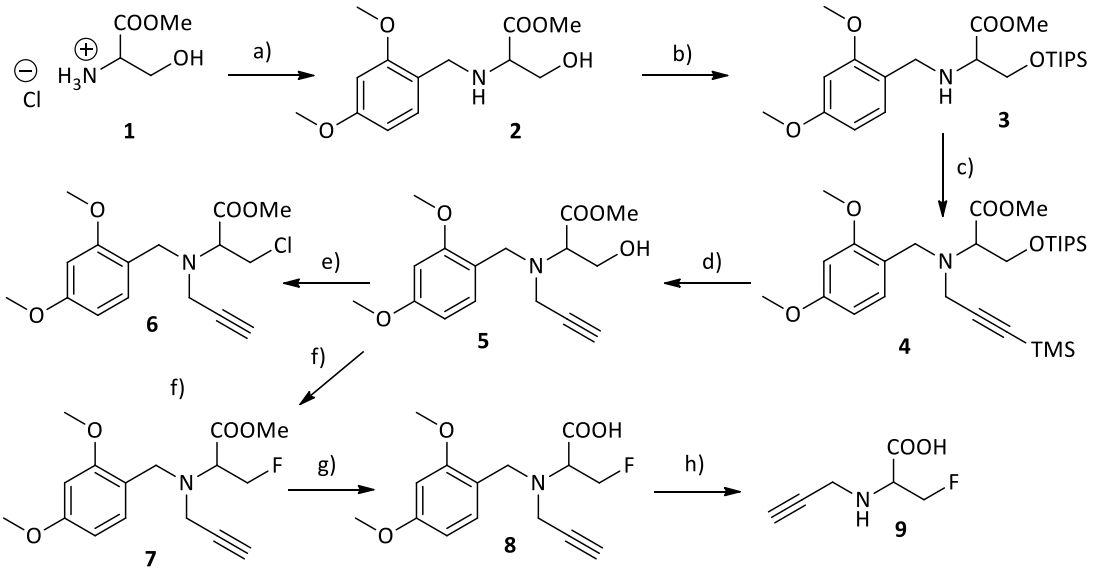

Scheme 1. Synthesis of the alkyne-functionalized reference compound **9** and labeling precursor **6**. **a**) 2,4-dimethoxybenzyl aldehyde, methanol, sodium cyanoborohydride; **b**) triisopropylsilyl chloride, dimethylformamide, imidazole; **c**) 3-bromo-1-(trimethylsilyl)-1-propyne, acetonitrile, Cs_2CO_3; **d**) tetrabutylammonium fluoride in tetrahydrofuran (1M); **e**) *p*-toluenesulfonyl chloride, acetonitrile, trimethylamine; **f**) (diethylamino)sulfur trifluoride, dichloromethane; **g**) lithium hydroxide (1M, aq.), tetrahydrofuran, *tert*.-butanol; **h**) trifluoroacetic acid, dichloromethane.

Subsequently, the radiolabeling of the protected precursor **6** was optimized, whereas different parameters like base concentration, precursor concentration, solvent, reaction time and reaction temperature were screened. Besides conventional heating using an oil-bath, a microwave supported-synthesis was investigated as well (Table 1).

Table 1: Optimization of the ^{18}F-labeling of the chloro-precursor 6.

Precursor (mg)	T [°C]	Base [µmol]	Solvent	Reaction-time [min]	Conversion[d] [%]
1	140[a]	6[b]	DMF	5	53±11
1	120	3[b]	DMF	20	11
1	120	6[b]	DMF	10	13
1	140[a]	12[b]	DMF	5	30
1	140	6[b]	DMF	3	6
1	140	24[b]	DMF	20	23
3	120	3[b]	DMF	20	8
3	120	6[b]	DMF	3	5
3	140[a]	3[b]	DMF	5	8
3	140	6[b]	DMF	10	10
6	120	6[b]	DMF	5	13
1	140	6[b]	DMSO	10	65±9
1	140	3[b]	DMSO	20	48
1	140[a]	6[b]	DMSO	5	77±6
1	140	14[c]	DMF	20	22
1	140	7[c]	DMF	20	44
1	140[a]	3.5[c]	DMF	5	33
1	120	3.5	DMF	10	8
1	120	7	DMF	20	15

a) microwave-supported, pre-run of 1 min mandatory; b) K_2CO_3; c) Cs_2CO_3; d) conversion determined by analytical radio-TLC.

Initially, the amount of precursor and amount of base were screened, whereas $[K\subset2.2.2]^+$/carbonate and dimethylformamide were considered as a solid and reliable system. The use of 1 mg (3 µmol) precursor **6** in 1 mL dimethylformamide gave the highest RCYs. Increasing or decreasing the amount of precursor led to a drop in RCY. The amount of base played a crucial role in two ways. First, if the amount of base was below 3 µmol, no ^{18}F-labeling could be observed. On the other hand, partial deprotection occurred during the labeling step, which additionally increased under higher concentrations of base. The temperature dependency was investigated using a

conventional oil-bath as well as microwave-supported heating. By using the microwave, highest RCYs were obtained, however, similarly the partly deprotected product **[^{18}F]8** was observed. Radiolabeling at 120 °C in an oil-bath resulted in low RCYs, but an increase in temperature to 140 °C led to improved RCYs of 30%. Subsequently, the solvent system and the base itself were screened and optimized. Besides the [K⊂2.2.2]$^{+}$/carbonate system, cesium carbonate was used in the same concentration. It turned out, that higher RCYs could be obtained with cesium carbonate. As expected, here a strong temperature dependency could be seen, too. The most promising results were obtained during the solvent screening. Acetonitrile led to no RCYs under all tested conditions, but the use of dimethyl sulfoxide led to RCYs up to 77±6% using the microwave-supported setup. Labeling under conventional heating led to similar RCYs of 65±9. Moreover, no partial deprotection was observed yielding the desired protected prosthetic group **[^{18}F]7**. The use of the cesium carbonate system in the standard system led to no RCY, thus the microwave-supported radiosynthesis using [K⊂2.2.2]$^{+}$/carbonate (6 µmol) and 1 mg (3 µmol) **6** in dimethyl sulfoxide was superior towards all other conditions.

The protected prosthetic group **[^{18}F]7** was deprotected using 3.3M hydrochloric acid solution at 100 °C for 10 min, which led to the final prosthetic group **[^{18}F]9**. The 2,4-dimethoxybenzyl protecting group is very resistant against acidic aqueous cleavage, therefore, relatively harsh conditions had to be applied (Scheme 2). Additionally, a sequential deprotection was performed, where in a first step the methyl ester was cleaved by addition of sodium hydroxide solution and in a second step the 2,4-dimethoxybenzyl group was cleaved using 3.3M hydrochloric acid (Figure 1).

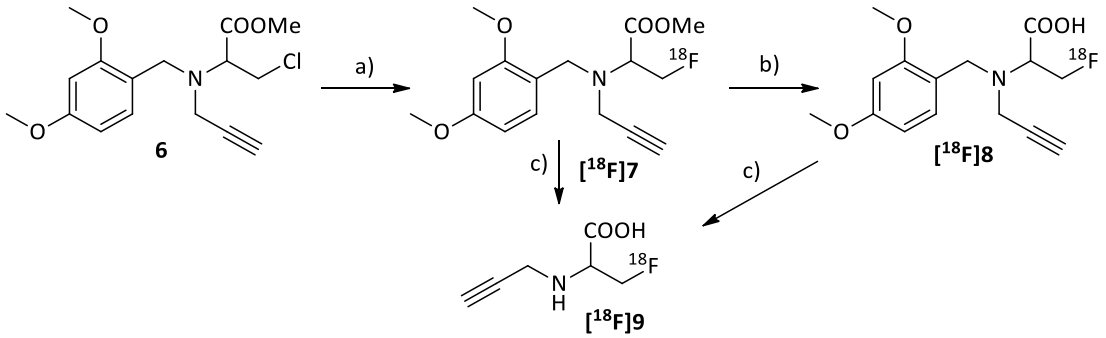

Scheme 2. Radiolabeling of the prosthetic group **[^{18}F]7** and subsequent deprotection. **a**) [K⊂2.2.2]$^{+}$/^{18}F^{-}, DMSO, 140 °C, 10 min; **b**) sodium hydroxide (3.3 M), 60 °C, 5 min; **c**) hydrochloric acid (3.3 M), 100 °C, 15 min.

Isolation of the final ^{18}F-labeled prosthetic group was carried out by evaporation of the solvent of the product fraction obtained after semi-preparative HPLC, because neither a C18 phase cartridge nor a cation exchange cartridge was able to trap **[^{18}F]9** sufficiently, resulting in an overall RCY of 28±5%.

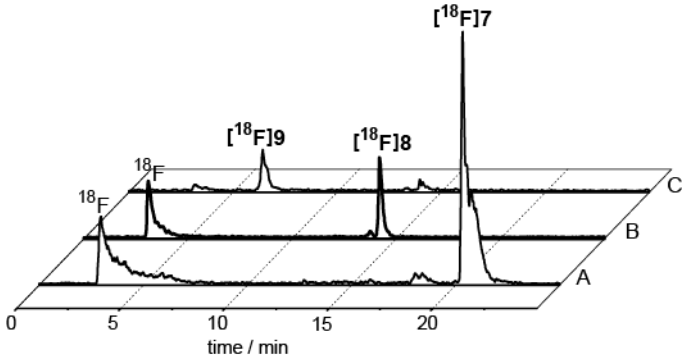

Figure 1. Radiosynthesis of **[^{18}F]9**. **A**) ^{18}F-labeling of precursor **6**. **B**) Addition of sodium hydroxide for methyl ester cleavage. **C**) Addition of hydrochloric acid for 2,4-dimethoxybenzyl cleavage, yielding **[^{18}F]9**. Peak intensities in **A**, **B** and **C** are not normalized.

The superior ^{18}F-labeling conditions ([K⊂2.2.2]$^{+}$/carbonate, dimethyl sulfoxide, 140 °C, 10 min) were applied to synthesize the prosthetic group **[^{18}F]9**. To test the viability of **[^{18}F]9** it was reacted in a copper(I)-catalyzed cycloaddition with the azido-functionalized cRGD peptide **10** as a model system of a highly relevant targeting vector (Scheme 3).[15,26,27] The (non-optimized) ^{18}F-click reaction gave the desired peptide **[^{18}F]10** in yields of 15%,

showing that the new prosthetic group is suitable for convenient ^{18}F-labeling of sensitive molecules under very mild conditions (40 °C, PBS buffer, 20 min).

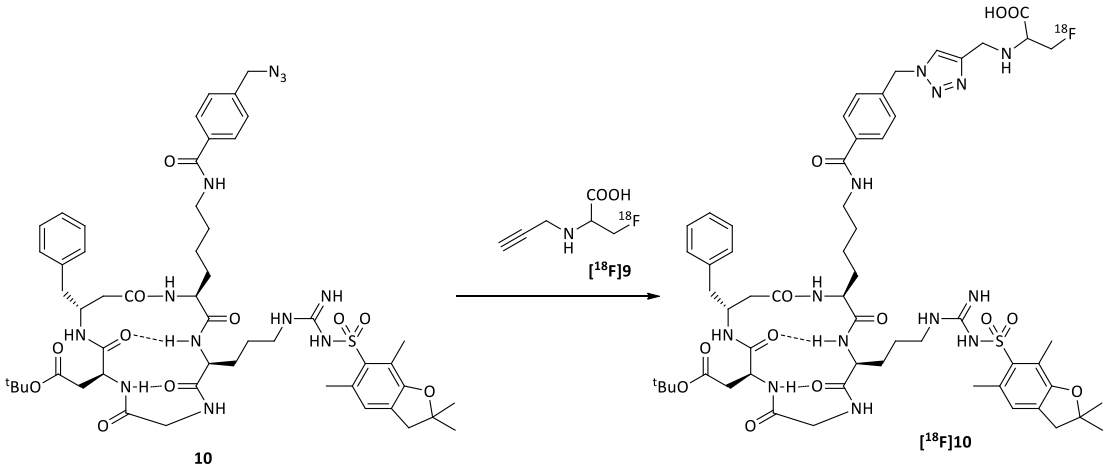

Scheme 3. CuAAC of the protected azido-functionalized cRGD (**10**) and prosthetic group **[^{18}F]9**. Model reaction of **[^{18}F]9** with a biologically highly relevant molecule (azido-cRGD). Click reaction conditions: copper sulfate (20 µmol), sodium ascorbate (100 µmol), 40 °C, PBS buffer, 20 min.Radiolabeling using prosthetic groups, especially for ^{18}F-labeling, gained more and more interest due to the alteration of molecules to be labeled. Throughout molecules become more complex with many and various functionalities, which aggravate direct ^{18}F-labeling. Moreover, the molecules are mostly sensitive to heat or base which makes direct ^{18}F-labeling impossible.

The here reported synthesis strategy enables for the first time the ^{18}F-labeling of a serine derivative, which is carrying an alkyne moiety to participate on CuAACs. High radiochemical yields (28±5% over two radioactive steps) were obtained, showing the huge potential of multi-step, but convenient ^{18}F-labeling strategies. The synthesis turned out to be very facile and robust, although it includes two radioactive steps. Moreover, the amino acid analog is assumed to have no significant, rather a positive influence on the metabolism/pharmacokinetics *in vivo* and represents a promising approach for ^{18}F-click labeling of sensitive and complex structures, especially peptides, proteins and other amino acid-based molecules.[16,17]

Further investigations towards the biocompatibility and advantages of the introduction of the ^{18}F-labeled serine-based prosthetic group itself as well as the influence on the *in vivo* behavior of various biomolecules will be investigated to demonstrate the unique

properties of this prosthetic group. The here reported ^{18}F-labeled prosthetic group could certainly cope with current demands for ^{18}F-labeling of sensitive biomolecules, leading to the ability to introduce more compounds to PET imaging and ultimately adding more flexibility to the field of ^{18}F-labeling and PET chemistry.

References:

(1) Johnsson, N.; Johnsson, K. *ACS Chem. Biol.* **2007**, *2*, 31–38.

(2) Prante, O.; Einsiedel, J.; Haubner, R.; Gmeiner, P.; Wester, H.-J.; Kuwert, T.; Maschauer, S. *Bioconjugate Chem.* **2007**, *18*, 254–62.

(3) Sutcliffe-Goulden, J. L.; O'Doherty, M. J.; Marsden, P. K.; Hart, I. R.; Marshall, J. F.; Bansal, S. S. *Eur. J. Nucl. Med. Mol. Imaging* **2002**, *29*, 754–9.

(4) Chang, Y. S.; Jeong, J. M.; Lee, Y.-S.; Kim, H. W.; Rai, G. B.; Lee, S. J.; Lee, D. S.; Chung, J.-K.; Lee, M. C. *Bioconjugate Chem.* **2005**, *16*, 1329–33.

(5) Bauman, A.; Piel, M.; Schirrmacher, R.; Rösch, F. *Tetrahedron Lett.* **2003**, *44*, 9165–9167.

(6) Comagic, S.; Piel, M.; Schirrmacher, R.; Höhnemann, S.; Rösch, F. *Appl. Radiat. Isot.* **2002**, *56*, 847–51.

(7) Chi, D. Y.; Kilbourn, M. R.; Katzenellenbogen, J. A.; Welch, M. J. *J. Org. Chem.* **1987**, *52*, 658–664.

(8) Coenen, H. H.; Elsinga, P. H.; Iwata, R.; Kilbourn, M. R.; Pillai, M. R. A.; Rajan, M. G. R.; Wagner, H. N.; Zaknun, J. J. *Nucl. Med. Biol.* **2010**, *37*, 727–40.

(9) Cai, L.; Lu, S.; Pike, V. W. *Eur. J. Org. Chem.* **2008**, *2008*, 2853–2873.

(10) Okarvi, S. M. *Med. Res. Rev.* **2004**, *24*, 357–97.

(11) Wester, H. J.; Hamacher, K.; Stöcklin, G. *Nucl. Med. Biol.* **1996**, *23*, 365–72.

(12) Poethko, T.; Schottelius, M.; Thumshirn, G.; Hersel, U.; Herz, M.; Henriksen, G.; Kessler, H.; Schwaiger, M.; Wester, H.-J. *J. Nucl. Med.* **2004**, *45*, 892–902.

(13) Sirion, U.; Kim, H. J.; Lee, J. H.; Seo, J. W.; Lee, B. S.; Lee, S. J.; Oh, S. J.; Chi, D. Y. *Tetrahedron Lett.* **2007**, *48*, 3953–3957.

(14) Li, Z.-B.; Wu, Z.; Chen, K.; Chin, F. T.; Chen, X. *Bioconjugate Chem.* **2007**, *18*, 1987–94.

(15) Ross, T. L.; Honer, M.; Lam, P. Y. H.; Mindt, T. L.; Groehn, V.; Schibli, R.; Schubiger, P. A.; Ametamey, S. M. *Bioconjugate Chem.* **2008**, *19*, 2462–70.

(16) Marik, J.; Hausner, S. H.; Gagnon, M. K. J.; Sutcliffe, J. L. *J. Labelled Compd. Radiopharm.* **2007**, *50*, S39.

(17) Hausner, S. H.; Marik, J.; Gagnon, M. K. J.; Sutcliffe, J. L. *J. Med. Chem.* **2008**, *51*, 5901–4.

(18) Rameda, T.; Bergmann, R.; Wüst, F. *Lett. Drug Des. Discov.* **2007**, *4*, 279–285.

(19) Schieferstein, H.; Betzel, T.; Fischer, C. R.; Ross, T. L. *EJNMMI Res.* **2013**, *3*, 68.

(20) Maschauer, S.; Einsiedel, J.; Haubner, R.; Hocke, C.; Ocker, M.; Hübner, H.; Kuwert, T.; Gmeiner, P.; Prante, O. *Angew. Chem. Int. Ed. Engl.* **2010**, *49*, 976–9.

(21) Wester, H. J.; Herz, M.; Weber, W.; Heiss, P.; Senekowitsch-Schmidtke, R.; Schwaiger, M.; Stöcklin, G. *J. Nucl. Med.* **1998**, *40*, 205–212.

(22) Krasikova, R. N.; Kuznetsova, O. F.; Fedorova, O. S.; Belokon, Y. N.; Maleev, V. I.; Mu, L.; Ametamey, S.; Schubiger, P. A.; Friebe, M.; Berndt, M.; Koglin, N.; Mueller, A.; Graham, K.; Lehmann, L.; Dinkelborg, L. M. *J. Med. Chem.* **2011**, *54*, 406–10.

(23) Yang, D.; Kuang, L. R.; Cherif, A; Tansey, W.; Li, C.; Lin, W. J.; Liu, C. W.; Kim, E. E.; Wallace, S. *J. Drug Targeting* **1993**, *1*, 259–67.

(24) Wang, L.; Zha, Z.; Qu, W.; Qiao, H.; Lieberman, B. P.; Plössl, K.; Kung, H. F. *Nucl. Med. Biol.* **2012**, *39*, 933–43.

(25) Choe, Y. S.; Lee, K.-H. *Curr. Pharm. Des.* **2007**, *13*, 17–31.

(26) Almutairi, A.; Rossin, R.; Shokeen, M.; Hagooly, A.; Ananth, A.; Capoccia, B.; Guillaudeu, S.; Abendschein, D.; Anderson, C. J.; Welch, M. J.; Fréchet, J. M. J. *Proc. Natl. Acad. Sci. U. S. A.* **2009**, *106*, 685–90.

(27) Yoshida, Y.; Sakakura, Y.; Aso, N.; Okada, S.; Tanabe, Y. *Tetrahedron* **1999**, *55*, 2183–2192.

(28) Holschbach, M. H.; Olsson, R. A.; Bier, D.; Wutz, W.; Sihver, W.; Schüller, M.; Palm, B.; Coenen, H. H. *J. Med. Chem.* **2002**, *45*, 5150–6.

(29) Nussbaumer, P.; Baumann, K.; Dechat, T.; Harasek, M. *Tetrahedron* **1991**, *41*, 4591–4602.

Supplementary Data

Highly Polar ^{18}F-Labeled Serines for Convenient Amino Acid-based Click-Labeling of Biomolecules

Hanno Schieferstein, Tobias L. Ross*

Institute of Nuclear Chemistry, Johannes Gutenberg-University Mainz, Mainz 55128, Germany

Radiopharmaceutical Chemistry, Department of Nuclear Medicine, Hannover Medical School, Hannover 30623, Germany

I. Organic Syntheses of *L*-serine derivatives

I.1 General

Reagents and solvents were purchased from Sigma-Aldrich Co. (St. Louis, MO, USA), Acros (Geel, Belgium), or Merck AG (Darmstadt, Germany) and used without further purification. Reactions were monitored by thin layer chromatography (performed on Merck silica gel 60 F254, not modified, pre-coated silica gel on aluminum-supported plates) or high-performance liquid chromatography (HPLC). ^{1}H and ^{13}C nuclear magnetic resonance spectra were recorded on Bruker 400 MHz spectrometer. Chemical shifts (δ) to solvent are reported in parts per million (ppm) relative to tetramethylsilane and referenced. Low-resolution mass spectra (LR-MS) were recorded on Agilent 6100 Series Single Quadrupole LC/MS and high-resolution mass spectra (HR-MS) were recorded on either a Micromass Quattro Micro API LC-ESI or a Finnigan MAT90-Spectrometer.

Radiosyntheses were performed manually in a lead-shielded fume hood (starting activities ≤5 GBq [^{18}F]fluoride) using conventional heating or a focused laboratory microwave (CEM Discover, Matthews, NC, USA) in the following mode: 1-min pre-run, 5-min reaction time, and a maximum power of 300 W.

I.2 Synthesis of the alkyne *L*-serine labeling precursor

*Methyl 2-((2,4-dimethoxybenzyl)amino)-3-hydroxypropanoate (**2**)*

To a solution of *L*-serine methylester hydrochloride **1** (1 g, 6.42 mmol) and 2,4-dimethoxybenzaldehyde (1,06 g, 6.42 mmol) in dry methanol (15 mL), triethylamine (898.8 µL, 6.42 mmol) were added and stirred for 30 min at RT. Then sodium cyanoboronhydride (800 mg, 12.7 mmol) were added in one portion. The reaction was stirred overnight, dichloromethane (20 mL) were added and the organic layer was

extracted 3-times (5 mL) with sodium bicarbonate solution (1M). The organic phase was dried over sodium sulfate, the solvent evaporated and the mixture purified by column chromatography (ethyl acetate), giving a pale yellow oil (996 mg, 3.7 mmol, 50%).

^{1}H-NMR ($CDCl_3$, 400MHz): δ [ppm] = 2.58 (br s, 1H, -O*H*), 3.42 (dd, 1H, $^{3}J_{H-H}$ = 4.5 Hz, $C_{alpha}H$), 3:62 (q, 1H, $^{3}J_{H-H}$ = 6.3 Hz, CH_2-OH), 3.69 (s, 3H, COOCH_3), 3.75-3.78 (d, 2H, $^{3}J_{H-H}$ = 10 Hz CH_2-NH), 3.80-3.82 (q, 1H, $^{3}J_{H-H}$ = 6.3 Hz, CH_2-OH), 3.82 (s, 3H, Ar-OCH_3), 3.84 (s, 3H, Ar-OCH_3), 6.46 (dd, 1H, $^{4}J_{H-H}$ = 2.5 Hz, Ar-*H*), 6.47 (d, 1H, Ar-*H*), 7.11 (d, 1H, $^{3}J_{H-H}$ = 7.9 Hz, Ar-*H*).

^{13}C-NMR ($CDCl_3$, 100MHz): δ [ppm] = 47.02 (NH-*C*H_2Ar), 52.09 (COO*C*H_3), 55.31 (O*C*H_3), 55.38 (O*C*H_3), 61.53 (C_{alpha}), 61.91 (*C*H_2-OH), 98.59 (Ar-*C*H), 103.73 (Ar-*C*H), 119.88 (Ar-*C*), 130.51 (Ar-*C*H), 158.74 (Ar-*C*-OCH_3), 160.41 (Ar-*C*-OCH_3), 173.43 (C=O).

MS (ESI positive): 270.1 $[M+H]^+$

HRMS: calcd for C13H20NO5 270.1341, found 270.1346.

*Methyl 2-((2,4-dimethoxybenzyl)amino)-3-((triisopropylsilyl)oxy)-propanoate (**3**)*

Compound **2** (200 mg, 0.74 mmol) and triisopropylsilyl chloride (174 μL, 157 mg, 0.81 mmol) were dissolved in dimethylformamide (10 mL) and cooled to 0 °C, after imidazole (100 mg,1.48 mmol) was added in one portion. The reaction was stirred overnight, quenched with water (20 mL) and extracted 3-times with 10 mL dichloromethane. The combined organic phases were dried over sodium sulfate and the solvent removed under vaccuum. Purification via silica column purification (ethyl acetate:hexanes/2:1) gave **3** as a pale yellow oil (215 mg, 0.5 mmol, 68%).

^{1}H-NMR ($CDCl_3$, 400MHz): δ [ppm] = 1.02-1.09 (m, 21H, Si(C_3H_7)$_3$), 3.48 (t, 1H, $^{3}J_{H-H}$ = 5.3 Hz, C_{alpha}), 3.69 (s, 3H, COOCH_3), 3.73-3.86 (m, 2H, CH_2-NH), 3.81 (s, 6H, ArC-OCH_3) 3.92-3.97 (m, 2H, CH_2-OH), 6.43-6.46 (m, 2H, Ar-*H*), 7.17 (d, 1H, $^{3}J_{H-H}$ = 7.9 Hz, Ar-*H*).

^{13}C-NMR ($CDCl_3$, 100MHz): δ [ppm] = 11.84 (C_{tert}(C-(C_2H_6)$_3$), 17.85 (C_{tert}-(C_2H_6)$_3$), 46.97 (NH-CH$_2$Ar), 51.68 (Ar-OCH$_3$), 55.38 (Ar-OCH$_3$), 62.61 (C_{alpha}), 64.69 (CH$_2$-OH), 98.35 (Ar-CH), 103.80 (Ar-CH), 130.42 (Ar-C), 158.61 (Ar-C-OCH$_3$), 160.18 (Ar-C-OCH$_3$), 173.73 (C=O).

MS (ESI positive): 426.2 $[M+H]^+$

HRMS: calcd for C22H40NO5Si 426.2676, found 426.2676.

*Methyl 2-((2,4-dimethoxybenzyl)(3-(trimethylsilyl)prop-2-yn-1-yl)amino)-3-((triisopropyl-silyl)oxy)propanoate (**4**)*

After dissolving **3** (100 mg, 0.25 mmol) in dry acetonitile (4 mL), 3-bromo-1-(trimethylsilyl)-1-propyne (41 μL, 48 mg, 0.25 mmol), dissolved in dry acetonitrile (2 mL) was added and the reaction mixture was heated to 55 °C. The addition of cesium carbonate (114 mg, 0.35 mmol) resulted in a brown precipitate after 30 min of reaction time. The reaction was quenched with water (15 mL) after 1 h of reaction time, followed by an extraction (3 x 10 mL dichlromethane). The combined organic phases were dried over sodium sulfate and purfified using silica column chromatography (ethyl acetate:hexanes/5:1), obtaining **4** as a colorless oil (105 mg, 0.2 mmol, 85%).

^{1}H-NMR ($CDCl_3$, 400MHz): δ [ppm] = 0.02 (s, 9H, Si(CH_3)$_3$), 1.04-1.08 (m, 21H, Si-(C_3H_7)$_3$), 3.51 (s, 2H,NH-CH_2-C), 3.70-3.77 (m, 1H, $C_{alpha}H$), 3.71-3.90 (m, 2H,CH_2-NH), 3.74 (s, 3H, COOCH_3), 3.80 (s, 3H, Ar-OCH_3), 3.81 (s, 3H, Ar-OCH_3), 4.04-4.18 (m, 2H, C_{alpha}-CH_2-OTIPS), 6.44-6.48 (m, 2H, Ar-H), 7.27 (d, 1H, $^{3}J_{H\text{-}H}$ = 8.0 Hz Ar-H).

^{13}C-NMR ($CDCl_3$, 100MHz): δ [ppm] = 0.08 (Si-(CH$_3$)$_3$), 11.88 (C_{tert}(C-(C_2H_6)$_3$), 17.90 (C_{tert}-(C_2H_6)$_3$), 41.39 (N-CH$_2$), 48.65 (NH-CH$_2$-C≡CTMS), 51.28 (COOCH_3), 55.34 (OCH$_3$), 63.25 (C_{alpha}-CH$_2$-OTIPS), 66.20 (C_{alpha}), 89.37 (CH$_2$-C≡CTMS), 98.48 (Ar-CH), 102.48 (CH$_2$-C≡C-Si), 103.84 (Ar-CH), 119.06 (Ar-C), 131.36 (Ar-CH), 159.00 (Ar-C-OCH$_3$), 160.16 (Ar-C-OCH$_3$), 172.42 (C=O).

MS (ESI positive): 536.3 $[M+H]^+$

HRMS: calcd for C28H50NO5Si2 536.3228 found 536.3238

*Methyl 2-((2,4-dimethoxybenzyl)(prop-2-yn-1-yl)amino)-3-hydroxy-propanoate (**5**)*

To a solution of **4** (500 mg, 0.93 mmol) in THF (2 mL), tetrabutylammonium fluoride (1M in THF, 4 mL) was added and stirred at room temperature for 16 h. Subsequently, the solvent was removed and purified via silica column chromatography (ethyl acetate:hexanes/1:3), giving **5** as a colorless oil (230 mg, 0.75 mmol, 80%).

^{1}H-NMR ($CDCl_3$, 400MHz): δ [ppm] = 2.26 (t, 1H, $^{4}J_{H\text{-}H}$ = 2.5 Hz -C≡C*H*), 3.36 (s, 3H, Ar-CH_3), 3.51 (dd, 1H, $^{3}J_{H\text{-}H}$ = 17 Hz, CH_2-C≡C), 3.59-4.06 (dd, 2H, $^{3}J_{H\text{-}H}$ = 13 Hz, CH_2-N), 3.75 (s, 3H, COOCH_3), 3.75-3.79 (m, 1H, C_{alpha}-*H*), 3.82 (s, 3H, Ar-OCH_3), 3.84 (s, 3H, Ar-OCH_3), 3.84 (t, 1H, -CH_2-OH), 3.93 (t, 1H, -CH_2-OH), 6.45 (dd, 1H, $^{3}J_{H\text{-}H}$ = 8.2 Hz, Ar-*H*), 6.48 (d, 1H, $^{4}J_{H\text{-}H}$ = 2.4 Hz, Ar-*H*), 7.15 (d, 1H, $^{3}J_{H\text{-}H}$ = 8.2 Hz, Ar-*H*).

^{13}C-NMR ($CDCl_3$, 100MHz): δ [ppm] = 40.14 (N-*C*H_2), 47.94 (*C*H_2-C≡CH), 51.33 (COO*C*H_3), 55.32 (O-*C*H_3), 55.41 (O-*C*H_3), 58.96 (*C*H_2-OH), 64.52 (C_{alpha}), 72.84 (C≡*C*H), 79.83 (CH_2-*C*≡CH), 98.92 (Ar-*C*H), 103.67 (Ar-*C*H), 117.98 (Ar-*C*), 132.03 (Ar-*C*H), 158.78 (Ar-*C*-OCH_3), 160.70 (Ar-*C*-O*C*H_3), 171.41 (C=O).

MS (ESI positive): 308.1 $[M+H]^+$, 330.1 $[M+Na]^+$

HRMS: calcd for C16H21NO5Na 330.1317, found 330.1328.

*Methyl 3-chloro-2-((2,4-dimethoxybenzyl)(prop-2-yn-1-yl)amino)-propanoate (**6**)*

Compound **5** (230 mg, 0.75 mmol) and *p*-toluenesulfonyl chloride (286 mg, 1.5 mmol) were dissolved in dry acetonitrile (5 mL) and cooled to 0 °C. Triethylamine (280 µL, 203 mg, 2 mmol) were pre-dissolved in dry acetonitrile (2 mL) and added slowly to the reaction mixture. The mixture was then allowed to warm up to RT, stirred for another 48 h and the solvent was removed. Column chromatography (ethyl acetate:hexanes/1:5) afforded the product **6** as a pale yellow oil (183 mg, 0.56 mmol, 75%).

^{1}H-NMR ($CDCl_3$, 400MHz): δ [ppm] = 2.28 (t, 1H, $^{4}J_{H\text{-}H}$ = 2.5 Hz C≡C*H*), 3.00-3.27 (ddd, 2H, $^{3}J_{H\text{-}H}$ = 13.5 Hz C_{alpha}-CH_2-Cl), 3.37 (s, 2H, N-CH_2-C≡CH), 3.70 (s, N-CH_2-Ar), 3.78 (s, 3H,

COOC*H*$_3$), 3.81 (s, 3H, Ar-OC*H*$_3$), 3.82 (s, 3H, Ar-OC*H*$_3$), 4.38 (m, 1H, C_{alpha}*H*), 6.44-6.47 (m, 2H, ArC-*H*), 7.17-7.19 (d, 1H, $^3J_{H\text{-}H}$ = 8.9 Hz ArC-*H*).

^{13}C-NMR ($CDCl_3$, 100MHz): δ [ppm] = 42.53 (*C*H$_2$-C≡CH), 51.36 (N-*C*H$_2$), 52.77 (COO*C*H$_3$), 53.62 (C_{alpha}), 55.29 (O-*C*H$_3$), 52.77 (O-*C*H$_3$), 57.62 (C_{alpha}-*C*H$_2$-Cl), 73.07 (C≡*C*H), 78.91 (CH$_2$-*C*≡CH), 98.50 (Ar*C*-H), 103.84 (Ar*C*-H), 118.29 (Ar-*C*), 131.30 (Ar-*C*H), 158.98 (Ar-*C*-OCH$_3$), 160.40 (Ar-*C*-OCH$_3$), 169.69 (C=O).

MS (ESI positive): 326.2 $[M+H]^+$

HRMS: calcd for C16H20NO4NaCl 348.0979, found 348.0970.

I.3 Synthesis of the alkyne *L*-serine reference compound

*Methyl 2-((2,4-dimethoxybenzyl)(prop-2-yn-1-yl)amino)-3-fluoro-propanoate (**7**)*

To a solution of **5** (30 mg, 0.1 mmol) in dry dichloromethane (2 mL) (diethylamino)sulfur trifluoride (13 µL, 15.7 mg, 0.01 mmol) was added at room temperature. The reaction mixture was stirred for another 2 h before quenched with water (5 mL) and extracted with dichloromethane (3 x 5 mL). The combined organic phases were dried over sodium sulfate and the solvent evaporated. Silica column chromatography (ethyl acetate:hexanes/1:4) gave a colorless oil (26 mg, 0.08 mmol, 80%).

^{1}H-NMR ($CDCl_3$, 400MHz): δ [ppm] = 2.27 (t, 1H, $^4J_{H\text{-}H}$ = 1.5, Hz C≡C*H*), 3.06 (m, 1H, C_{alpha}*H*), 3.49 (m, 2H, N-C*H*$_2$-C≡C), 3.73 (m, 2H, N-C*H*$_2$-Ar), 3.78 (s, 3H, COO-C*H*$_3$), 3.83 (s, 6H, Ar-OC*H*$_3$), 5.07 (s, 1H, $^2J_{H\text{-}H}$ = 49 Hz, C*H*$_2$-F), 5.19 (s, 1H, $^2J_{H\text{-}H}$ = 49 Hz, C*H*$_2$-F), 6.47-6.49 (m, 2H, ArC-*H*), 7.23-7.25 (d, 1H, $^3J_{H\text{-}H}$ = 6.8 Hz, ArC-*H*).

^{13}C-NMR ($CDCl_3$, 100MHz): δ [ppm] = 42.89 (N-*C*H$_2$-C≡C), 51.79 (N-*C*H$_2$-Ar), 52.25 (N-*C*H$_2$-Ar), 54.85 (C_{alpha}), 55.35 (Ar-O*C*H$_3$), 55.44 (Ar-O*C*H$_3$), 73.13 (C≡*C*H), 78.86 (CH$_2$-*C*≡CH), 88.47 (*C*H$_2$-F), 90.32 (*C*H$_2$-F), 98.52 (Ar-*C*H), 103.94 (Ar-*C*H), 118.47 (Ar-*C*), 131.30 (Ar-*C*), 158.95 (Ar*C*-OCH$_3$), 160.25 (Ar*C*-OCH$_3$), 169.11 (C=O).

^{19}F-NMR ($CDCl_3$, 376 MHz): δ [ppm] = -192.75.

MS (ESI positive): 310.1 $[M+H]^+$

HRMS: calcd for C16H21NO4F 310.1455, found 310.1464.

*2-((2,4-dimethoxybenzyl)(prop-2-yn-1-yl)amino)-3-fluoropropanoic acid (**8**)*

Deprotection of **7** (45 mg, 0.14 mmol) was performed by adding a 1M lithium hydroxide solution (1 mL) to **7** in THF (1 mL) and *tert*-butanol (1 mL). After 2 h at 40 °C, the formed two layers were separated. The solvents of the organic layer were removed under vacuum, re-dissolved in dichloromethane (2 mL) and filtered. After solvent removal *in vacuo*, compound **8** as yellow solid (28 mg, 0.09 mmol, 65%).

^{1}H-NMR ($CDCl_3$, 400MHz): δ [ppm] = 2.24 (t, 1H, $^4J_{H\text{-}H}$ = 2.5 Hz, C≡C*H*), 2.98 (m, 1H, $C_{alpha}H$), 3.31 (m, 2H, N-CH_2-C≡CH), 3.64 (dd, $^3J_{H\text{-}H}$ = 12.9 Hz, N-CH_2-Ar), 3.74 (s, 3H, Ar-OCH_3), 3.75 (s, 3H, Ar-OCH_3), 4.93 (m, 1H, $^2J_{H\text{-}H}$ = 49.3 Hz, C_{alpha}-CH_2-F), 5.06 (m, 1H, $^2J_{H\text{-}H}$ = 49.3, Hz C_{alpha}-CH_2-F), 6.39-6.41 (m, 2H, ArC-*H*), 7.19 (d, 1H, $^3J_{H\text{-}H}$ = 8.7 Hz, ArC-*H*).

^{13}C-NMR ($CDCl_3$, 100MHz): δ [ppm] = 41.90 (N-*C*H_2), 51.81 (N-*C*H_2-Ar), 55.27 (Ar-O*C*H_3), 55.70 (Ar-O*C*H_3), 55.91 (C_{alpha}), 73.84 (-C≡*C*H), 78.54 (CH_2-*C*≡CH), 89.74 (*C*H_2-F), 91.54 (*C*H_2-F), 98.82 (Ar*C*-H), 104.14 (Ar*C*-H), 118.15 (Ar-*C*), 131.87 (Ar-*C*H), 158.80 (Ar*C*-OCH_3), 160.35 (Ar*C*-OCH_3), 175.59 (C=O).

^{19}F-NMR ($CDCl_3$, 376 MHz): δ [ppm] = -192.75.

MS (ESI positive): 296.2 $[M+H]^+$

HRMS: calcd. for C15H18NO4NaF 318.1124, found 318.1118.

*3-fluoro-2-(prop-2-yn-1-ylamino)propanoic acid (**9**)*

To a solution of **8** (20 mg, 0.06 mmol) in dichloromethane (1 mL) anhydrous trifluoroacetic acid (2 mL) was added and stirred at room temperature for 72 h until the solution turned purple. Subsequently, methanol was added and the mixture was co-evaporated three times leading to the formation of a solid. The heterogeneous reaction

mixture was filtered, washed with methanol (3 x 1 mL) and the solvent was removed *in vacuo* yielding a yellow oil (8.7 mg, 0.06 mmol, quant.).

^{1}H-NMR (MeCN-d_3, 400MHz): δ [ppm] = 2.95 (m, 1H, C≡C*H*), 3.66 (m, 2H, N-C*H*$_2$-C≡CH), 4.39 (C_{alpha}*H*), 5.32 (m, 1H, C_{alpha}-C*H*$_2$-F), 5.38 (m, 1H, C_{alpha}-C*H*$_2$-F).

^{13}C-NMR (MeCN-d_3, 100MHz): δ [ppm] = 47.41 (N-*C*H$_2$), 55.34 (*C*$_{alpha}$), 77.64 ((-C≡*C*H), 78.32 (CH$_2$-*C*≡CH), 83.73 (*C*H$_2$-F), 85.89 (*C*H$_2$-F), 167.43 (C=O).

^{19}F-NMR (MeCN-d_3, 376 MHz): δ ppm] = -197.72

MS (ESI positive): 147.2 [M+H+H]

HRMS: calcd for C6H9FNO2 146.0612, found 146.0613.

II ^{18}F-labeling of the alkyne precursor

II.1 General radiolabeling methods

N.c.a. [^{18}F]fluoride was produced via the ^{18}O(p,n)^{18}F nuclear reaction. Isotopically enriched [^{18}O]water (97% enrichment) was irradiated by a 18 MeV proton beam and trapped on an anion exchange resin (Sep-Pak light Waters Accell Plus QMA cartridge), which was pre-conditioned with 1M potassium carbonate solution (10 ml) and rinsed with pure water (20 ml). Elution of the QMA cartridge was performed either with a Kryptofix 2.2.2/carbonate solution or with a cesium carbonate solution. The reaction kinetic was screened and optimized due to the amount of precursor, reaction temperature and reaction time, meaning that aliquots were taken after 1, 3, 5, 10, 20 min after addition of the activity to the precursor.

II.1.1 Carbonate/Kryptofix 2.2.2 labeling

^{18}F-fluoride was eluted from the QMA cartridge with a solution (1 mL) containing Kryptofix 2.2.2 (15 mg) and potassium carbonate (2 mg, 15 µmol) in dry acetonitrile. After elution the aqueous acetonitrile was azeotropically dried by heating under helium streaming at 86 °C for 20 min. Within this time dry acetonitrile (3 x 1 mL) was added and

evaporated to yield the final dry $[K\subset 2.2.2]^+/^{18}F^-$ complex. To the dried complex the desired solvent, acetonitrile, dimethylformamide or dimethyl sulfoxide, was added (1 mL) and an aliquot (200 µL/400 µL) was used for kinetic studies.

II.1.2 Cesium carbonate labeling

Elution of the ^{18}F-flouride from the QMA cartridge was done using a methanolic cesium carbonate solution (1 mL), containing cesium carbonate (12 mg, 37 µmol), dissolved in water (10 µL) and methanol (990 µL). The azeotropic drying was performed using a helium stream and heating to 86 °C for 20 min. During drying dry acetonitrile (3 x 1 mL) was added and evaporated, yielding the dry ^{18}F-tetrabutylammonium fluoride. This was re-dissolved in the desired solvent (1 mL), acetonitrile, dimethylformamide or dimethyl sulfoxide, and aliquots (100 µL/ 200 µL/ 400 µL) were used for kinetic studies.

II.2 Synthesis of 3-[^{18}F]fluoro-2-(prop-2-yn-1-ylamino)propanoic acid ([^{18}F]9)

After azeotropic drying of the ^{18}F-fluoride, the $[K\subset 2.2.2]^+/^{18}F^-$ complex was dissolved in dimethyl sulfoxide (0.6 mL) and transferred into a microwave vial containing the chlorine precursor **6** dissolved in dry dimethyl sulfoxide (0.4 mL). The reaction time was 5 min at 140 °C with a pre-heating time of 1 min, followed by the quench of the labeling reaction with water (1 mL) and injection into a semi-preparative HPLC system at a flow of 3.6 mL/min, whereas **A** is an aqueous ammonium formate buffer (5mM) and **B** is acetonitrile. The following method was used: 0-5 min 100% **A** (isocratic), 5-18 min 0-95% **B** (gradient), 18-22 95% **B** (isocratic), 22-25 5-100% **A** (gradient). After purification via semi-preparative HPLC the fraction was diluted with water (15 mL/ratio 1:4) and fixed on a Strata™ X SPE cartridge (Phenomenex). The fixed protected prosthetic group was eluted with acetonitrile (1 mL) into a reaction vessel and the acetonitrile removed (260 mbar, 70 °C, 20 mL/min helium flow). Deprotection was done using an aqueous 3.3M hydrochloric acid solution (0.5 mL) at 100 °C for 15 min. After neutralization of the reaction mixture using an aqueous 3.3M sodium hydroxide solution (0.5 mL). Additionally, 0.1M ammonium formate buffer (1 mL) was added and the mixture injected in a semi-preparative HPLC

system. The purified unprotected prosthetic group was collected and the solvents removed (100 mbar, 80 °C, 50 mL/min helium flow). The dried prosthetic group was re-dissolved in PBS buffer and used for the subsequent copper(I)-catalyzed cycloaddition. The overall RCY was 28±5% with an overall reaction time of 125 min (2 steps).

II.3 Copper(I)-catalyzed cycloaddition of [^{18}F]9 and azido-functionalized cRGD as model system

The unprotected prosthetic group **[^{18}F]9** was dissolved in PBS buffer (500 µL) and copper(II) sulfate (20 µmol) in 20 µL PBS buffer as well as the cRGD (1 mg, 1.1 µmol) in 440 µL PBS buffer were added. Subsequently, sodium ascorbate (100 µmol) in 40 µL PBS buffer was added and the mixture was reacted at 40 °C for 15 min. Analytical radio-HPLC was performed using the method described above at a flow of 3.6 mL/min: 0-5 min 100% **A** (isocratic), 5-18 min 0-95% **B** (gradient), 18-22 95% **B** (isocratic), 22-25 5-100% **A** (gradient). The final ^{18}F-labeled cRGD was obtained in 15% yield (determined by analytical radio-HPLC).

Synthesis and Evaluation of Boron Folates for Boron-Neutron-Capture-Therapy (BNCT)

Kathrin Kettenbach, Hanno Schieferstein, Catrin Grunewald, Dorothée Iffland, Christian Schütz, Gabriele Hampel, Nicolas Bings, Tobias L. Ross*

Institute of Nuclear Chemistry, Johannes Gutenberg-University Mainz, 55128 Mainz, Germany

Institute of Inorganic Chemistry and Analytical Chemistry, Johannes Gutenberg-University Mainz, 55128 Mainz, Germany

Radiochemistry/Radiopharmacy, Department of Nuclear Medicine, Hannover Medical School, 30623 Hannover, Germany

Introduction

The boron neutron capture therapy (BNCT) is a radiation therapy, which can selectively damage tumor cells, whereas the surrounding healthy tissue is not spared. This therapy uses a ^{10}B-pharmaceutical, which accumulates in the tumor tissue and is subsequently irradiated with thermal neutrons. The resulting nuclear reaction ^{10}B(n,α)^{7}Li provides an α-particle and a ^{7}Li-nucleus, which both deposit their energy with a high linear energy transfer (LET).

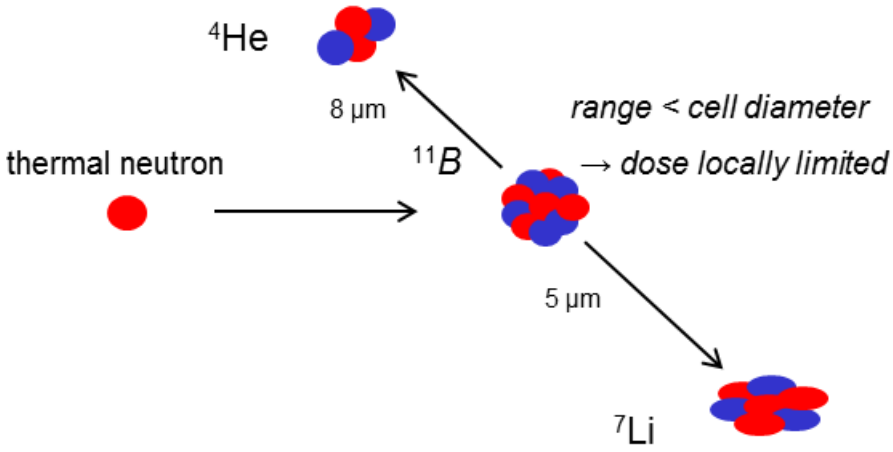

Figure 1: Irradiation and nuclear reaction of boron-10 with thermal neutrons.

Because of the low range of only 5-9 µm, which is below one cell diameter, those high-energy particles do not harm the surrounding healthy tissue.[1] Therefore BNCT is predominantly used as radiation scalpel for the therapy of malignant glioma[2,3], but also for recurrent head and neck tumors.[4] To obtain good therapeutic responses the boron compound has to be internalized into the tumor cells in concentrations of about 20 µg ^{10}B/g tissue to deploy its lethal effect.[5] It has also been reported that a prolonged retention of the boron compound in the tumor cells is essential to give a good tumor to normal tissue contrast and to ease time management and patient care.[6] The reduction of the background levels could be accomplished by introducing the FR-targeting concept, which enables a fast clearance from normal tissue due to the targeting effect.[7] Thus, there is a demand for a target, which allows a selective transportation of boron drugs into cancer cells, but not into healthy tissues. Additionally, the targeting vector should

furthermore allow a facile linkage of ^{10}B-delivery agents without loss of affinity of the targeting molecule to its targeting site.

So far the clinical established boron phenylalanine (BPA) or sodium boron mercaptate (BSH) use either inefficient (BPA) or passive (BSH) targeting for accumulation at target sites.[8–10] Nevertheless they are still clinically used for patients due to the lack of novel boron agents for BNCT, which satisfy the biological demands.

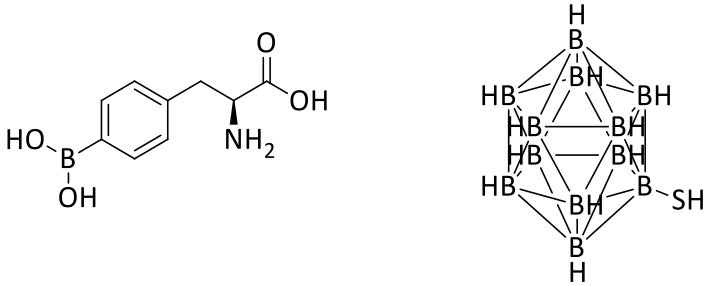

boron phenylalanine **sodium boron mercaptate**

Figure 2: The clinical “gold standard” BPA (boron phenylalanine) and BSH (sodium boron mercaptate).

BPA, an amino acid derivative, which accumulates in the tumor tissue due to the higher amino acid need of such highly proliferating cells, has been extensively investigated.[11,12] The major uptake process of BPA via the *L*-amino acid transporter (LAT 1) is based on a bidirectional 1:1 amino acid exchange, which showed promising results, but lacks an efficient trapping in the tumor cells.[8,9] Because of this insufficiency high blood levels of BPA are required and limits the time period for treatment after intravenous (i.v.) infusion.[12,13] Besides this active targeting concept, BSH uses the enhanced permeability and retention (EPR) effect for accumulation at target sites.[10,14] One major advantage of BSH is the high boron content due to its cluster structure, which makes it interesting for a coupling to a targeting vector.

An already proven targeting structure is the FR, which is (over)expressed on many human carcinomas and therefore provides an ideal oncological target due to a very restricted expression in normal healthy tissue.[15,16] The FR-targeting concept has been used for numerous molecular imaging as well as therapy approaches.[17,18] It has been shown that

the FR is (over)expressed in more than 50% of all human types of cancer, but the expression in normal tissue is limited to the kidneys, the lungs, placenta and *Plexus choroidus*, making the FR a very suitable target for BNCT.[15,16,18]

As already mentioned there is a demand for novel ^{11}B-pharmaceuticals, which accumulate selectively at target sites, because both clinically used boron pharmaceuticals are still not ideal for the application in BNCT.

The aim of this work was to combine the well-established BNCT with the highly specific and effective FR-targeting concept to improve tumor therapy.

Materials and Methods

Synthetic and Analytic Materials and Supplies

Protected pteroic acid was kindly provided by Merck & Cie AG (Switzerland). All other reagents were purchased from Acros Organics, Bachem, Deutero, Fisher-Scientific, Fluka, Lancaster, Merck, Sigma-Aldrich, Solvay-Organics and VWR. ^{1}H NMR spectra were recorded using an AC-300-Spektrometer (300-MHz-T-NMR-spectrometer AC 300, Bruker Analytik GmbH) in $CDCl_3$ or DMSO-d_6. For ^{11}B NMR spectra we used an Avance III-HD-400-Spektrometer (400 MHz) and for ^{13}C NMR spectra an Avance II-400-Spektrometer (400 MHZ). Chemical shifts for ^{1}H NMR were referenced to tetramethylsilane (0.00 ppm) and ^{13}C NMR they were calibrated to the solvent signals ($CDCl_3$: 77.0 ppm and DMSO-d_6: 39.5 ppm). FD and ESI mass spectrometry were performed on a MAT 95-spectrometer from Finnigan. For the boron detection we used an ICP-MS 7500 CE from Agilent respectively 4500 from Hewlett-Pachard (HP).

Synthesis

To synthesize the boron folates, a folate derivative was linked via a copper-catalyzed azide-alkyne cycloaddition (CuAAC) with a boron cluster (carboran and BSH), which is depicted in Scheme 1. A built-up synthesis was necessary to ensure regioselectivity. A at the γ-position derivatized boron folate was synthesized by first coupling azido spacer to a γ-protected glutamate, which was subsequently coupled to an alkyne maleimidecarboran via CuAAC. The alkyne maleimidecarboran was synthesized starting from maleimide anhydride and propargyl amine. Afterwards the carborane or BSH was coupled through a Michael addition reaction of the maleiimide and the thiol function of the boron clusters. In the last step the protected folic acid was deprotected using basic conditions.

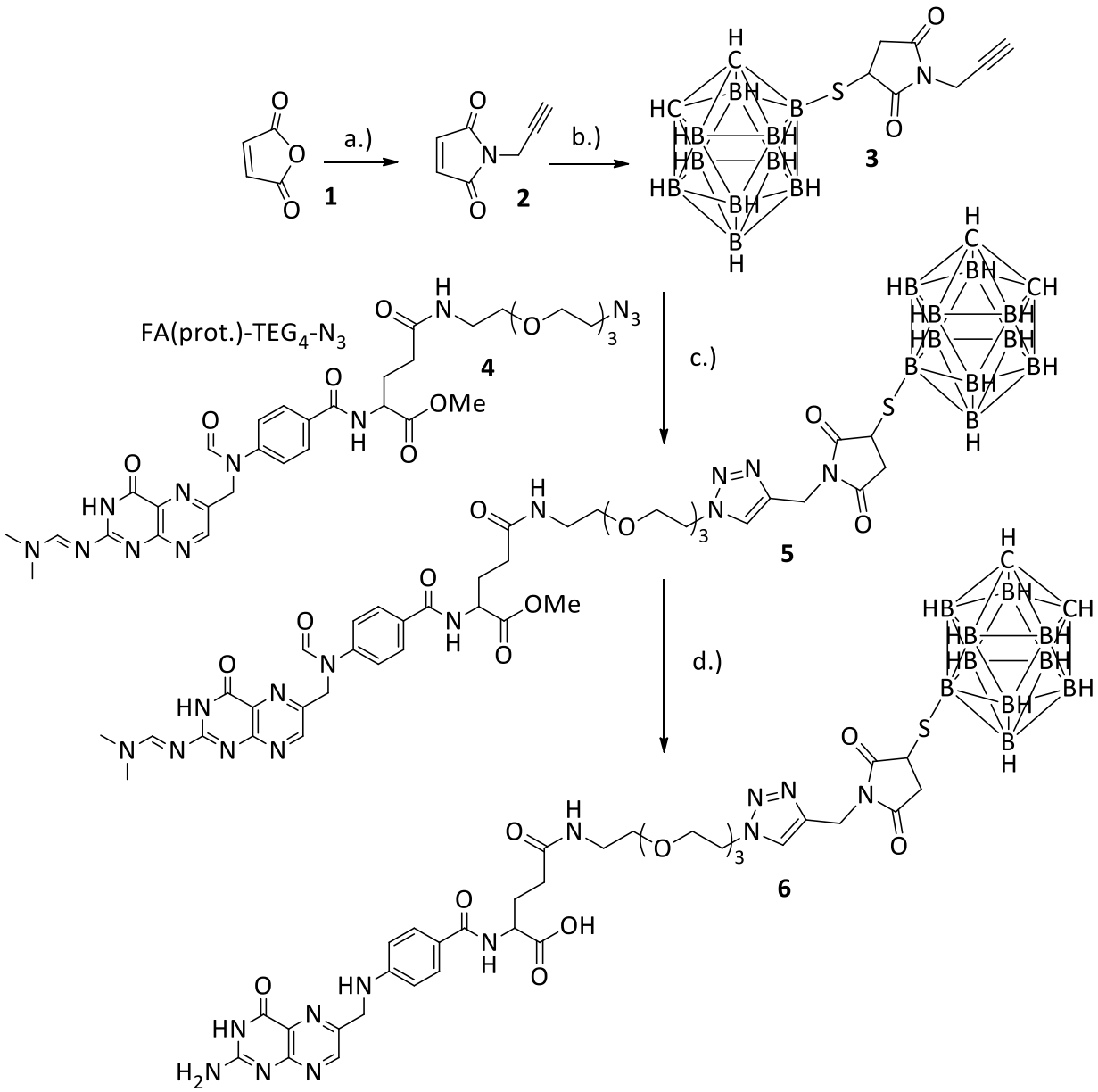

Scheme 1: Synthesis of the carboranfolate. a) maleic anhydride, toluene, 1 h, RT, $ZnCl_2$, HMDS, 2 h, 120°C; b.) MeCN, 0.2 M NaAc, 3 h, RT; c.) MeCN, $Cu(Ac)_2$, sodium ascorbate, 3 h, RT; d.) 1M NaOH, 12 h, RT, 2M HCl

The N^2-*N,N*-Dimethylaminomethylen-10-formyl-α-O-methyl-γ-(11-azido-3,6,9-trioxa-undecan-1-yl)folicacidamide (**4**) (protected) was synthesized according Schieferstein et al.[19]

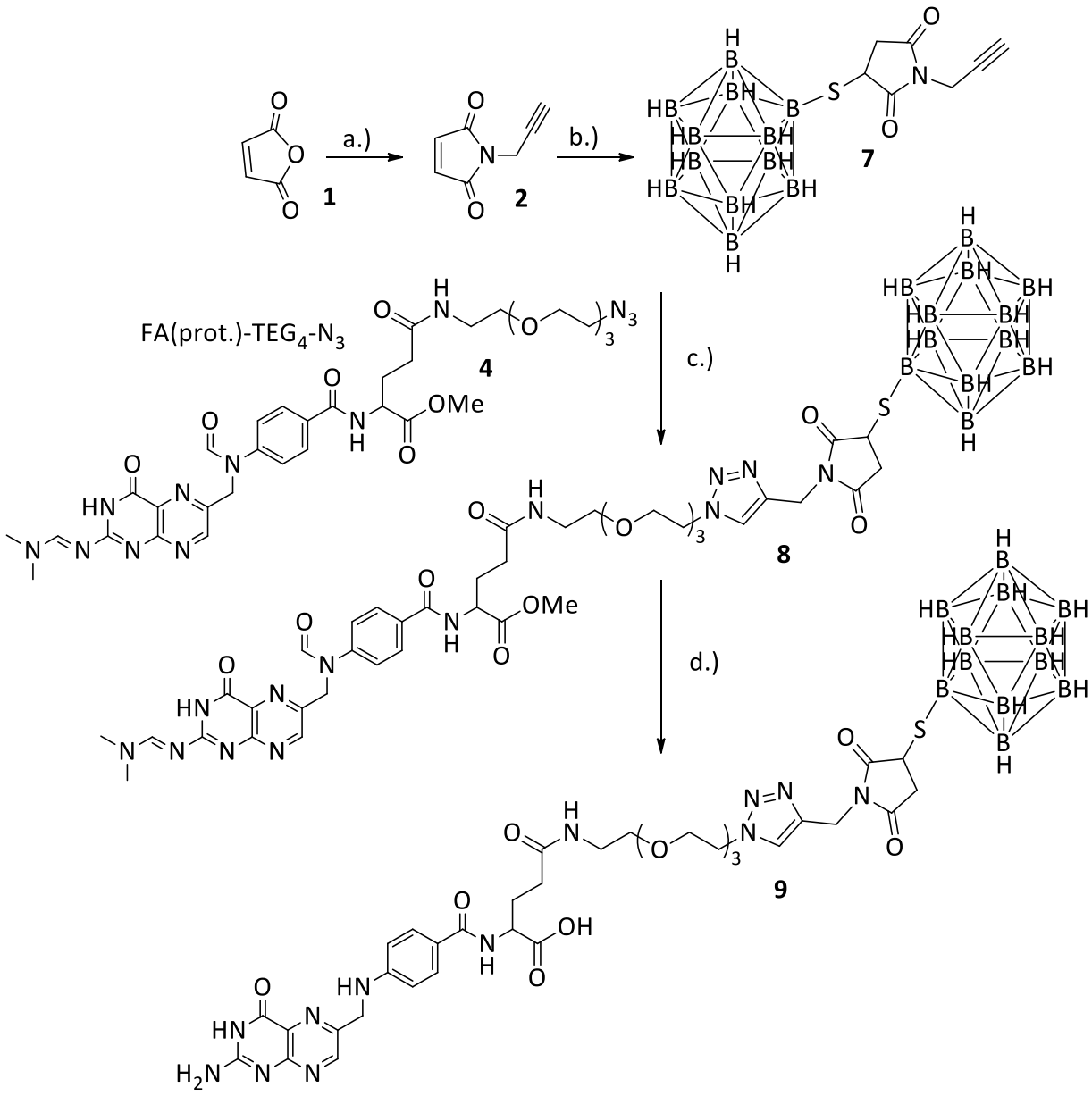

Scheme 2: Synthesis of the BSH-folate. a) maleic anhydride, toluene, 1 h, RT, $ZnCl_2$, HMDS, 2 h, 120°C; b.) MeCN, 0.2M NaAc, 3 h, RT; c.) MeCN, $Cu(Ac)_2$, sodium ascorbate, 3 h, RT; d.) 1M NaOH, 12 h, RT, 2M HCl. The N^2-N,N-Dimethylaminomethylen-10-formyl-α-O-methyl-γ-(11-azido-3,6,9-trioxa-undecan-1-yl)folic acid amide (**4**) (protected) was synthesized according Schieferstein et al.[19]

Synthesis of 1-(2-Propyn-1-yl)-1H-pyrrole-2,5-dione

Maleic anhydride (1.99 g, 19.3 mmol) (**1**) was dissolved in toluene (25 mL) and propargyl amine (1.06 g, 19.3 mmol) in toluene (10 mL) was added drop wise while stirring. The reaction mixture was stirred for 1 h at room temperature. Subsequently zinc chloride (2.63 g, 2 mmol) was added and the reaction mixture was heated to 120°C. Hexamethyldisilazane (HMDS) (6.11 mL, 3 mmol) in toluene (5mL) was added drop wise over 30 min. The reaction mixture was then refluxed for an additional hour before it was poured in 0.5M hydrochloride acid (50 mL). The aqueous phase was extracted with ethyl acetate (three times with 10 mL each). The product **2** was obtained as colorless oil (1.03 g, 7.65 mmol, 40%). ^{1}H NMR (300 MHz, $CDCl_3$): δ (ppm) = 6.73 (s, 2H, CH-CON), 4.26 (d, 2H, N-CH_2-CCH), 2.19 (t, 1H, CH-C-CH_2). MS (FD) m/z (% rel Int.): 135.7 ($[M]^+$, 100). Calculated ($C_7H_7NO_2$): 135.03

*Synthesis of 1-(2-Propyn-1-yl)-1H-pyrrole-2,5-dione-3-thiol-(9-mercapto-1,2-dicarba-closo-dodecane-borane) (**3**)*

1-(2-Propyn-1-yl)-1H-pyrrole-2,5-dione (**2**) (150 mg, 1.11 mmol) and 9-Mercapto-1,2-dicarba-closo-dodecane-borane were dissolved each in 5 mL acetonitrile and then combined. To start the reaction 0.2M sodium acetate solution (600 µL) was added and the reaction mixture was stirred for 3 h at room temperature. The product was extracted with dichloromethane (3 x 10 mL each) and the solvent was removed under reduced pressure before purification by column chromatography. Compound **3** was obtained as colorless oil (263 mg, 0.84 mmol, 75%). ^{1}H NMR (300 MHz, $CDCl_3$): δ (ppm) = 2.19 (s, 1 H, CH_2-C-CH), 2.72 (d, 1H, N-CO-CH_2), 2.77 (d, 1H, N-CO-CH_2), 3.24 (dd, 1H, S-CH), 4.25 (s, 2H, CH_2-C-CH). ^{11}B NMR (128.4 MHz, $CDCl_3$): δ (ppm) = -14.68 (t, 6B), -9.37 – 8.16 (d, 2B), -3.07 – 1.90 (d, 1B), 5.73 (s, 1B). ^{13}C NMR (100 MHz, $CDCl_3$): δ (ppm) = 28.03 (N-C-CO), 39.53 (CO-CH_2-CH-S), 41.26 (CO-CH_2-CH-S), 48.81 (Carba-C), 53.37 (Carba-C), 71.58 (CH-C-CH_2), 76.72 (CH-C-CH_2), 173.86 (N-CO-CH_2), 175.25 (N-CO-CH-S). MS (FD) m/z (% rel Int.): 334.19 ($[M+Na]^+$, 100), 646.40 ($[M+Na]^{2+}$). Calculated ($C_9H_{17}B_{10}NO_2S$): 313.19

*Synthesis of 1-(1,2,3-Triazo-4-N-ethyl-pyrrole-2,5-dione-3-thiol-(9-mercapto-1,2-dicarba-closo-dodecan-boran))3,6,9-trioxaundecan-1-yl)folicacidamide (**5**)*

The protected folic acid derivative **4** (60 mg, 0.08 mmol), **3** (27 mg, 0.08 mmol) and copper(II)acetate monohydrate (5.4 mg, 0.03 mmol) were dissolved in acetonitrile (2 mL, each) and combined. Subsequently sodium ascorbate (30 mg, 0.14 mmol) in water (400 µL) was added and the reaction mixture was stirred for 3 h at room temperature before it was extracted with dichloromethane (3 x 10 mL each). The product N^2-*N,N*-dimethylaminomethylene-10-formyl-α-O-methyl-γ-(11-(triazo-N-ethyl-pyrrole-2,5-dione-3-thiol-(9-mercapto-1,2-dicarba-closo-dodecane-borane)) 3,6,9-trioxaundecane-1-yl)folic acid amide (**5**) was obtained as a yellow solid (45 mg, 0.043mmol, 52%) after purification by column chromatography. ^{1}H NMR (300 MHz, $CDCl_3$): δ (ppm) = 1.59 (t, 2 H, TEG-NH-CO-CH_2), 1.93 – 2.08 (t, 2H, TEG-NH-CO-CH_2-CH_2), 2.39 (d, 6 H, CH_3-N-CH_3), 2.66 (s, 1 H, Carba-S-CH-CH_2), 3.30 (d, 2H, TEG-O-CH_2CH_2), 3.49 – 3.56 (d, 8H, TEG), 3.70 (d, 2H, TEG-O-NH-CH_2), 3.85 (s, CO-O-CH_3), 3.98 (d, 1 H, Carba-S-CH), 4.01 (t, 2H, TEG-O-CH_2-CH_2-N-N-N-), 4.05 (d,2H, TEG-O-CH_2-CH_2-N-N-N-), 4.09 (s, 2H, N-C-CH_2-N-CO), 4.40 (t, 1H, CO-NH-CH-$COOCH_3$), 5.34 (d, 2H, Carba-S-CO-N-CH_2), 7.62 (s, 1H, Carba-S-CO-N-CH_2-C-CH), 7.66 (s, 1H, CH_3-N-CH), 7.73 (d, 2H, CO-N-PhenylH), 7.78 (d, 2H, CO-N-CH_2PhenylH), 7.87 (s, 2H, NH), 7.98 (s, 1H, N-CH=O). ^{11}B NMR(128.4 MHz, $CDCl_3$): δ (ppm) = -14.05 (t, 6B), -9.53 – 8.22 (d, 2B), -3.25 – 2.23 (d, 1B), 5.56 (s, 1B). ^{13}C NMR (100 MHz, $CDCl_3$): δ (ppm) = 26.06 (1C, TEG-NH-CO-CH_2-CH_2), 26.66 (1C, TEG-NH-CO-CH_2-CH_2), 35.24 (1C, Carba-S-CH-CH_2), 36.60 (1C, Carba-S-CH), 39.45 (1C, TEG-CH_2-NH), 39.59 (2C, N-$(CH_3)_2$), 41.48 (1C, Carba-S-pyrrolle-2,5-dione-CH_2), 48.48 (1C, $COOCH_3$), 51.81 ($(CH_3)_2$N-CH-N-CH-N-C-N-CH-C-CH_2), 51.67 (Pter-NH-CH-COOMe), 52.01 (Carba-S-male-triaza-CH_2), 66.06 (Carba-S-male-triaza-CH_2-CH_2), 70.39 (2C, Carba-S-male-triaza-CH_2-CH_2-O-CH_2), 70.52 (2C, Carba-S-male-triaza-CH_2-CH_2-O-CH_2-$_{CH2)}$, 122.49 – 149.67 (12C, aromat.), 157.64 (1C, $(CH_3)_2$N-CH), 162.34 (N-CO), 170.42 (1C, COOMe), 172.54 (TEG-NH-CO), 174.69 (1C, Carba-S-CH-CO), 175.01 (1C, Carba-S-CH-CH_2CO). MS (FD) m/z (% rel Int.): 1073.58 ($[M+Na]^+$, 50). Calculated ($C_{41}H_{59}B_{10}N_{13}O_{11}S$): 1051.51

To remove the protection groups **5** (17 mg, 0.016 mmol) was dissolved in 1 M sodium hydroxide solution (1 mL) and stirred for 12 h at room temperature. The solution was acidified using 2M hydrochloride solution (500 µL) to precipitate the product. The precipitate was centrifuged and washed with water (2 x 1 mL). The product 11-triazo-*N*-ethyl-pyrrole-2,5-dione-3-thiol-(9-mercapto-1,2-dicarba-closo-dodecane-borane)3,6,9-trioxaundecane-1-yl)folic acid amide (**6**) was obtained as a yellow solid (13.3 mg, 0.014, 87%). ^{1}H NMR (300 MHz, DMSO-d_6): δ (ppm) = 1.90 (m, 1H, TEG-NH-CO-CH_2-CH_2), 2.02 (m, 1H, TEG-NH-CO-CH_2-CH_2), 2.20 (t, 2H, TEG-NH-CO-CH_2-CH_2), 2.92 (s, 2H, Carba-S-CH_2), 3.16 (d, 2H, TEG-CH_2CH_2-NH), 3.45 (t, 8H, TEG), 3.79 (d, 2H, N-N-N-CH_2-TEG), 3.76 (d, 2H, N-N-N-CH_2-CH_2-O) 4.25 (t, 2H, N-CH-C-CH_2-NH), 4.45 (d, 1H, NH-CH-COOH), 4.48 (d, 2H, N-N-N-C-CH_2) 6.61 (t, 2H, NH-CH), 7.17 (d, 1H, N-N-N-C-CH), 7.63 (t, 2H, HN-C-CH-CH-C-CO) 8.64 (s, 1H, N-CH-C-N) . ^{11}B NMR (128.4 MHz, DMSO-d_6): δ (ppm) = -13.68 (t, 6B), -8.40 (d, 2B), -3.02(d, 1B), 5.80 (s, 1B). ^{13}C NMR (100 MHz, DMSO-d_6): δ (ppm) = 27.00 (1C, TEG-NH-CO-CH_2-CH_2), 32.40 (1C, TEG-NH-CO-CH_2-CH_2), 51.81 ($(CH_3)_2$N-CH-N-CH-N-C-N-CH-C-CH_2), 56.29 (Carba-S-male-triaza-CH_2), 69.20 (Carba-S-male-triaza-CH_2-CH_2), 69.98 (2C, Carba-S-male-triaza-CH_2-CH_2-O-CH_2), 75.78 (2C, Carba-S-male-triaza-CH_2-CH_2-O-CH_2-CH_2), 120.05 – 147.40 (12C, aromat.), 172.15(1C, COOH), 174.28 (1C, Carba-S-CH-CO), 181.41 (1C, Carba-S-CH-CH_2CO). MS (FD) m/z (% rel Int.): 954.63 ($[M]^+$, 17), 972.64 ($[M + Na]^+$, 40), 994.67 ($[M + 2\ Na]^+$, 52). Calculated ($C_{36}H_{52}B_{10}N_{12}O_{10}S$): 954.45

*Synthesis of 1-(2-Propyn-1-yl)-1H-pyrrole-2,5-dione-3-thiol-(mercapto-closo-dodecaborate (**7**)*

Compound **2** (124 mg, 1.11 mmol) and mercapto-closo-dodecaborat disodium salt (220 mg, 1.11 mmol) were dissolved in acetonitrile (5 mL, each) and combined. To start the reaction 0.2M sodium acetate solution (600 µL) were added and the reaction mixture was stirred for 3 h at room temperature before it was extracted with dichloromethane (3 x 10 mL each). The solvent was removed under reduced pressure. The product *N*-propargyl-3-thiol-(mercapto-closo-dodecaborat)maleimid (**7**) was obtained as a colorless oil (299 mg, 0.84 mmol, 92%) after purification by column chromatography. ^{1}H NMR (300 MHz,

DMSO-d_6): δ (ppm) = 2.49 (d, 1 H, CH_2-C-CH), 3.13 (d, 1H, N-CO-CH_2), 3.34 (d, 1H, N-CO-CH_2), 3.36 (d, 1H, S-CH), 4.05 (d, 2H, CH_2-C-CH). ^{11}B NMR (128.4 MHz, DMSO-d_6): δ (ppm) = -18.59 bis -14.73 (t, 10B), -9.02 bis -7.14 (d, 2B). ^{13}C NMR (100 MHz, DMSO-d_6): δ (ppm) = 27.54 (N-C-CO), 39.36 (CO-CH_2-CH-S), 41.67 (CO-CH_2-CH-S), 73.74 (CH-C-CH_2), 78.59, (CH-C-CH_2), 176.48 (N-CO-CH_2), 177.80 (N-CO-CH-S). MS (FD) m/z (% rel Int.): 353.16 ($[M+Na]^+$, 100), 732.42 ($[M+Na]^{2+}$, 20), 1088.62 ($[M+Na]^{3+}$, 15). Calculated ($C_7H_{17}B_{12}NO_2S$): 331.9

*Synthesis of 11-(1,2,3-Triazo-4-N-ethyl-pyrrole-2,5-dione-3-thiol-(mercapto-closo-dodeca borate)) 3,6,9-trioxaundecan-1-yl)folic acid amide (**8**)*

The protected folic acid derivative **4** (35 mg, 0.05 mmol), **7** (17 mg, 0.05 mmol) and copper(II) acetate monohydrate (3.2 mg, 0.02 mmol) were dissolved in acetonitrile (2 mL, each) and combined. Subsequently sodium ascorbate (16 mg, 0.08 mmol) in water (400 µL) was added and the reaction mixture was stirred for 3 h at room temperature. The reaction mixture was extracted with dichloromethane (3 x 10 mL each) and the solvent was removed under reduced pressure. The product N^2-*N,N*-dimethyl-aminomethylen-10-formyl-α-O-methyl-γ-(11-(triazo-N-ethyl- pyrrole-2,5-dione -3-thiol-(mercapto-closo-dodecaborat))3,6,9-trioxaundecan-1-yl)folic acid amide (**8**) was obtained as a yellow solid (53 mg, 0.05 mmol, 68%). ^{1}H NMR (300 MHz, DMSO-d_6): δ (ppm) = 1.59 (t, 2 H, TEG-NH-CO-CH_2), 1.93 – 2.08 (t, 2H, TEG-NH-CO-CH_2-CH_2), 2.39 (d, 6 H, CH_3-N-CH_3), 2.66 und 3.03 (s, 1 H, Carba-S-CH-CH_2), 3.30 (d, 2H, TEG-O-CH_2CH_2), 3.49 – 3.56 (d, 8H, TEG), 3.70 (d, 2H, TEG-O-NH-CH_2), 3.85 (s, CO-O-CH_3), 3.98 (d, 1 H, Carba-S-CH), 4.01 (t, 2H, TEG-O-CH_2-CH_2-N-N-N-), 4.05 (d,2H, TEG-O-CH_2-CH_2-N-N-N-), 4.09 (s, 2H, N-C-CH_2-N-CO), 4.40 (t, 1H, CO-NH-CH-$COOCH_3$), 5.34 (d, 2H, Carba-S-CO-N-CH_2), 7.62 (s, 1H, Carba-S-CO-N-CH_2-C-CH), 7.66 (s, 1H, CH_3-N-CH), 7.73 (d, 2H, CO-N-PhenylH), 7.78 (d, 2H, CO-N-CH_2PhenylH), 7.87 (s, 2H, NH), 7.98 (s, 1H, N-CH=O). ^{11}B NMR (128.4 MHz, DMSO-d_6): δ (ppm) = -15.15 (d, 10B), -7.11 (d, 2B). ^{13}C NMR (100 MHz, DMSO-d_6): δ (ppm) = 27.54 (1C, TEG-NH-CO-CH_2-CH_2), 29.46 (1C, TEG-NH-CO-CH_2-CH_2), 36.28 (2C, Carba-S-CH-CH_2, Carba-S-CH), 39.33 (1C, TEG-CH_2-NH), 40.37 (2C, N-$(CH_3)_2$), 41.65 (1C, Carba-S-maleimid-CH_2), 50.87 (1C,

$COOCH_3$), 51.91 (Pter-NH-CH-COOMe), 52.52 (2C, $(CH_3)_2$N-CH-N-CH-N-C-N-CH-C-CH_2, Carba-S-male-triaza-CH_2), 62.08 (Carba-S-male-triaza-CH_2-CH_2), 70.05 (2C, Carba-S-male-triaza-CH_2-CH_2-O-CH_2), 70.62 (2C, Carba-S-male-triaza-CH_2-CH_2-O-CH_2-CH_2), 118.55 – 133.29 (12C, aromat.), 156.91 (1C, $(CH_3)_2$N-CH), 161.27 (1C, NH-CO-CN), 162.81 (N-CO), 165.26 (1C, Phenyl-CO-NH), 171.6 (1C, COOMe), 174.31 (TEG-NH-CO), 176.49 (1C, Carba-S-CH-CO), 177.80 (1C, Carba-S-CH-CH_2CO). MS (FD) m/z (% rel Int.): 1075.35 ($[M+Na]^+$, 5). Calculated ($C_{39}H_{59}B_{12}O_{11}S$): 1049.53

To remove all protection groups **8** (30 mg, 0,03 mmol) was dissolved in 1M sodium hydroxide solution (1mL) and stirred for 12 h at room temperature. The solution was acidified with 2M hydrochloride solution (500 µL) to precipitate the product. The precipitate was centrifuged and washed with water (2 x 1 mL, each). The product **9** was obtained as a yellow solid (5.3 mg, 0.006 mmol, 20%). ^{1}H NMR (300 MHz, DMSO-d_6): δ (ppm) = 1.77 (t, 1H, TEG-NH-CO-CH_2-CH_2), 2.11 (s, 1H, TEG-NH-CO-CH_2-CH_2), 2.15 (s, 2H, TEG-NH-CO-CH_2-CH_2), 3.43 (s, 2H, Carba-S-CH_2), 3.47 (d, 2H, TEG-CH_2CH_2-NH), 3.73 – 3.95 (t, 8H, TEG), 4.08 (d, 2H, N-N-N-CH_2-CH_2-O), 4.43 (d, 2H, N-N-N-CH_2-TEG), 4.48 (t, 2H, N-CH-C-CH_2-NH), 4.96 (d, 1H, NH-CH-COOH, 2H, N-N-N-C-CH_2) 6.65 – 8.88 (5 H, aromat.). ^{11}B NMR (128.4 MHz, DMSO-d_6): δ (ppm) = -15.21 (s, 12 B). ^{13}C NMR (100 MHz, DMSO-d_6): δ (ppm) = 29.15 (1C, TEG-NH-CO-CH_2-CH_2), 29.46 (1C, TEG-NH-CO-CH_2-CH_2), 34.16 (2C, Carba-S-CH-CH_2, Carba-S-CH), 38.43 (1C, TEG-CH_2-NH), 45.66 (1C, Carba-S-maleimid-CH_2), 47.44 (Pter-NH-CH-COOMe), 66.36 (Carba-S-male-triaza-CH_2-CH_2), 70.22 (2C, Carba-S-male-triaza-CH_2-CH_2-O-CH_2), 125.98 – 133.27 (12C, aromat.), 166.57 (1C, Phenyl-CO-NH). MS (FD) m/z (% rel Int.): 950.65 ($[M]^+$, 10), 954.62 ($[M]^+$, 9), 976.61 ($[M + Na]^+$, 6), 994.61 ($[M + 2\ Na]^+$, 45). Calculated ($C_{34}H_{52}B_{12}N_{12}O_{10}S$): 952.48

Biological evaluation

For the evaluation of **6** and **9** human KB cells derived from human cervical carcinoma were used. The cell line KB was obtained from DSMZ and cultured in DMEM medium with 10% FBS (fetal bovine serum), 1 % PEST (penicillin and streptomycin) and 1% MEM (non-essential amino acid). Cells were grown at 37 °C in a humidified atmosphere containing 5% CO_2.

Two days before the experiment the cells were sowed in petri dishes and cultivated at 37 °C and 5% CO_2. The boron folates (**6** and **9**) were dissolved in PBS buffer in different concentrations for the in vitro studies. After the incubation at 37 °C for 1.5 h or 2.5 h, cells were washed with PBS buffer and then with acidic glacial acid buffer (pH 3) to remove the receptor bound folate. The cells were trypsinized and collected as a pellet via centrifugation. Reference experiments using BPA were conducted as described above. Each experiment was carried out three times in triplicates for each setup (incubation time and concentration).

The boron content of the cell pellets, the washing solution and stripping buffer was measured via ICP-MS and normalized to one million cells. After BPA incubation the cell pellets were dissolved in nitric acid and hydrogen peroxide solution (1 mL, each). For the analysis 1 mL of this solution was spiked with concentrated ammonia solution, beryllium, rhodium standard (50 µL, each) and rinse solution (2.9 mL), which consist of butanol (2.5%), EDTA (0.05%), Triton X-100 (0.05%) and ammonia solution (1.0%). The beryllium and rhodium is used as an internal standard to detect fluctuation during measurement due to temperature variation or salification. For the boron folate probes a microwave supported digestion was used. Cell pellets were dissolved in nitric acid (4 mL) and hydrogen peroxide solution (32%, 4 mL). To analyze the washing solution and stripping buffer 200 µL were dissolved in nitric acid and hydrogen peroxide solution (3.9 mL, each). The probes were then heated up to 200 °C within 10 minutes and this temperature was hold for 10 min. The temperature was then raised up to 240 °C and hold constant for 20 min before cooling down to room temperature.

Results

The aim of this work was to combine BNCT with the FR-targeting concept to provide a higher boron accumulation in tumor tissue and to improve tumor therapy using BNCT. Therefore folic acid was conjugated to a boron carrying system (boron cluster) to assure a selective and effective transportation of the boron pharmaceutical into the tumor cells via the folate receptor. Therefore an γ-azido oligoethylene folate synthesized using a protocol described by Schieferstein et al.[19] The carboran as well as the BSH cluster were coupled to a linker system via Michael addition if a thiol and maleimide, which in turn was coupled to the azido folate via CuAAC. The final carboran folate **6** could be obtained within six reaction steps with a total yield of 7%. The BSH-folate **9** could be obtained in an overall yield of 3%. Afterwards **6** and **9** were tested *in vitro*.

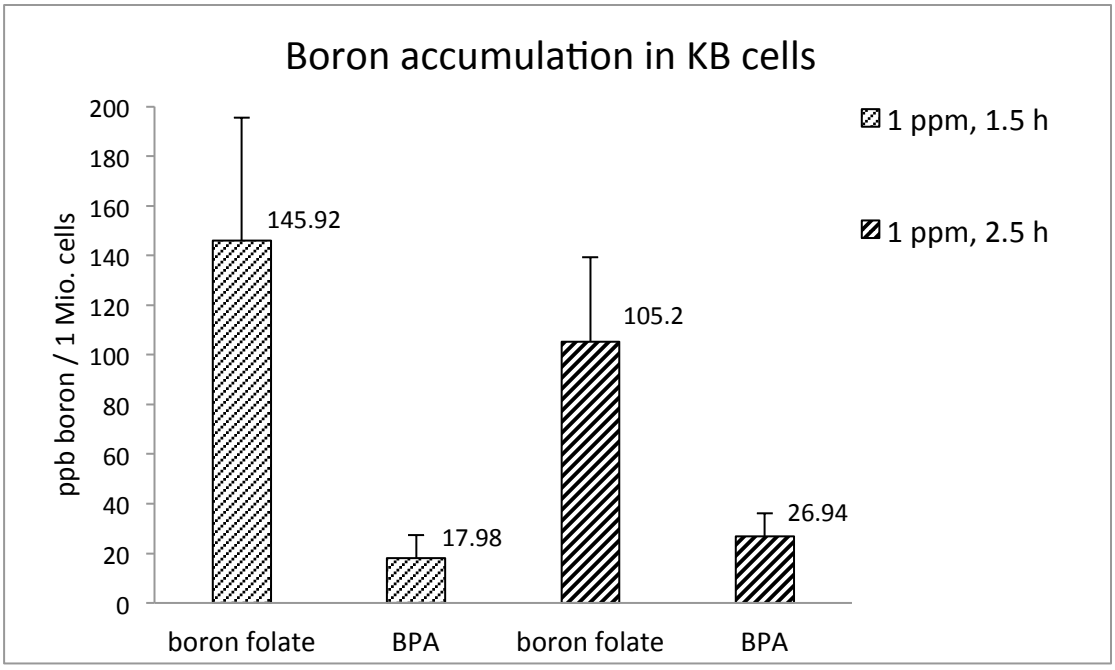

Figure 3: Boron accumulation in KB cells after incubation with carboran folate in comparison to BPA uptake at 1 ppm.

The boron amount for each setting (incubation concentration and time) was normalized to one million cells. In figure 3 the boron amount of the carboran folate **6** compared to BPA for an incubation concentration of 1 ppm and at 1.5 h and 2.5 h can be seen. The boron concentration after 1.5 h is 145.92 ppm/1 million cells, whereas the BPA reached

only levels of 17.98 ppm/1 million cells. After 2.5 h the boron concentration slightly decreased for the carboran folate to 105.2 ppm/1 million cells and the BPA concentration stayed almost constant.

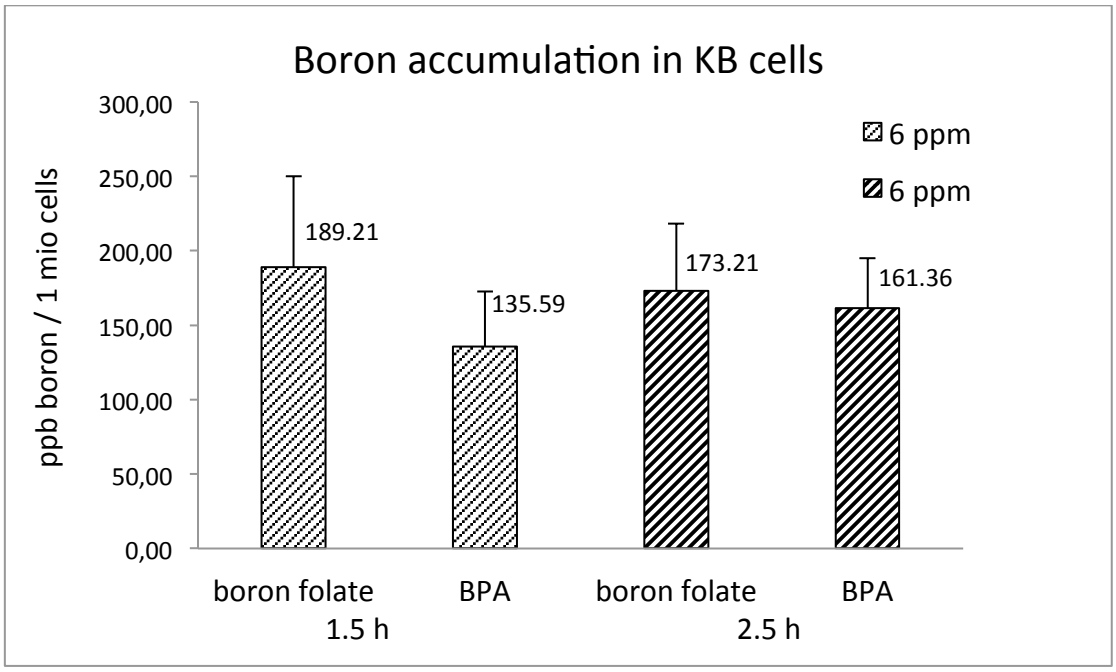

Figure 4: Boron accumulation in KB cells after incubation with carboran folate in comparison to BPA uptake for 6 ppm.

Figure 4 displays uptake studies of the carboran folate **9** and BPA at incubation concentrations of 6 ppm. Like in the experiments described before, the incubation time was set at 1.5 h and 2.5 h respectively. The boron concentrations of the carboran folates were 189.59 ppm/1 million cells (1.5 h) and 173.21 ppm/1 million cells after 2.5 h incubation time. BPA concentrations reached 135.59 ppm/1 million cells (1.5 h) and increased slightly to 161.36 ppm/1 million cells.

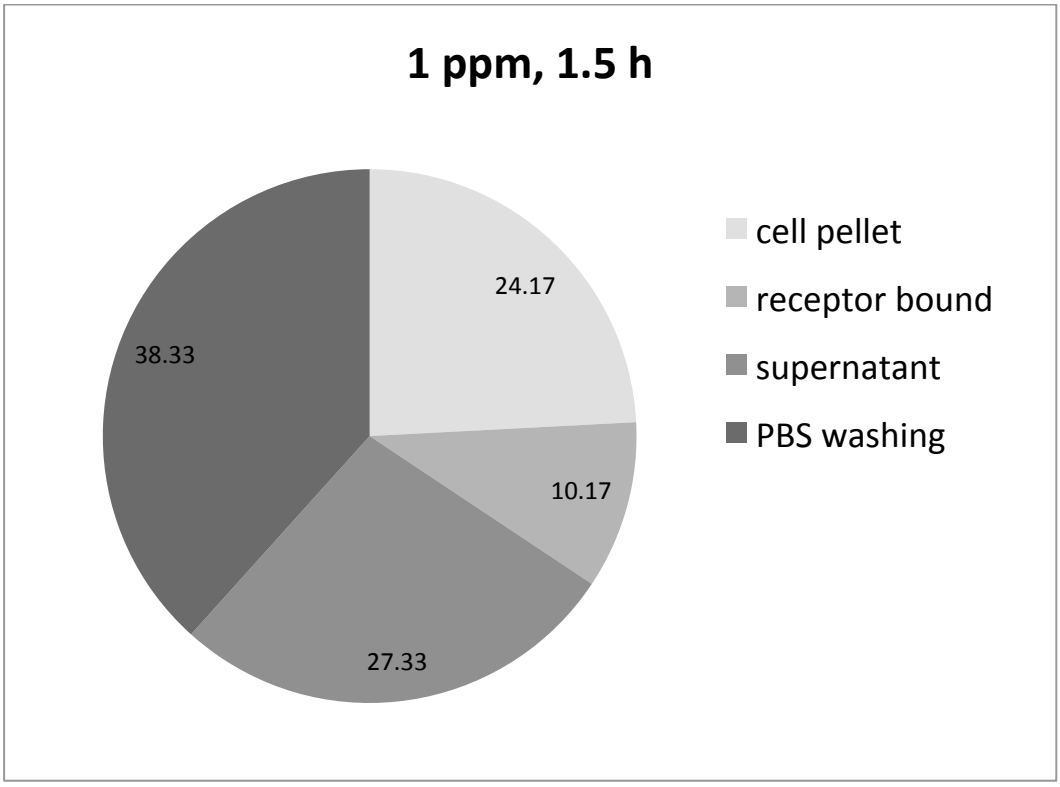

Figure 5: boron distribution after incubation with carboran **6** folate within one probe.

In figure 5 the boron distribution within one probe as an example for incubation with carboran folate with a concentration of 1 ppm and an incubation time of 1.5 h can be seen. The pie chart shows that nearly 25% of the applied boron folate was internalized and additional 10% was receptor bound at the end of the incubation time. One third of the incubated carboran folate stayed in the supernatant after 1.5 h of incubation. The other third was found in the PBS washing fraction. The distribution pattern did not change if a higher starting concentration of 6 ppm was used.

Discussion

Two novel boron folates, a carboran folate as well as a BSH-folate was synthesized in six steps with an overall yields of 7% respectively 3%. Considering the complexity of those molecules and that their multi-step syntheses, the total synthesis yields were very satisfactorily. The final coupling of the folate moiety and the boron cluster was achieved through CuAAC under mild and regioselective conditions. Since the boron clusters both were only available carrying thiol groups for derivatization, a Michael addition reaction seemed very suitable. Therefore the linker molecule **2** was synthesized, which was able to do Michael additions and participate in CuAACs. Both synthetic approaches display the successful syntheses of two novel derivatives, which can be used for active targeting in BNCT. The incubation studies on human KB cells clearly showed an increased boron accumulation in the cells compared with BPA due to the active FR-targeting. Moreover a clear tendency could be observed by considering the initial concentration of carboran folate. By increasing the concentration of carboran folate from 1 ppm to 6 ppm only a little increase of boron in the cells could be measured. But the BPA concentration in the cells increased and reached almost the same boron levels as for FR-targeting after 1.5 h or 2.5 h. However, taking a look at the at the low concentrations (1 ppm) of carboran folate for reaching a sort of plateau and comparing the uptake levels of BPA at the same concentrations, it becomes clear that FR-targeting resulted in 5-times higher boron concentrations in the cells. Considering the setup of the measurements, it can be seen, that also 10% of the carboran folate have been bound to the receptor, but not internalized. However, this fraction would also have a lethal effect on tumor cells, because of the spatial proximity. Furthermore, the carboran folate shows extra advantages compared to BPA, beside an increased accumulation in the tumor cells. Additionally folates are known to show a longer retention time in tumor tissue than BPA or BSH.[7,20,] Both, BPA and show a high efflux from tumor tissue after infusion.[21] Compared to this, the tumor concentrations retain almost constant even after 24 hours, whereas the blood concentrations already decrease after one hour, which is shown by Fani et al. for ^{68}Ga- and ^{111}In-labeled folate derivatives.[7] This allows enables to start with the therapy

several hours after infusion of the boron folate, leading to very good tumor-to-blood-levels and therefore to a lower background. This reduces the damage of healthy tissues during irradiation with thermal neutrons. Furthermore a reduced systematically applied dose among of pharmaceutical due to the higher boron charging of the boron cluster could be achieved.

With those promising results concerning the higher accumulation of targeted novel boron drugs in tumor cells, biodistribution studies are ongoing to evaluate the novel compounds *in vivo*. Furthermore incubation studies with higher boron folate concentrations up to 50 ppm to gain more information about possible saturation effects of the folate receptor are under investigation.

In conclusion we can say, that we synthesized two novel folate derivatives, which are conjugated to a boron cluster to have the ability for BNCT. Furthermore, one of the folate derivatives has been evaluated in *in vitro* experiments showing promising results due a 5-times higher uptake in cells than BPA. These results display the high potential of the FR-targeting concept in BNCT.

Acknowledgments

The authors thank Merck & Cie AG (Switzerland) for kindly providing protected pteroic acid. Hanno Schieferstein thanks the research cluster SAMT for financial support.

References

(1) Slatkin, D. N. *Brain* **1991**, *114*, 1609–1629.

(2) Farr, L. E.; Sweet, W. H.; Robertson, J. S.; Foster, C. G.; Locksley, H. B.; Sutherland, D. L.; Mendelsohn, M. L.; Stickley, E. E. *Am. J. Roentgenol. Radium Ther. Nucl. Med.* **1954**, *71*, 279–293.

(3) Chadha, M.; Capala, J.; Coderre, J. A.; Elowitz, E. H.; Iwai, J.; Joel, D. D.; Liu, H. B.; Wielopolski, L.; Chanana, A. D. *Int. J. Radiat. Oncol. Biol. Phys.* **1998**, *40*, 829–834.

(4) Kato, I.; Ono, K.; Sakurai, Y.; Ohmae, M.; Maruhashi, A.; Imahori, Y.; Kirihata, M.; Nakazawa, M.; Yura, Y. *Appl. Radiat. Isot.* **2004**, *61*, 1069–1073.

(5) Barth, R. F.; Soloway, A. H.; Fairchild, R. G.; Brugger, R. M. *Cancer* **1992**, *70*, 2995–3007.

(6) Barth, R.; H Vicente, M. G.; Harling, O.; Kiger, W. S.; Riley, K.; Binns, P.; Wagner, F.; Suzuki, M.; Aihara, T.; Kato, I.; Kawabata, S. *Radiat. Oncol.* **2012**, *7*, 146.

(7) Fani, M.; Wang, X.; Nicolas, G.; Medina, C.; Raynal, I.; Port, M.; Maecke, H. R. *Eur. J. Nucl. Med. Mol. Imaging* **2011**, *38*, 108–19.

(8) Meier, C.; Ristic, Z.; Klauser, S.; Verrey, F. *EMBO J.* **2002**, *21*, 580–9.

(9) Yoshimoto, M.; Kurihara, H.; Honda, N.; Kawai, K.; Ohe, K.; Fujii, H.; Itami, J.; Arai, Y. *Nucl. Med. Biol.* **2013**, *40*, 625–9.

(10) Maeda, H.; Wu, J.; Sawa, T.; Matsumura, Y.; Hori, K. *J. Controlled Release* **2000**, *65*, 271–84.

(11) Savolainen, S.; Kortesniemi, M.; Timonen, M.; Reijonen, V.; Kuusela, L.; Uusi-Simola, J.; Salli, E.; Koivunoro, H.; Seppälä, T.; Lönnroth, N.; Välimäki, P.; Hyvönen, H.; Kotiluoto, P.; Serén, T.; Kuronen, A.; Heikkinen, S.; Kosunen, A.; Auterinen, I. *Phys. Med.* **2013**, *29*, 233–48.

(12) Coderre, J. a; Elowitz, E. H.; Chadha, M.; Bergland, R.; Capala, J.; Joel, D. D.; Liu, H. B.; Slatkin, D. N.; Chanana, a D. *J. Neurooncol.* **1997**, *33*, 141–52.

(13) Kankaanranta, L.; Seppälä, T.; Koivunoro, H.; Saarilahti, K.; Atula, T.; Collan, J.; Salli, E.; Kortesniemi, M.; Uusi-Simola, J.; Mäkitie, A.; Seppänen, M.; Minn, H.; Kotiluoto, P.; Auterinen, I.; Savolainen, S.; Kouri, M.; Joensuu, H. *Int. J. Radiat. Oncol. Biol. Phys.* **2007**, *69*, 475–82.

(14) Matsumura, Y.; Maeda, H. *Cancer Res.* **1986**, 6387–6392.

(15) Weitman, S. D.; Lark, R. H.; Coney, L. R.; Fort, D. W.; Frasca, V.; Zurawski, V. R.; Kamen, B. A. *Cancer Res.* **1992**, *52*, 3396–3401.

(16) Garin-Chesa, P.; Campbell, I.; Saigo, P. E.; Lewis, J. L.; Old, L. J.; Rettig, W. J. *Am. J. Pathol.* **1993**, *142*, 557–67.

(17) Siegel, B. A.; Dehdashti, F.; Mutch, D. G.; Podoloff, D. A.; Wendt, R.; Sutton, G. P.; Burt, R. W.; Ellis, P. R.; Mathias, C. J.; Green, M. A.; Gershenson, D. M. *J. Nucl. Med* **2003**, *44*, 700–707.

(18) Ross, J. F.; Chaudhuri, P. K.; Ratnam, M. *Cancer* **1994**, *73*, 2432.

(19) Schieferstein, H.; Betzel, T.; Fischer, C. R.; Ross, T. L. *EJNMMI Res.* **2013**, *3*, 68.

(20) Ichikawa, H.; Taniguchi, E.; Fujimoto, T.; Fukumori, Y. *Appl. Radiat. Isot.* **2009**, *67*, S111–4.

(21) Obayashi, S.; Kato, I.; Ono, K.; Masunaga, S.-I.; Suzuki, M.; Nagata, K.; Sakurai, Y.; Yura, Y. *Oral Oncol.* **2004**, *40*, 474–82.

^{18}F-Radiolabeling and Evaluation of Folate-pHPMA Conjugates via PET

H. Schieferstein, A. Kelsch, A. Reibel, K. Koynov, M. Barz, H.G. Buchholz, N. Bausbacher, O. Thews, R. Zentel, T.L. Ross

[1]Institute of Nuclear Chemistry, Johannes Gutenberg University, Mainz, Germany

[2]Institute of Organic Chemistry, Johannes Gutenberg University, Mainz, Germany

[3]Institute of Physiology and Pathophysiology, University Medicine Mainz, Mainz, Germany

[4] Max Planck Institute for Polymer Research, 55128 Mainz, Germany

[5]Department of Nuclear Medicine, University Medical Center Mainz, Mainz, Germany

[6]Institute of Physiology, University Halle, Halle, Germany

Introduction

Based on the visionary work of H. Jatzkewitz[1] and H. Ringsdorf[2], who introduced the concept of macromolecular-based drug delivery systems, many diverse macromolecular systems, which can be summarized under the expression “polymer therapeutics”, were investigated up to now.[3,4] Particularly the biocompatible and in some cases biodegradable polymers have entered clinical trials and are used as anticancer conjugates, numerous being HPMA-based conjugates.[3,5–7] Up to now the influence of different architectures of pHPMA-based carrier systems has already been investigated using fluorine-18 for short-term PET studies or iodine-131 for long-term *in vivo* studies.[8–11] It has been shown that the accumulation of untargeted pHPMA in the tumor, reaches its best contrast levels after 168 h.[10] Thus 2 h short-term micro PET studies do always suffer the slow kinetics of the enhanced permeability and retention (EPR) effect, resulting in limited contrast levels.[12] Additionally, different tumor entities show marked variations of the EPR effect, which limits passive targeting.[11,13] For enhancing the tumor accumulation of polymeric systems that active targeting is favorable and might accelerate specific accumulation at target sites.[14,15] The potential of active targeting could already be demonstrated by addressing the immune system and inducing a specific immune response, to that effect an immune stimulus is protected from degradation.[16] Keeping the enormous potential of active targeting in mind, surprisingly there is –to the best of our knowledge- no clinical proof for successful targeting of nanoparticles. One reason is for sure the complex conjugation of targeting structures like antibodies to nano-sized objects. Thus, small molecules may be an easier target, especially when the binding side is disease associated, like in the case of folates.[17,18]

This makes folic acid an attractive targeting vector for macromolecular drug delivery systems. Folic acid by itself has a very high affinity to the FR ($K_d \sim 10^{-10}$ M).[19–21] Besides, the FR is very tolerant towards the size of cargo, and is able to bind and internalize – predominantly by clathrine mediated endocytosis- even big molecules, like

macromolecular folate conjugates, up to sizes of 100 nm.[22] An enhanced folate-mediated *in vitro* uptake of macromolecular systems, e.g. micells[23–27] dendrimers,[28,29] coated inorganic nanoparticles[30–32], or liposomes[33–35].

However, at present the body distribution of different polymeric architectures and the effect of different chemical bonding of folate on the *in vivo* behavior have not fully understood. Polymeric nanoparticles described in literature, dealing with FA, are mostly based on polyethylene oxide (PEO), but only little attention has been paid on pHPMA. The biggest advantage of using pHPMA is its multifunctionality. Nowadays, pHPMA can be synthesized via controlled radical polymerization techniques, such as reversible addition-fragmentation chain transfer (RAFT) polymerization in combination with the reactive ester approach.[36,37] Up to date the incorporation of folic acid into the side-chains of pHPMA has already been described by Barz and coworkers as well as the group of McCormick, who investigated the cell uptake of pHPMA due to folate conjugation and variation of folate content.[38,39] The benchmark for the development of the here reported folic acid pHPMA conjugates via copper(I)-catalyzed cycloaddition, was set on these findings, and therefore the incorporation of about 10% folic acid into the polymer side chains was chosen. Beyond the already proven increased uptake in *in vitro* experiments, there are still unanswered questions regarding the *in vivo* behavior of folate-pHPMA conjugates, whereas non-targeted polymeric systems have been sufficiently evaluated *in vivo*.[9,11] Thus, the FR-targeting concept addressing the FR on the cell surface, was investigated in combination with these polymeric systems. The aim of this work was to investigate by positron emission tomography (PET) how high and low molecular weight folate-pHPMA conjugates behave *in vivo* with respect to tumor accumulation and contrast ratios in the Walker-256 carcinoma model of the rat.

Experimental Section

Materials

All chemicals were reagent grade, obtained from Aldrich and Acros and used without further purification, unless indicated otherwise. Oregon green cadaverin was purchased from Invitrogen. All solvents were of analytical grade. Pentafluorophenol was obtained from Fluorochem (Great Britain, U.K.) and distilled prior to use. Dioxane and dimethylsulfoxide (DMSO) used in the syntheses were freshly distilled from a sodium/potassium mixture. 2,2'-Azobis-(isobutyronitrile) (AIBN) was recrystallized from diethyl ether and stored at −7 °C. Deuterated chloroform-d_1 was purchased from Deutero GmbH, dried, and stored over molecular sieves. Dialyses were performed with Cellu SepH1 membranes (Membrane Filtration Products, Inc.) with a nominal molecular weight cutoff of 1000 g/mol and Spectra/Por membranes (Roth) with a nominal molecular weight cutoff of 3500 g/mol. The building block *N2-N,N*-dimethylaminomethylene-10-formylpteoric acid was generously provided by Merck & Cie AG, Schaffhausen, Switzerland.

Characterization

^{1}H and ^{13}C nuclear magnetic resonance spectra were recorded on either a Bruker 300 MHz or 400 MHz spectrometer. Chemical shifts (δ) to solvent are reported in parts per million (ppm) relative to tetramethylsilane and referenced; the following abbreviations are used in the experimental section for the description of ^{1}H NMR spectra: singlet (s), doublet (d), triplet (t), multiplet (m), broad (br). The chemical shifts of complex multiplets are given as the range of their occurrence. Low-resolution mass spectra (LR-MS) and high-resolution mass spectra (HR-MS) were recorded on either a Micromass Quattro micro API LC-ESI or a Finnigan MAT90-Spectrometer. Reactions were monitored by thin layer chromatography (TLC, performed on Merck silica gel 60 F254, not modified, pre-coated silica gel on aluminum-supported plates).

Synthesis of 2-(2-(2-(prop-2-yn-1-yloxy)ethoxy)ethoxy)ethanamine

The 2-(2-(2-(prop-2-yn-1-yloxy)ethoxy)ethoxy)ethyl 4-methylbenzenesulfonate was prepared in analogy to the literature and used as starting material for further sntheses.[40] Potassium phthalimide (342 mg, 1 mmol), 2-(2-(2-(prop-2-yn-1-yloxy)ethoxy)ethoxy)ethyl 4-methylbenzenesulfonate and catalytic amounts of potassium iodide were dissolved in a mixture of dry dimethylformamide (10 mL) and dry ethanol (5 mL) and heated at 110 °C overnight. The dimethylformamide was removed under vacuum, the residue re-dissolved in ethanol (15 mL), hydrazine hydrate (150 µL) was added and refluxed overnight until a white precipitate was formed. Subsequently, half-concentrated hydrochloric acid (15 mL) was added and the crude reaction mixture was refluxed for another 45 min. The removal of ethanol was done under vacuum and the crude reaction mixture filtered and washed with 2 M hydrochloric acid (2 x 5 mL). The pH-value of the filtrate was adjusted to 12 using sodium hydroxide, extracted with ethyl acetate (3 x 15 mL) and dried over sodium sulfate. The removal of the solvent yielded 2-(2-(2-(prop-2-yn-1-yloxy)ethoxy)ethoxy)ethanamine (151 mg, 0.8 mmol, 80%) as a yellow oil.

^{1}H NMR (300 MHz, $CDCl_3$): δ [ppm] = 4.18 (2H, d, O-CH_2-C≡CH), 3.70-3.48 (m, 8H, O-CH_2-CH_2), 3.49 (t, 2H, N-CH_2-CH_2), 2.85 (t, 2H, N-CH_2-CH_2), 2.40 (t, 1H, C≡C*H*), 2.08 (-NH_2).

Synthesis of the HPMA-based polymers

Synthesis of 4-cyano-4-((thiobenzoyl)sulfanyl)pentanoic acid (CTP)

4-cyano-4-((thiobenzoyl)sulfanyl)pentanoic acid was used as chain transfer agent (CTA) and synthesized according to literature in a 3-step reaction.[41]

Synthesis of pentafluorophenyl methacrylate (PFPMA)

PFPMA was prepared according to the literature.[36]

Synthesis of macro-CTA

RAFT polymerization of PFPMA using CTP was performed in a Schlenk tube[42,43], loaded with PFPMA and 2,2'-azobis(isobutyronitrile) (AIBN), (molar ratio monomer/CTA/AIBN: 50/1/0.1) and finally dissolved in absolute dioxane. After three freeze–vacuum–thaw cycles, the mixture was stirred at 70 °C for 16 h. Afterwards the polymeric solution was precipitated 3 times in hexane, isolated by centrifugation and dried for 12 h at 30 °C under vacuum. A pink powder with a yield of 79% was obtained. ^{1}H-NMR ($CDCl_3$): δ [ppm] 1.9-2.7 (br), 1.2-1.7 (br). ^{19}F-NMR ($CDCl_3$): δ [ppm] -162.6 (br), -157.3 (br), -150 to -152 (br).

Removal of dithiobenzoate end group

The dithiobenzoate end group was removed according to the procedure reported by Perrier et al.[44] Therefore a 25-fold molar excess of ACVA was added to the polymer dissolved in dioxane. After four hours of heating the solution at 80 °C, the polymer was precipitated in hexane twice and collected by centrifugation. The polymer was dried under vacuum for 18 h; a colorless powder could be obtained. Yield: 91%. The absence of the dithiobenzoate endgroup was confirmed by UV–vis spectroscopy.

Polymer analogous reaction of homopolymers

For radioactive labeling of polymers the protocol was applied as follows.

200 mg of P-R without dithioester endgroup were dissolved in 2.5 mL of abs. dioxane. Exemplary for P1-R (Mn = 12,800 g/mol) 8.6 mg of tyramine and 12.8 mg of triethylamine were diluted in a DMSO/dioxane mixture and added to the vessel. After stirring for 6 hours at 60 °C, 89 mg of alkyne spacer in 500 µL dioxane as well as 96.2 mg of triethylamine were added and the solution stirred for 1 day. Thereafter, 30.6 mg of 2-hydroxypropylamine and 136.2 mg of triethylamine were added and the solution further stirred for 48 hours. For final removal of reactive ester side groups 61.2 mg of 2-hydroxypropylamine were additionally added the next morning. The solution was

precipitated two times in diethyl ether, centrifuged and finally dissolved in a DMSO/water solution for dialysis. After lyophilization a white, crystalline powder with a yield of 68% could be obtained. ^{1}H-NMR (400 MHz, DMSO-d_6) δ [ppm]: 0.60-1.40 (br), 1.45-2.40 (br), 2.72-3.07 (br), 3.22-3.43 (s), 3.44-3.60 (br), 3.61-3.90 (br), 4.06-4.22 (s), 4.50-4.83 (br), 6.60-6.76 (br) and 6.89-7.04 (br). For additional fluorescent labeling, 200 mg of P1-R were diluted in 2.5 mL of absolute dioxane and 3.92 mg of Oregon Green 488 cadaverine as well as 0.53 mg of triethylamine were added. After stirring for 6 h alkyne spacer, 2-hydroxypropylamine and triethylamine were added, as described by the procedure above.

Characterization of the Copolymers.

All ^{19}F NMR spectra were recorded on a Bruker 400 MHz FT- NMR spectrometer. Chemical shifts (δ) are given in ppm relative to CCl_3F. All measurements were accomplished at room temperature and spectroscopic data were analyzed using ACDLabs 9.0 1D NMR Manager. Polymers were dried at 40 °C overnight under vacuum and subsequently characterized by size exclusion chromatography (SEC). SEC was performed in tetrahydrofurane (THF) as solvent using the following system: pump PU 1580, auto sampler AS 1555, UV-detector UV 1575, RI-detector RI 1530 from Jasco, and miniDAWN Tristar light scattering detector from Wyatt. Columns were used from MZ Analysentechnik, 300x8.0 mm: MZ-Gel SDplus 102 Å, MZ-Gel SDplus 104 Å, and MZ-Gel SDplus 106 Å. The elution diagrams were analyzed using the ASTRA 4.73.04 software from Wyatt Technology. Calibration was done using polystyrene standards. The flow rate was 1 mL/min at a temperature of 25 °C and the salt content was 0.1 mmol/mL.

Synthesis of γ-(11-azido-3,6,9-trioxaundecanyl)folic acid amide

The folic acid derivate was prepared in analogy to the literature.[40]

General procedure for the synthesis of the folate-pHPMA conjugates

pHPMA (20 mg) was dissolved in 500 µL of phosphate buffered saline (PBS buffer) followed by the addition of copper sulfate (3.2 µg, 0.02 µmol) in 500 µL PBS buffer and sodium ascorbate (39 µg, 0.2 µmol) in 500 µL PBS buffer. After 15 minutes of stirring at RT the azido-folate (0.1 mg, 0.15 µmol) in 200 µL PBS buffer was added and the reaction mixture was protected from sunlight and allowed to react for another 16 h. Purification was accomplished using a GE PD-10 Desalting Column (M_r 5000), pre-conditioned with Milli-Q water. Fractions were analyzed using UV/Vis spectroscopy and sodium permanganate staining leading to 15 mg of the desired folate-pHPMA conjugate.

Characterization of the folate-pHPMA conjugates

Characterization of the folate-pHPMA derivatives was done ^{1}H NMR spectroscopy. Folate incorporation was calculated through the oligoethylene spacer signal ratios before and after folate conjugation.

Aggregation behavior of the folate-pHPMA conjugates

The aggregation behavior of the pHPMA polymers was investigated via fluorescence correlation spectroscopy (FCS) using a commercial setup (Zeiss, Germany), which is described in details elsewhere.[45] Concentrations, similar to the blood concentrations of pHPMA, folate-pHPMA conjugate (0.02 mg/mL) as well as blocking agent (0.04 mg/mL), were used.

Radiolabeling

The radiolabeling using [^{18}F]FETos was done in analogy to Herth et al. [8]

For synthesis of 2-[^{18}F]fluoroethyl-1-tosylate ([^{18}F]FETos), a Sykam S 1100 pump and a Knauer UV-detector (K-2501) HPLC system were used. Size exclusion chromatography (SEC) of ^{18}F-labeled polymers was performed using a GE HiTrap Desalting Column, Sephadex G-25 Superfine, and a Merck Hitachi System equipped with two L-7100 pumps,

a L-7400 UV detector, a D-7000 D-Line, an L-7250 autosampler, a L-7300 column oven and a Gina-Star radiodetector.

Animal experiments

For animal experiments the rat Walker 256 mammary carcinoma cell line was used. The cell line was grown in culture in RPMI medium supplemented with 10 mM L-glutamine and 10% fetal calf serum (FCS) at 37 °C under a humidified 5% CO_2 atmosphere and sub-cultivated twice per week. For tumor implantation male Sprague-Dawley rats (Charles River Wiga, Sulzfeld, Germany; body weight 180 to 400 g) housed in the animal care facility of the University of Mainz were used in this study. All experiments had previously been approved by the regional animal ethics committee and were conducted in accordance with the German Law for Animal Protection and the UKCCCR Guidelines.[46] Animals were allowed access to food and acidified water *ad libitum* before the investigation. Solid carcinomas Walker-256 cells were heterotopically induced by injection of cell suspension (0.4 mL approx. 10^4 cells/µL) subcutaneously into the dorsum of the hind foot. Tumors grew as flat, spherical segments and replaced the subcutis and corium completely. Volumes were determined by measuring the three orthogonal diameters (d) of the tumors and using an ellipsoid approximation with the formula: V = d1 x d2 x d3 x π/6. Tumors were used when they reached a volume of between 0.5 to 4.0 mL approx. 7 to 14 days after tumor cell inoculation.

Ex vivo biodistribution studies

For *ex vivo* biodistribution studies animals were injected with ^{18}F-labeled folate-pHPMA conjugate (1 mg in 1 mL isotonic sodium chloride solution, 5.5-23.7 MBq, light and heavy conjugate) intravenously (i.v.) in the tail vein. For blockade studies the rats were injected i.v. in the tail vein with native folic acid (2 mg/kg BW) 3 min before tracer administration. After 120 or 240 min post injection (p.i.), the animals were sacrificed and different organs (kidney, liver, lung, spleen, heart, skeletal muscle, small intestine, testis, blood) as well as the tumors were excised. The samples were weighted, minced and measured in a Perkin

Elmer 2470 Wizard2 γ-counter to calculate the percentage of injected dose per gram tissue.

In vivo micro PET studies

For PET measurements, rats were anaesthetized with isofluran (3%) and polymers were injected into the tail. The µPET imaging was performed on a microPET Focus 120 small animal PET (Siemens/Concorde, Knoxville, USA). During PET measurements the animals were placed in supine position and breathed room air spontaneously. Dynamic PET studies were acquired in listmode. The injected activity of radiolabeled polymers was 19.0±1.3 MBq (in 500-900 µL isotonic saline). Blocking experiments were performed using native folic acid (2 mg/kg) injected 3 min prior to tracer administration. The PET listmode data were histogrammed into 25 frames and reconstructed using OSEM2D algorithm. Volumes-of-interests (VOIs) were defined for tumor and reference tissue (testis). The testis was used as a reference since it was in the field of view when imaging the tumors on the feet and because the tissue concentration was relatively constant between all animals on a low level. Time activity curves (TAC) were obtained with varying time frames (1.5-10 min) for a total measuring interval of 120 min. Ratios of tumor to reference tissue were calculated from integral images between 15’ and 120’ after polymer injection.

Results and Discussion

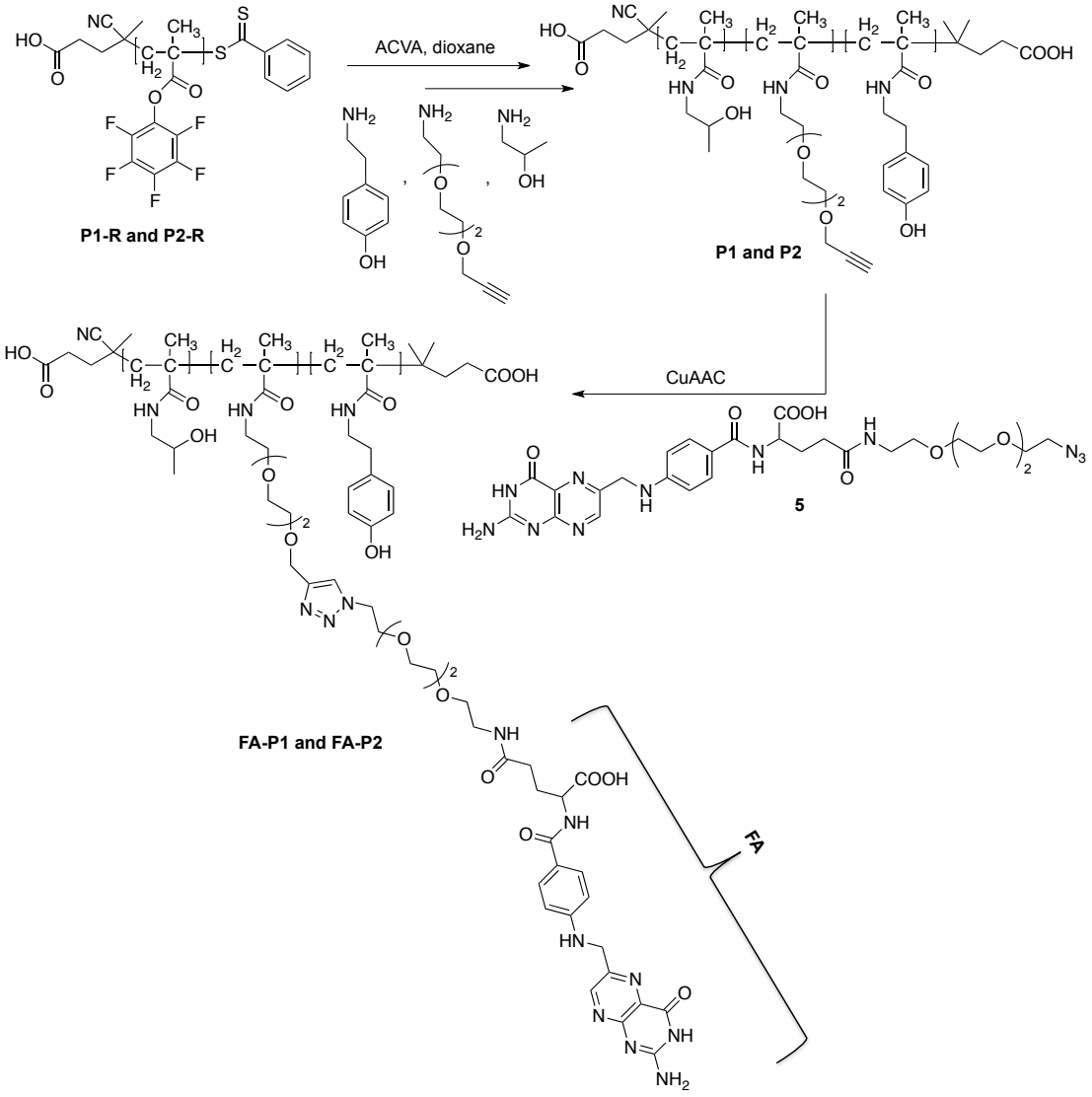

Scheme 1: Polymer synthesis and conjugation of the azido folate (FA) to the polymer side chain.

Synthetic concept of small and large folate-pHPMA conjugates

It has been shown that it is possible to influence the biodistribution of polymeric systems by simply varying their size, molecular weight or composition.[10,11]

The pHPMA polymers were synthesized using the reactive ester approach (Scheme 1). Therefore we synthesized well-defined high and low molecular weight polypentafluorophenylmathacrylate polymers (**P1-R**, **P2-R**) with narrow dispersities (Đ) of

1.2 for the low molecular weight polymer and 1.4 for the high molecular weight polymer (Table 1). The reactive precursor polymers (**P1-R**, **P2-R**) were precisely characterized and later on transferred into pHPMA polymers bearing further alkyne moieties for the attachment of targeting vectors (**P1** and **P2**). Therefore, precursor polymers were aminolyzed using 2-(2-(2-(prop-2-yn-1-yloxy)ethoxy)ethoxy)ethanamine, 2-hydroxyproylamine, -(2-(2-(prop-2-yn-1-yloxy)ethoxy)ethoxy)ethanamine and tyramine. In the case of fluorescence-labeling OG was used instead of tyramine (**P1-OG**, **P2-OG**). The 2-(2-(2-(prop-2-yn-1-yloxy)ethoxy)ethoxy)ethanamine was synthesized in 3 steps (see supporting information).

Thus, in the next step coupling of the folate derivative to the polymer can be achieved through copper catalyzed azide-alkyne cycloaddition (CuAAc). Since Barz and coworkers showed, at least 10% folate incorporation were needed to enhance uptake, we used the same amount of folate.[49] Both polymers were also labeled with Oregon Green 488 cadaverin (OG) for FCS measurements (**P1-OG**, **P2-OG**). So the aggregation behavior of hydrophilic HPMA polymers and the compared hydrophobic folate could be investigated, since it has been reported that already 10% of hydrophobic segments led to aggregate formation.[51] The incorporation of the alkyne spacer was determined by ^{1}H NMR, resulting in 10% alkyne incorporation for all polymers. These polymers were coupled to a previously synthesized azido-folate using CuAAc to give the final polymers (**FA-P1**, **FA-P2**, **FA-P1-OG**, **FA-P2-OG**). The folate-conjugates were purified using size exclusion chromatography (SEC; Sephadex G-25) and lyophilized. After derivatization and purification the ratio of the oligoethylene parts of precursor-click polymers (**P1**, **P2**, **P1-OG**, **P2-OG**) and folate-polymer conjugates (**FA-P1**, **FA-P2**, **FA-P1-OG**, **FA-P2-OG**) was determined by ^{1}H NMR spectroscopy. The percentage of incorporated folate was calculated using these ratios and remained constant at 8% for all polymers (Table 1). Additionally the incorporation of tyramine into the polymer side chain (3%) enables the radiolabeling with fluorine-18 and therefore to track the folate-pHPMA conjugates *in vivo*.

Table 1. Characterization of pHPMA and folate-pHPMA conjugates

Polymer	M_n [g/mol]	M_w [g/mol]	Đ	Tyramine content[2]	Aklyne content[2]	Folic acid content[2]
P1-R	12,800[1]	16,000[1]	1.2[1]	-	-	-
P2-R	64,000[1]	91,500[1]	1.4[1]	-	-	-
P1	8,000[3]	10,000[3]	1.2[3]	3%	10%	-
P2	40,000[3]	57,000[3]	1.4[3]	3%	10%	-
FA-P1	10,500[3]	13,000[3]	1.2[3]	3%	10%	8%
FA-P2	52,500[3]	75,000[3]	1.4[3]	3%	10%	8%
P1-OG[4]	8,000[3]	10.000[3]	1.2[3]	-	10%	-
P2-OG[4]	40,500[3]	58,000[3]	1.4[3]	-	10%	-
FA-P1-OG[4]	10,800[3]	13.000[3]	1.2[3]	-	10%	8%
FA-P2-OG[4]	53,500[3]	76,500[3]	1.4[3]	-	10%	8%

[1] = Determination by GPC in THF as solvent ; [2] = Tyramine-, alkyne spacer- and folic acid incorporation ratio determined by ^{1}H-NMR spectroscopy after polymeranalogous reaction; [3] = Calculated from the molecular weight of the reactive ester polymer P-R determined by GPC in THF as solvent; [4] = Oregon Green Cadaverine was incorporated during polymeranalogous reaction (1 mol%).

FCS studies

Since folate moieties are hydrophobic segment, aggregate formation like reported by Barz et al. can occure. Fluorescence correlation spectroscopy[52] was used to measure the hydrodynamic radii of the studied folate-pHPMA conjugates and inspect their aggregation behavior in the presence or absence of folic acid. Typical FCS autocorrelation curves (ACC) for the lower molecular weight HPMA polymer (**P1-OG**) and its folate conjugate (**FA-P1-OG**) are shown in Figure 1A. As can be seen the curves are almost identical. By fitting them with an appropriate model function[51,52] the values of 2.0 nm and 2.2 nm were determined for the hydrodynamic radii of **P1-OG** and **FA-P1-OG** respectively. Adding 0.04 μmol of folic acid to the **FA-P1-OG** solution, which corresponds with the blood concentration during blockade in 1 mL blood, did not induce aggregation as evident from the corresponding ACC curve (Figure 1A). That corresponds to small diffusing fluorescent species with hydrodynamic radius of about 2.2 nm. The behavior of the high molecular weight polymers, however, is qualitatively different. While, in the solution of the net HPMA polymer (**P2-OG**) only individual polymer chains with hydrodynamic radius of

around 3.3 nm are observed, the folate conjugate **FA-P2-OG** shows strong aggregation even in the absence of free folic acid. The corresponding correlation curve (Figure 1B) is strongly affected by the presence of large aggregates with an average radius in the order of 100 nm that coexist in the solution together with the individually diffusing polymer chains. The addition of folic acid to the solution does not significantly affect the aggregation behavior of the **FA-P2-OG** as evident from corresponding ACC (Figure 1B).[51]

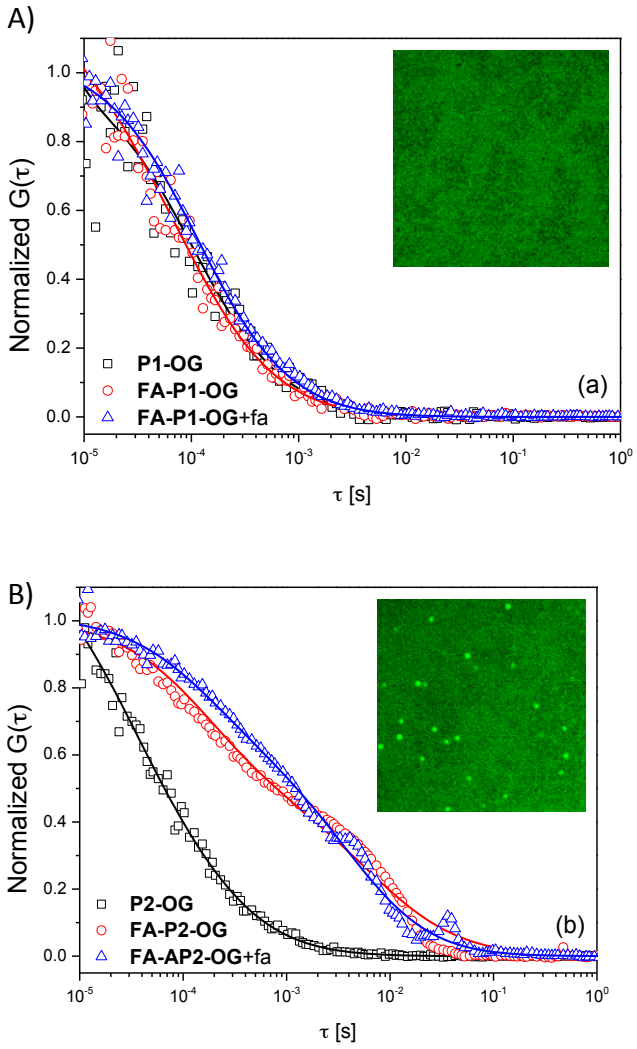

Figure 1. Normalized FCS autocorrelation curves measured for the low (**A**) and high (**B**) molecular weight pHPMA polymers in aqueous solutions. The square symbols correspond to the net polymers, the circles to the folate conjugates in the absence of folic acid and the triangles to the folate conjugates in the presence of folic acid. The insets show representative CLSM images (100 µm x 100 µm) of the FCS cell in the latter case.

Radiolabeling using [^{18}F]fluoroethyl tosylate and purification

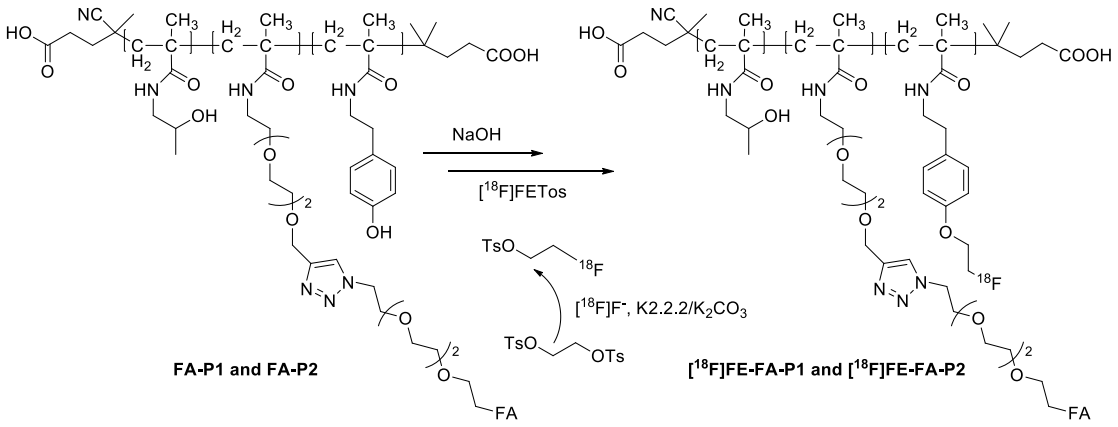

Scheme 2. Radiolabeling of **FA-P1** and **FA-P2** using [^{18}F]FETos.

The radiolabeling was facilitated as already described by Herth et al. using [^{18}F]fluoroethyl tosylate (Scheme 2).[8] The amount of precursor was held constant (3 mg) as well as the amount of base (5 µmol), obtaining radiochemical yields (RCY) of 10% for the low molecular weight polymer and 5% for the high molecular weight polymer (Table 2). For purification the crude reaction mixture was injected into a size exclusion HPLC system, using 0.9% isotonic sodium chloride solution as solvent and three GE HiTrap (5mL) columns.

Table 2. Radiolabeling of the folate-pHPMA conjugates

Polymer	M_n [g/mol]	M_w [g/mol]	RCY
[^{18}F]FE-FA-P1	10,500	13,000	10±2
[^{18}F]FE-FA-P2	52,500	75,000	5±3

Animal experiments

PET imaging

To investigate the *in vivo* behavior µPET experiments were performed, allowing quantification of the tracer uptake in different organs and in the tumors (Walker-256 mammary carcinoma of the rat). Figures 2A+B show whole body images of the polymer distribution 120 min after i.v. injection of the low mw (**[^{18}F]FE-FA-P1**) or high mw (**[^{18}F]FE-FA-P2**) polymers. Comparable to the untargeted homopolymers the low mw polymer showed highest concentration in the kidney (indicating a high renal excretion) whereas the high mw polymer (**[^{18}F]FE-FA-P2**) accumulated mainly in the liver (Li) and renal clearance was only of minor importance (Figures 2A+B).[9]

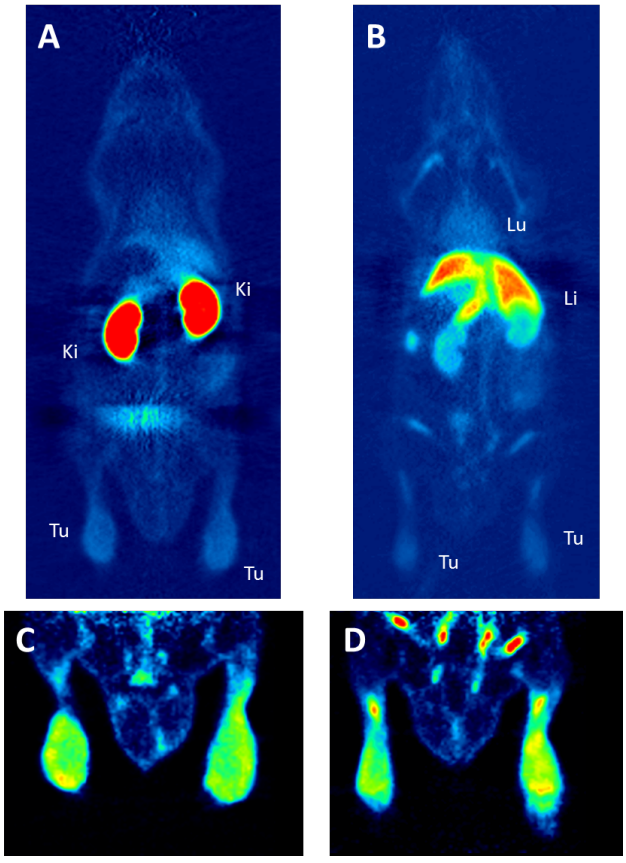

Figure 2. Representative µPET imgaes of the whole body distribution (**A**+**B**) and the tumor accumulation (**B**+**C**) of the low molecular weight (A+C, **[^{18}F]FE-FA-P1**, Mw=10.5 kDa) and high molecular weight (**B**+**D**, **[^{18}F]FE-FA-P2**, Mw=52.5 kDa) pHPMA-folate conjugates. Tu: tumor, Ki: kidney, Li: liver, Lu: lung.

PET imaging also showed a clear polymer accumulation in the tumors implanted on the hindfood dorsum (Figure 2C+D). In order to quantify the tumor uptake *in vivo*, the intratumoral activity was normalized to the reference tissue in the field of view (testis) and time activity curves (TACs) were calculated. Referencing the testis enables to gauge the fluctuations based on perfusion and diffusion of the tracers. Figure 3 shows the averaged TACs over the 120 min observation period of the polymer-folate conjugates without and with blockade by native folate as well as the tumor accumulation of the labeled untargeted pHPMA. After an initial redistribution within the first 20 min after injection the low mw polymer (Figure 3A, solid line) reaches a stable plateau over the complete observation period, which was almost twice as high as the polymer without folate conjugation (dotted line). Blockade of the FR with native folate tumor accumulation led to a markedly reduced (dashed line) intratumoral concentration, which tends to decrease over time (Figure 3). The high mw polymer was taken up into the tumor even stronger than the low mw counterpart (Figure 4) which is the opposite behavior found in previous measurements with polymers without folate conjugation.[9] The time course of tumor uptake of the high mw folate-polymer shows some differences to the small polymer (Figure 3B). Without blocking the polymer showed a reduced initial redistribution phase followed by a more or less continuous increase in tumor uptake. With folate blocking the time course during the first hour was comparable to that without blocking. However, afterwards the intratumoral activity in blocked animals was continuously decreasing (Figure 3B) indicating a constant redistribution and elimination. After 2 h a significant difference (approximately 20%) between blocked and non-blocked animals was reached (Figure 4).

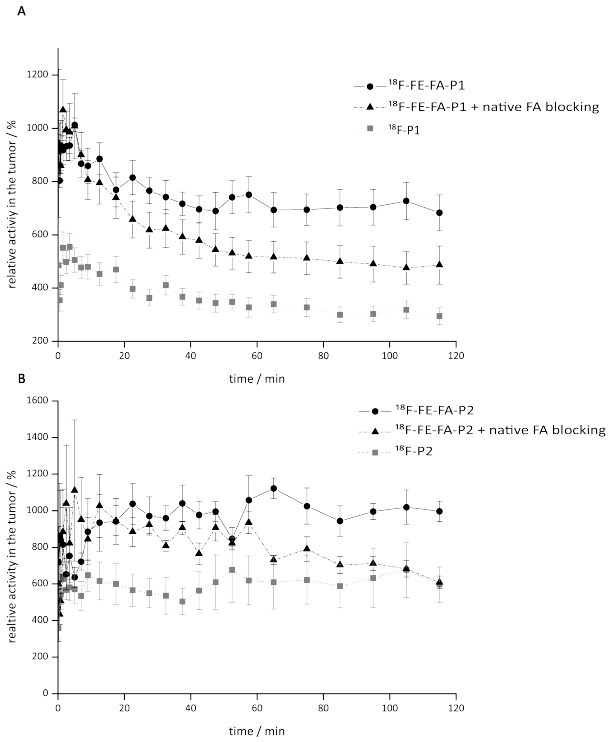

Figure 3. Time activity curves of the intratumoral accumulation of (**A**) the low mw and (**B**) the high mw polymer. Solid curves show the respective folate-pHPMA conjugates without blocking whereas dashed lines indicate activites with native FA blocking. Dotted lines show tumor accumulation of the pHPMA polymers without FA-conjugation. Values were normalized to the concentration of the reference tissue (testis). n=2-7.

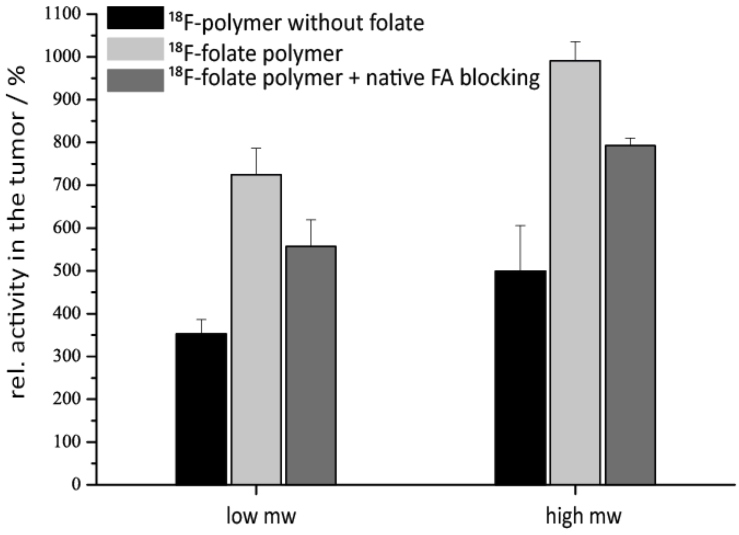

Figure 4. Comparison of uptake of the small and large pHPMA polymers in Walker-256 carcinomas) determined by PET imaging (intratumoral activity over the period from 15’ to 120’ after polymer injection normalized to the reference tissue testis). Shown are the values for the polymer without folate moiety and folate-polymer conjugates without or with simultaneous blocking by free folate. n=2-7.

One possible explanation for the differences in the uptake kinetics between the low and high mw conjugates could be the fact that the large polymers more easily formed aggregates due to their higher fraction of lipophilic folate residues compared the HPA. By this the hydrodynamic radius (which is already larger in high mw polymers) further increases leading to a reduced diffusive uptake but also slower redistribution (Figure 3).

The higher number of folates per polymer molecule could also explain the observed difference in the relative accumulation of the low and high mw polymers (Figure 4). But also the faster redistribution of unbound low mw polymers out of the tumor could contribute to the observed differences.

Ex vivo biodistribution

The Tables 3 and 4 show the biodistribution of **[^{18}F]FE-FA-P1** and **[^{18}F]FE-FA-P2** in tumor bearing rats. Table 3 lists the biodistribution data of the low mm folate-pHPMA conjugate (**[^{18}F]FE-FA-P1**). As seen in the PET images (Figure 2A) the highest accumulation of **[^{18}F]FE-FA-P1** was found in the kidneys and remained almost constant over 240 min, which is consistent with the findings that low molecular weight polymers ran through renal excretion.[8,9] Under blockade conditions the accumulation of **[^{18}F]FE-FA-P1** after 120 min or 240 min did only slightly decrease. The low accumulation in the liver after 120 min or 240 min indicates the relatively minor importance of the hepatic elimination of the low mw folate-HPMA conjugate. The liver uptake was also almost independent from the blocking with free folate.

Table 3. Biodistribution study of **[^{18}F]FE-FA-P1**

Organ or tissue	120 min p.i. (*n* = 3)	120 min p.i. blockade (*n* = 3)	240 min p.i. (*n* = 3)	240 min p.i. blockade* (*n* = 3)
%ID/g in:				
Lung	0.76 ± 0.71	0.38 ± 0.10	0.29 ± 0.16	0.22 ± 0.08
Liver	1.78 ± 0.84	0.68 ± 0.22	1.01 ± 0.18	0.89 ± 0.23
Spleen	0.74 ± 0.36	0.71 ± 0.57	0.55 ± 0.10	0.42 ± 0.16
Kidneys	18.51 ± 3.56	16.89 ± 1.40	20.31 ± 3.65	19.72 ± 3.97
Muscle	0.08 ± 0.19	0.08 ± 0.21	0.06 ± 0.03	0.07 ± 0.03
Heart	0.19 ± 0.03	0.20 ± 0.02	0.17 ± 0.06	0.18 ± 0.05
Blood	0.32 ± 0.16	0.46 ± 0.04	0.25 ± 0.08	0.37 ± 0.07
Intestine (empty)	0.35 ± 0.07	0.27 ± 0.03	0.31 ± 0.06	0.29 ± 0.12
Testicles	0.10 ± 0.01	0.13 ± 0.01	0.11 ± 0.07	0.11 ± 0.04
Tumor	0.46 ± 0.04	0.43 ± 0.04	0.44 ± 0.11	0.44 ± 0.17

---

*In the blockade group, each animal received 2 mg/kg BW of folic acid in PBS 3 min before radiotracer injection.

In contrast, the high mw folate-pHPMA conjugate (**[^{18}F]FE-FA-P2**) showed under non-blocking conditions highest activity levels in the liver after 120 min and 240 min (Table 4).[9] During folate blockade the accumulation of **[^{18}F]FE-FA-P2** was only slightly reduced after 120 min. Interestingly increased blood activity levels due to an reduced renal clearance could not be observed, and highest activity levels were found in the liver and spleen. The accumulation of **[^{18}F]FE-FA-P2** in the kidneys over time changed not significantly. Due to blockade with native folic acid the kidney accumulation increased from 3.99%ID/g to 5.84%ID/g after 120 min, but this could be because of residual urine in the kidney tubuli. Comparing the absolute polymer concentration in the tumor biodistribution experiments show that the low mw polymer shows higher concentrations, which seems to be contradictory to the PET experiments (Figure 4).

Table 4. Biodistribution study of **[^{18}F]FE-FA-P2**

Organ or tissue	120 min p.i. (*n* = 3)	120 min p.i. blockade (*n* = 3)	240 min p.i. (*n* = 3)	240 min p.i. blockade* (*n* = 3)
%ID/g in:				
Lung	0.29 ± 0.07	0.14 ± 0.09	0.17 ± 0.13	0.13 ± 0.07
Liver	5.57 ± 1.10	5.21 ± 0.36	5.74 ± 0.62	4.97 ± 1.17
Spleen	1.82 ± 0.11	1.36 ± 0.92	1.72 ± 0.18	1.50 ± 0.32
Kidneys	3.99 ± 0.40	5.84 ± 2.00	4.02 ± 0.57	4.15 ± 0.92
Muscle	0.03 ± 0.01	0.03 ± 0.02	0.03 ± 0.01	0.04 ± 0.01
Heart	0.15 ± 0.03	0.13 ± 0.02	0.10 ± 0.03	0.11 ± 0.03
Blood	0.47 ± 0.08	0.36 ± 0.20	0.34 ± 0.13	0.30 ± 0.04
Intestine (empty)	0.19 ± 0.04	0.19 ± 0.06	0.16 ± 0.01	0.17 ± 0.04
Testicles	0.06 ± 0.01	0.05 ± 0.01	0.04 ± 0.01	0.05 ± 0.01
Tumor	0.28 ± 0.06	0.27 ± 0.11	0.31 ± 0.13	0.21 ± 0.03

---

*In the blockade group, each animal received 2 mg/kg BW of folic acid in PBS 3 min before radiotracer injection.

However, it has to be taken into account that in the PET analysis the tumor concentration was normalized to the value in the reference tissue in the field of view (testis). If this ratio is calculated for the biodistribution data (Figure 5) the PET and *ex vivo* data become more comparable, especially by considering the imaging aspect (best contrast levels). However, minor differences are still obvious. In contrast to the PET images the *ex vivo* biodistribution experiments after 120 min reveal no marked difference between the tumor accumulation of the low and high mw polymers (Figure 5). In contrast, after 240 min the high mw polymer showed a markedly higher concentration in the tumor as compared to the low mw counterpart (which was seen in the PET experiments). One reason for the differences at 120 min might be that with PET imaging also the blood compartment of the tumor is measured. Since with the high mw polymer the blood

concentration is markedly higher than with the low mw polymer PET imaging may overestimate the tumor uptake. However, after 4 h, when the EPR effect takes place the better tumor uptake of **[^{18}F]FE-FA-P2** becomes visible also in the *ex vivo* biodistribution.

Blockade experiments (*ex vivo* biodistribution) with free folate led to a marked reduction in tumor accumulation. The efficiency of blockade stayed also constant over 240 min, indicating no loss of blocking potency over time. These results underline the great potential of the active targeting concept using a folate-mediated binding/uptake of macromolecular drug delivery systems. Besides, the scope of the low and high mw polymer-conjugates have to be differentiated. Obviously, the low mw polymer meets the demands for FR-targeted therapy approaches due to its well-characterized nature and higher absolute tumor accumulation. In contrast the high mw polymer displays a higher tumor to testis ratio giving better contrast levels for imaging purposes even if aggregation has been observed. This better imaging contrast with lower background levels makes this system an interesting candidate for multimodal imaging in combination with other techniques.

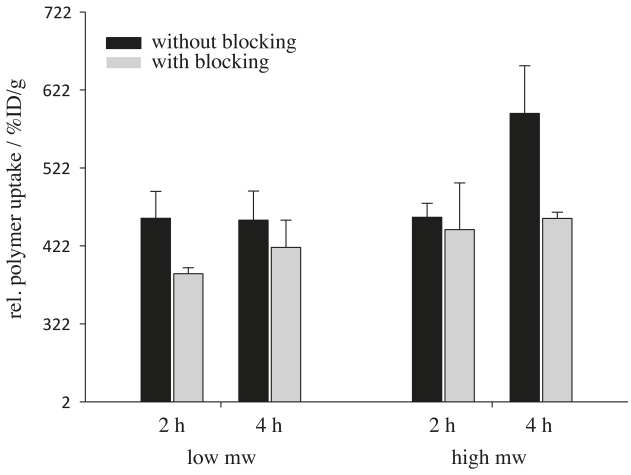

Figure 5: Intratumoral polymer uptake in Walker-256 mammary carcinomas determined by biodistribution measurements 120 min and 240 min after polymer application under non-blockade and blockade conditions. In the blockade group, each animal received 2 mg/kg BW of folic acid in PBS 3 min before radiotracer injection.

Conclusion

The synthesis and characterization of alkyne-functionalized low and high mw pHPMA homopolymers and their coupling to a folate derivative via CuAAC could be accomplished. FCS measurements showed aggregation of the high mw conjugates after coupling to folate. The folate-pHPMA conjugates were ^{18}F-labeled using [^{18}F]FETos and their *in vivo* behavior investigated in the Walker carcinoma model of the rat. The *in vivo* analysis showed that the low mw conjugates have the highest absolute tumor accumulation, whereas the best tumor to testis (reference region) ratios could be achieved. These findings indicate two fields of application. Thus, the low mw polymer is perfectly suitable for drug delivery due to its higher absolute tumor accumulation (2.5-fold higher compared to untargeted pHPMA), whereas the high mw polymer provides the better contrast levels during imaging. Ultimately, this work clearly displays the high potential of the FR-targeting concept to macromolecular systems either for drug delivery or molecular imaging.

Acknowledgement

The authors thank Merck & Cie AG (Switzerland) for kindly providing protected pteroic acid. Hanno Schieferstein thanks the research cluster SAMT for financial support.

References

(1) Ringsdorf, H. *J. Polym. Sci. Poym. Symp* **1975**, *51*, 135–153.

(2) Jatzkewitz, H. *Hoppe-Seyler's Z. Physiol. Chem.* **1954**, *297*, 149–156.

(3) Duncan, R. *Nat. Rev. Drug Discov.* **2003**, *2*, 347–60.

(4) Lammers, T.; Kiessling, F.; Hennink, W. E.; Storm, G. *J. Controlled Release* **2012**, *161*, 175–87.

(5) Duncan, R. *Adv. Drug Deliv. Rev.* **2009**, *61*, 1131–48.

(6) Duncan, R.; Vicent, M. J. *Adv. Drug Deliv. Rev.* **2010**, *62*, 272–82.

(7) Barz, M.; Luxenhofer, R.; Zentel, R.; Vicent, M. J. *Polym. Chem.* **2011**, *2*, 1900.

(8) Herth, M. M.; Barz, M.; Moderegger, D.; Allmeroth, M.; Jahn, M.; Thews, O.; Zentel, R.; Rösch, F. *Biomacromolecules* **2009**, *10*, 1697–703.

(9) Allmeroth, M.; Moderegger, D.; Biesalski, B.; Koynov, K.; Rösch, F.; Thews, O.; Zentel, R. *Biomacromolecules* **2011**, *12*, 2841–9.

(10) Lammers, T.; Kühnlein, R.; Kissel, M.; Subr, V.; Etrych, T.; Pola, R.; Pechar, M.; Ulbrich, K.; Storm, G.; Huber, P.; Peschke, P. *J. Controlled Release* **2005**, *110*, 103–18.

(11) Allmeroth, M.; Moderegger, D.; Gündel, D.; Koynov, K.; Buchholz, H.-G.; Mohr, K.; Rösch, F.; Zentel, R.; Thews, O. *Biomacromolecules* **2013**, *14*, 3091–101.

(12) Matsumura, Y.; Maeda, H. *Cancer Rev.* **1986**, 6387–6392.

(13) Lammers, T.; Aime, S.; Hennink, W. E.; Storm, G.; Kiessling, F. *Acc. Chem. Res.* **2011**, *44*, 1029–38.

(14) Seymour, L. W.; Ferry, D. R.; Anderson, D.; Hesslewood, S.; Julyan, P. J.; Poyner, R.; Doran, J.; Young, A. M.; Burtles, S.; Kerr, D. J. *J. Clin. Oncol.* **2002**, *20*, 1668–76.

(15) Qian, Z. M.; Li, H.; Sun, H.; Ho, K. *Pharmacol. Rev.* **2002**, *54*, 561–587.

(16) Nuhn, L.; Hartmann, S.; Palitzsch, B.; Gerlitzki, B.; Schmitt, E.; Zentel, R.; Kunz, H. *Angew. Chem. Int. Ed. Engl.* **2013**, 10652–10656.

(17) Parker, N.; Turk, M. J.; Westrick, E.; Lewis, J. D.; Low, P. S.; Leamon, C. P. *Anal. Biochem.* **2005**, *338*, 284–93.

(18) Leamon, C. P.; Low, P. S. *Proc. Natl. Acad. Sci. U. S. A.* **1991**, *88*, 5572–6.

(19) McHugh, M. *J. Biol. Chem.* **1979**, *254*, 11312–11318.

(20) Kamen, B. a; Capdevila, a *Proc. Natl. Acad. Sci. U. S. A.* **1986**, *83*, 5983–7.

(21) Müller, C.; Dumas, C.; Hoffmann, U.; Schubiger, P. A.; Schibli, R. *J. Organomet. Chem.* **2004**, *689*, 4712–4721.

(22) Leamon, C. P.; Low, P. S. *Proc. Natl. Acad. Sci. U. S. A.* **1991**, *88*, 5572–6.

(23) Lu, Y.; Low, P. S. *Adv. Drug Deliv. Rev.* **2002**, *54*, 675.

(24) Lee, E. S.; Na, K.; Bae, Y. H. *J. Controlled Release* **2003**, *91*, 103.

(25) Yoo, H. S.; Park, T. G. *J. Controlled Release* **2004**, *96*, 273.

(26) Pasut, G.; Canal, F.; Dalla Via, L.; Arpicco, S.; Veronese, F. M.; Schiavon, O. *J. Controlled Release* **2008**, *127*, 239.

(27) York, A. W.; Zhang, Y.; Holley, A. C.; Guo, Y.; Huang, F.; McCormick, C. L. *Biomacromolecules* **2009**, *10*, 936.

(28) Quintana, A.; Raczka, E.; Piehler, L.; Lee, I.; Myc, A.; Majoros, I.; Patri, A. K.; Thomas, T.; Mule, J.; Baker, J. R. *Pharm. Res.* **2002**, *19*, 1310.

(29) Chandrasekara, D.; Sistlaa, R.; Ahmadb, F. J.; Kharb, R. K.; Diwan, P. V *Biomaterials* **2007**, *28*, 504.

(30) Pan, D.; Turner, J. L.; Wooley, K. L. *Chem. Commun.* **2003**, 2400.

(31) Choi, H.; Choi, S. R.; Zhou, R.; Kung, H. F.; Chen, I. *Acad. Radiol.* **2004**, *11*, 996.

(32) Sonvico, F.; Mornet, S.; Vasseur, S.; Dubernet, C.; Jaillard, D.; Degrouard, J.; Hoebeke, J.; Duguet, E.; Colombo, P.; Couvreur, P. *Bioconjugate Chem.* **2005**, *16*, 1181.

(33) Anderson, K. E.; Eliot, L. A.; Stevenson, B. R.; Rogers, J. A. *Pharm. Res.* **2001**, *18*, 316.

(34) Lee, R. J.; Low, P. S. *J. Biol. Chem.* **1994**, *269*, 3198.

(35) Lee, R. J.; Low, P. S. *Biochim. Acta.* **1995**, *1233*, 134.

(36) Eberhardt, M.; Théato, P. *Macromol. Rapid Commun.* **2005**, *26*, 1488–1493.

(37) Eberhardt, M.; Mruk, R.; Zentel, R.; Theato, P. *Eur. Polym. J.* **2005**, *41*, 1569–1575.

(38) Barz, M.; Canal, F.; Koynov, K.; Zentel, R.; Vicent, M. J. *Biomacromolecules* **2010**, *11*, 2274–82.

(39) York, A. W.; Zhang, Y.; Holley, A. C.; Guo, Y.; Huang, F.; McCormick, C. L. *Biomacromolecules* **2009**, *10*, 936–43.

(40) Schieferstein, H.; Betzel, T.; Fischer, C. R.; Ross, T. L. *EJNMMI Res.* **2013**, *3*, 68.

(41) Thang, S. H.; Chong, B. Y. K.; Mayadunne, R. T. A.; Moad, G.; Rizzardo, E. *Tetrahedron Lett.* **1999**, *40*, 2435–2438.

(42) Theato, P. *J. Polym. Sci., Part A Polym. Chem.* **2008**, *46*, 6677–6687.

(43) Barz, M.; Luxenhofer, R.; Zentel, R.; Kabanov, A. V *Biomaterials* **2009**, *30*, 5682–90.

(44) Perrier, S.; Takolpuckdee, P.; Mars, C. A. *Macromolecules* **2005**, *38*, 2033–2036.

(45) Barz, M.; Canal, F.; Koynov, K.; Zentel, R.; Vicent, M. J. *Biomacromolecules* **2010**, *11*, 2274–2282.

(46) Workman, P.; Aboagye, E. O.; Balkwill, F.; Balmain, a; Bruder, G.; Chaplin, D. J.; Double, J. a; Everitt, J.; Farningham, D. a H.; Glennie, M. J.; Kelland, L. R.; Robinson, V.; Stratford, I. J.; Tozer, G. M.; Watson, S.; Wedge, S. R.; Eccles, S. a *Br. J. Cancer* **2010**, *102*, 1555–77.

(47) Hemmelmann, M.; Kurzbach, D.; Koynov, K.; Hinderberger, D.; Zentel, R. *Biomacromolecules* **2012**, *13*, 4065–74.

(48) Koynov, K.; Butt, H.-J. *Curr. Opin. Colloid Interface Sci.* **2012**, *17*, 377–387.

Biodistribution of ^{18}F-labeled nanoparticles stabilized by HPMA-based Block Copolymers

Annette Kelsch*, Hanno Schieferstein*, Nicole Bausbacher, Matthias Miederer, Tobias L. Ross, Katharina Landfester, Rudolf Zentel

* both authors have contributed equally

Institute of Organic Chemistry, Johannes Gutenberg University, Mainz, Germany

Institute of Nuclear Chemistry, Johannes Gutenberg University, Mainz, Germany

Department of Nuclear Medicine, University Medical Center Mainz, Mainz, Germany

Max Planck Institute for Polymer Research, 55128 Mainz, Germany

Introduction

The term “nanomedicines” describes an area that deals with the medical application of nanoparticular systems for the treatment of malignancies.[1] Such systems include polymer drug conjugates, polymer protein conjugates as well as organic or inorganic nanoparticles.[1] The major advantage of those systems is the ability to load drugs and therefore to change the biodistribution pattern compared to the free drug, which has already been reported.[2] Furthermore it has been demonstrated that encapsulation or conjugation of drugs to polymeric systems led to a reduced metabolization or renal excretion.[3] The used nanoparticles, e.g. polymeric colloids, have several advantages like a stable shape, a defined interface and the ability to encapsulate sensitive cargos underlining their unique role in the area of drug delivery.[4] Therefore Kelsch and coworkers recently described the synthesis of nanoparticles using the miniemulsion technique in combination with the solvent evaporation approach.[5] In this case p((HPMA)-*b*-(LMA)) copolymers were employed to act as surfactants during the miniemulsion process due to their low critical micelle concentration (CMC).[6] These surface-active polymers are permanently stuck to the hydrophobic core, whereas the hydrophilic segments (HPMA) always pointed to the outside. The introduction of an oligoethylene-based spacer, which carries an azido-moiety for copper(I)-catalyzed azide-alkyne cycloadditions (CuAAC), is a common concept for labeling macromolecular structures.[7] This moiety enables the ^{18}F-labeling of the nanoparticles to investigate their *in vivo* behavior. Up to now, many approaches have been made for radiolabeling of macromolecular systems, but numerous used long-lived positron emitters, mostly radiometals or iodine.[8,9] This entails the use of chelates, which can change the architecture and pharmacokinetics of the macromolecular systems.[8,10] Since ^{18}F is one of the clinically most used radionuclides for diagnostic purposes using the positron emission tomography (PET), many approaches have been made to investigate the *in vivo* behavior of macromolecular systems.[9,11–13] Besides the neat ^{18}F-labeling strategy by using 2-[^{18}F]fluoroethyl tosylate alternative labeling concepts have been explored, whereas a special role was assigned to ^{18}F-click labeling. The formed 1,4-disubstituted-1,2,3-triazoles

have proven to be very stable under physiological conditions and showed similar characteristics to amide bonds.[14] This labeling approach has been used for ^{18}F-labeling of predominantly peptide structures, since the reaction conditions are meant to be very mild.[15,16] These mild conditions of the CuAAC and high yields enabled to radiolabel nanoparticles consisting of an iron oxide core and an aminated polysaccharide layer for dervatization[7] or an iron oxide core coated with dextran[17].

In this work we report the synthesis of ^{18}F-labeled nanoparticles consisting of poly(DL) lactic acid (PDLLA) as core material stabilized via p((HPMA)-*b*-(LMA)) copolymers as surfactants. The big advantage of these systems is on the one hand the biodegradable core and on the other hand the multifunctionality of the hydrophilic segment of the p((HPMA)-*b*-(LMA)) surfactants. Thus, these clinically relevant colloids were ^{18}F-labeled and biodistribution as well as micro PET studies were conducted using a mouse model to investigate the *in vivo* behavior of those systems.

Materials and Methods

All chemicals were reagent grade, obtained from Aldrich and Acros and used without further purification, unless indicated otherwise. Oregon green cadaverin was purchased from Invitrogen. All solvents were of analytical grade. Pentafluorophenol was obtained from Fluorochem (Great Britain, U.K.) and distilled prior to use. Dioxane and dimethylsulfoxide (DMSO) used in the syntheses were freshly distilled from a sodium/potassium mixture. 2,2'-Azobis-(isobutyronitrile) (AIBN) was recrystallized from diethyl ether and stored at −7 °C. Deuterated chloroform-d_1 was purchased from Deutero GmbH, dried, and stored over molecular sieves. Dialyses were performed with Cellu SepH1 membranes (Membrane Filtration Products, Inc.) with a nominal molecular weight cutoff of 1000 g/mol and Spectra/Por membranes (Roth) with a nominal molecular weight cutoff of 3500 g/mol.

Characterization

^{1}H and ^{13}C nuclear magnetic resonance spectra were recorded on either a Bruker 300 MHz or 400 MHz spectrometer. Chemical shifts (δ) to solvent are reported in parts per million (ppm) relative to tetramethylsilane and referenced; the following abbreviations are used in the experimental section for the description of ^{1}H NMR spectra: singlet (s), doublet (d), triplet (t), multiplet (m), broad (br). The chemical shifts of complex multiplets are given as the range of their occurrence. Low-resolution mass spectra (LR-MS) and high-resolution mass spectra (HR-MS) were recorded on either a Micromass Quattro micro API LC-ESI or a Finnigan MAT90-Spectrometer. Reactions were monitored by thin layer chromatography (TLC, performed on Merck silica gel 60 F254, not modified, pre-coated silica gel on aluminum-supported plates).

Synthesis of 4-cyano-4-((thiobenzoyl)sulfanyl)pentanoic acid (CTP)

4-cyano-4-((thiobenzoyl)sulfanyl)pentanoic acid was used as chain transfer agent (CTA) and synthesized according to literature in a 3-step reaction.[18]

Synthesis of pentafluorophenyl methacrylate (PFPMA)

PFPMA was prepared according to the literature.[19]

Synthesis of macro-CTA

RAFT polymerization of PFPMA using CTP was performed in a Schlenk tube[20,21], loaded with PFPMA and 2,2'-azobis(isobutyronitrile) (AIBN), (molar ratio monomer/CTA/AIBN: 50/1/0.1) and finally dissolved in absolute dioxane. After three freeze–vacuum–thaw cycles, the mixture was stirred at 70 °C for 16 h. Afterwards the polymeric solution was precipitated 3 times in hexane, isolated by centrifugation and dried for 12 h at 30 °C under vacuum. A pink powder with a yield of 79% was obtained. ^{1} H-NMR ($CDCl_3$): δ [ppm] 1.9-2.7 (br), 1.2-1.7 (br). ^{19}F-NMR ($CDCl_3$): δ [ppm] -162.6 (br), -157.3 (br), -150 to -152 (br).

Synthesis of block copolymer

Block copolymer was prepared in analogy to literature.[22] The macro-CTA, obtained in the above-mentioned polymerization, LMA and AIBN (molar ratios monomer/macroCTA/AIBN: 4/1/0.17) were dissolved in absolute dioxane. After three freeze–vacuum–thaw cycles the tube was immersed in an oil bath at 70 °C. After polymerization time of 2 d, the solution was precipitated twice in ethanol. After removal of the supernatant the precipitate was dried for 12 h at 30 °C under vacuum, obtaining a slightly pink powder with a yield of 88%. ^{1}H-NMR ($CDCl_3$): δ [ppm] 1.9–2.6 (br), 1.0–1.7 (br), 0.8–0.9 (br t). ^{19}F-NMR ($CDCl_3$): δ [ppm] -162.2 (br), -157.1 (br), -152 to – 150 (br).

Removal of dithiobenzoate end group

The dithiobenzoate end group was removed according to the procedure reported by Perrier et al.[23] Therefore a 25-fold molar excess of AIBN was added to the polymer dissolved in dioxane. After four hours of heating the solution at 80 °C, the polymer was precipitated in hexane twice and collected by centrifugation. The polymer was dried under vacuum for 18 h; a colorless powder could be obtained. Yield: 91%. The absence of the dithiobenzoate endgroup was confirmed by UV–vis spectroscopy.

Postpolymerization modification of block copolymers

Precursor polymer (200 mg) without dithioester endgroup was dissolved in abs. dioxane (4 mL). Azido spacer (15.6 mg) dissolved in dioxane (500 µL) as well as triethylamine (14.4 mg) were added and the solution stirred for 1 day. Thereafter, 2-hydroxypropylamine (54.2 mg) and triethylamine (146.0 mg) were added and the solution further stirred for 48 hours. For final removal of reactive ester side groups 2-hydroxypropylamine (108.4 mg) were additionally added. The solution was dissolved in a DMSO/water solution for dialysis. After lyophilization a white powder with a yield of 69% could be obtained. ^{1}H-NMR (400 MHz, DMSO-d_6) δ [ppm]: 0.60-1.38 (br), 1.41-2.00 (br), 2.62-3.10 (br), 3.19-3.43 (s), 3.41-3.80 (br), 4.50-4.83 (br) and 6.90-7.70 (br).

Synthesis of the 2-(2-(2-(prop-2-yn-1-yloxy)ethoxy)ethoxy)ethyl 4-methylbenzenesulfonate

The labeling precursor was synthesized according to the literature.[24]

Click reaction to the ^{18}F-labeled nanoparticles

The ^{18}F-labeling of 2-(2-(2-(prop-2-yn-1-yloxy)ethoxy)ethoxy)ethyl 4-methylbenzenesulfonate was done according to the literature.[24] After the ^{18}F-labeled prosthetic group was trapped on a Phenomenx StrataX C18 cartridge, 3-(2-(2-(2-[^{18}F]fluoroethoxy)ethoxy)ethoxy)prop-1-yne was eluted into a reaction vessel using acetonitrile (1 mL). The acetonitrile was evaporated (70 °C, 300 mbar, 30 mL/min helium flow) and dissolved in PBS buffer (500 μL). To the dissolved 3-(2-(2-(2-[^{18}F]fluoroethoxy)ethoxy)ethoxy)prop-1-yne copper sulfate (20 μmol in 20 μL) was added. The reaction mixture was stirred for 2 min until the miniemulsion (80 μL, solid content 0.42 w%) was added. After addition of sodium *L*-ascorbate (50 μmol, 20 μL) the reaction mixture was stirred for 20 min at room temperature until injection into a size exclusion HPLC system. Size exclusion chromatography (SEC) of ^{18}F-labeled polymers was performed using a GE HiTrap Desalting Column, Sephadex G-25 Superfine, and a Merck Hitachi System equipped with two L-7100 pumps, a L-7400 UV detector, a D-7000 D-Line, an L-7250 autosampler, a L-7300 column oven and a Gina-Star radio detector.

Animal experiments

For animal experiments C57BL/6 mice (Charles River Wiga, Sulzfeld, Germany; body weight 25-35 g) housed in the animal care facility of the University of Mainz were used in this study. All experiments had previously been approved by the regional animal ethics committee and were conducted in accordance with the German Law for Animal Protection and the UKCCCR Guidelines.[25] Animals were allowed access to food and acidified water *ad libitum* before the investigation.

Biodistribution

For *ex vivo* biodistribution studies animals were injected with ^{18}F-labeled nanoparticle emulsion (2.5 - 3 MBq) intravenously (i.v.) in the tail vein. After 30 or 120 min post injection (p.i.), the animals were sacrificed and different organs (kidney, liver, lung, spleen, heart, skeletal muscle, small intestine, testis, blood) were excised. The samples were weighted, minced and measured in a Perkin Elmer 2470 Wizard2 γ-counter to calculate the percentage of injected dose per gram tissue.

Micro PET studies

For PET measurements, mice were anaesthetized with isofluran (2.5%) and nanoparticles were injected into the tail. The micro PET imaging was performed on a microPET Focus 120 small animal PET (Siemens/Concorde, Knoxville, USA). During PET measurements the animals were placed head first prone (HFS) and breathed room air spontaneously. Dynamic PET studies were acquired in listmode. The injected activity of radiolabeled polymers was 2.5±0.5 MBq (in 150-200 µL isotonic saline). The PET listmode data were histogrammed into 13 frames and reconstructed using OSEM2D algorithm.

Results & Discussion

The here synthesized and first reported nanoparticles, having a PDLLA core and an p((HPMA)-*b*-(LMA)) shell, which is modified with azido oligoethylene spacers, were ^{18}F-labeled using the highly selective and high yielding CuAAC. The ^{18}F-labeled nanoparticles were used for preliminary *ex vivo* biodistribution and *in vivo* micro PET studies.

Synthetic concept of azido-functionalized p((HPMA)-b-(LMA)) polymers

By applying the RAFT polymerization technique in combination with the reactive ester approach well-defined HPMA-based block copolymers with very narrow molecular weight

distributions were synthesized.[22] Via polymer analogous reaction an azido oligoethylene-based spacer in the hydrophilic part was introduced (Scheme 1).

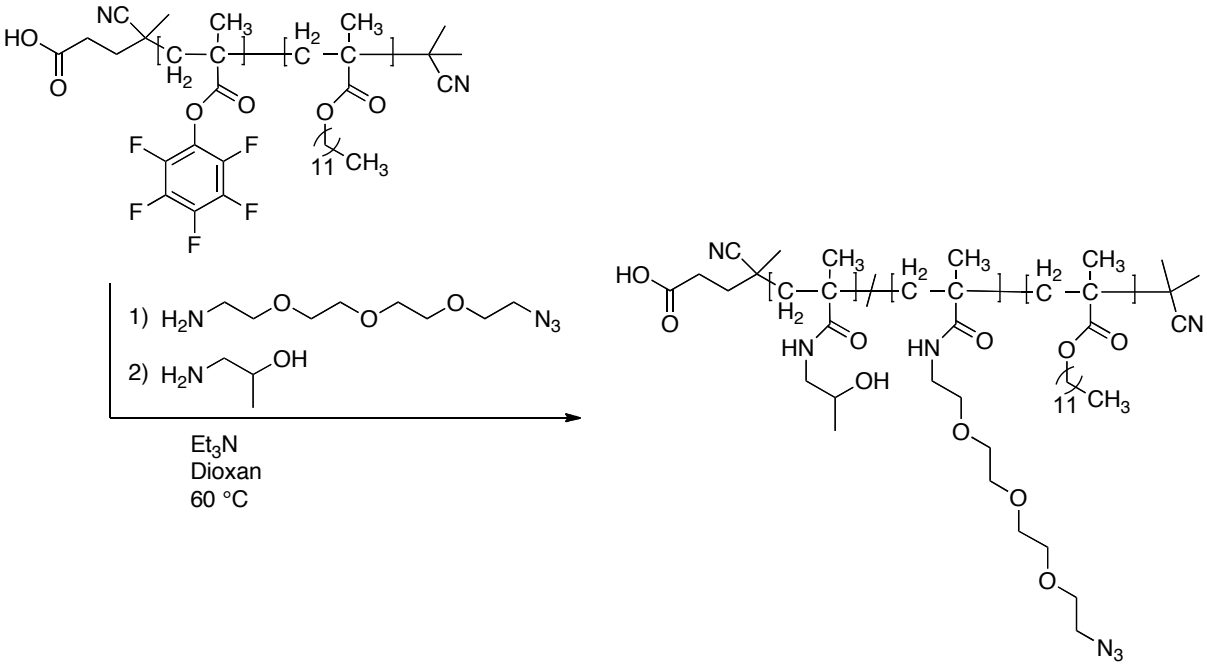

Scheme 1. Synthetic pathway to HPMA-LMA block copolymers functionalized with an azido spacer in the hydrophilic segment.

Azido-functionalized PDLLA-nanoparticles via miniemulsion technique

In our previous work we showed that HPMA/LMA block copolymers were well suited for the preparation of PDLLA nanoparticles via miniemulsion technique in combination with solvent evaporation.[5] Additionally, it has been shown that these nanoparticles were nontoxic and moderately taken up by HeLa cells. To study the *in vivo* behavior via micro PET imaging an azido-functionalized HPMA-based block copolymer was introduced to the miniemulsion technique for the preparation of azido-functionalized colloids (Figure 1). Therefore the block copolymer was dissolved in the continuous phase (water) whereas the disperse phase (chloroform) consisted of PDLLA. After high shear, nanodroplets were formed followed by evaporation of the organic solvent. Stable particles could be obtained with sizes of around 200 nm. The morphology of the PDLLA nanoparticles was visualized by scanning electron microscopy (SEM) and is shown in Figure 2. All particles show a spherical shape and have a relatively low dispersity. The incorporation of the azido-

functionalized spacer into the hydrophilic part led them to extend to the outside, which is necessary for the radioactive labeling. Slightly deformed particles visible on the SEM image (Figure 2) were due to melting of PDLLA under the electron beam.

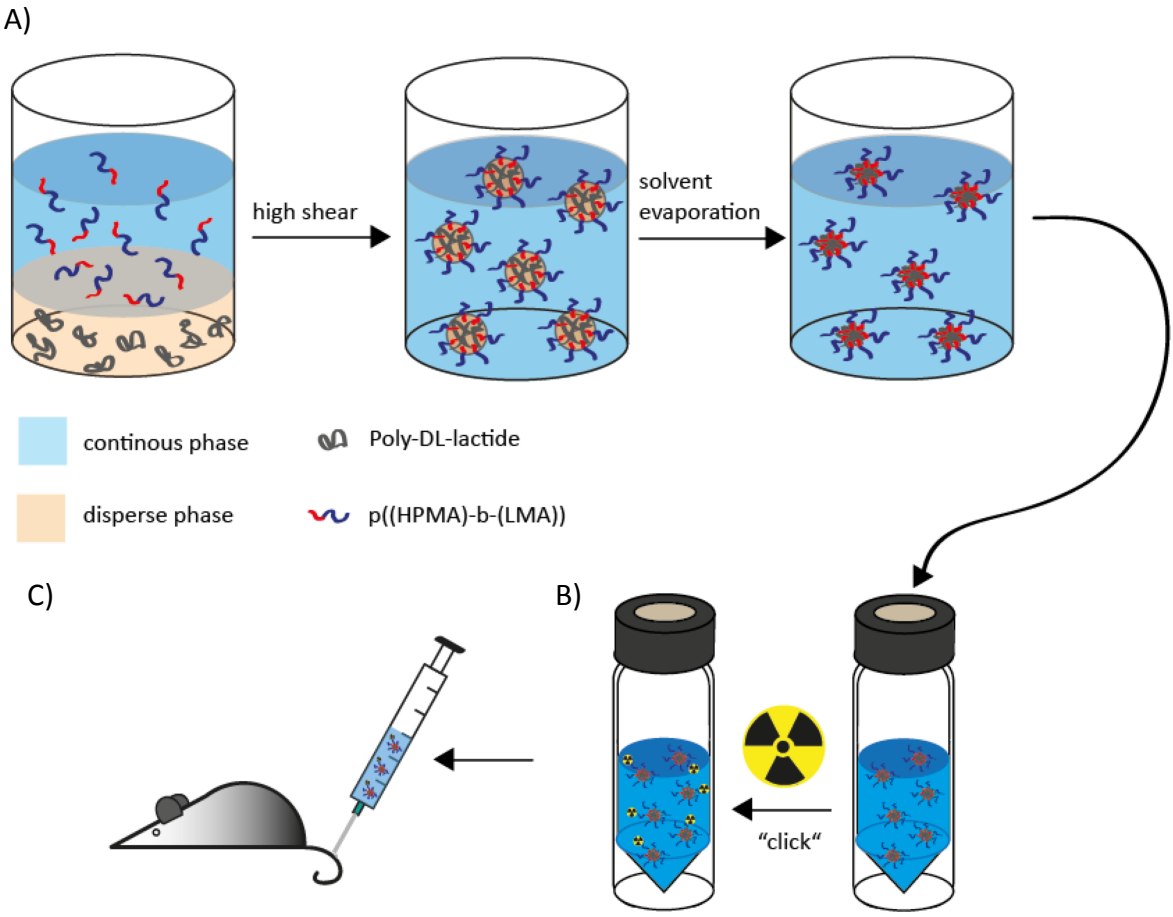

Figure 1. A) Synthesis of PDLLA nanoparticles via miniemulsion technique stabilized by P((HPMA/Azido-OEG)-*b*-(LMA)); B) ^{18}F-labeling of the azido-functionalized surfactant using CuAAC; C) *in vivo* evaluation of the ^{18}F-labeled nanoparticles.

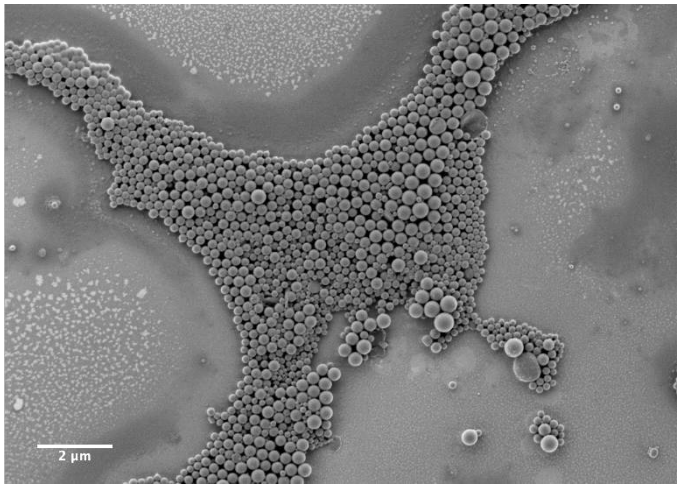

Figure 2. SEM image of the unlabeled azido-functionalized nanoparticles for CuAAC; *D* = 200 nm.

Radiochemistry

The radiolabeling could be achieved in a two-step synthesis. First, the ^{18}F-labeled prosthetic group was synthesized in high radiochemical yields (RCYs) and purity as already described in literature.[24] For the second step, the ^{18}F-click reaction had to been screened and optimized, because the PDLLA core is very sensitive towards heat (Table 1). Thus, reaction temperatures up to 40 °C were screened for the ^{18}F-click reaction. Another important factor was the solvent optimization, since the nanoparticles decomposed if organic solvents were present. Therefore only aqueous media were used, whereas a PBS-buffered system was the most promising, since its slight basic character supports CuAACs.[26] Table 1 displays the screening procedure of the ^{18}F-click reaction, showing that a system containing 1:2.5 ratio of copper(I) sulfate and sodium *L*-ascorbate at slightly elevated temperatures (40 °C) gave the best results. The usage of higher amounts of copper(I) sulfate led to no significant increase or decrease of the RCY. However, the increase of the azido-functionalities resulted in poor RCYs. Furthermore, the dependency of the amount of sodium *L*-ascorbate was tested, leading to decomposition of the nanoparticles if too much *L*-ascorbate was used- due to the high redox potential in the reaction mixture.[27] A strong dependency on reaction times was observed. It could be clearly seen that after 10 min the RCYs were low even under the optimized conditions. Not until 10 min reaction time the RCYs increased from 6% to 32%. Purification of the ^{18}F-

labeled nanoparticles was achieved via size exclusion chromatography and directly formulated in isotonic sodium chloride solution with an overall RCY of 8±3% (Figure 3).

Table 1. Screening and optimization of the ^{18}F-click reaction.

Amount miniemulsion[a] [µL]	$CuSO_4$ [µmol]	Na ascorbate [µmol]	Time [min]	Temperature [°C]	Conversion[b] [%]
50	20	100	15	RT	0
50	20	100	20	RT	3
70	20	50	20	RT	10
70	20	50	5	40	6
70	20	50	10	40	17
70	20	50	20	40	32
70	20	100	20	40	7
70	40	250	20	40	0
100	20	50	20	40	0
100	20	100	20	40	4
150	20	50	20	40	0
500	20	50	20	40	0
700	20	50	20	40	0

[a] solid content of the miniemulsion was 0.42 w%. [b] the conversion was determined by size exclusion chromatography.

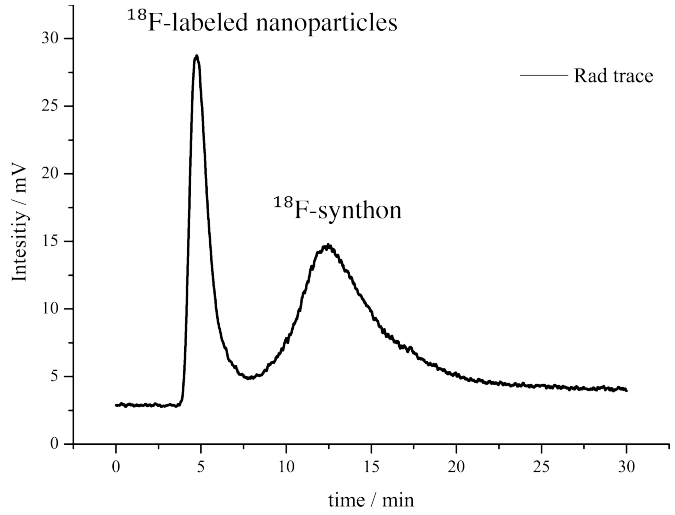

Figure 3. Purification of the ^{18}F-labeled nanoparticles using size exclusion chromatography.

Ex vivo biodistribution and in vivo micro PET experiments

To investigate the *in vivo* behavior of these novel ^{18}F-labeled nanoparticles preliminary biodistribution and micro PET experiments were performed using wild-type mice (C57BL/6). The maximum intensity projection (MIP) of the 30 min PET scan clearly displays the kidneys and the bladder (Figure 4A). Whereas almost no activity could be found in the liver and lungs as expected for large nanoparticles of sizes around 200 nm.[11]

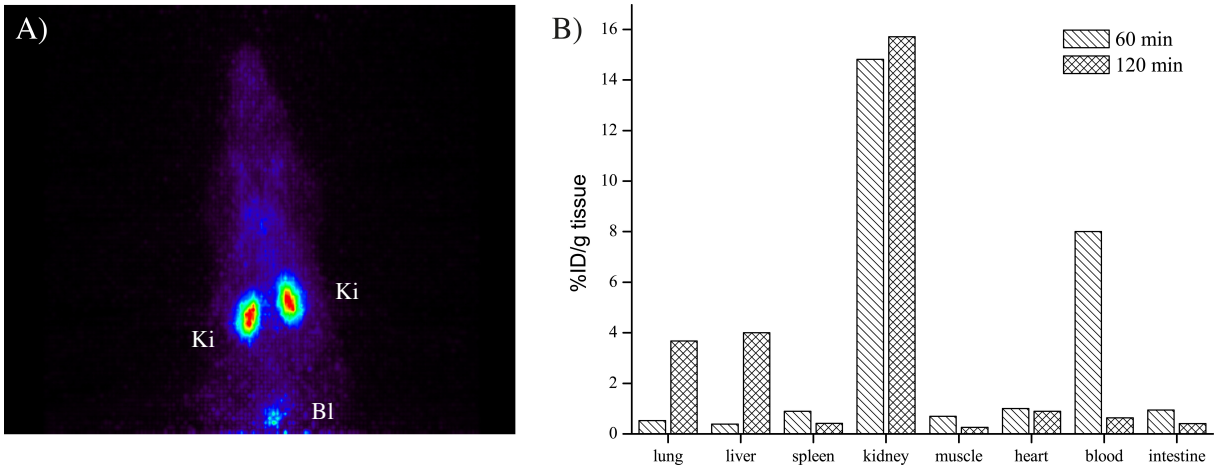

Figure 4. A) MIP of a 30 min micro PET scan of a C57BL/6 mouse injected with 2 MBq of the ^{18}F-labeled nanoparticles; Ki: kidney, Bl: bladder. B) Biodistribution of the ^{18}F-labeled nanoparticles after 60 min and 120 min after i.v. injection.

The *ex vivo* biodistribution displays an interesting behavior of the ^{18}F-labeled nanoparticles, showing the distribution pattern of both, macromolecules below and above the renal threshold (Figure 4B).[11] Obviously, the accumulation of the nanoparticles was predominantly in the kidneys, indicating that molecules under the renal threshold were administered. In contrast the blood levels after 1 h were 8%ID/g showing a prolonged circulation in the blood. After 2 h the blood levels decreased below 1%ID/g, and a redistribution of the activity was found. Thus, an accumulation in the lung (4%ID/g) and liver (4%ID/g) was observed, which is corresponding to macromolecules above the renal threshold. By comparing the remaining organs like spleen, heart, muscle and intestines a decrease of activity over time (120 min) could be observed. The before mentioned behavior in the blood, liver, lungs and in contrast the also observed accumulation on the kidneys could be referred to an equilibrium of surfactant in solution

and on the shell of the labeled nanoparticle, but further investigations have to be carried out. However, this work depicts for the first time the synthesis and ^{18}F-click labeling of azido-functionalized nanoparticles consisting of a PDLLA core and an HPMA-*b*-LMA copolymer on the surface as surfactant.

Conclusion

The suitability and uniqueness of nanoparticles as drug delivery systems have been demonstrated and reported many times.[28,29] The here reported nanoparticles consisting of a biodegradable PDLLA core with the ability to load lipophilic drugs and a surface that is stabilized through HPMA-*b*-LMA copolymers as surfactants, seem to be promising candidates as drug delivery systems. Additionally, the incorporation of azido functionalities in the hydrophilic surface segment enabled us the ^{18}F-click labeling of these nanoparticles for the first time and to track them *in vivo* to investigate their fate in the organism. The encouraging results will serve as base frame for future work to improve these systems as drug carriers.

Acknowledgements

Hanno Schieferstein thanks the research cluster SAMT for financial support.

References

(1) Duncan, R. *Nat. Rev. Drug Discov.* **2003**, *2*, 347–60.

(2) Haag, R.; Kratz, F. *Angew. Chem. Int. Ed. Engl.* **2006**, *45*, 1198–215.

(3) Matsumura, Y.; Maeda, *Cancer Research* **1986**, 6387–6392.

(4) Landfester, K. *Angew. Chem. Int. Ed. Engl.* **2009**, *48*, 4488–507.

(5) Kelsch, A.; Tomcin, S.; Rausch, K.; Barz, M.; Mailänder, V.; Schmidt, M.; Landfester, K.; Zentel, R. *Biomacromolecules* **2012**, *13*, 4179–87.

(6) Barz, M.; Luxenhofer, R.; Zentel, R.; Kabanov, A. V *Biomaterials* **2009**, *30*, 5682–90.

(7) Devaraj, N. K.; Keliher, E. J.; Thurber, G. M.; Nahrendorf, M.; Weissleder, R. *Bioconjugate Chem.* **2009**, *20*, 397–401.

(8) Kobayashi, H.; Wu, C.; Kim, M. K.; Paik, C. H.; Carrasquillo, J. a; Brechbiel, M. W. *Bioconjugate Chem.* **1999**, *10*, 103–11.

(9) Lammers, T.; Kühnlein, R.; Kissel, M.; Subr, V.; Etrych, T.; Pola, R.; Pechar, M.; Ulbrich, K.; Storm, G.; Huber, P.; Peschke, P. *J. Control. Release* **2005**, *110*, 103–18.

(10) Fani, M.; Del Pozzo, L.; Abiraj, K.; Mansi, R.; Tamma, M. L.; Cescato, R.; Waser, B.; Weber, W. a; Reubi, J. C.; Maecke, H. R. *J. Nucl. Med.* **2011**, *52*, 1110–8.

(11) Allmeroth, M.; Moderegger, D.; Biesalski, B.; Koynov, K.; Rösch, F.; Thews, O.; Zentel, R. *Biomacromolecules* **2011**, *12*, 2841–9.

(12) Allmeroth, M.; Moderegger, D.; Gündel, D.; Koynov, K.; Buchholz, H.-G.; Mohr, K.; Rösch, F.; Zentel, R.; Thews, O. *Biomacromolecules* **2013**, *14*, 3091–101.

(13) Herth, M. M.; Barz, M.; Moderegger, D.; Allmeroth, M.; Jahn, M.; Thews, O.; Zentel, R.; Rösch, F. *Biomacromolecules* **2009**, *10*, 1697–703.

(14) Ross, T. L. *Curr. Radiopharm.* **2010**, *3*, 202–223.

(15) Li, Z.-B.; Wu, Z.; Chen, K.; Chin, F. T.; Chen, X. *Bioconjugate Chem.* **2007**, *18*, 1987–94.

(16) Rameda, T.; Bergmann, R.; Wüst, F. *Lett. Drug Des. Discov.* **2007**, *4*, 279–285.

(17) Nahrendorf, M.; Keliher, E.; Marinelli, B.; Waterman, P.; Feruglio, P. F.; Fexon, L.; Pivovarov, M.; Swirski, F. K.; Pittet, M. J.; Vinegoni, C.; Weissleder, R. *Proc. Natl. Acad. Sci. U. S. A.* **2010**, *107*, 7910–5.

(18) Thang, S. H.; Chong, B. Y. K.; Mayadunne, R. T. A.; Moad, G.; Rizzardo, E. *Tetrahedron Lett.* **1999**, *40*, 2435–2438.

(19) Eberhardt, M.; Théato, P. *Macromol. Rapid Commun.* **2005**, *26*, 1488–1493.

(20) Theato, P. *J. Polym. Sci., Part A Polym. Chem.* **2008**, *46*, 6677–6687.

(21) Barz, M.; Luxenhofer, R.; Zentel, R.; Kabanov, A. V *Biomaterials* **2009**, *30*, 5682–90.

(22) Barz, M.; Tarantola, M.; Fischer, K.; Schmidt, M.; Luxenhofer, R.; Janshoff, a; Theato, P.; Zentel, R. *Biomacromolecules* **2008**, *9*, 3114–8.

(23) Perrier, S.; Takolpuckdee, P.; Mars, C. A. *Macromolecules* **2005**, *38*, 2033–2036.

(24) Schieferstein, H.; Betzel, T.; Fischer, C. R.; Ross, T. L. *EJNMMI Res.* **2013**, *3*, 68.

(25) Workman, P.; Aboagye, E. O.; Balkwill, F.; Balmain, a; Bruder, G.; Chaplin, D. J.; Double, J. a; Everitt, J.; Farningham, D. a H.; Glennie, M. J.; Kelland, L. R.; Robinson, V.; Stratford, I. J.; Tozer, G. M.; Watson, S.; Wedge, S. R.; Eccles, S. A. *Br. J. Cancer* **2010**, *102*, 1555–77.

(26) Kolb, H. C.; Finn, M. G.; Sharpless, K. B. *Angew. Chemie Int. Ed.* **2001**, *40*, 2004–2021.

(27) Chan, T. R.; Hilgraf, R.; Sharpless, K. B.; Fokin, V. V. *Org. Lett.* **2004**, *6*, 2853–5.

(28) Moghimi, S. M.; Hunter, a C.; Murray, J. C. *FASEB J.* **2005**, *19*, 311–30.

(29) Panyam, J.; Labhasetwar, V. *Adv. Drug Deliv. Rev.* **2012**, *64*, 61–71.

List of Publications

"A simple, rapid method for the preparation of [^{11}C]formaldehyde"

Jacob M. Hooker, Matthias Schönberger, **Hanno Schieferstein**, and Joanna S. Fowler, *Angew. Chem., Int. Ed.*, ***2008***, 47, 5989-5992.

"A new polar ^{18}F-labelled folic acid derivative via ^{18}F-click-chemistry"

Hanno Schieferstein, Cristina Müller, Tobias L. Ross, *J. Labelled Compd. Radiopharm.* ***2011***, 54, S11

"In vivo evaluation of pegylated [^{18}F]harmine derivatives: Selective reversible MAO-A inhibitors"

Hanno Schieferstein, Markus Piel, Nicole Bausbacher and Frank Roesch, *J. Nucl. Med.*, ***2012***, 53 (Supplement 1), 1612

"Fluorine-18 labeling approach for HPMA-based polymers via click chemistry

Doeothea Moderegger, Mareli Allmeroth, **Hanno Schieferstein**, Hans-Georg Buchholz, Oliver Thews, Rudolf Zentel, Frank Rösch

"^{18}F-labeled folic acid derivatives for imaging of the folate receptor via positron emission tomography"

Hanno Schieferstein, Tobias L. Ross, *J. Labelled Compd. Radiopharm.*, ***2013***, 56, 432-440.

"^{18}F-click labeling and preclinical evaluation of a new ^{18}F-folate for PET imaging"

Hanno Schieferstein, Thomas Betzel, Cindy R. Fischer, Tobias L. Ross, *EJNMMI Res.*, *2013*, 3:68.

"Folate receptor targeted delivery of supramolecular drug-carriers monitored by PET"

H. Schieferstein, Annette Kelsch, Barbara Biesalski, Hans-Georg Buchholz, Dorothea Moderegger, Mareli Allmeroth, Nicole Bausbacher, Oliver Thews, Frank Roesch, Rudeolf Zentel, Tobias L. Ross, *J. Labelled Compd. Radiopharm.,* ***2013****, 56, S183*

"Total evaluation of a new polar ^{18}F-labeled PEG-click-folate"

Hanno Schieferstein, Thomas Betzel, Cindy R. Fischer, Tobias L. Ross, *J. Labelled Compd. Radiopharm.,* ***2013***, 56, S183

"Total evaluation of ^{18}F-labeled harmol derivatives"

Hanno Schieferstein, Markus Piel, Friderike Beyerlein, Hartmut Lüddens, Nicole Bausbacher, Hans-Georg Buchholz, Tobias L. Ross and Frank Rösch

"Highly Polar ^{18}F-Labeled Serines for Convenient Amino Acid-based Click-Labeling of Biomolecules"

Hanno Schieferstein, Tobias L. Ross

submitted